UNIVERSITÀ DEGLI STUDI DI PADOVA

DIPARTIMENTO DI INGEGNERIA INDUSTRIALE

DOTTORATO DI RICERCA IN INGEGNERIA INDUSTRIALE

CURRICULUM: INGEGNERIA DEI MATERIALI

CICLO XXXI

FUNCTIONALIZED POLYMER-DERIVED BIOCERAMICS FOR BONE TISSUE ENGINEERING

Direttore della scuola:
Ch.mo Prof. Paolo Colombo

Coordinatore d'indirizzo:
Ch.mo Prof. Enrico Bernardo

Supervisore:
Ch.ma Prof.ssa Monica Dettin

Co-Supervisore:
Ch.mo Prof. Enrico Bernardo

Dottorando:
Annj Zamuner

Abstract

Bioceramic foams, typically containing Ca or Ca-Mg silicates, as wollastonite ($CaSiO_3$) and diopside ($CaMgSi_2O_6$), can be obtained from the thermal treatment of preceramic polymers (silicone resins) containing micro- and nano-sized filler powders. This innovative process is advantageous because of its simplicity, the limited processing temperature and the microstructural homogeneity. These foams can simulate the natural porous internal structure of human bones, and both physical and mechanical characteristics can be modulated by varying the parameters of bioceramic formation process, consequently can be considered as promising scaffolds for bone tissue engineering. The silicate scaffolds were functionalized to add a biochemical component miming organic structure of bone, thus improving the surface-to-cells interactions, complying with the new approach of "biochemical functionalization". The nonapeptide (HVP) from the h-Vitronectin protein (sequence 352-360) was covalently and selectively anchored on wollastonite-diopside (W/D) foams' surfaces. In addition, a dimeric analogue (2HVP) was designed in order to increase ionic interactions with cellular GAGs and two HVP retro-inverted sequences (DHVP, retro-inverted peptide of HVP, and D2HVP, retro-inverted peptide of 2HVP) were synthesized to increase the stability toward proteolytic degradation under physiological conditions. A first screening, through *in vitro* bioassays showed that D2HVP gave the best results in terms of h-Osteoblasts (HOB) adhesion, proliferation, gene expression without inducing cytotoxicity when anchored to W/D foams. In particular, HOB proliferation showed a 15-folds increase for D2HVP functionalized samples with respect to the silanized foams at 6 days. A next-generation scaffold in addition to the ability to "communicate" with the surrounding cells, has to improve angiogenesis by promoting the formation of an interconnected and stable vascular network, because angiogenesis is fundamental for implant's survival and long term integration. In order to reach this goal, we combined the proved bioactivity of D2HVP functionalized polymer-derived silicate foams with the several properties of self-assembling peptides (SAPs). Preliminary *in vitro* screenings were carried out to understand how different cell types (i.e. macrophages, osteoblasts and HUVECs), involved in the processes of inflammatory response, osseointegration and angiogenesis, respond to scaffolds produced by SAPs. The results of these preliminary assays showed that EAK is able to induce the formation of longer HUVEC's tubule structures, and to promote the highest increase in HOB proliferation and YAP1 expression. *In vivo* assays confirmed the osteoconductive and osteoinductive properties of D2HVP peptide. All W/D scaffolds showed external and internal cell colonization with formation of new blood vessels (neoangiogenesis). Only W/D foams functionalized with D2HVP were able to stimulate the process of ectopic mineralization. *In vivo* results showed that EAK enriched with the pro-angiogenic sequence TIM (from Tß4) grafted to the SAP itself, have a synergistic effect in promoting mineralization. Finally, we proposed a different covalent and selective functionalization methodology that, requiring only mild reactions' conditions and aqueous solutions can be easily transferred to all types of polymer-derived bioglass (e.g. Mg/Sr doped hardystonite), for improving their bioactivity.

Contents

Abstract I

1 Introduction 1
1.1 Tissue Engineering 1
1.2 Angiogenesis 2
1.2.1 Steps of angiogenesis 3
1.2.2 Vascularization strategies 5
1.2.3 Angiogenesis assay 6
1.3 Bone tissue 7
1.3.1 Bone tissue Engineering 9
1.3.1.1 Scaffolds for BTE 11
1.3.1.2 Self-assembling peptides 14
1.3.1.3 Biochemical factors 17
1.3.1.4 Chemoselective ligation 22
1.3.2 Cells 23
1.3.2.1 Human Osteoblasts 23
1.3.2.2 Human Umbilical Vein Endothelial Cells 25
1.3.2.3 Human Leukemic Monocytes 28
1.4 Biochemical functionalization 31
1.5 Aim of the research 33
1.6 References 35

2 SAP screening 51
2.1 Abstract 51
2.2 Human Osteoblasts 52
2.2.1 Results and discussion 52
2.2.2 Conclusions 53
2.2.3 Materials and methods 54
2.2.3.1 Peptide synthesis, characterization and purification 54
2.2.3.2 Preparation of peptide solutions 54
2.2.3.3 Cell Tissue culture, seeding, fixation and permeabilisation 55
2.2.3.4 Cell staining 55
2.2.3.5 Preparation of SAPs coatings 56
2.2.3.6 HOB proliferation assays 57
2.2.3.7 Imaging and image analysis 57
2.2.3.8 Statistical analysis 57

2.3 HUVECs 58
2.3.1 Results and discussion 58
2.3.2 Conclusions 65
2.3.3 Materials and methods 65
2.3.3.1 Cell Tissue culture, seeding, fixation and permeabilisation 65
2.3.3.2 Cell Staining 66
2.3.3.3 Preparation of SAP/Gelatin coatings 66
2.3.3.4 SAPs/matrigel assays 67
2.3.3.5 HUVEC proliferation assays 68
2.3.3.6 Imaging and image analysis 68
2.3.3.7 Measuring HUVEC networks' architecture 69
2.3.3.8 Statistical analysis 69
2.4 Macrophages 70
2.4.1 Results and discussion 70
2.4.2 Conclusions 77
2.4.3 Materials and methods 77
2.4.3.1 THP-1 Cell Culture 77
2.4.3.2 HUVEC Cell Culture 78
2.4.3.3 SAP/gelatin coatings and incubation time optimization 78
2.4.3.4 THP-1 Adhesion assay on SAP/gelatin coated plate 79
2.4.3.5 Staining THP-1 cells with Hoechst and Phalloidin 79
2.4.3.6 Imaging and quantification of adherent cells 79
2.4.3.7 Polarisation of THP-1 derived Macrophages 80
2.4.3.8 M1 and M2 Immunofluorescence analysis 81
2.4.3.9 Matrigel/HUVEC angiogenesis assay on SAP-polarised M1/M2 82
2.4.3.10 Measuring HUVEC networks' architecture 83
2.4.3.11 Statistical analysis 83
2.5 References 84

3 Wollastonite-Diopside foams 87
3.1 Abstract 87
3.2 Results and discussion 88
3.2.1 *In vitro* assays 88
3.2.2 *In vivo* assays 92
3.2.2.1 Qualitative histological analysis 93
3.2.2.2 Histomorphometric analysis 98
3.3 Conclusions 104
3.4 Materials and methods 106
3.4.1 W/D foams synthesis and characterization 106

3.4.2 Adhesive peptides synthesis and characterization 107
3.4.2.1 HVP characterization 107
3.4.2.2 2HVP characterization 108
3.4.2.3 DHVP characterization 108
3.4.2.4 D2HVP characterization 108
3.4.3 Non-adhesive peptide synthesis and characterization 108
3.4.4 Self-assembling peptide synthesis and characterization 109
3.4.4.1 EAK 109
3.4.4.2 AoaEAK 110
3.4.5 Pro-angiogenic peptide synthesis and characterization 111
3.4.6 Chemoselective ligation of EAK and G7TIM 112
3.4.7 W/D foams functionalization 112
3.4.7.1 Selective and covalent functionalization 112
3.4.7.2 SAP embedding 113
3.4.8 Crushing strength test 114
3.4.9 *In vitro* bioassays 114
3.4.9.1 Adhesion assay 114
3.4.9.2 Proliferation assay 115
3.4.9.3 Cytotoxicity assay 115
3.4.9.4 Quantitative real time polymerase chain reaction 115
3.4.10 *In vivo* bioassays 116
3.4.10.1 Histological analysis 118
3.4.10.2 Histomorphometric analysis 119
3.4.11 Statistical analysis 120
3.5 References 120

4 Mg/Sr doped hardystonite foams 123
4.1 Abstract 123
4.2 Results and Discussion 124
4.3 Conclusions 133
4.4 Materials and Methods 134
4.4.1 Mg/Sr doped Hardystonite foams synthesis and characterization 134
4.4.2 Adhesive peptides synthesis and characterization 136
4.4.3 Self-assembling peptide synthesis and characterization 137
4.4.4 HT foams functionalization 137
4.4.4.1 Selective and covalent functionalization 137
4.4.4.2 SAP embedding 138
4.4.5 *In vitro* bioassays 138
4.4.6 Statistical analysis 138

4.5 References 138

5 Final conclusions 141

Abbreviations 145

Chapter 1

Introduction

1.1 Tissue Engineering

The actually worldwide recognized term "Tissue engineering" was first introduced to the scientific committee at a bioengineering panel meeting of the National Science Foundation in 1987, and the first meeting focused on this subject was carried out during the following year[1]. Tissue engineering (TE) has developed to become a prominent interdisciplinary field of regenerative medicine, involving the collaborative efforts of clinicians, biologists and engineers. The ultimate goal of TE is to develop biological substitutes that mimic natural tissue and 'restore, maintain or improve tissue function or a whole organ' *in vivo*[2]. This can be required following loss of hard or soft tissue due to trauma, cancer, chronic and congenital disease[3].

With the ageing population expected to rise to 2 billion by 2050 (United Nations World Population Ageing, 2017) the occurrence of degenerative diseases, such as osteoporosis, Alzheimer's and cardiovascular disease are increasing. As a consequence, the need for the replacement of diseased tissue to improve quality of life is paramount. Although the implementation of synthetic biomaterials, artificial devices and organ transplantation have been able to meet demands so far, it has led to a large cost burden on health services, and concerns surrounding immunogenicity, biocompatibility and organ shortage are inevitable[4]. TE represents a potential solution, with the emergence of bone regeneration for orthopaedic conditions, skin reconstruction for burns, and drug delivery, to name a few.

In order to achieve the ultimate aim of tissue engineering, three vital components are required (**Fig 1.1**); a biomaterial scaffold to provide the structural microenvironment for cell attachment, growth stimulating factors to encourage cell differentiation and cells as building blocks for tissue generation. Nonetheless, formation of an interconnected and stable vascular network for long term survival, functionality and integration represents a major challenge to overcome[5].

Once implanted, tissue engineered scaffolds aim to drive cells to the site of the defect to induce tissue regeneration. In order to achieve this, the scaffold must integrate with the

tissue and enable repopulation and remodelling by host cells. This large-scale cell migration[6]is a significant factor for scaffold success, and hence culminating a detailed understanding of the physical and mechanical properties of the three-dimensional extracellular environment, such as stiffness and topography, is key.

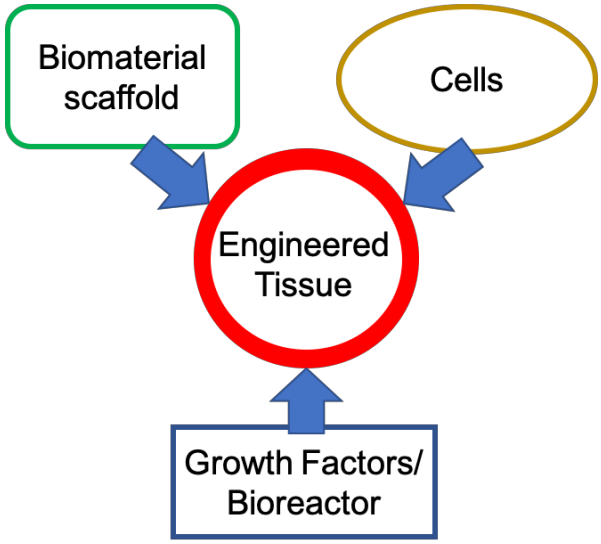


Figure 1.1. The triad of tissue engineering, to repair and regenerate tissue[7].

Ultimately, the hindrance of cell invasion and migration coincides with lack of vascularisation and eventually cell necrosis[8], which refers to uncontrolled cell death in response to injury, such as lack of oxygenated blood supply[9].

1.2 Angiogenesis

Vasculature, in the form of arteries, veins and capillaries, exists as an organised hierarchal network that transports blood to and from tissues, to provide oxygen, and nutrients, remove waste products and carry biochemical molecules[10]. The process of blood vessel formation is implicated in both physiological and pathological conditions, ranging from early development, wound healing, repair, and homeostasis in health, to the emergence of tumour growth, chronic wounds and rheumatoid arthritis in disease[11]. Two fundamental mechanisms of blood vessel formation can be distinguished; vasculogenesis and angiogenesis. Vasculogenesis is defined as the *de novo* formation of blood vessels that occurs during early embryological development, Mesoderm derived endothelial precursors, angioblasts, differentiate into endothelial cells (EC) to form a primitive vascular cord, and eventually a primary capillary plexus. In this manner, the major blood vessels of the body are formed[12].

The majority of vascular expansion and remodelling in utero and adulthood is governed by angiogenesis, which refers to the process of blood vessel sprouting from pre-existing vessels[13–15]. This process plays a significant role in wound healing, because the newly formed blood vessels permit the delivery of oxygen and nutrients to support tissue growth[16], and allow the removal of waste products produced during tissue repair[17]. In the field of regenerative medicine, which focuses on replacing or regenerating human tissue and/or organs, one of the major challenges is to induce new blood vessels growth within the defected area, in order to support the demand of the newly formed tissue. As previously said, angiogenesis is also an important aspect in the field of tissue engineering, which focuses on facilitating regrowth of damaged tissue by applying a combination of scaffolds, cells and biochemical factors, because angiogenesis could prevent hypoxia, apoptosis and tissue necrosis at the site of implantation[18]. Particularly, scaffolds larger than 200-500 µm must be accompanied by angiogenesis in order to survive after implantation[19]. Moreover, inflammatory cells (i.e. macrophages and neutrophiles) require interaction with vessel wall and its basement membrane to transmigrate into the site of injury and induce inflammatory response[16]. Furthermore, abnormal or incomplete angiogenesis is one of the cause of almost all chronic wounds or delayed healing, including arterial, diabetic, pressure and venous ulcers[20]. Therefore, understand what drives and inhibits angiogenesis is important for the future development of new treatment for ischaemic injuries, tissue engineering and regenerative medicine.

1.2.1 Steps of Angiogenesis

The angiogenic process is characterised by either sprouting angiogenesis, or intussusceptive angiogenesis. Sprouting angiogenesis (**Fig 1.2**) is initiated by the production of a pro-angiogenic growth factor, Vascular Endothelial Growth Factor-A (VEGF-A), which is released by cells in a hypoxic state; a deprivation of oxygen to tissues. Quiescent endothelial cells become activated to tip cells and migrate towards the VEGF-A gradient.

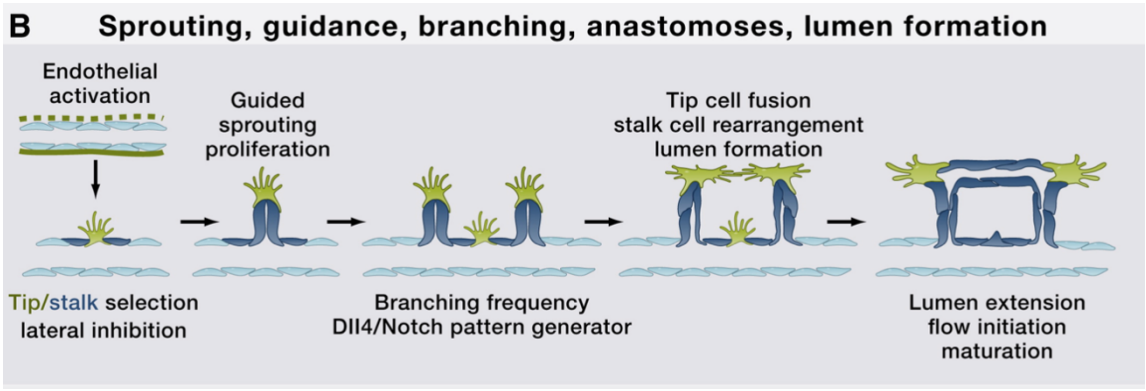


Figure 1.2. Steps of vessels Sprouting[14].

The induction of long, actin-rich cellular extensions called filopodia, facilitate tip cell migration to guide capillary sprout formation and vascular patterning. Directional polarity is expressed by the presence of VEGF2 receptors on filopodia[21] which enable sensing of the extracellular environment for varying concentrations of VEGF-A. Alongside this, the numerous filopodia probe the extracellular matrix (ECM), to recognise ECM mechanics[22] and composition, to dictate the formation of integrin mediated adhesion complexes that act as anchoring sites to the local ECM fibres. Studies have highlighted the close association between ECM mechanical properties, primarily stiffness, and cellular responses, by means of cytoskeletal organisation and focal adhesion[23,24]. In the context of tumour behaviour, angiogenic outgrowth correlated with increased matrix stiffness[25] and upregulation of angiogenic growth factors[26].

Following attachment to the substratum through adhesion complexes, the actin filaments of the filopodia generate a traction force to cause cell cytoskeleton contractility and pull the tip cells in the direction of the pro-angiogenic signal. Proteolytic degradation of the ECM from secretion of proteases, such as matrix metalloproteinases (MMPs), subsequently enables ECM remodelling to allow vascular growth. Concurrently, neighbouring endothelial stalk cells, which are proliferating in nature and have less filopodia, proliferate behind the tip cell to promote sprout elongation, lumenization and formation of the basement membrane. Phenotypic differentiation of ECs to tip and stalk cells is dynamic and controlled by the intricate balance of VEGF-A and delta-like ligand (DLL4) and Notch signalling[27]. VEGF-A stimulates the activity of DLL4 present on the tip cell, which interacts with Notch receptors on neighbouring stalk cells, to supress conversion to a tip cell phenotype. Activated notch signalling in stalk cells down regulates VEGF receptors (VEGFR2) to desensitise ECs to the VEGF-A gradient. This lateral inhibition allows the branching frequency to be regulated so that vacuole development can occur to form a vascular lumen. As neighbouring sprouts converge, tip cells combine to cause lumen anastomosis and establish vessel connections. With reduced levels of VEGF-A, differentiation to phalynx cells occurs, which go on to form the inner layer of quiescent endothelial cells of the newly formed vessel. Recruitment of mural cells, including pericytes and smooth muscle cells (SMCs), assist with vessel stabilisation and perfusion.

Alternatively, intussusceptive angiogenesis, also called splitting or non-sprouting angiogenesis, is characterised by the development of an intussusceptive pillar that internally splits the lumen of a pre-existing capillary plexus. The process involves reorganisation of intercellular junctions and recruitment of pericytes and myofibroblasts to deposit ECM, in an attempt to remodel vascular beds. In contrast to sprouting angiogenesis, limited research and experimental models that investigate the precise mechanisms of intussusceptive angiogenesis exist, with notions suggesting it's biological

relevance in organ specific angiogenesis[28] and impact of haemodynamic forces, such as laminar shear stress[29].

1.2.2 Vascularization strategies

Ideal tissue engineered scaffolds are designed to facilitate cell adhesion, promote proliferation or differentiation and cell infiltration through sufficient interconnected porosity and a large surface area to volume ratio[30]. Several strategies to promote successful vascularisation have been proposed (**Fig 1.3**):

- the use of pro-angiogenic growth factors such as VEGF, basic fibroblast growth factor (bFGF) and platelet derived growth factor (PDGF) in cell loaded scaffolds[31];
- cell transplantation with endothelial cells or mesodermal stem cells as precursors for vessel formation;
- the use of co-culture systems such as seeding endothelial cells and mural cells in a 3D scaffold[32];
- bioreactors for mechanical stimulation[33];
- optimising chemical architecture of biomaterials, and employing microfabrication techniques, such as lithography and micro contact printing[34].

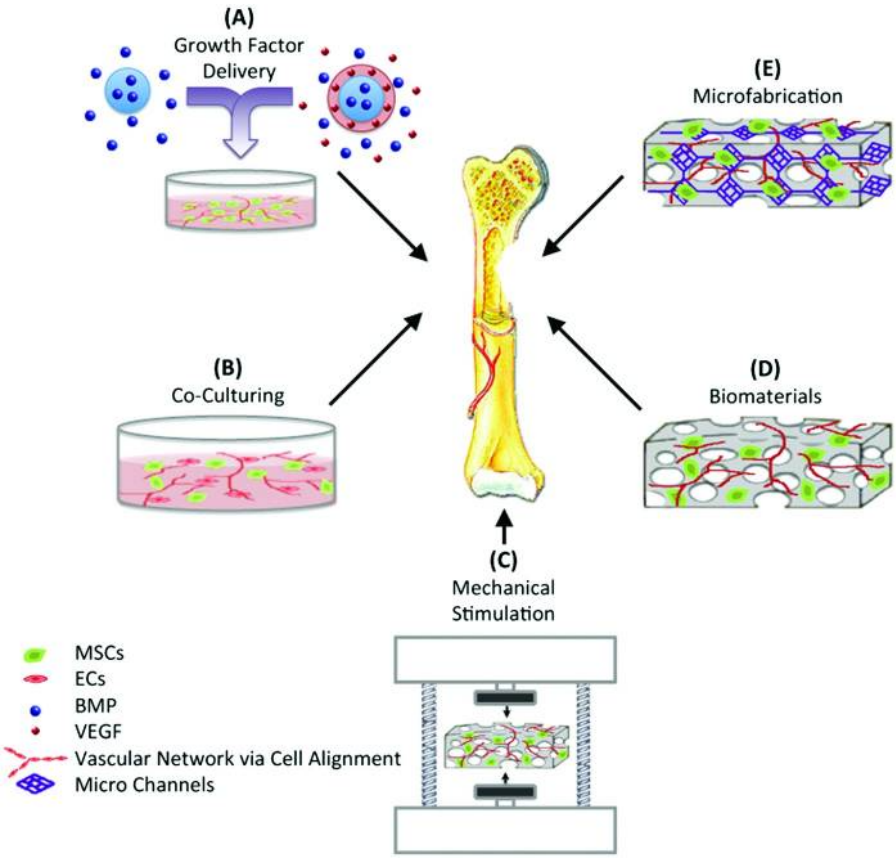


Figure 1.3. Schematic showing of different vascularization strategies[35].

Another strategy consists in modulating inflammation using cytokines (e.g. interleukin 4) to activate pro-angiogenic macrophages (M2 macrophages)[19].

However, the ideal solution remains elusive, as advantages and drawbacks exist for many of the vascularisation approaches. For instance, growth factor delivery can be performed through binding growth factor proteins with nanoparticles[36] or with encapsulation to allow a controlled rate of degradation, along with the simultaneous delivery of growth factors to emulate the complexity required for vessel growth. Shun *et al.* demonstrated enhanced vascularisation and formation of mature vessels with co-immobilisation of multiple angiogenic growth factors[37]. On the other hand, integration of growth factors is limited by the short half-life *in vivo*, for instance, VEGF has a half-life of 6-8 hours[35] and hence this requires a sustained and controlled method of delivery for continuity. Moreover, infusions of growth factors generally require concentrations that are above physiological levels, which can lead to protein denaturation. Direct administration of high dose VEGF is associated with toxicity and risk of tumour development, and there is minimal spatial temporal control of release through the scaffold[35]. Induction of vascularisation following implantation is associated with a time delay for host cell infiltration to form anastomoses within the scaffold, and thus stimulating vascularisation after implantation is not necessarily the ideal option.

Recently, studies have shown the advantage of cultivating preformed microvessels by encapsulating endothelial cells and stromal cells on scaffolds to mimic the extracellular environment i.e. hydrogels or biologically derived scaffolds, before implantation. This approach avoids the delay in oxygenation of scaffold cells and enables rapid vascularisation to improve cell survival *in vivo*[38,39]. Overall, the need to develop a successful and clinically applicable vascularisation strategy for tissue engineering still remains.

1.2.3 Angiogenesis assay

Angiogenesis still represents an area of active research and many of studies are still ongoing in order to understand what factors, materials and cells drive or inhibit angiogenesis. In the recent years, numerous *in vitro* models have been developed for angiogenesis assays to replace animal models, that best resemble human physiology but are expensive and subjected to legal restrictions[13].*In vitro* models are classified in: 2D, 2.5D and 3D models according to the arrangement of cells and matrix[40].

- 2D models: endothelial cells are placed directly on hard tissue culture polystyrene (TCSP)'s surface. With this model, it's possible to promote the development of focal adhesion.

- 3D models: endothelial cells are dispersed within a hydrogel composed of one or more components from the extra cellular matrix (ECM), such as collagen, fibrin or their peptides, etc.
- 2.5D models: endothelial cells are seeded between hard TCSP surface and a soft matrix, or on top of the soft matrix hydrogel. This model combines the benefits of 2D and 3D models.

Matrigel is one type of matrix hydrogel commonly used for *in vitro* models. Matrigel is an ECM-like hydrogel composed of collagen, laminin and nidogen produced by Engelbreth Holm Swarm (EHS) mouse sarcoma cells. Matrigel is stored at 4°C in its liquid form, while when incubated at 37°C for bioassays it gelified due to proteins polymerization[41]. When endothelial cells are seeded on top of Matrigel, they can arrange themselves in network of cords (**Fig 1.4**), whilst this doesn't happen when seeded on TCSP plates.

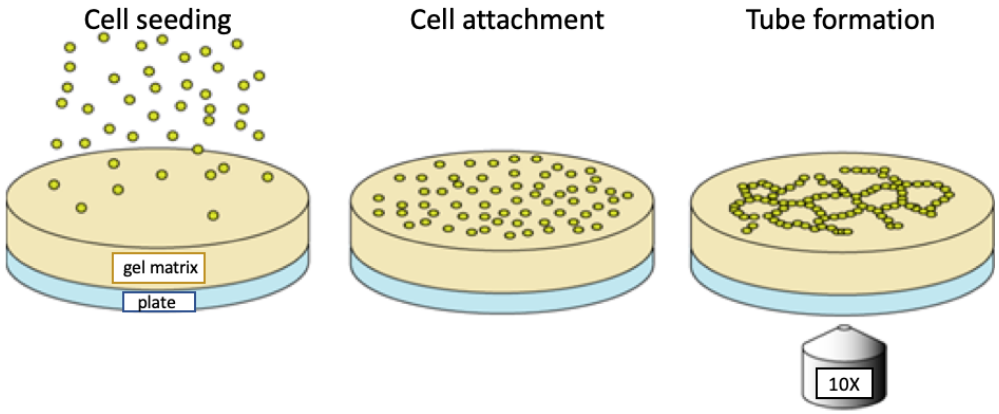


Figure 1.4. Endothelial cells cultured on Matrigel to form tubules and nodes. Scheme adapted from www.bio1000.com.

Concluding, Matrigel assays are advantageous since they resemble the *in vivo* ECM environment due to the presence of numerous proteins, but Matrigel composition strongly differs from different batches and does not encourage cell proliferation or lumen formation, therefore it cannot be used for vasculogenesis studies[13].
Collagen and fibrin are also used in 3D and 2.5D assays as they potentially trigger endothelial cells proliferation, angiogenesis and vasculogenesis[13,42,43].

1.3 Bone tissue

Bone is a complex hierarchically structured family of materials that includes a network of cells and their interconnected cell processes[44]. Bone tissue is mainly composed by four types of cells: osteoblasts, bone lining cells, osteocytes, and osteoclasts[45,46]. The precursor

of these cells is constituted by mesenchymal stromal cells (hMSCs), which represent a small fraction within the bone marrow.The principal functions of bones are locomotion, support and protection of soft tissues, calcium and phosphate storage, and harbouring of bone marrow[47,48]. Despite its inert appearance, bone is a highly dynamic organ that is continuously resorbed by osteoclasts and neo-formed by osteoblasts[49].Recent studies revealed the presence of two different materials, the major material being the well-known ordered arrays of mineralized collagen fibrils and associated macromolecules, and the minor component being a relatively disordered material composed of individual collagen fibrils with no preferred orientation, with crystals of carbonated hydroxyapatite inside and possibly between fibrils, and extensive ground mass[44] (**Fig 1.5**).

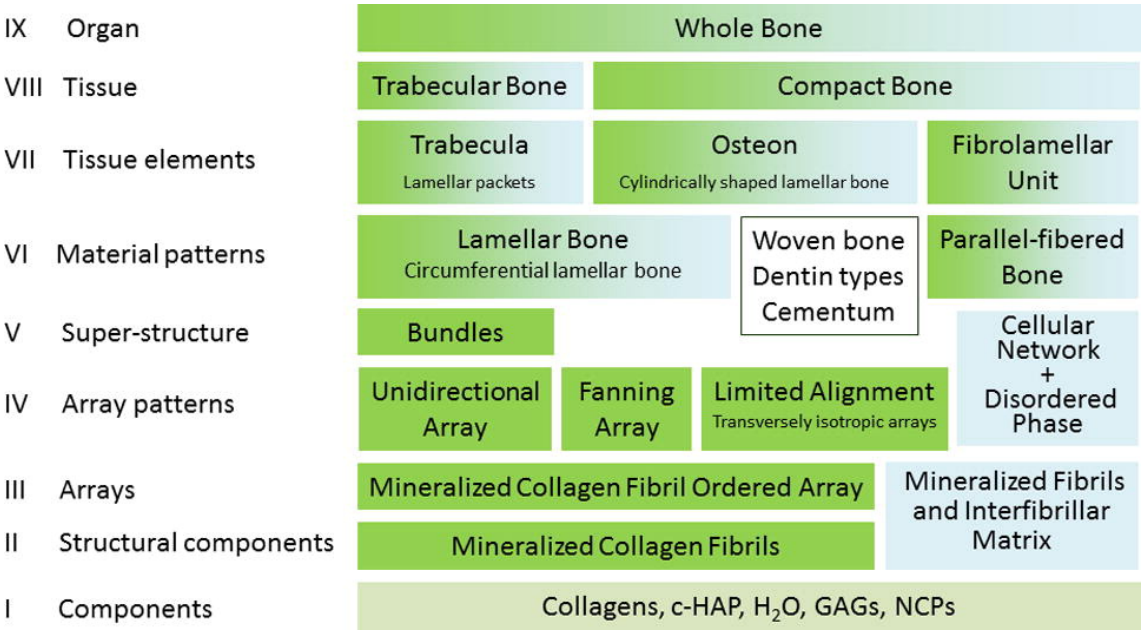


Figure 1.5. Hierarchical organization of bone. c-HAP: carbonated hydroxyapatite; GAGs: glycosaminoglycans; NCPs: non-collagenous proteins.[44]

Accordingly to their shape, bones can be classified into long, short and flat bones. An adult long bone presents a diaphysis, the central part of the bone, and two epiphyses at the two edges. The structure of the bone is different between the two regions (**Fig 1.6**): the diaphysis consists mainly in cortical bone, whilst the epiphyses and the inner part of the diaphysis is mainly composed by cancellous or trabecular bone[50].

Cortical bone is a dense and highly mineralized bone tissue that represent the 80% of the mass of the bone tissue in the body and it's mainly responsible of the mechanical and structural properties of the bone[51]. The other 20% of the mass is composed by trabecular bone, a porous structure composed by lattice of plates and rods known as trabecula[52,53]. The bone tissue is a mineralized connective tissue mainly composed of mineral, organic matrix, cells and water[49], where the major mineral content consists of hydroxyapatite

$Ca_{10}(PO_4)_6OH_2$[53]. The organic matrix is mainly composed of collagen Type I (~90%), but it contains also non-collagenous proteins (~10%) like fibronectin, osteocalcin, osteopontin, osteonectin and bone sialoprotein[54,55].

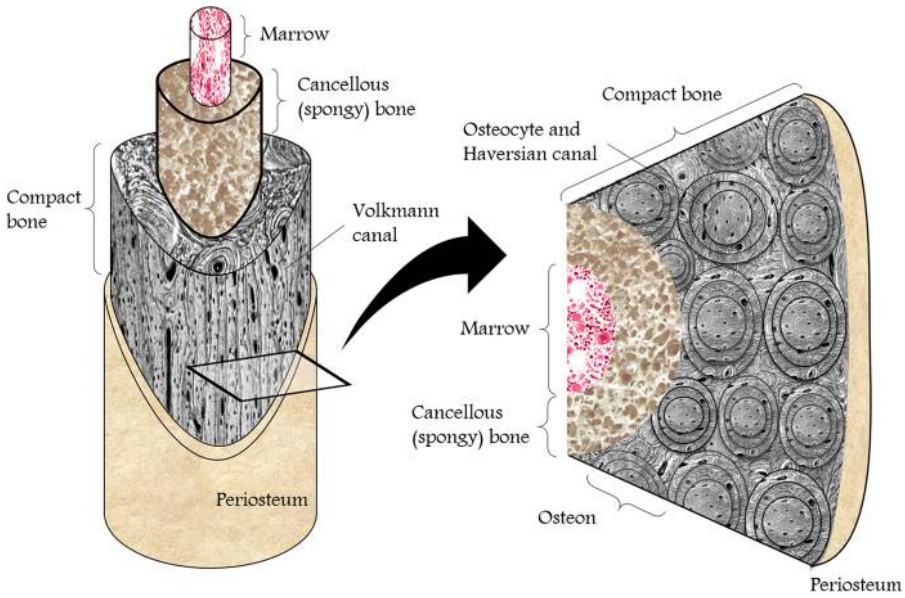


Figure 1.6. Long bone anatomy[56].

1.3.1 Bone Tissue Engineering

The gain in life expectancy during the twentieth century ranks as one of the most extraordinary social and medical achievements but it is accompanied by an increase in age-related pathologies such as obesity, osteoporosis, bone disorders and allied conditions[57,58].

Tissue engineering and regenerative medicine focus on the restoration of form and function to tissue insufficiencies. In the context of bone, a clinical osseous insufficiency is defined as a discontinuity in bone integrity resulting from trauma, congenital malformation or surgical resection[59].

As the incidence of bone diseases is increasing steeply, the field of bone tissue engineering (BTE) is attracting more and more attention. Nowadays, autografts represent the gold standard in bone implant since the histocompatibility and lack of immunogenic reactions guarantee osteogenesis, osteoconduction and osseointegration[58,60,61]. Osteogenesis is the process during which osteoprogenitor cells mature into osteoblasts, which subsequently mineralize and form bone tissue[62].

Osteoconduction refers to the process by which bone forms on a surface. With respect to biomaterials, osteoconduction is measured by the ability of an implant to support the growth of bone in a 3D manner at a defect site[63].

Finally, osteoinduction describe the process of recruitment of immature osteoprogenitor cells to a wound site and the subsequent differentiation of these cells into osteoblasts

under the influence of a diffusible bone morphogenetic protein[64]. However, additional surgical procedures and risk of inflammation, infection and chronic pain at donor site complicate autogenous bone implants whereas the limited supply of autografts do not meet the needs for large bone fractures[65,66]. Thus, the quest for regeneration in critically sized bone defects has inspired a search for clinically efficacious tissue-engineering therapeutics that has spanned over two decades[67].

Therefore, engineered substitutes ensuring the biocompatibility, osteoconduction and early implant loading are required[68,69].

The building blocks to assemble tissue-engineered therapies that fulfil the demanding biological performance standards required for bone regeneration include cells, signalling molecules and scaffolds[67] (**Fig 1.7**).

Specifically, we must achieve the precise, predictable coordination of cell responses with matrix scaffolds and biological signalling molecules to match the dynamics of physiological fracture repair[67].

Since osseointegration and long-term success of the implant are determined by the complex reactions taking place at the tissue-material interface, in bone tissue engineering one of the most relevant issue is to recreate the ability of autogenous grafts to communicate with the surrounding biological environment. Thus, cell adhesion, proliferation, migration and differentiation are induced by coordinate transmembrane signalling occurring in cells approaching the surface of the implant and are mandatory for implant colonization[70–72].

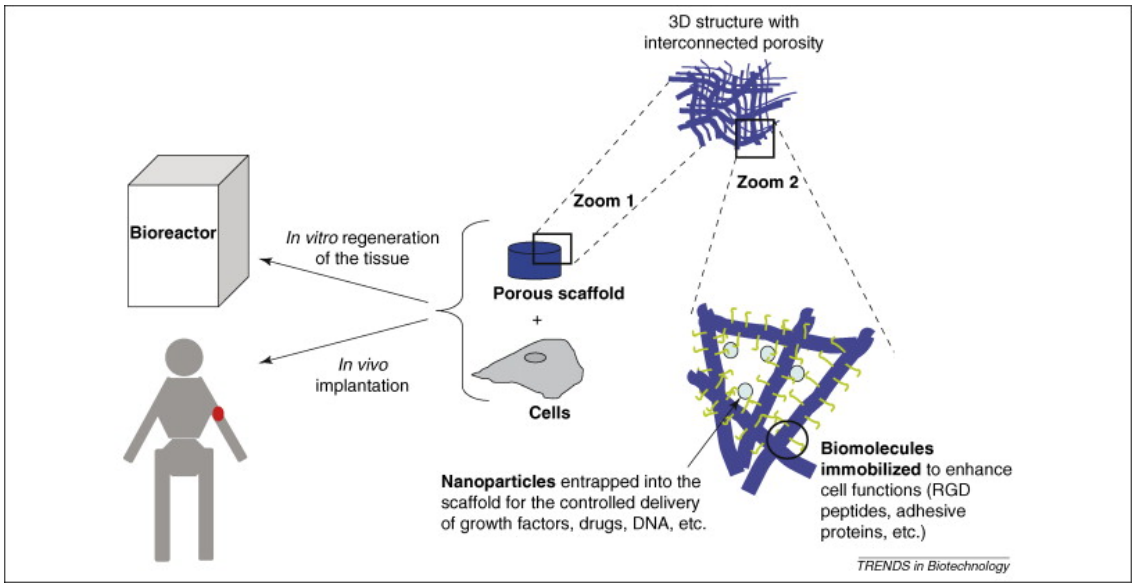


Figure 1.7. Schematic representation of bone tissue engineering[73].

1.3.1.1 Scaffolds for BTE

An engineered substitute for BTE needs a three-dimensional scaffold that provide the environment to support and guide cell adhesion, growth and proliferation in order to promote the formation of new tissue[74].

The general criteria in designing an appropriate scaffold graft for successful BTE includes the type of material, its architecture and porosity, surface chemistry and osteoinductivity as well as mechanical strength[75] (**Tab 1.1**).

Table 1.1.Criteria and their functional considerations for the design of scaffolds used in BTE applications[75].

CRITERIA	FUNCTION
Biocompatibility	Ability to perform its function in the host tissue without eliciting any immune response.
Biodegradability	Tunable rate of degradation to match growth of new bone tissue as scaffold gets replaced by new bone.
Mechanical properties	Sufficient mechanical strength to provide temporary support to the defect region and withstand in vivo loading forces.
Microarchitecture	Interconnected scaffold structures to uniformly distribute stresses throughout scaffold.
Osteoinductivity	Osteoinductive properties to recruit and differentiate osteoprogenitors to the defect region.
Porosity	Large surface area: volume and pore size to allow for tissue in-growth, neovascularisation, mass transport and osteogenesis.
Surface properties	Appropriate chemical and topographical properties for influencing cellular adhesion, proliferation and differentiation.

First of all, the material needs to be biocompatible and not provoking adverse physiological response from the host.

Ideally, the scaffold should serve to provide a temporary structure which subsequently degrades in tandem with new tissue formation over time, so the rate of degradation of the scaffold has to be close to the regeneration rate of the natural tissue[75,76].

The ease of manufacturability and clinical handling are also essential in filling up the gap defects. Nowadays, the use of increasingly sophisticated technologies (e.g. computed tomography and magnetic resonance) for imaging the defect region, allows for the customisation of scaffold size and shape to fit the defect region, using manufacturing methods such as fused deposition modelling[77] and 3D printing[75,78].

Biomaterials for BTE can be classified broadly into two main categories: inorganic and organic materials, which include both naturally derived and synthetic components. Inorganic materials, such as beta tricalcium phosphate (ß-TCP), hydroxyapatite (HA) and bioactive glasses, have long been used because of their similarities in structure and composition to the inorganic elements of bone itself[79].

Among the benefits of inorganic biomaterials are their compressive strength (which is often equal to, or greater than bone tissue) and potential for osteoconductivity[80].

The main disadvantage regarding the use of these materials is their brittle nature, which can be problematic in high load-bearing biological applications[67].

The alternatives to inorganic materials are organic polymers, which can be either naturally occurring, such as collagen[81], chitosan[82], hyaluronic acid[83], cellulose[84], alginate[85]and silk, or chemically synthesized polymers.

Generally, naturally derived biomaterials are characterized by biocompatibility, enabling adhesion and migration of cells within their structures, by the way, the major limitations of naturally derived polymers include difficulties in processing and purification that lead to high cost, though the most important disadvantage is that none of the naturally derived organic biomaterials has adequate mechanical properties[67].

Synthetic polymers can be produced on large scale, they are cost efficient and it's possible to tailor the mechanical and physical characteristics to the application, but they are not biologically recognized, since they lack of the natural recognition sites, especially in comparison to naturally derived polymers that have ECM-binding domains, mandatory to communicate with cells[86].

In the last years, many synthetic biomaterials with tuneable micro- and macro-scale features have being developed. Microscale features include composition, architecture and binding groups, whereas macroscale features include porosity, stiffness and elasticity[67].

The most commonly used synthetic materials are biodegradable polymers such as polylactic acid (PLA), polyglycolic acid (PGA), the copolymer PLGA, polycaprolactone (PCL).

Composites are materials that combine the desirable properties of ceramics and polymersin order to achieve a synergistic effect in their resultant properties[87].Typically, bioceramics are added as fillers or coatings to the polymer matrix to improve the mechanical proprieties and induce enhanced bioactivity[88].

Alternatively, composite made using a porous bioceramic scaffold coated with polymer has been prepared too; in this case, the polymer was introduced to strengthen the bioglass scaffold structure[89].

In composites' fabrication, both degradable and non-degradable polymers have been used, but the latter normally have low biocompatibility and tent to create a fibrotic capsule around the implant[90]. Much effort has been devoted to overcome this problem, and several composites based on a combination of biodegradable polymers and bioceramics have been suggested[91–94].

Nowadays, nano-bioceramic/polymer composites are acquiring great interest due to their potential to improve host tissue/cell interaction[95].

The development of a smart composite biomaterial with nanoscale interaction between the bioactive inorganic phase and the organic one could allow the degradation of the

scaffold as a single material and not with two degradation rates related to the two separated phases[96].

In the last years, lots of interest has been devoted to the development of multifunctional bioceramics that combine the properties of porous bioactive scaffolds and the therapeutic value of ions release[90]. For this reason, bioactive glass has been doped with various trace elements to provide smart strategy for the controlled *in situ* delivery.

Studies demonstrated that the controlled released into the cellular environment of Mg, Sr, Cu, Ga or Co may lead to therapeutic effects such as promotion of angiogenesis and antibacterial effect[97–99].

New strategies for BTE scaffold fabrication are emerging with the purpose of improving scaffold performance together with developing even more sustainable processing routes[90].

In this regard, an innovative method based on preceramic polymers containing micro- and nano-sized fillers has been developed to successfully produce highly porous bioactive glass scaffolds[100].

Bioglass ceramics from preceramic polymers and fillers

Highly amorphous bioceramic foams can be obtained from the thermal treatment of preceramic polymers, in the form of silicone resins, containing micro and nano-sizedfiller powders.

Fillers can be active or passive, the first react with the decomposition products of the preceramic polymer to create new phases, whilst the latter don't modify the composition of the polymer-derived ceramic phase[101].

Simply by changing the starting nano-sized active fillers, this method allows to obtain different types of ceramics such as wollastonite, diopside, akermanite, hardystonite, fluoroapatite etc[101–104].

The process consists in a very simple processing technique that involves three steps:

1. preparation of polymer/fillers mixture
2. curing step at 300-350°C in which the liquid silicone can be easily foamed by water release, in turn due to the decomposition of hydrated sodium phosphate or borax (used as foaming agents)
3. ceramic conversion of the silicone foam into glass-ceramic foam by heating at moderate temperatures (generally below 1400°C)[101].

The main advantages of this process are:

- preceramic polymers, as silicone resins, are commercially available at reasonable prices;
- the simple processing procedure that involves two thermal treatments at low temperature;

- the possibility of using polymer processing techniques to achieve complex shapes;
- bothporosity and mechanical properties can be easily adjusted simply modifying the starting precursors (micro- or nano-sized powders and silicones) and/or adding a glass filler to obtain a positive impact on the structural integrity of the scaffold[102];
- the reactions occurring between the bioceramic and the soaking medium do not cause large changes of the pH, that is fundamental to have a suitable environment for host cells after implantation[100].

The 3D porous structure, with open and interconnected porosity (higher than 75%), and the mechanical properties, with compressive strength that reaches 2 MPa (but can be further increased adding glass fillers) fulfilled the requirements for being promising scaffolds for BTE.

Preliminary *in vitro* bio-assays on wollastonite-diopside and wollastonite-hydroxycarbonate apatite scaffolds showed positive results in terms of bioactivity, biocompatibility as well as osteogenic potential[102,105].

1.3.1.2 Self-assembling peptides

Recently, the use of self-assembling peptides (SAPs) as scaffolds for cell growth has become important in the field of tissue engineering.

Self-assembly can be defined as "the spontaneous association of molecules, through non-covalent bonds and under equilibrium conditions, into stable, structurally well-defined aggregates"[106].

SAPs represent a particular class of molecules characterized by the ability to organize themselves into ordered structures by creating non-covalent bonds such as Van der Waals forces, hydrogen and ionic bonds, and hydrophobic interactions. These molecules allow to obtain 2D or 3D structures to be used to promote multidimensional cell-cell interactions and increase cell density.

EAK 16-II (AEAEAKAKAEAEAKAK) was the first synthetic self-assembly peptide discovered in 1993 by S. Zhang as fragment of a yeast protein named Zuotin, that was initially identified for its ability to bind to left handed Z-DNA[107].

The class of self-assembling peptides was divided into five main types[108]:

- Type I, or "Molecular Lego": they form hydrogels that can be used in the creation of scaffolds;
- Type II, or "molecular switches";
- Type III: "molecular hooks" and "molecular velcro", are peptides used in surface treatments;

- Type IV: group of nano-peptide tubes and "molecular capsules" for the transport of genes and proteins;
- Type V: "molecular cavities" for biomineralization[109].

The process of self-assembly is related to both the intrinsic nature of the individual amino acids and their position in the sequence.

It is, therefore, possible to obtain a specific secondary structure by selecting and conveniently arranging the amino acids in sequence[110]. The peptides for self-aggregation must have two characteristics: the complementarity (i.e. the repetition of a particular charge distribution within the sequence) and the structural compatibility.

The type I ionic-complementary peptides, meet both requirements being characterized by the alternation of positive and negative residues.

The configurations of charges have been classified into various moduli: modulus I, − + − + − + − +, modulus II, − − + + − − + +, modulus III, − − − + + +, and modulus IV, − − − − + + + +[108].Peptides belonging to this class generally assume, in different solvents, a secondary β-sheet structure, where each β-sheet plane has an ionic-shaped face with positively and negatively charged side chains and a hydrophobic face (**Fig 1.8**).

Thanks to both ionic and hydrophobic interactions, the numerous β-sheet planes can be assembled in three-dimensional structures with interwoven nanofibers, which have been shown to have a diameter of 10-20nm and pore size of 50-200nm[107]. The subsequent hydrogels have a high water content of above 99%, thus aiding diffusional transport of oxygen, nutrients and bioactive factors, and favouring cell ingrowth[111].

Many are the conditions that determine and influence the process among which the concentration of the peptide in solution, the presence of monovalent positive ions, the pH, the temperature and time[112].

Hong *et al.* and Fung *et al.* showed that EAK16-II forms fibrillar assemblies in pure water at near neutral pH, above a certain critical concentration of peptide (around 0.3mg peptide/mL water)[113–115].

Because the fibrillar aggregates disappeared at the critical concentration, Fung *et al.* called it a critical aggregation concentration (CAC). These SAPs' hydrogels have been used as scaffolds for the growth of different types of cells[41,112,116–121] and a particular type of self-assembling peptide, called RADA, is marketed with the name of PuraMatrix.

SAPs can be easily coupled with biologically active motifs e.g. RGD (Arginine-Glycine-Aspartic Acid), the fibronectin sequence for cell attachment, without disrupting the self-assembly. In this way, the self-assembled scaffolds are able to mimic the ECM architecture to promote cell adhesion, proliferation and form implantable tissue constructs.

Self-assembling peptides can also be used for drug delivery, and growth factors can be simply embedded in the hydrogel or can be conjugated via chemoselective ligation[122–124] (paragraph 1.3.1.4).

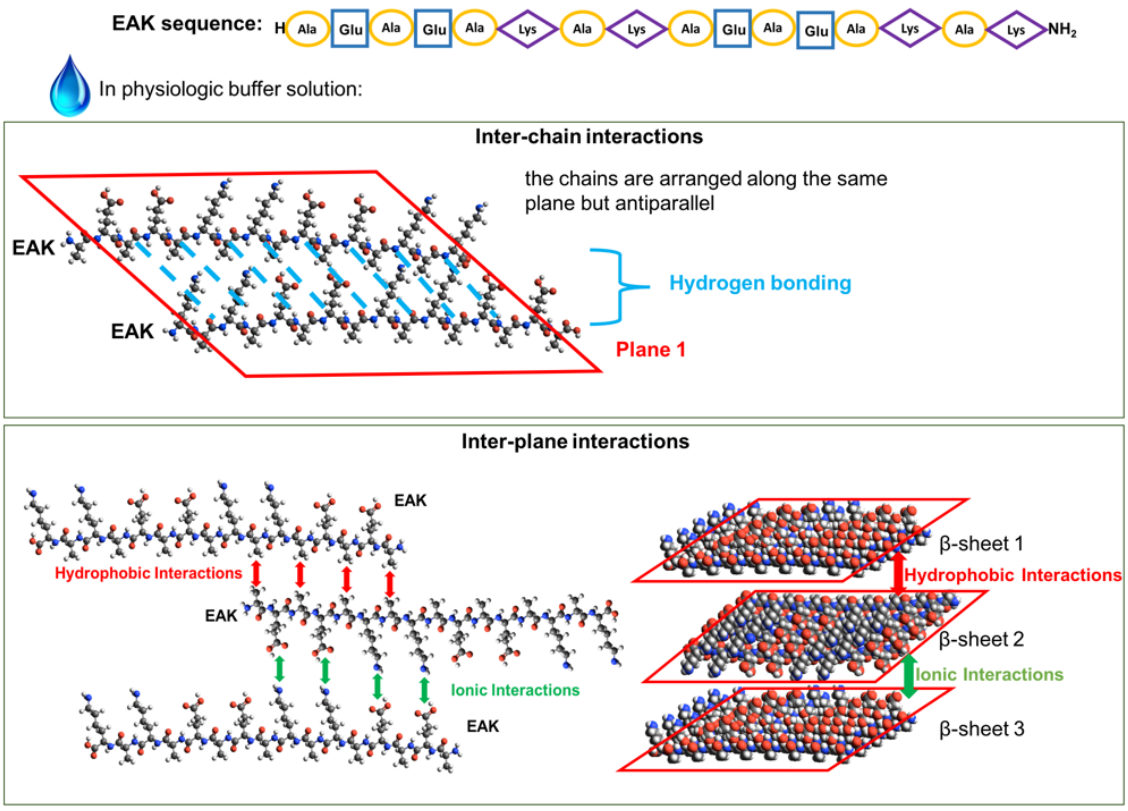


Figure 1.8. Scheme of peptide self-assembling. The sequence of EAK: hydrophobic amino acids are circled in yellow, hydrophilic amino acids are in blue squares (acid amino acids, negatively charged at neutral pH) or in violet diamonds (basic amino acids, positively charged at neutral pH)[112].

Self-assembling peptides have found application in various clinical fields: as substrates for neurite growth and synapse formation[125,126]; as promoters of injectable nanofibers for intramyocardial microenvironments for endothelial cells[127]; as scaffolds for cartilage development and repair; as biomaterials in bone restoration therapies[128].

Other studies have shown that SAP scaffolds can encourage angiogenesis with the development of robust vessel networks, making them more suitable then conventional scaffold grafting[19,129].

Although SAPs' angiogenic potential have been demonstrated there are still unexplored correlated fields such as their effect on macrophage polarization, which plays an important role in regulating angiogenesis and wound healing.

1.3.1.3 Biochemical factors

In order to achieve a new suitable substitute through tissue engineering techniques, it is essential that cell adhesion and proliferation processes take place on the scaffold. These processes are basic for the formation and maintenance of the structure of new tissues, and therefore, for their correct functioning.

Moreover, cell adhesion is directly related to cell growth, migration and differentiation, in fact, many cell types are "anchor-dependent", i.e. they cannot express their functions, and therefore proliferate, until they have joined the support.

Adhesion can be mediated by the presence of numerous proteins:

- fibronectin, collagen, laminin, vitronectin, of the extracellular matrix (ECM);
- actin and vinculin, of the cytoskeleton;
- integrin, of the cell membrane.

The interactions between these proteins and the corresponding receptors induce the transduction of signals which influence cell adhesion, growth, proliferation and tissue formation[130,131].

Adhesion can occur between adjacent cells or between cells and support, which for biological tissues, is represented by the ECM.

Integrin is a membrane receptor that play an extremely important role for cell-cell and cell-matrix interaction and recognition mechanisms. Integrin is a heterodimer containing two distinct chains: α and β subunits. This family of glycoproteins consists in a large extracellular domain, a hydrophobic zone immersed in the membrane, and a short cytoplasmic tail. This latter has a very important role in communication between the extracellular environment and the cytoplasm.

Some proteins of integrin's family are able to recognize short signal peptide sequences of other proteins, especially in fibronectin of the ECM. Fibronectin is a long and flexible adhesive protein, normally present in the form of dimers with the two units bound by a disulphide bridge.

Cell proliferation is strictly dependent on the adhesion process, and it's equally critical for the growth of new tissue.

Cell mitosis, necessary for proliferation, is induced by growth factors, such as bFGF[132].

In conclusion, to achieve an ideal substitute for BTE it is fundamental to take into consideration the ability of the scaffold to mimic the ECM. This ability that is more evident in natural scaffolds can be increased in synthetic scaffolds in two different ways:

- indirectly modifying the surface chemistry, thus influencing protein adsorption and growth factor entrapment;
- through the direct introduction of biochemical factors such as peptide sequences and growth factors by surface functionalization[90,133].

Initially, surface functionalization was carried out with cell adhesive proteins, proteins has many disadvantages as high costs, insolubility and can be easily denatured. Therefore, the "peptide mimicry technique" allows the individuation inside the whole protein, of the shortest biologically active fragment that can be easily reproduced by synthesis. In this way, it is possible to use smaller sequences named peptides, which are more stable, cheap, soluble, and are easily obtained in large quantity with a high purity grade, but they are in most of the cases less active then proteins[134] and enzyme cleavable[135,136].

There are many modifications to peptides that can be made to increase their thermal and protease stability, such as cyclization, substitution of amino acids not critical for biological effects, the use of non-natural amino acids, and D-amino acids[58,137–139]. Bioactive peptides are short sequences of amino acids that mimic the function of biological molecules. In particular, they can have very different specific functions, for example: adhesive peptides[140], antimicrobial peptides[141], pro-angiogenic peptides[142,143] and etc.

Adhesive peptides

Adhesive peptides are short amino acid (AA) sequences that contain the minimal motif required to specifically bind to a cell receptor responsible for the cell adhesion[140]. Several types of artificial substrates for TE have been conjugated with adhesion sequences (**Fig 1.9**). These functionalized synthetic systems have been shown to improve tissue integration of titanium implants[144], induce cell spreading in 3D cell culture[145], and reduce scar formation[146].

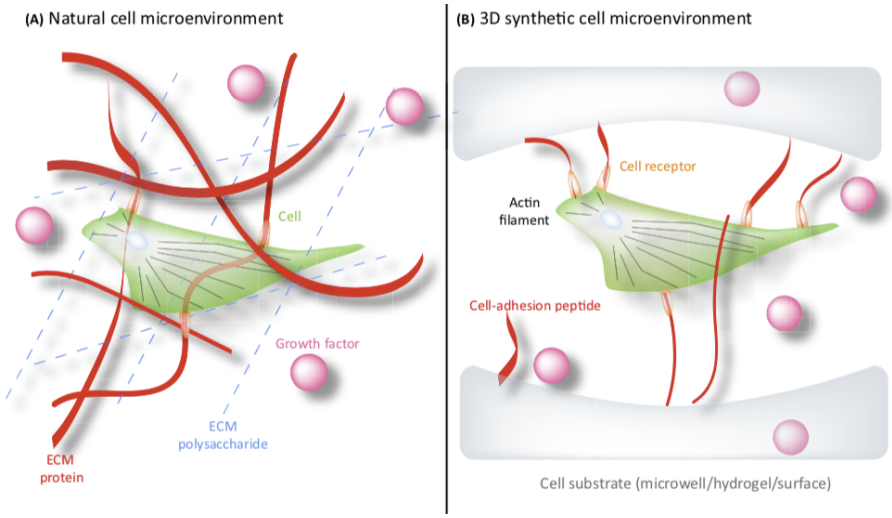


Figure 1.9. Comparison between natural tissue and synthetic scaffold cell microenvironment. (A) In the native ECM, cells attach through cell receptors to polysaccharides and proteins. (B) 3D synthetic cell microenvironment made of a substrate with defined mechanical properties functionalized with peptide sequences able to bind to cell receptors. The addition of soluble biological signals, like growth factors, to the artificial matrix can further assist reproducing the native tissue[140].

As reported by Huettner *et al.*, despite these peptides have allowed great advances in biomedical materials, a search on three databases (PubMed, Scopus, and Web of Science) for articles published between 1970 and early 2018 on adhesive peptides used to functionalize scaffolds reveals a shortage of investigated peptides.

The majority (89%) of the published studies used the RGD sequence, first discovered in 1984 by Pierschbacher and Ruoslahtias a cell-binding region in fibronectin that targets the integrin receptor. The second and third most reported, IKVAV and YIGSR, both isolated from the laminin sequence, represented only 6% and 4% of the publications, respectively. Other marginal adhesive peptides such as DGEA, PHRSN, and PRARI represented less than 1% of the literature[140].

In addition to these adhesive sequences, has been demonstrated that a nonapeptide (HVP) from the h-Vitronectin protein (sequence 352-360) selectively enhances osteoblast adhesion through an osteoblast-specific mechanism which involves interactions between membrane glycosaminoglycans (GAGs) and the heparin binding sites on ECM proteins[71]. A dimeric analogue (2HVP) was designed in order to increase ionic interactions with cellular GAGs and two HVP retro-inverted sequences (DHVP = retro-inverso peptide of HVP, and D-2HVP = retro-inverso peptide of 2HVP) were synthesized to increase the stability toward proteolytic degradation under physiological conditions. In that study, HVP peptides' series has been covalently and selectively anchored on glass surfaces with a protocol easily transferable to surfaces widely used in BTE such as titanium, titanium alloys, and bioglass ceramics. The authors demonstrated that, unlike L-peptides, retro-inverted peptides were not degraded by foetal bovine serum proteolytic enzymes and that D-2HVP, grafted to glass surfaces, efficiently improved h-osteoblasts adhesion and spreading, increased intracellular calcium levels and stimulated expression of integrin binding sialoprotein, vitronectin and secreted phosphoprotein 1, proteins involved in bone formation.

Finally, osteoblasts cultured on D-2HVP-functionalized glasses showed focal adhesion contacts with the surfaces and elongated cellular shape with several protrusions confirming the role of this retro-inverted peptide in presenting proper extracellular cues[58].

Pro-angiogenic peptides

Insufficient vascularization currently limits the size and complexity for all tissue engineering approaches.

The field of tissue engineering has made remarkable progress in developing tissues to restore, augment, or replace the function of damaged tissues within the body[147–149]. However, the success of engineered tissues has been limited to thin tissues, with engineering larger, more complex structures, like long bone reconstruction, slowed by

challenges associated with development of necessary vascularization to sustain growing/remodelling tissues[150].

Pro-angiogenic approaches have largely focused on delivery of angiogenic proteins including vascular-, endothelial-, fibroblast-, or platelet-derived growth factor[151,152]. The delivery of these factors is considered one of the more straightforward pro-angiogenic approaches; it is simpler and more controllable than cell- and gene- based therapies, and many pro-angiogenic proteins are commercially available[153]. However, a simple injection of these factors is an inefficient and ineffectual delivery method, as proteins suffer from poor localization and rapid clearance[154].

Alternatively, the use of pro-angiogenic peptides, allows the delivery at higher concentrations to target tissue thanks to their smaller size.

Many pro-angiogenic peptides are obtain through the peptide mimicry technique from the bioactive region of pro-angiogenic growth factors[155,156], other peptides consist of entirely novel sequences[157], and others mimic the ECM[158,159].

A selection of pro-angiogenic peptides that have shown promising results are summarized in **Table 1.2**.

Table 1.2.A selection of pro-angiogenic peptides[142]

Pro-angiogenic peptide	Sequence	Source	Demonstrated effects	Reference
Qk	KLTWQEL YQLKYKG I	α-helix region of VEGF	Causes similar signaling and *in vitro* effects to full-length VEGF. *In vivo*, Qk increased vessel density in ischemic hind limbs and Matrigel plugs, as well as the rate of cutaneous wound closure	Santulli *et al.* (2009), Finetti *et al.* (2012)
PAB2-1c	(C*VRKIEI VRKK)2–Ahx–Ahx–Ahx–RKRKLERI AR–NH2	Mimic of PDGF	Stimulates cell proliferation, migration, and collagen gel contraction similar to full-length PDGF in vitro	Lin *et al.* (2007)
T7 vasculotide	(PEG-CHHHRHS F) tetramer	Tie-2-binding region of Ang1	Increases serum-free cell survival and cell migration as compared to controls in vitro. Increases vessel number and size when delivered from Matrigel, and increase the rate of diabetic wound closure when delivered using Intrasite Topical Gel *in vivo*	Van Slyke *et al.* (2009), Slyke (2011)
GHK, GHK-Cu, or $SPARC_{120-122}$	GHK	Cu^{2+}-binding region of SPARC	Induces a wide range of cellular effects, including reducing inflammatory while increasing anti-inflammatory factors, increasing extracellular matrix protein production, and matrix metalloproteinase expression. *In vivo* effects have been shown ranging from increasing vascularization in the rabbit eye, increasing the rate of uncomplicated and diabetic wound healing, and inhibiting gastric ulcer formation	Pickart (2008)

Comb1	DINECEIGAPAGEETEVTVEGLEPG	Combination of the epidermal growth factor -like domains of fibrillin 1 and tenascin X	Increases cell proliferation, tube formation, and sprouting compared to controls *in vitro*. Increased chemically impaired cutaneous wound healing when co-delivered daily with UN3	Demidova-Rice *et al.* (2011, 2012)
UN3	NH_2-ELLESYIDGRPTATSEYQTFFNPR-amide	Previously unknown peptide fragment from platelet lysate	Significantly increased cell migration, proliferation, and tube formation *in vitro*. Significantly increased vessel density in impaired cutaneous wounds. Increased chemically impaired cutaneous wound healing when co-delivered daily with Comb1	Demidova-Rice *et al.* (2012)
KRX-725	MRPYDANKR	Second intercellular loop of sphingosine 1-phosphate (S1P) 3	Increases aortic ring sprouting as compared to controls with greater smooth muscle cell co-localization to endothelial cells than VEGF. Increases in vascularization of the rabbit cornea were obtained by co-treatment with KRX-725 and VEGF or bFGF as compared to factors alone	Ben-Sasson *et al.* (2003)
Pep-12	NYLTHRQ	Ig-like domain II of VEGF receptor 1	Facilitates integrin-mediated cell adhesion and cause tube formation *in vitro*. Significantly increases angiogenesis in the rabbit cornea as compared to controls, albeit to a lesser extent than VEGF	Soro *et al.* (2008)
LL-37	LLGDFFRKSKEKIGKEFKRIVQRIKDFLRNLVPRTES	The 134–170 amino acid region of the human cationic anti-microbial protein 18	Originally identified as an anti-microbial peptide produced in response to inflammation or infection, it was shown to have pro-angiogenic effects in addition to anti-microbial action. LL-37 caused dose-dependent increases in cell proliferation and increased collateral blood flow, capillary density, and blood velocity in a rabbit hind-limb ischemia model	Koczulla *et al.* (2003)
YR or RoY	YPHIDSLGHWRR	Identified by phage display for binding to endothelial cells	Increased cell proliferation and migration *in vitro*. Increases vessel density when injected into a mouse ear and hindlimb reperfusion when delivered intramuscularly	Hardy *et al.* (2007, 2008)
AcSDKP	AcSDKP	A naturally expressed regulator of hematopoiesis found in bone marrow	AcSDKP increases cell migration and tube formation, with increasing then decreasing responses as the concentration is increased beyond the optimal dose. Similar results were seen *in vivo* using the Matrigel plug assay, with greater vascularization induced with 10^{-9} M than 10^{-5} M of peptide	Liu *et al.* (2003)

A selection of pro-angiogenic peptides, all which are in pre-clinical testing. Standard amino acid abbreviations are used. C*, disulfide bridge; Ahx, aminohexanoic acid; Ac, acetyl.

Recently Conconi at al., designed and synthesized three peptide sequences containing the N-terminus (TYB4-n), the central part (TYB4-i) or the C-terminus (TYB4-c) of Thymosin-ß4 (Tß4), a G-actin sequestering peptide involved in regeneration and remodelling of injured tissues. This group demonstrated that Tß4-derived peptides exert both *in vitro* and *in vivo* pro-angiogenic effects[160].

In this PhD research study, TYB4-n, that showed the higher effectiveness then the other sequences[160], has been conjugated to the self-assembling peptide EAK through

chemoselective ligation. In fact, Kim *et al.*[161] demonstrated that the self-assembling peptide RADA 16-II when covalent bonded with substance P (SP, a systemically acting injury-inducible wound messenger that accelerates wound healing by mobilizing stromal cells[162], that induces angiogenesis and tissue repair through an enhanced recruitment of autologous stem cells[163]), prevented fibrosis and enabled substance P realise until 28 days, leading to an enhanced recruitment of MSCs extending their angiogenic activity when compared both to non-bonded SP and RADA 16-II. In the following chapters, we will always refer to TYB4-n peptide as TIM.

1.3.1.4 Chemoselective ligation

Bioconjugation consists in binding covalently biomolecules to solid supports or in conjugating two or more biomolecules to obtain a compound having the combined properties of its components. In this way, natural or synthetic molecules can be chemically combined to create unique compounds with appropriately engineered characteristics.

Chemoselective ligation represents a bioconjugation between two biological molecules in aqueous medium and mild conditions, in the absence of activating substances, but simply through a selective reaction between a group present in one peptide and another specific group located in a protein or another peptide sequence.

To let the reaction occur, it is necessary to modify in advance one specific group of the protein or peptide; for this purpose Francis *et al.* developed a technique for modifying the peptide amine terminal into an aldehyde or ketone group, through a reaction with pyridoxal-5-phosphate (PLP) under mild conditions: aqueous solution at pH 6.5 and temperature of 37°C[122,164]. The reaction yield varies according to the type of residual present as N-terminal of the sequence: it is high in case the residue is Ala, Gly, Asp, Glu or Asn, or very low if the residue is Cys, Ser, His, Thr, Trp or Pro[122], but the yield can be increased simply through the insertion of a flexible spacer[123].

In **Figure 1.10** is reported in a schematic way the reactions that take place during a biomimetic transamination conjugation through pyridoxal-5-phosphate (PLP) addition proposed by J.M. Gilmore *et al*.

The purpose of most protein conjugation procedures is to create stable products with maintenance of the native state and biological activity. Ideally, any derivatization should result in a protein that behaves exactly like its native form, but with an added functionality imparted by what has been bioconjugated to it. In this project, the chemoselective ligation technique was used to conjugate the self-assembling peptide EAK with the pro-angiogenic peptide G7TIM, where G7 is a flexible spacer (i.e. Glycine-7-aminoheptanoic acid) introduced in the sequence to increase the yield of the transamination reaction (reaction **2** of **Fig 1.10**)[123].

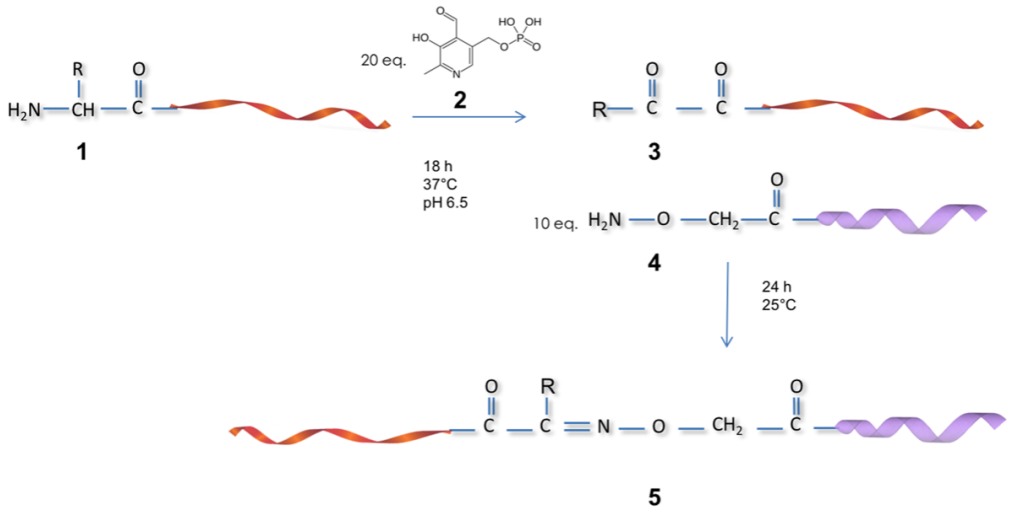


Figure 1.10. Biomimetic transamination through pyridoxal-5-phosphate (**2**) addition modifies the N-terminus of protein/peptides (red tape, **1**) introducing a reactive ketone/aldehyde group (**3**). This group is conjugated with the aminooxy group of another biomolecule (pink tape, **4**) obtaining the formation of an oxime (**5**)[123].

1.3.2 Cells

After scaffolds and biochemical factors, the last of the three main components that TE needs is represented by cells (**Fig 1.1**)[7].

In this research project, human osteoblasts (HOB), human umbilical vein endothelial cells (HUVECs) and human leukemic monocytes (TCP1) have been used for *in vitro* biological assays.

1.3.2.1 Human Osteoblasts

Osteoblasts are cuboidal cells that are located along the bone surface comprising 4-6% of the total resident bone cells and are largely known for their bone forming function, thus exerting a crucial role in the achievement and maintenance of a correct bone mass, which is accomplished through a close cross-talk with the other bone cells: osteoclasts and osteocytes[165].

Osteoblasts are derived from mesenchymal stem cells (MSCs).

The commitment of MSCs towards the osteoprogenitor lineage requires the expression of specific genes, following timely programmed steps, including the synthesis of bone morphogenetic proteins (BMPs) and members of the Wingless (Wnt) pathways[166] (**Fig 1.11, A**).

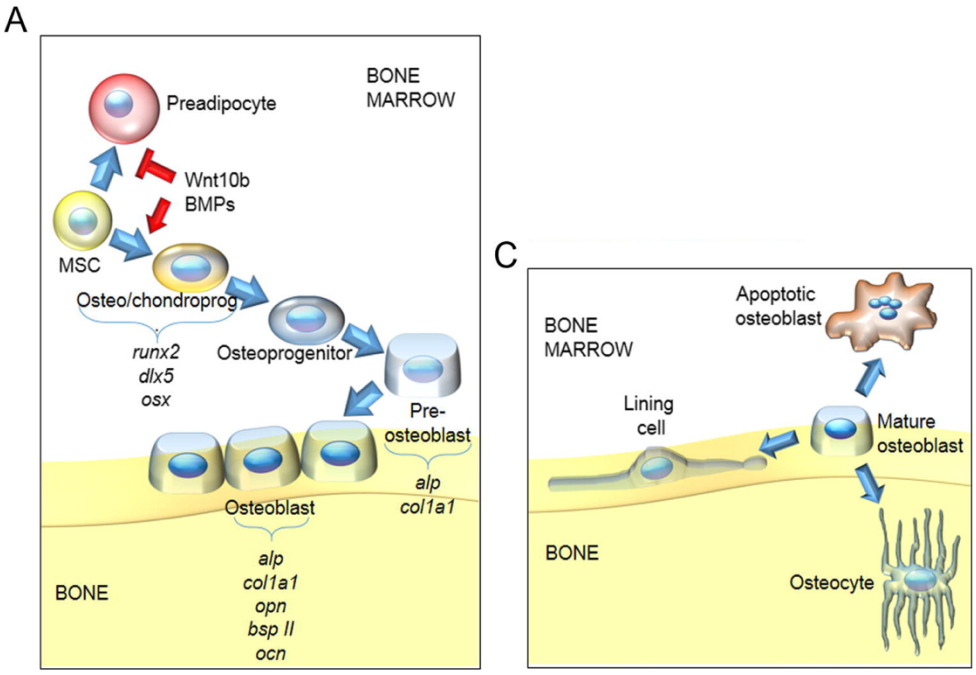


Figure 1.11. Osteoblast differentiation and fate. (**A**) Schematic representation of the multistep process of osteoblast differentiation. (**B**) Schematic representation of the possible fate of a mature osteoblast: lining cell, osteocyte or apoptosis[165].

The expressions of Runt-related transcription factors 2 (Runx2), Distal-less homeobox 5 (Dlx5), and osterix (Osx) are crucial for osteoblast differentiation[49,165,167]. Additionally, Runx2, also known as core binding factor alpha1 (cbfa1), is a master gene of osteoblast differentiation[167,168]and has demonstrated to upregulate osteoblast-related genes such as ColIA1, ALP, BSP, BGLAP, and OCN[169].

Once a pool of osteoblast progenitors expressing Runx2 and ColIA1 has been established during osteoblast differentiation, there is a proliferation phase. In this phase, osteoblast progenitors show alkaline phosphatase (ALP) activity, and are considered pre-osteoblasts[49,165].

The transition of pre- osteoblasts to mature osteoblasts is characterized by an increase in the expression of Osx and in the secretion of bone matrix proteins such as osteocalcin (OCN), bone sialoprotein (BSP) I/II, and collagen type I.

Moreover, the osteoblasts undergo morphological changes, becoming large and cuboidal cells[167,170–172]. Mature osteoblasts eventually be trapped in the bone matrix just deposed and mineralized[165]. Some of these osteoblasts show cytoplasmic processes towards the bone matrix and reach the osteocyte processes[173].

At this stage, the mature osteoblasts can undergo apoptosis or become osteocytes or bone lining cells[174](**Fig 1.11, B**). Bone lining cells are quiescent flat shaped osteoblasts

covering the bone surface, functionally representing the resting phase ofthe bone remodelling process[165]. A likely role of these cells is to prevent the direct interaction between osteoclasts and bone matrix, when bone resorption should not occur[165,175].

1.3.2.2 Human Umbilical Vein Endothelial Cells

Human endothelial cells (EC) cultured *in vitro* are a simple experimental system that allows for the study of diverse facets of the normal endothelial biology and mechanisms underlying the vascular pathology[176].

Besides for fundamental research, human umbilical vein endothelial cells (HUVECs) are often the model system of choice for the bio-pharmaceutical industry and preclinical assays since they have several advantages[177].

HUVECs are primary, non-immortalized cells of human origin, they are relatively easy to isolate without contamination of other cell types and umbilical veins are readily available[178]. They are widely used due to their low cost, and simple techniques for isolating them from umbilical cords, which are normally resected after childbirth and because they can be easily made to proliferate in a laboratory setting.

HUVECs were first isolated and cultured *in vitro* in the 1970s by Jaffe and others[179–182]. Confluent HUVECs can differentiate into a monolayer of tightly packed cells, the so-called cobblestone phenotype, that resembles endothelium morphology *in vivo* (**Fig 1.12**)[177].

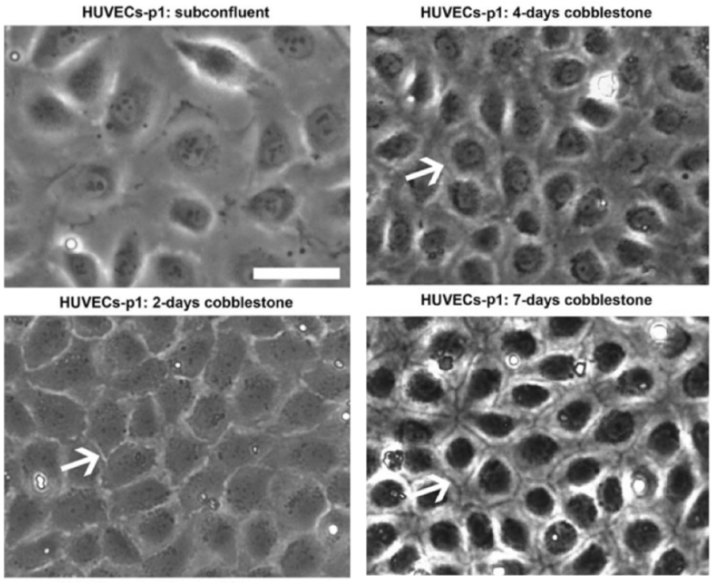


Figure 1.12. Establishment of a tight, mature cobblestone monolayer of HUVECs (passage 1, p1) assessed by phase contrast microscopy. At ‘‘subconfluent’’ state cells are spread and divide actively. When the monolayers get confluent, cells are more compact and stop proliferating by contact inhibition. In unripe cobblestone cultures (“2-days cobble- stone”) cell limits are bright. As cobblestone cells mature (“4-days cobblestone”), cell limits get dark until they become distinct lines (“7-days cobblestone”). Arrows point out cell peripheries. Scale bar: 50 μm[177].

In the latest years, much interest has been devoted on the effects of the transcription co-activators, Yes-associated protein (YAP) and WW domain containing transcription regulator (TAZ) on endothelial mechanotransduction.[183]
Recently, Neto *et al.* demonstrated that endothelial YAP/TAZ drive proliferation in response to mechanical stimulation at the cell-cell junction, and not in response to VEGF. In this way, endothelial YAP/ TAZ provide a cell intrinsic mechanism of locally controlling cell densities, in contrast to growth factor-mediated cell proliferation instructed by the surrounding tissue.
In second instance, endothelial YAP/TAZ increase VE-Cadherin turnover at cell-cell junctions, which is essential for cells to migrate and rearrange while maintaining the endothelial barrier at the same time[184].

Hippo signalling pathway and the mechanical regulation of YAP/TAZ

Transcription co-activators, Yes-associated protein (YAP) and WW domain containing transcription regulator (TAZ) have been of significant interest within mechanobiology studies, and are known to be downstream effectors of the Hippo Pathway, a kinase mediated signalling pathway involved in the regulation of cell proliferation, differentiation and organ morphogenesis[185].
Upon stimulation of the hippo pathway, YAP/TAZ becomes phosphorylated, causing localisation within the cytoplasm and preventing gene transcription.
Alternatively, inhibition of phosphorylation activates YAP/TAZ to stimulate nuclear translocation from the cytoplasm.
Nuclear accumulation of YAP/TAZ is a fundamental determinant of its role, as it facilitates up regulation of genes that drive cell proliferation, migration and anti-apoptosis[186,187]. In this manner, YAP/TAZ effectors of the Hippo pathway act as a mechanosensing mechanism that can be turned on or off by changes to ECM mechanics.
Contrastingly, studies have exemplified that Hippo mediated phosphorylation may not be sole inactivator of YAP/TAZ, as Wada *et al.* found the presence of phosphorylated YAP within the nucleus[188], and nuclear translocation still occurred when cells with phosphorylated YAP were treated with nuclear export inhibitors[189].
Mechanical stimuli, such as cell stretching and ECM stiffness are implicated in YAP/TAZ regulation[183](**Fig 1.13**).
Cell stretching incurs a mechanical stress that causes cytoskeleton remodelling in order to conform to the morphological changes. In doing so, modification of cytoskeletal organisation causes the formation of F-actin stress fibres in certain areas of the cell as it stretches, leading to YAP/TAZ activation through nuclearaccumulation[183].

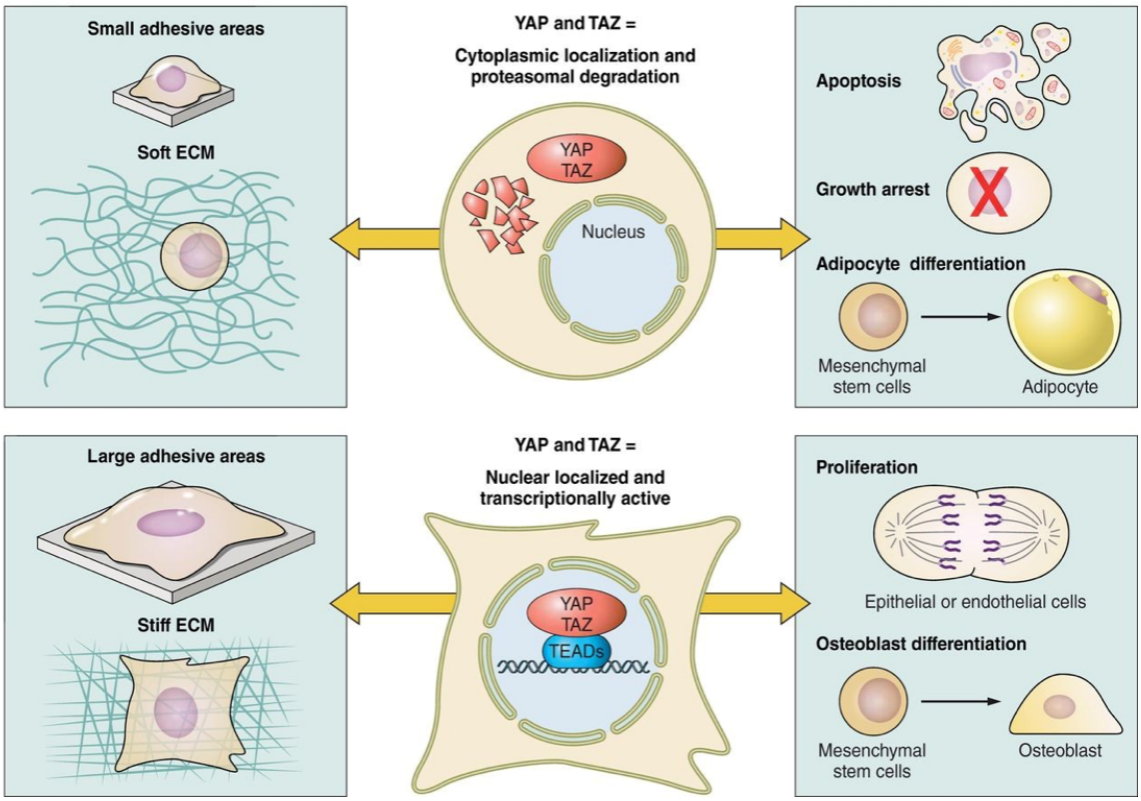


Figure 1.13 Representation of two modalities, cell spreading and ECM rigidity, by which mechanical cues affect YAP/TAZ activity and, in so doing, control multiple cell fate decisions[183].

The YAP/TAZ mechanotransductive response was emphasised in metalloprotease MT1-MMP mouse knockouts, where reduced proteolytic degradation and remodelling of the ECM prevented mesenchymal stem cells stretching. This directed YAP/TAZ to remain inactive, and interfered with the function of YAP/TAZ as a checkpoint to determine cell fate and differentiation.

YAP/TAZ in angiogenesis

The process of sprouting angiogenesis is highly dependent on the fine balance between EC proliferation and distribution, whereby there is an appropriate number of cells in the correct position to enable branching frequency and formation of a functional vascular network. Interaction of YAP/TAZ pattern expression may establish this, as Neto and colleagues recently observed in a mouse retina model that nuclear TAZ is highly expressed at the capillary sprout front.

YAP was predominantly found in all other areas of the cells and within more mature vessels[184].

These findings suggest the crucial role of endothelial YAP/TAZ in vascular development, through the promotion of cell migration and vessel maintenance.

Furthermore, deletion of YAP/TAZ instigated vascular defects by reducing cell migration and cell-cell coupling, and compromised VE-cadherin junctions, important for vascular remodelling. Uemura *et al.* demonstrated the correlation of endothelial nuclear YAP/TAZ and stimulated Bone morphogenetic protein 4 (BMP4) expression to drive osteogenesis for intramembranous ossification, highlighting the influence of YAP/TAZ in various other cell types[190]. In general, the complexity of the molecular relationship of YAP/TAZ with regulation of sprouting, proliferation and cell distribution in angiogenesis is largely unidentified. Various other biological effects of YAP/TAZ have also been proposed, such as transduction of VEGF signalling[191], regulation of focal adhesions complexes for cell adherence to the ECM[185] and influence on notch signalling to dictate differentiation[192]. YAP/TAZ is a key mechanosensor integrated within endothelial cells that enables mechanical force to induce biochemical signalling for cellular activity.

However, despite recent advances in understanding the Hippo-YAP/TAZ pathway, questions about how signalling is regulated *in vivo* still remain, and detailed knowledge of the mechanosensing mechanisms of endothelial cells that would enable translation to scaffold engineering is scarce.

1.3.2.3 Human leukemic monocytes

Macrophages are myeloid cells derived from monocytes that circulate in the blood[193,194]. Once monocytes are present in the blood vessel and enter the tissue, they differentiate into long-lived macrophages with specific functions[193].

Although macrophages are well known for their fundamental roles in innate immune response, they can also adopt a variety of context-specific phenotypes in respond to environmental triggers, allowing them to function in various physiological processes, such as angiogenesis and tissue repair (**Fig 1.14**)[195].

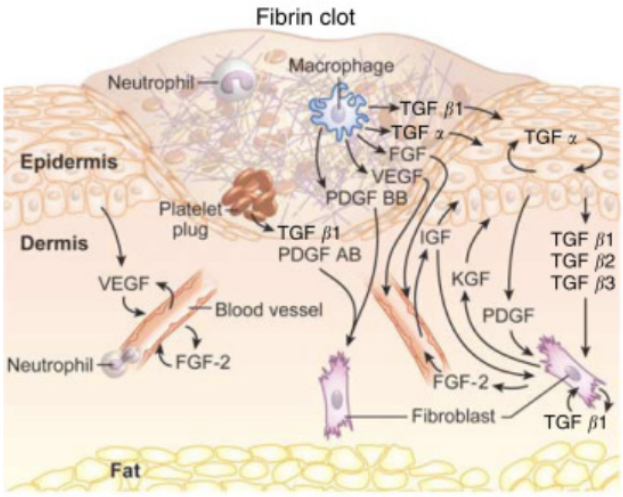


Figure 1.14. Macrophages aiding angiogenesis and wound healing[195].

In the last years, many studies demonstrated that macrophages can contribute to angiogenesis in different ways:

- macrophages can facilitate anastomosis between the tip cells of newly formed vessels[14,196];
- macrophages can produce cytokines, e.g. VEGF, FGF and IGF, that aid angiogenesis directly[20];
- macrophages can produce matrix metalloproteinase-9 (MMP-9), which degrades ECM thereby realising the sequestered VEGF[197] and it act also as a potent stimulator for vascular remodelling, allowing the endothelial cells to migrate[43];
- macrophages can facilitate fibroblast proliferation and ECM production, thus stabilising newly formed blood vessels[198].

During healing process, macrophages are able to polarise into two different phenotypes: Pro-inflammatory M1 phenotype (activated macrophages), or Anti-inflammatory M2 phenotype (alternatively activated macrophages)[199]. M1 and M2 macrophages show different morphology, and while *in vitro* M1 appears elongated and firmly adherent, M2 appears more rounded and less adherent[197]. M1 and M2 precise roles in angiogenesis are still not well understood, and whether M1 or M2 is the more pro-angiogenic phenotype remains a controversy.

Zajac *et al.* reported M2 to be more angiogenic than M1 due to the ability of M2 to produce proMMP-9, a pro-angiogenic enzyme, whereas M1 produces the same enzyme alongside with its inhibitor (i.e. tissue inhibitor of metalloproteinases-1, TIMP-1). In 2015, another *in vivo* experiment published in *Angiogenesis* reaffirmed that M2 phenotype plays a more crucial role in angiogenesis rather than M1 phenotype. This because M2 macrophages were found at the site where angiogenesis was induced[200], but only one year later another study gave an opposite result[194], demonstrating that polarising macrophages towards a more pro-inflammatory profile (M1) could increase their angiogenic potential when compared to M2. The authors suggested that the secretion of inflammatory factor is the reason why M1 can induce better vessel growth, as already suggested in past studies[201,202], but this could be affected by the use of an *in vitro* model that couldn't completely resemble the normal physiological environment. The most recent review on this topic, claims that both macrophages phenotypes are important for angiogenesis, concluding that M1 produce pro-inflammatory cytokines to initiate angiogenesis in the early stage of tissue repair, whilst M2 macrophages stabile angiogenesis by promoting fibroblast proliferation, recruiting pericytes and encouraging ECM production in the later stages (**Fig 1.15**)[198].

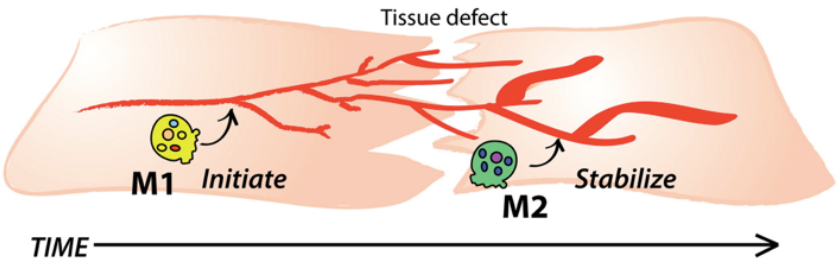


Figure 1.15. Suggested functions of M1 and M2 macrophages phenotypes in angiogenesis[198].

Due to the important role of macrophages in wound healing and angiogenesis, in the last years lots of effort has been given to investigate on possible macrophage-based therapy. Macrophages can be functionalised using the following strategies (**Fig 1.16**)[198]:

1. delivery of *ex vivo* activated or polarised macrophages to the injury's site to aid healing;
2. delivery of molecules (e.g. macrophage colony stimulating factor) to increase macrophage population at the site of injury;
3. delivery of M1/M2 inhibiting or activating molecules to treat conditions due to excessive or insufficient macrophages polarisation;
4. design of biomaterials/scaffolds able to manipulate macrophages phenotype in order to promote angiogenesis within the graft, resulting in a better integration with the host tissue.

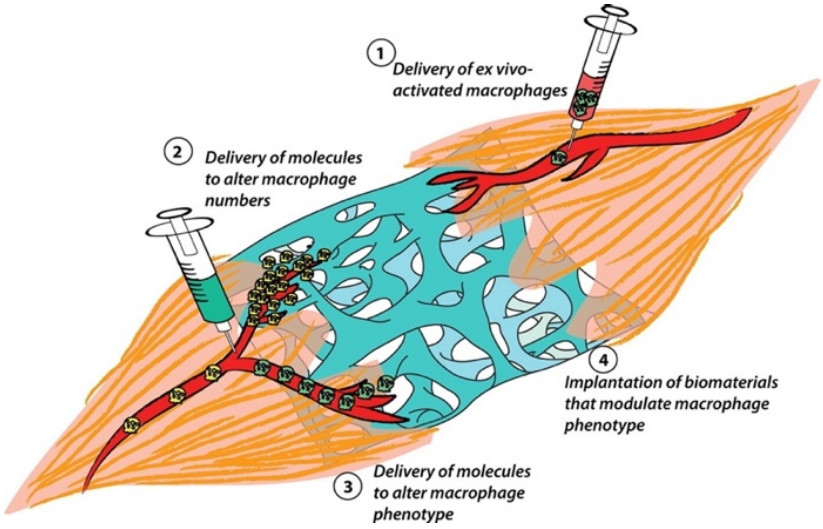


Figure 1.16. Strategies to manipulate macrophage in regenerative medicine[198].

In this research project, we study how different self-assembling peptides can influence macrophages behaviour and polarisation, and the subsequent effect on HUVECs, which is

a novel approach that has gained increasing attention in regenerative medicine research[203,204].

1.4 Biochemical functionalization

As reported before, osseointegration and long-term success of a TE implant are determined by several complex reactions occurring at the tissue-material interface. In BTE, one of the most relevant issue is to recreate the ability of autogenous grafts to communicate with the surrounding biological environment[58]. Evidence in the last decade suggests that the properties of the insoluble microenvironment can guide cell behaviours such as adhesion, proliferation, morphology and differentiation[70,72].
The combination of soluble and insoluble signals regulates cell behaviour together with mechanical cues from the substrate (**Fig 1.17**)[205,206].

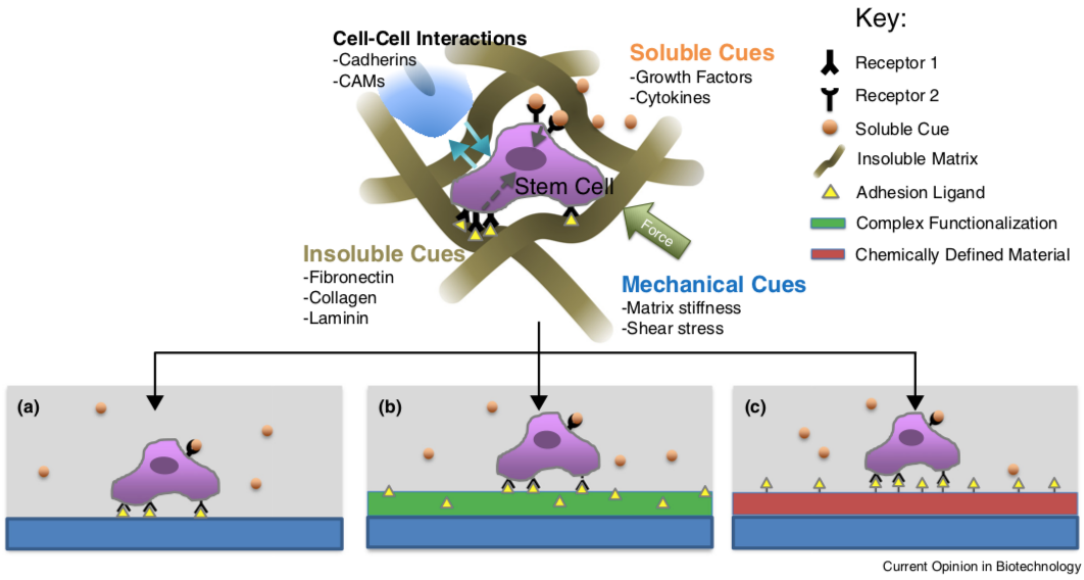


Figure 1.17. Cell culture systems can reproduce aspects of the cell microenvironment. (a) Cells cultured on untreated material adhere to adsorbed serum proteins and interact with soluble signals. (b) Complex biological functionalization adds insoluble cues derived from the extracellular matrix. (c) Chemically defined, functionalizable materials (red) enable tailored presentation of bioactive ligands[206].

The growing knowledge about molecular processes driving cell adhesion and growth have focused the treatment of biomaterial surfaces on improving the surface-to-cells interactions, complying with the new approach of "biochemical functionalization"[58].
Biomaterials for TE represent all those synthetic and natural materials specifically designed and used in biomedical applications as constituents of prosthetic components. The history of biomaterials can be summarized in three fundamental stages:

- 1st generation biomaterials: the material is bio-inert, it minimizes chemical/physical interactions between the organism and the material itself.
- 2nd generation biomaterials: the material is bioactive, it integrates quickly with the host tissue causing controlled reactions in the physiological environment, or it is re-absorbable, and it gradually degrades in the body without causing rejection or toxicity problems.
- 3rd generation biomaterials: the material is both bioactive and re-absorbable; these last materials represent the present and the future of biomaterials.

Third-generation biomaterials are also called biomimetic materials, as they interact with adjacent tissues through mechanisms of biomolecular recognition[130].In order to improve biomaterial's bioactivity, allowing it to establish advantageous interactions with the biological environment, it is possible to use the so called "biochemical functionalization", that consists in applying organic molecules (such as adhesive sequences or growth factors) able to "talk" with cells of the host. Different techniques have lately been adopted to optimize biological properties of bone implants[207,208]. In the past years, proteins and/or small peptide sequences have been conveyed at the interface between material and biological environment in different ways (**Fig 1.18**):

(i) through superficial adsorption of biologically active molecules; (ii) including the biomolecules within a resorbable carrier (generally a polymer) used as coating of the scaffold, in this way the release of the biomolecules takes place over time during the degradation of the carrier; (iii) anchoring the molecules to the surface through a covalent bond.

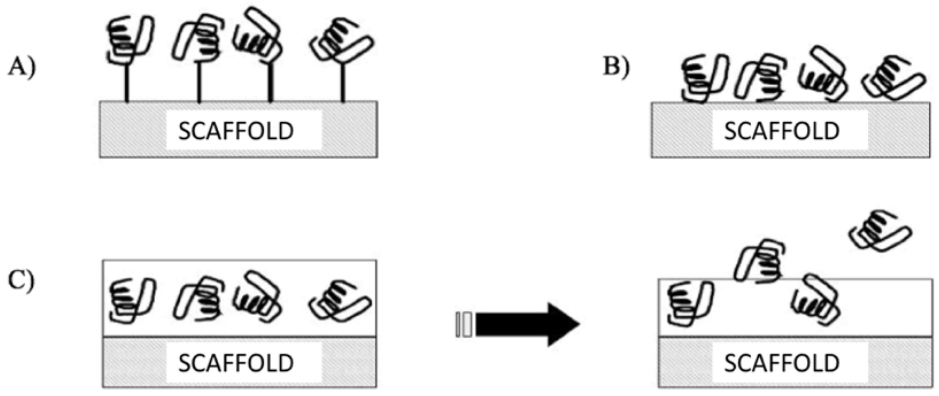


Figure 1.18. Anchoring through covalent bond in presence of a spacer (A), superficial adsorption of biologically active molecules (B) and of a protein from a carrier (C).

One of the most promising approach for TBE substitutes, involves the decoration of surfaces of the implant with adhesive sequences or osteogenic growth factors[209] using sophisticated strategies to ensure selective bonds and appropriate and functional spatial orientation (**Fig 1.19**)[124,210–214]. Peptides are covalently anchored to different surfaces

(e.g. glass, quartz, metal oxides and synthetic polymers) through different techniques depending on the type of chemical groups available on the implant's surface[215,216]. Moreover, additional molecules acting as spacers are used during the anchoring process to immobilize the bioactive peptide while preserving the ideal flexibility for receptor interaction[217].

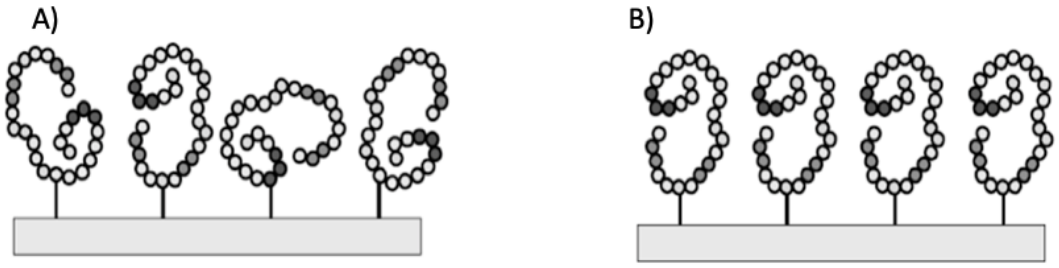


Figure 1.19. Aspecific (A) and specific (B) covalent functionalization

Several strategies have been developed for proteins' or bioactive peptides' grafting: a) the use of aminoalkyltrialkoxysilane to bind the amino groups to oxides; b) the insertion of a thiol group in the biomolecule to exploit the link between this group and gold surfaces; c) the use of titanium substrates coated with polypyrrole; d) the synthesis of copolymers containing poly (L-lysine) as coating for surface linking, or poly (ethylene glycol) conjugated to bioactive peptide[218].

The scientific community however hardly questioned the practicability of bioactive surfaces mainly because adhesive sequences grafted onto biomaterials surfaces might be masked by serum proteins *in vivo* thus nullifying the functionalization[58].

To overcome this criticism, Battista *et al.* have recently demonstrated that cells dig into the physio-adsorbed protein layer and gain the submerged chemically bound adhesion motifs to establish a firmer adhesive structure and build thicker stress fibres enhancing the mechanical stability of the cytoskeleton[219].

1.5 Aim of the research

Nowadays the growing interest in the field of tissue engineering stimulates the research for substitutes ever more biocompatible, bioresorbable and able to allow a better and faster healing of the patient.

The aim of this project is the design of a bone substitute that includes more peculiarities / characteristics among those indicated as basic:

1. scaffolds with good biomechanical properties of wollastonite-diopside and hardystonite with interconnected porosity;

2. selective covalent functionalization with adhesive peptides, specific for osteoblasts and resistant to serum proteases;
3. filling of porosity with ionic-complementary self-assembling peptides, also enriched with pro-angiogenic sequences, to promote angiogenesis and modulate the inflammatory response. In this way, one of the aim of this project is to combine the proved bioactivity of previously developed polymer-derived silicate foams (based on wollastonite-diopside and hardystonite) with the several properties of self-assembling peptides in order to obtain an ideal scaffold specific for bone tissue regeneration.

After the obtainment of a bioceramic scaffold with adequate mechanical and physico-chemical properties, the growing knowledge about molecular processes driving cell adhesion and growth have focused the treatment of implant surfaces on improving the surface-to-cells interactions, complying with the new approach of "biochemical functionalization".

Between the different techniques that have been lately adopted to optimize biological properties of bone implants[207,208], in this project we followed a promising approach involving the decoration of implant's surface with adhesive sequences[209] using sophisticated strategies to ensure selective bonds and appropriate/functional spatial orientation[121,210,211,214]. This functionalization method is for the first time applied to bioceramics, in fact, in literature only few research groups functionalized ceramic scaffolds with bioactive peptides/proteins but using non-covalent[220] or nonspecific[221,222] ways.

In the present study, the nonapeptide (HVP) from the h-Vitronectin protein (sequence 352-360) will be covalently and selectively anchored on bioceramic surfaces. In addition, a dimeric analogue (2HVP) will be designed in order to increase ionic interactions with cellular GAGs and two HVP retro-inverted sequences (DHVP, retro-inverted peptide of HVP, and D2HVP, retro-inverted peptide of 2HVP) will be synthesized to increase the stability toward proteolytic degradation under physiological conditions[58].

A first screening trough *in vitro* bioassays will permit us to understand which of the adhesive peptides gives the best results in terms of HOB adhesion, proliferation, gene expression and cytotoxicity when anchored to W/D foams.

In order to develop an increasingly more complete scaffold, which, in addition to the ability of communicating with the biological environment, thus favouring osseointegration, can improve angiogenesis by promoting the formation of an interconnected and stable vascular network, we will combine the proved bioactivity of functionalized polymer-derived silicate foams with the several properties of SAPs.

The idea consists in creating a sort of "soft scaffold into a hard scaffold", where the second is represented by the porous bioglass ceramic, while the first is the SAP-hydrogel

that fills all the internal porosity creating a more suitable environment for cell growth and angiogenesis.

Preliminary work will be done in order to understand how the different cell types involved in the processes of inflammatory response, osseointegration and angiogenesis (i.e. macrophages, osteoblasts and HUVECs) respond to the different stimuli from different kinds of SAPs. For this reason, macrophages, osteoblasts and HUVECs will be seeded *in vitro* on five different self-assembling peptides' hydrogels (i.e. EAK, EAbuK, DAR, EAOrn and EYK, see **Table I** from Gambaretto *et al.*[110]) to evaluate adhesion, proliferation, YAP/TAZ expression (in HOB and HUVECs) and the formation of HUVECs' tubular structures on matrigel assays.

The final scaffold for *in vivo* assay in mice model, will be prepared by covalent and selectively binding the adhesive peptide that will give the best results *in vitro* to W/D foams and then embedding the latter in SAP solution.

Eventually, hydrogel of self-assembling peptide can be used also to vehicle biochemical motifs such as pro-angiogenic sequences, and in this project the enrichment of SAP with the pro-angiogenic sequence TIM from Tß4, suitably grafted to the SAP itself will be tested in *in vivo* assay to evaluate its angiogenic potential and how it can influence new calcium deposition on the scaffold.

Finally, the same covalent and specific functionalization's strategy will be tested on another bioceramic based on hardystonite enriched with Mg^{2+} and Sr^{2+} ions. In this way, we want to understand whether the proposed methodology can also be transferred to other types of polymer-derived bioceramics, or if it's necessary to modify the functionalization method, introducing mild reaction conditions.

1.6 References

1. Nerem, R. M. & Sambanis, A. Tissue engineering: from biology to biological substitutes. *Tissue Eng.* **1,** 3–13 (1995).
2. Howard, D., Buttery, L. D., Shakesheff, K. M. & Roberts, S. J. Tissue engineering: strategies, stem cells and scaffolds. *J. Anat.* **213,** 66–72 (2008).
3. Bressan, E. *et al.* Biopolymers for Hard and Soft Engineered Tissues: Application in Odontoiatric and Plastic Surgery Field. *Polymers (Basel).* **3,** 509–526 (2011).
4. Edgar, L. *et al.* Heterogeneity of Scaffold Biomaterials in Tissue Engineering. *Materials (Basel).* **9,** 332 (2016).
5. Rouwkema, J. & Khademhosseini, A. Vascularization and Angiogenesis in Tissue Engineering: Beyond Creating Static Networks. *Trends Biotechnol.* **34,** 733–745 (2016).
6. Lutolf, M. P. & Hubbell, J. A. Synthetic biomaterials as instructive extracellular

microenvironments for morphogenesis in tissue engineering. *Nat. Biotechnol.* **23,** 47–55 (2005).

7. O'Brien, F. J. Biomaterials & scaffolds for tissue engineering. *Mater. Today* **14,** 88–95 (2011).
8. Phelps, E. A. & García, A. J. Engineering more than a cell: vascularization strategies in tissue engineering. *Curr. Opin. Biotechnol.* **21,** 704–709 (2010).
9. Golstein, P. & Kroemer, G. Cell death by necrosis: towards a molecular definition. *Trends Biochem. Sci.* **32,** 37–43 (2007).
10. Filipowska, J., Tomaszewski, K. A., Niedźwiedzki, Ł., Walocha, J. A. & Niedźwiedzki, T. The role of vasculature in bone development, regeneration and proper systemic functioning. *Angiogenesis* **20,** 291–302 (2017).
11. Yoo, S. Y. & Kwon, S. M. Angiogenesis and Its Therapeutic Opportunities. *Mediators Inflamm.* **2013,** 1–11 (2013).
12. Tang, D. G. & Conti, C. J. Endothelial cell development, vasculogenesis, angiogenesis, and tumor neovascularization: an update. *Semin. Thromb. Hemost.* **30,** 109–17 (2004).
13. Nakatsu, M. N. & Hughes, C. C. W. An optimized three-dimensional in vitro model for the analysis of angiogenesis. *Methods Enzymol.* **443,** 65–82 (2008).
14. Potente, M., Gerhardt, H. & Carmeliet, P. Basic and Therapeutic Aspects of Angiogenesis. *Cell* **146,** 873–887 (2011).
15. Bodnar, R. J. Chemokine Regulation of Angiogenesis During Wound Healing. *Adv. Wound Care* **4,** 641–650 (2015).
16. Li, J., Zhang, Y.-P. & Kirsner, R. S. Angiogenesis in wound repair: Angiogenic growth factors and the extracellular matrix. *Microsc. Res. Tech.* **60,** 107–114 (2003).
17. Favia, G. *et al.* Accelerated wound healing of oral soft tissues and angiogenic effect induced by a pool of aminoacids combined to sodium hyaluronate (AMINOGAM). *J. Biol. Regul. Homeost. Agents* **22,** 109–16
18. Garg, T., Singh, O., Arora, S. & Murthy, R. Scaffold: a novel carrier for cell and drug delivery. *Crit. Rev. Ther. Drug Carrier Syst.* **29,** 1–63 (2012).
19. Kumar, V. A. *et al.* Highly Angiogenic Peptide Nanofibers. *ACS Nano* **9,** 860–868 (2015).
20. Morgan, C. & Nigam, Y. Naturally derived factors and their role in the promotion of angiogenesis for the healing of chronic wounds. *Angiogenesis* **16,** 493–502 (2013).
21. Gerhardt, H. *et al.* VEGF guides angiogenic sprouting utilizing endothelial tip cell filopodia. *J. Cell Biol.* **161,** 1163–1177 (2003).
22. Heckman, C. A. & Plummer, H. K. Filopodia as sensors. *Cell. Signal.* **25,** 2298–

2311 (2013).

23. Jacquemet, G., Hamidi, H. & Ivaska, J. Filopodia in cell adhesion, 3D migration and cancer cell invasion. *Curr. Opin. Cell Biol.* **36,** 23–31 (2015).
24. Mason, B. N., Califano, J. P. & Reinhart-King, C. A. in *Engineering Biomaterials for Regenerative Medicine* 19–37 (Springer New York, 2012). doi:10.1007/978-1-4614-1080-5_2
25. Bordeleau, F. *et al.* Matrix stiffening promotes a tumor vasculature phenotype. *Proc. Natl. Acad. Sci.* **114,** 492–497 (2017).
26. Zhao, D. *et al.* Substrate stiffness regulated migration and angiogenesis potential of A549 cells and HUVECs. *J. Cell. Physiol.* **233,** 3407–3417 (2018).
27. Blanco, R. & Gerhardt, H. VEGF and Notch in tip and stalk cell selection. *Cold Spring Harb. Perspect. Med.* **3,** a006569 (2013).
28. Makanya, A. N., Hlushchuk, R. & Djonov, V. G. Intussusceptive angiogenesis and its role in vascular morphogenesis, patterning, and remodeling. *Angiogenesis* **12,** 113–123 (2009).
29. Weinstein, N., Mendoza, L., Gitler, I. & Klapp, J. A Network Model to Explore the Effect of the Micro-environment on Endothelial Cell Behavior during Angiogenesis. *Front. Physiol.* **8,** (2017).
30. Loh, Q. L. & Choong, C. Three-Dimensional Scaffolds for Tissue Engineering Applications: Role of Porosity and Pore Size. *Tissue Eng. Part B Rev.* **19,** 485–502 (2013).
31. Young, S. *et al.* Dose Effect of Dual Delivery of Vascular Endothelial Growth Factor and Bone Morphogenetic Protein-2 on Bone Regeneration in a Rat Critical-Size Defect Model. *Tissue Eng. Part A* **15,** 2347–2362 (2009).
32. Zhou, J. *et al.* The repair of large segmental bone defects in the rabbit with vascularized tissue engineered bone. *Biomaterials* **31,** 1171–1179 (2010).
33. Von Offenberg Sweeney, N. *et al.* Cyclic strain-mediated regulation of vascular endothelial cell migration and tube formation. *Biochem. Biophys. Res. Commun.* **329,** 573–582 (2005).
34. Leslie-Barbick, J. E., Shen, C., Chen, C. & West, J. L. Micron-Scale Spatially Patterned, Covalently Immobilized Vascular Endothelial Growth Factor on Hydrogels Accelerates Endothelial Tubulogenesis and Increases Cellular Angiogenic Responses. *Tissue Eng. Part A* **17,** 221–229 (2011).
35. Nguyen, L. H. *et al.* Vascularized Bone Tissue Engineering: Approaches for Potential Improvement. *Tissue Eng. Part B Rev.* **18,** 363–382 (2012).
36. Anderson, S. M., Siegman, S. N. & Segura, T. The effect of vascular endothelial growth factor (VEGF) presentation within fibrin matrices on endothelial cell branching. *Biomaterials* **32,** 7432–7443 (2011).

37. Sun, G. *et al.* Functional neovascularization of biodegradable dextran hydrogels with multiple angiogenic growth factors. *Biomaterials* **32,** 95–106 (2011).
38. Sukmana, I. Bioactive polymer scaffold for fabrication of vascularized engineering tissue. *J. Artif. Organs* **15,** 215–224 (2012).
39. Montaño, I. *et al.* Formation of Human Capillaries In Vitro : The Engineering of Prevascularized Matrices. *Tissue Eng. Part A* **16,** 269–282 (2010).
40. Pebworth, M.-P., Cismas, S. A. & Asuri, P. A Novel 2.5D Culture Platform to Investigate the Role of Stiffness Gradients on Adhesion-Independent Cell Migration. *PLoS One* **9,** e110453 (2014).
41. Gelain, F., Bottai, D., Vescovi, A. & Zhang, S. Designer Self-Assembling Peptide Nanofiber Scaffolds for Adult Mouse Neural Stem Cell 3-Dimensional Cultures. *PLoS One* **1,** e119 (2006).
42. Koh, W., Stratman, A. N., Sacharidou, A. & Davis, G. E. In vitro three dimensional collagen matrix models of endothelial lumen formation during vasculogenesis and angiogenesis. *Methods Enzymol.* **443,** 83–101 (2008).
43. Spiller, K. L. *et al.* The role of macrophage phenotype in vascularization of tissue engineering scaffolds. *Biomaterials* **35,** 4477–4488 (2014).
44. Reznikov, N., Shahar, R. & Weiner, S. Bone hierarchical structure in three dimensions. *Acta Biomater.* **10,** 3815–26 (2014).
45. Buckwalter, J. A., Glimcher, M. J., Cooper, R. R. & Recker, R. Bone biology. I: Structure, blood supply, cells, matrix, and mineralization. *Instr. Course Lect.* **45,** 371–86 (1996).
46. Downey, P. A. & Siegel, M. I. Bone biology and the clinical implications for osteoporosis. *Phys. Ther.* **86,** 77–91 (2006).
47. Robling, A. G., Castillo, A. B. & Turner, C. H. Biomechanical and molecular regulation of bone remodeling. *Annu. Rev. Biomed. Eng.* **8,** 455–98 (2006).
48. Datta, H. K., Ng, W. F., Walker, J. A., Tuck, S. P. & Varanasi, S. S. The cell biology of bone metabolism. *J. Clin. Pathol.* **61,** 577–87 (2008).
49. Florencio-Silva, R., Sasso, G. R. da S., Sasso-Cerri, E., Simões, M. J. & Cerri, P. S. Biology of Bone Tissue: Structure, Function, and Factors That Influence Bone Cells. *Biomed Res. Int.* **2015,** 421746 (2015).
50. Di Luca, A., Van Blitterswijk, C. & Moroni, L. The osteochondral interface as a gradient tissue: from development to the fabrication of gradient scaffolds for regenerative medicine. *Birth Defects Res. C. Embryo Today* **105,** 34–52 (2015).
51. Ratner, B. D., Hoffman, A. S., Schoen, F. J. & Lemons, J. E. *Biomaterials Science: an introduction to materials in medicine*. (Elsevier, 2004). doi:10.1016/C2009-0-02433-7
52. Yamada, S., Tadano, S. & Fukasawa, K. Micro-cantilever bending for elastic

modulus measurements of a single trabecula in cancellous bone. *J. Biomech.* **49,** 4124–4127 (2016).

53. Acton, A. Q. *Advances in Bioartificial Materials and Tissue Engineering Research and Application*. (2013).
54. Hall, B. K. *Bones and cartilage: developmental and evolutionary skeletal biology*. (2005).
55. Feng, X. Chemical and Biochemical Basis of Cell-Bone Matrix Interaction in Health and Disease. *Curr. Chem. Biol.* **3,** 189–196 (2009).
56. Bienz, M. & Saad, F. Androgen-deprivation therapy and bone loss in prostate cancer patients: a clinical review. *Bonekey Rep.* **4,** (2015).
57. Meling, T., Harboe, K. & Søreide, K. Incidence of traumatic long-bone fractures requiring in-hospital management: A prospective age- and gender-specific analysis of 4890 fractures. *Injury* **40,** 1212–1219 (2009).
58. Zamuner, A. *et al.* Smart biomaterials : Surfaces functionalized with proteolytically stable osteoblast-adhesive peptides. *Bioact. Mater.* **2,** 121–130 (2017).
59. Hollinger, J. & Wong, M. E. K. The integrated processes of hard tissue regeneration with special emphasis on fracture healing. *Oral Surgery, Oral Med. Oral Pathol. Oral Radiol. Endodontology* **82,** 594–606 (1996).
60. Hallman, M. & Thor, A. Bone substitutes and growth factors as an alternative/complement to autogenous bone for grafting in implant dentistry. *Periodontol. 2000* **47,** 172–192 (2008).
61. Rickert, D., Slater, J. J. R. H., Meijer, H. J. A., Vissink, A. & Raghoebar, G. M. Maxillary sinus lift with solely autogenous bone compared to a combination of autogenous bone and growth factors or (solely) bone substitutes. A systematic review. *Int. J. Oral Maxillofac. Surg.* **41,** 160–167 (2012).
62. Van de Putte, K. A. & Urist, M. R. Osteogenesis in the interior of intramuscular implants of decalcified bone matrix. *Clin. Orthop. Relat. Res.* **43,** 257–70
63. Albrektsson, T. & Johansson, C. Osteoinduction, osteoconduction and osseointegration. *Eur. Spine J.* **10 Suppl 2,** S96-101 (2001).
64. Urist, M. R. Bone: formation by autoinduction. 1965. *Clin. Orthop. Relat. Res.* 4–10 (2002).
65. Nkenke, E. *et al.* Morbidity of harvesting of bone grafts from the iliac crest for preprosthetic augmentation procedures: A prospective study. *Int. J. Oral Maxillofac. Surg.* **33,** 157–163 (2004).
66. Barone, A., Ricci, M., Mangano, F. & Covani, U. Morbidity Associated With Iliac Crest Harvesting in the Treatment of Maxillary and Mandibular Atrophies: A 10-Year Analysis. *J. Oral Maxillofac. Surg.* **69,** 2298–2304 (2011).
67. Shrivats, A. R., McDermott, M. C. & Hollinger, J. O. Bone tissue engineering:

state of the union. *Drug Discov. Today* **19,** 781–786 (2014).

68. Al-Nawas, B. & Schiegnitz, E. Augmentation procedures using bone substitute materials or autogenous bone – a systematic review and meta-analysis. *Eur. J. Oral Implant.* **7,** 219–234 (2014).
69. Amini, A. R., Laurencin, C. T. & Nukavarapu, S. P. Bone Tissue Engineering: Recent Advances and Challenges. *Crit. Rev. Biomed. Eng.* **40,** 363–408 (2012).
70. Hughes, D. E., Salter, D. M., Dedhar, S. & Simpson, R. Integrin expression in human bone. *J. Bone Miner. Res.* **8,** 527–33 (1993).
71. Brun, P. *et al.* Mechanisms underlying the attachment and spreading of human osteoblasts: from transient interactions to focal adhesions on vitronectin-grafted bioactive surfaces. *Acta Biomater.* **9,** 6105–15 (2013).
72. Ramazanoglu, M. & Oshi, Y. in *Implant Dentistry - A Rapidly Evolving Practice* (InTech, 2011). doi:10.5772/16936
73. Engel, E., Michiardi, A., Navarro, M., Lacroix, D. & Planell, J. A. Nanotechnology in regenerative medicine: the materials side. *Trends Biotechnol.* **26,** 39–47 (2008).
74. Zander, N. E., Orlicki, J. A., Rawlett, A. M. & Beebe, T. P. Quantification of protein incorporated into electrospun polycaprolactone tissue engineering scaffolds. *ACS Appl. Mater. Interfaces* **4,** 2074–81 (2012).
75. Liu, Y., Lim, J. & Teoh, S.-H. Review: Development of clinically relevant scaffolds for vascularised bone tissue engineering. *Biotechnol. Adv.* **31,** 688–705 (2013).
76. Lannutti, J., Reneker, D., Ma, T., Tomasko, D. & Farson, D. Electrospinning for tissue engineering scaffolds. *Mater. Sci. Eng. C* **27,** 504–509 (2007).
77. Zein, I., Hutmacher, D. W., Tan, K. C. & Teoh, S. H. Fused deposition modeling of novel scaffold architectures for tissue engineering applications. *Biomaterials* **23,** 1169–85 (2002).
78. Leukers, B. *et al.* Hydroxyapatite scaffolds for bone tissue engineering made by 3D printing. *J. Mater. Sci. Mater. Med.* **16,** 1121–4 (2005).
79. Damien, C. J. & Parsons, J. R. Bone graft and bone graft substitutes: a review of current technology and applications. *J. Appl. Biomater.* **2,** 187–208 (1991).
80. Schmitz, J. P., Hollinger, J. O. & Milam, S. B. Reconstruction of bone using calcium phosphate bone cements: a critical review. *J. Oral Maxillofac. Surg.* **57,** 1122–6 (1999).
81. Nillesen, S. T. M. *et al.* Increased angiogenesis and blood vessel maturation in acellular collagen-heparin scaffolds containing both FGF2 and VEGF. *Biomaterials* **28,** 1123–31 (2007).
82. Rodríguez-Vázquez, M., Vega-Ruiz, B., Ramos-Zúñiga, R., Saldaña-Koppel, D. A. & Quiñones-Olvera, L. F. Chitosan and Its Potential Use as a Scaffold for Tissue

Engineering in Regenerative Medicine. *Biomed Res. Int.* **2015,** 821279 (2015).

83. Kang, S.-W. *et al.* Surface modification with fibrin/hyaluronic acid hydrogel on solid-free form-based scaffolds followed by BMP-2 loading to enhance bone regeneration. *Bone* **48,** 298–306 (2011).
84. Tengood, J. E., Kovach, K. M., Vescovi, P. E., Russell, A. J. & Little, S. R. Sequential delivery of vascular endothelial growth factor and sphingosine 1-phosphate for angiogenesis. *Biomaterials* **31,** 7805–12 (2010).
85. Kolambkar, Y. M. *et al.* An alginate-based hybrid system for growth factor delivery in the functional repair of large bone defects. *Biomaterials* **32,** 65–74 (2011).
86. Koh, C. J. Tissue Engineering, Stem Cells, and Cloning: Opportunities for Regenerative Medicine. *J. Am. Soc. Nephrol.* **15,** 1113–1125 (2004).
87. Callister, W. D. J. & Rethwisch, D. G. *Materials Science and Engineering: An Introduction, 9th Edition*. (Wiley, 2013).
88. Mohamad Yunos, D., Bretcanu, O. & Boccaccini, A. R. Polymer-bioceramic composites for tissue engineering scaffolds. *J. Mater. Sci.* **43,** 4433–4442 (2008).
89. Chen, Q. Z., Thompson, I. D. & Boccaccini, A. R. 45S5 Bioglass®-derived glass–ceramic scaffolds for bone tissue engineering. *Biomaterials* **27,** 2414–2425 (2006).
90. Baino, F., Novajra, G. & Vitale-Brovarone, C. Bioceramics and Scaffolds: A Winning Combination for Tissue Engineering. *Front. Bioeng. Biotechnol.* **3,** 202 (2015).
91. Kasuga, T., Ota, Y., Nogami, M. & Abe, Y. Preparation and mechanical properties of polylactic acid composites containing hydroxyapatite fibers. *Biomaterials* **22,** 19–23 (2001).
92. Deng, X., Hao, J. & Wang, C. Preparation and mechanical properties of nanocomposites of poly(D,L-lactide) with Ca-deficient hydroxyapatite nanocrystals. *Biomaterials* **22,** 2867–73 (2001).
93. Ambrosio, A. M., Sahota, J. S., Khan, Y. & Laurencin, C. T. A novel amorphous calcium phosphate polymer ceramic for bone repair: I. Synthesis and characterization. *J. Biomed. Mater. Res.* **58,** 295–301 (2001).
94. Xu, H. Synergistic reinforcement of in situ hardening calcium phosphate composite scaffold for bone tissue engineering. *Biomaterials* **25,** 1029–1037 (2004).
95. Erol-Taygun, M., Zheng, K. & Boccaccini, A. R. Nanoscale Bioactive Glasses in Medical Applications. *Int. J. Appl. Glas. Sci.* **4,** 136–148 (2013).
96. Jones, J. R. New trends in bioactive scaffolds: The importance of nanostructure. *J. Eur. Ceram. Soc.* **29,** 1275–1281 (2009).
97. Mourino, V., Cattalini, J. P. & Boccaccini, A. R. Metallic ions as therapeutic

agents in tissue engineering scaffolds: an overview of their biological applications and strategies for new developments. *J. R. Soc. Interface* **9,** 401–419 (2012).

98. Hoppe, A., Güldal, N. S. & Boccaccini, A. R. A review of the biological response to ionic dissolution products from bioactive glasses and glass-ceramics. *Biomaterials* **32,** 2757–2774 (2011).
99. Wang, M. *et al.* Improved osteogenesis and angiogenesis of magnesium-doped calcium phosphate cement via macrophage immunomodulation. *Biomater. Sci.* **4,** 1574–1583 (2016).
100. Fiocco, L. *et al.* Novel processing of bioglass ceramics from silicone resins containing micro- and nano-sized oxide particle fillers. *J. Biomed. Mater. Res. Part A* **102,** 2502–2510 (2014).
101. Elsayed, H. *et al.* Development of bioactive silicate-based glass-ceramics from preceramic polymer and fillers. *J. Eur. Ceram. Soc.* **35,** 731–739 (2015).
102. Fiocco, L. *et al.* Bioactive Wollastonite-Diopside Foams from Preceramic Polymers and Reactive Oxide Fillers. *Materials (Basel).* **8,** 2480–2494 (2015).
103. Bernardo, E. *et al.* Novel akermanite-based bioceramics from preceramic polymers and oxide fillers. *Ceram. Int.* **40,** 1029–1035 (2014).
104. Elsayed, H., Zocca, A., Franchin, G., Bernardo, E. & Colombo, P. Hardystonite bioceramics from preceramic polymers. *J. Eur. Ceram. Soc.* **36,** 829–835 (2016).
105. Fiocco, L., Li, S., Bernardo, E., Stevens, M. M. & Jones, J. R. Highly porous polymer-derived wollastonite-hydroxycarbonate apatite ceramics for bone regeneration. *Biomed. Mater.* **11,** 025016 (2016).
106. Moscatelli, A. Self-assembly: Block molecules separate. *Nat. Nanotechnol.* (2017). doi:10.1038/nnano.2017.93
107. Zhang, S., Holmes, T., Lockshin, C. & Rich, A. Spontaneous assembly of a self-complementary oligopeptide to form a stable macroscopic membrane. *Proc. Natl. Acad. Sci.* **90,** 3334–3338 (1993).
108. Zhang, S. Emerging biological materials through molecular self-assembly. *Biotechnol. Adv.* **20,** 321–39 (2002).
109. Zhang, S. Discovery and design of self-assembling peptides. *Interface Focus* **7,** 20170028 (2017).
110. Gambaretto, R., Tonin, L., Di Bello, C. & Dettin, M. Self-assembling peptides: sequence, secondary structure in solution and film formation. *Biopolymers* **89,** 906–15 (2008).
111. Tibbitt, M. W. & Anseth, K. S. Hydrogels as extracellular matrix mimics for 3D cell culture. *Biotechnol. Bioeng.* **103,** 655–63 (2009).
112. Zamuner, A. *et al.* Design of decorated self-assembling peptide hydrogels as architecture for mesenchymal stem cells. *Materials (Basel).* **9,** (2016).

113. Hong, Y., Legge, R. L., Zhang, S. & Chen, P. Effect of Amino Acid Sequence and pH on Nanofiber Formation of Self-Assembling Peptides EAK16-II and EAK16-IV. *Biomacromolecules* **4,** 1433–1442 (2003).
114. Hong, Y., Lau, L. S., Legge, R. L. & Chen, P. CRITICAL SELF-ASSEMBLY CONCENTRATION OF AN IONIC-COMPLEMENTARY PEPTIDE EAK16-I. *J. Adhes.* **80,** 913–931 (2004).
115. Fung, S. Y., Keyes, C., Duhamel, J. & Chen, P. Concentration Effect on the Aggregation of a Self-Assembling Oligopeptide. *Biophys. J.* **85,** 537–548 (2003).
116. Caplan, M. R., Schwartzfarb, E. M., Zhang, S., Kamm, R. D. & Lauffenburger, D. A. Control of self-assembling oligopeptide matrix formation through systematic variation of amino acid sequence. *Biomaterials* **23,** 219–227 (2002).
117. Zhang, S., Gelain, F. & Zhao, X. Designer self-assembling peptide nanofiber scaffolds for 3D tissue cell cultures. *Semin. Cancer Biol.* **15,** 413–420 (2005).
118. Wang, X., Horii, A. & Zhang, S. Designer functionalized self-assembling peptide nanofiber scaffolds for growth, migration, and tubulogenesis of human umbilical vein endothelial cells. *Soft Matter* **4,** 2388 (2008).
119. Chau, Y. *et al.* Incorporation of a matrix metalloproteinase-sensitive substrate into self-assembling peptides – A model for biofunctional scaffolds. *Biomaterials* **29,** 1713–1719 (2008).
120. Zhang, S. in *Amino Acids, Peptides and Proteins.* 40–65 (RSC Publishing, 2012). doi:10.1039/9781849734677-00040
121. Dettin, M. *et al.* Driving h-osteoblast adhesion and proliferation on titania: Peptide hydrogels decorated with growth factors and adhesive conjugates. *J. Pept. Sci.* **20,** (2014).
122. Gilmore, J. M., Scheck, R. A., Esser-Kahn, A. P., Joshi, N. S. & Francis, M. B. N-terminal protein modification through a biomimetic transamination reaction. *Angew. Chem. Int. Ed. Engl.* **45,** 5307–11 (2006).
123. Zamuner, A., Sica, G. & Dettin, M. Insertion of a Flexible Spacer Increases the Yield of Site-Specific Bioconjugation through N-Terminal Transamination. *Lett. Org. Chem.* **14,** (2017).
124. Dettin, M. *et al.* Driving h-osteoblast adhesion and proliferation on titania: Peptide hydrogels decorated with growth factors and adhesive conjugates. *J. Pept. Sci.* **20,** 585–594 (2014).
125. Holmes, T. C. *et al.* Extensive neurite outgrowth and active synapse formation on self-assembling peptide scaffolds. *Proc. Natl. Acad. Sci.* **97,** 6728–6733 (2000).
126. Schachner, M. Nervous engineering. *Nature* **405,** 747–748 (2000).
127. Davis, M. E. *et al.* Injectable self-assembling peptide nanofibers create intramyocardial microenvironments for endothelial cells. *Circulation* **111,** 442–50

(2005).

128. Misawa, H. *et al.* PuraMatrix facilitates bone regeneration in bone defects of calvaria in mice. *Cell Transplant.* **15,** 903–10 (2006).
129. Webber, M. J. *et al.* Supramolecular nanostructures that mimic VEGF as a strategy for ischemic tissue repair. *Proc. Natl. Acad. Sci.* **108,** 13438–13443 (2011).
130. Di Bello, C. & Bagno, A. *Interazioni tra biomateriali e tessuti*. (2009).
131. Park, K.-H., Na, K. & Chung, H.-M. Enhancement of the adhesion of fibroblasts by peptide containing an Arg-Gly-Asp sequence with poly(ethylene glycol) into a thermo-reversible hydrogel as a synthetic extracellular matrix. *Biotechnol. Lett.* **27,** 227–31 (2005).
132. Schultz, G. S. & Grant, M. B. Neovascular growth factors. *Eye (Lond).* **5 (Pt 2),** 170–80 (1991).
133. Hing, K. A. Bioceramic Bone Graft Substitutes: Influence of Porosity and Chemistry. *Int. J. Appl. Ceram. Technol.* **2,** 184–199 (2005).
134. Licht, T. Induction of pro-angiogenic signaling by a synthetic peptide derived from the second intracellular loop of S1P3 (EDG3). *Blood* **102,** 2099–2107 (2003).
135. West, J. L. & Hubbell, J. A. Polymeric Biomaterials with Degradation Sites for Proteases Involved in Cell Migration. *Macromolecules* **32,** 241–244 (1999).
136. Patterson, J. & Hubbell, J. A. Enhanced proteolytic degradation of molecularly engineered PEG hydrogels in response to MMP-1 and MMP-2. *Biomaterials* **31,** 7836–7845 (2010).
137. Diana, D. *et al.* Structural Determinants of the Unusual Helix Stability of a De Novo Engineered Vascular Endothelial Growth Factor (VEGF) Mimicking Peptide. *Chem. - A Eur. J.* **14,** 4164–4166 (2008).
138. Rozek, A., Powers, J.-P. S., Friedrich, C. L. & Hancock, R. E. W. Structure-Based Design of an Indolicidin Peptide Analogue with Increased Protease Stability † , ‡. *Biochemistry* **42,** 14130–14138 (2003).
139. Gentilucci, L., De Marco, R. & Cerisoli, L. Chemical Modifications Designed to Improve Peptide Stability: Incorporation of Non-Natural Amino Acids, Pseudo-Peptide Bonds, and Cyclization. *Curr. Pharm. Des.* **16,** 3185–3203 (2010).
140. Huettner, N., Dargaville, T. R. & Forget, A. Discovering Cell-Adhesion Peptides in Tissue Engineering: Beyond RGD. *Trends Biotechnol.* **36,** 372–383 (2018).
141. Sánchez-Gómez, S. & Martínez-de-Tejada, G. Antimicrobial Peptides as Anti-biofilm Agents in Medical Implants. *Curr. Top. Med. Chem.* **17,** 590–603 (2017).
142. Van Hove, A. H. & Benoit, D. S. W. Depot-Based Delivery Systems for Pro-Angiogenic Peptides: A Review. *Front. Bioeng. Biotechnol.* **3,** 102 (2015).
143. Mukherjee, A. K. *et al.* Characterization of a pro-angiogenic, novel peptide from Russell's viper (Daboia russelii russelii) venom. *Toxicon* **77,** 26–31 (2014).

144. Fraioli, R. *et al.* Surface guidance of stem cell behavior: Chemically tailored co-presentation of integrin-binding peptides stimulates osteogenic differentiation in vitro and bone formation in vivo. *Acta Biomater.* **43,** 269–281 (2016).
145. Attwood, S. J. *et al.* Adhesive ligand tether length affects the size and length of focal adhesions and influences cell spreading and attachment. *Sci. Rep.* **6,** 34334 (2016).
146. Sridar, S., Churchward, M. A., Mushahwar, V. K., Todd, K. G. & Elias, A. L. Peptide modification of polyimide-insulated microwires: Towards improved biocompatibility through reduced glial scarring. *Acta Biomater.* **60,** 154–166 (2017).
147. Macchiarini, P. *et al.* Clinical transplantation of a tissue-engineered airway. *Lancet* **372,** 2023–2030 (2008).
148. Raya-Rivera, A. *et al.* Tissue-engineered autologous urethras for patients who need reconstruction: an observational study. *Lancet* **377,** 1175–1182 (2011).
149. Atala, A., Bauer, S. B., Soker, S., Yoo, J. J. & Retik, A. B. Tissue-engineered autologous bladders for patients needing cystoplasty. *Lancet* **367,** 1241–1246 (2006).
150. Atala, A. Tissue Engineering and Regenerative Medicine: Concepts for Clinical Application. *Rejuvenation Res.* **7,** 15–31 (2004).
151. Papanas, N. & Maltezos, E. Growth Factors in the Treatment of Diabetic Foot Ulcers: New Technologies, Any Promises? *Int. J. Low. Extrem. Wounds* **6,** 37–53 (2007).
152. Losordo, D. W. Therapeutic Angiogenesis and Vasculogenesis for Ischemic Disease: Part I: Angiogenic Cytokines. *Circulation* **109,** 2487–2491 (2004).
153. Chu, H. & Wang, Y. Therapeutic angiogenesis: controlled delivery of angiogenic factors. *Ther. Deliv.* **3,** 693–714 (2012).
154. LAHAM, R. J. *et al.* Intracoronary and intravenous administration of basic fibroblast growth factor: myocardial and tissue distribution. *Drug Metab. Dispos.* **27,** 821–826 (1999).
155. Finetti, F. *et al.* Functional and pharmacological characterization of a VEGF mimetic peptide on reparative angiogenesis. *Biochem. Pharmacol.* **84,** 303–311 (2012).
156. Lane, T. F. SPARC is a source of copper-binding peptides that stimulate angiogenesis. *J. Cell Biol.* **125,** 929–943 (1994).
157. Hardy, B. *et al.* Angiogenesis induced by novel peptides selected from a phage display library by screening human vascular endothelial cells under different physiological conditions. *Peptides* **28,** 691–701 (2007).
158. Demidova-Rice, T. N., Geevarghese, A. & Herman, I. M. Bioactive peptides

derived from vascular endothelial cell extracellular matrices promote microvascular morphogenesis and wound healing in vitro. *Wound Repair Regen.* **19,** 59–70 (2011).

159. Demidova-Rice, T. N., Wolf, L., Deckenback, J., Hamblin, M. R. & Herman, I. M. Human Platelet-Rich Plasma- and Extracellular Matrix-Derived Peptides Promote Impaired Cutaneous Wound Healing In Vivo. *PLoS One* **7,** e32146 (2012).
160. Dettin, M. *et al.* In vitro and in vivo pro-angiogenic effects of thymosin-β4-derived peptides. *Cell. Immunol.* **271,** 299–307 (2011).
161. Kim, J. H., Jung, Y., Kim, B.-S. & Kim, S. H. Stem cell recruitment and angiogenesis of neuropeptide substance P coupled with self-assembling peptide nanofiber in a mouse hind limb ischemia model. *Biomaterials* **34,** 1657–1668 (2013).
162. Hong, H. S. *et al.* A new role of substance P as an injury-inducible messenger for mobilization of CD29+ stromal-like cells. *Nat. Med.* **15,** 425–435 (2009).
163. Ko, I. K. *et al.* Combined systemic and local delivery of stem cell inducing/recruiting factors for in situ tissue regeneration. *FASEB J.* **26,** 158–168 (2012).
164. Witus, L. S. & Francis, M. Site-Specific Protein Bioconjugation via a Pyridoxal 5'-Phosphate-Mediated N-Terminal Transamination Reaction. *Curr. Protoc. Chem. Biol.* **2,** 125–34 (2010).
165. Capulli, M., Paone, R. & Rucci, N. Osteoblast and osteocyte: Games without frontiers. *Arch. Biochem. Biophys.* **561,** 3–12 (2014).
166. Grigoriadis, A. E., Heersche, J. N. & Aubin, J. E. Differentiation of muscle, fat, cartilage, and bone from progenitor cells present in a bone-derived clonal cell population: effect of dexamethasone. *J. Cell Biol.* **106,** 2139–51 (1988).
167. Ducy, P., Zhang, R., Geoffroy, V., Ridall, A. L. & Karsenty, G. Osf2/Cbfa1: a transcriptional activator of osteoblast differentiation. *Cell* **89,** 747–54 (1997).
168. Komori, T. *et al.* Targeted disruption of Cbfa1 results in a complete lack of bone formation owing to maturational arrest of osteoblasts. *Cell* **89,** 755–64 (1997).
169. Fakhry, M., Hamade, E., Badran, B., Buchet, R. & Magne, D. Molecular mechanisms of mesenchymal stem cell differentiation towards osteoblasts. *World J. Stem Cells* **5,** 136–48 (2013).
170. Nakashima, K. *et al.* The novel zinc finger-containing transcription factor osterix is required for osteoblast differentiation and bone formation. *Cell* **108,** 17–29 (2002).
171. Glass, D. A. *et al.* Canonical Wnt signaling in differentiated osteoblasts controls osteoclast differentiation. *Dev. Cell* **8,** 751–64 (2005).
172. Hu, H. *et al.* Sequential roles of Hedgehog and Wnt signaling in osteoblast development. *Development* **132,** 49–60 (2005).

173. Manolagas, S. C. Birth and death of bone cells: basic regulatory mechanisms and implications for the pathogenesis and treatment of osteoporosis. *Endocr. Rev.* **21,** 115–37 (2000).
174. Jilka, R. L., Weinstein, R. S., Bellido, T., Parfitt, A. M. & Manolagas, S. C. Osteoblast programmed cell death (apoptosis): modulation by growth factors and cytokines. *J. Bone Miner. Res.* **13,** 793–802 (1998).
175. Del Fattore, A. & Teti, A. The Tight Relationship Between Osteoclasts and the Immune System. *Inflamm. Allergy-Drug Targets* **11,** 181–187 (2012).
176. Striker, G. E., Harlan, J. M. & Schwartz, S. M. Human endothelial cells in vitro. *Methods Cell Biol.* **21A,** 135–51 (1980).
177. Jiménez, N., Krouwer, V. J. D. & Post, J. A. A new, rapid and reproducible method to obtain high quality endothelium in vitro. *Cytotechnology* **65,** 1–14 (2013).
178. Manconi, F., Markham, R. & Fraser, I. S. Culturing endothelial cells of microvascular origin. *Methods Cell Sci.* **22,** 89–99 (2000).
179. Jaffe, E. A., Hoyer, L. W. & Nachman, R. L. Synthesis of antihemophilic factor antigen by cultured human endothelial cells. *J. Clin. Invest.* **52,** 2757–64 (1973).
180. Jaffe, E. A., Nachman, R. L., Becker, C. G. & Minick, C. R. Culture of human endothelial cells derived from umbilical veins. Identification by morphologic and immunologic criteria. *J. Clin. Invest.* **52,** 2745–56 (1973).
181. Jaffe, E. A., Hoyer, L. W. & Nachman, R. L. Synthesis of von Willebrand factor by cultured human endothelial cells. *Proc. Natl. Acad. Sci. U. S. A.* **71,** 1906–9 (1974).
182. Gimbrone, M. A., Cotran, R. S. & Folkman, J. Human vascular endothelial cells in culture. Growth and DNA synthesis. *J. Cell Biol.* **60,** 673–84 (1974).
183. Piccolo, S., Dupont, S. & Cordenonsi, M. The Biology of YAP/TAZ: Hippo Signaling and Beyond. *Physiol. Rev.* **94,** 1287–1312 (2014).
184. Neto, F. *et al.* YAP and TAZ regulate adherens junction dynamics and endothelial cell distribution during vascular development. *Elife* **7,** (2018).
185. Nardone, G. *et al.* YAP regulates cell mechanics by controlling focal adhesion assembly. *Nat. Commun.* **8,** 15321 (2017).
186. Zanconato, F., Cordenonsi, M. & Piccolo, S. YAP/TAZ at the Roots of Cancer. *Cancer Cell* **29,** 783–803 (2016).
187. Zanconato, F., Battilana, G., Cordenonsi, M. & Piccolo, S. YAP/TAZ as therapeutic targets in cancer. *Curr. Opin. Pharmacol.* **29,** 26–33 (2016).
188. Wada, K.-I., Itoga, K., Okano, T., Yonemura, S. & Sasaki, H. Hippo pathway regulation by cell morphology and stress fibers. *Development* **138,** 3907–3914 (2011).

189. Dupont, S. *et al.* Role of YAP/TAZ in mechanotransduction. *Nature* **474,** 179–183 (2011).
190. Uemura, M., Nagasawa, A. & Terai, K. Yap/Taz transcriptional activity in endothelial cells promotes intramembranous ossification via the BMP pathway. *Sci. Rep.* **6,** 27473 (2016).
191. Wang, X. *et al.* YAP/TAZ Orchestrate VEGF Signaling during Developmental Angiogenesis. *Dev. Cell* **42,** 462–478.e7 (2017).
192. Totaro, A. *et al.* YAP/TAZ link cell mechanics to Notch signalling to control epidermal stem cell fate. *Nat. Commun.* **8,** 15206 (2017).
193. Daigneault, M., Preston, J. A., Marriott, H. M., Whyte, M. K. B. & Dockrell, D. H. The Identification of Markers of Macrophage Differentiation in PMA-Stimulated THP-1 Cells and Monocyte-Derived Macrophages. *PLoS One* **5,** e8668 (2010).
194. Tattersall, I. W. *et al.* In vitro modeling of endothelial interaction with macrophages and pericytes demonstrates Notch signaling function in the vascular microenvironment. *Angiogenesis* **19,** 201–215 (2016).
195. Clark, R. A. F., Ghosh, K. & Tonnesen, M. G. Tissue engineering for cutaneous wounds. *J. Invest. Dermatol.* **127,** 1018–29 (2007).
196. Fantin, A. *et al.* Tissue macrophages act as cellular chaperones for vascular anastomosis downstream of VEGF-mediated endothelial tip cell induction. *Blood* **116,** 829–840 (2010).
197. Zajac, E. *et al.* Angiogenic capacity of M1- and M2-polarized macrophages is determined by the levels of TIMP-1 complexed with their secreted proMMP-9. *Blood* **122,** 4054–4067 (2013).
198. Spiller, K. L. & Koh, T. J. Macrophage-based therapeutic strategies in regenerative medicine. *Adv. Drug Deliv. Rev.* **122,** 74–83 (2017).
199. Ohradanova-Repic, A., Machacek, C., Fischer, M. B. & Stockinger, H. Differentiation of human monocytes and derived subsets of macrophages and dendritic cells by the HLDA10 monoclonal antibody panel. *Clin. Transl. Immunol.* **5,** e55 (2016).
200. Barbay, V. *et al.* Role of M2-like macrophage recruitment during angiogenic growth factor therapy. *Angiogenesis* **18,** 191–200 (2015).
201. Brancato, S. K. & Albina, J. E. Wound Macrophages as Key Regulators of Repair. *Am. J. Pathol.* **178,** 19–25 (2011).
202. Aplin, A. C. *et al.* Regulation of angiogenesis, mural cell recruitment and adventitial macrophage behavior by Toll-like receptors. *Angiogenesis* **17,** 147–161 (2014).
203. Mayer, A., Hiebl, B., Lendlein, A. & Jung, F. Support of HUVEC proliferation by pro-angiogenic intermediate CD163+ monocytes/macrophages: a co-culture

experiment. *Clin. Hemorheol. Microcirc.* **49,** 423–30 (2011).

204. Mayer, A., Roch, T., Kratz, K., Lendlein, A. & Jung, F. Pro-angiogenic CD14++ CD16+ CD163+ monocytes accelerate the in vitro endothelialization of soft hydrophobic poly(n-butyl acrylate) networks. *Acta Biomater.* **8,** 4253–4259 (2012).
205. Cheng, C. W., Solorio, L. D. & Alsberg, E. Decellularized tissue and cell-derived extracellular matrices as scaffolds for orthopaedic tissue engineering. *Biotechnol. Adv.* **32,** 462–484 (2014).
206. Krutty, J. D., Schmitt, S. K., Gopalan, P. & Murphy, W. L. Surface functionalization and dynamics of polymeric cell culture substrates. *Curr. Opin. Biotechnol.* **40,** 164–169 (2016).
207. Bierbaum, S., Hintze, V. & Scharnweber, D. Functionalization of biomaterial surfaces using artificial extracellular matrices. *Biomatter* **2,** 132–141 (2012).
208. Hassert, R. & Beck-Sickinger, A. G. Tuning peptide affinity for biofunctionalized surfaces. *Eur. J. Pharm. Biopharm.* **85,** 69–77 (2013).
209. Beutner, R., Michael, J., Schwenzer, B. & Scharnweber, D. Biological nano-functionalization of titanium-based biomaterial surfaces: a flexible toolbox. *J. R. Soc. Interface* **7 Suppl 1,** S93–S105 (2010).
210. Sapsford, K. E. *et al.* Functionalizing Nanoparticles with Biological Molecules: Developing Chemistries that Facilitate Nanotechnology. *Chem. Rev.* **113,** 1904–2074 (2013).
211. Dettin, M. *et al.* Assessment of novel chemical strategies for covalent attachment of adhesive peptides to rough titanium surfaces: XPS analysis and biological evaluation. *J. Biomed. Mater. Res. Part A* **91A,** 463–479 (2009).
212. Bagno, A. *et al.* Human osteoblast-like cell adhesion on titanium substrates covalently functionalized with synthetic peptides. *Bone* **40,** 693–699 (2007).
213. Maheshwari, G., Brown, G., Lauffenburger, D. A., Wells, A. & Griffith, L. G. Cell adhesion and motility depend on nanoscale RGD clustering. *J. Cell Sci.* **113 (Pt 1,** 1677–86 (2000).
214. Cacchioli, A., Ravanetti, F., Bagno, A., Dettin, M. & Gabbi, C. Human Vitronectin–Derived Peptide Covalently Grafted onto Titanium Surface Improves Osteogenic Activity: A Pilot In Vivo Study on Rabbits. *Tissue Eng. Part A* **15,** 2917–2926 (2009).
215. Conde, J. *et al.* Revisiting 30 years of biofunctionalization and surface chemistry of inorganic nanoparticles for nanomedicine. *Front. Chem.* **2,** 48 (2014).
216. Tallawi, M. *et al.* Strategies for the chemical and biological functionalization of scaffolds for cardiac tissue engineering: a review. *J. R. Soc. Interface* **12,** 20150254 (2015).

217. Nanci, A. *et al.* Chemical modification of titanium surfaces for covalent attachment of biological molecules. *J. Biomed. Mater. Res.* **40,** 324–35 (1998).
218. Dettin, M. *et al.* Covalent surface modification of titanium oxide with different adhesive peptides: Surface characterization and osteoblast-like cell adhesion. *J. Biomed. Mater. Res. Part A* **90A,** 35–45 (2009).
219. Battista, E. *et al.* Ligand engagement on material surfaces is discriminated by cell mechanosensoring. *Biomaterials* **45,** 72–80 (2015).
220. Borcard, F. *et al.* Chemical Functionalization of Bioceramics To Enhance Endothelial Cells Adhesion for Tissue Engineering. *J. Med. Chem.* **55,** 7988–7997 (2012).
221. Ehlert, N. *et al.* Amino-modified silica surfaces efficiently immobilize bone morphogenetic protein 2 (BMP2) for medical purposes. *Acta Biomater.* **7,** 1772–1779 (2011).
222. Schickle, K. *et al.* Synthesis of novel tricalcium phosphate-bioactive glass composite and functionalization with rhBMP-2. *J. Mater. Sci. Mater. Med.* **22,** 763–771 (2011).

Chapter 2

SAP screening

2.1 Abstract

In this first part of the PhD project, the influence of five different Type I, module II self-assembling peptides on three types of cells, fundamentally involved in tissue regeneration, has been investigated. For this reason, human osteoblasts, THP-1 monocytes and human umbilical vein endothelial cells have been cultivated on five self-assembling peptides: EAK, EAbuK, DAR, EAOrn and EYK (see **Table I** of Gambaretto *et al.*[1], pag.54).
Human osteoblasts (HOB) and Human umbilical vein endothelial cells (HUVECs) proliferation and YAP1 expression have been evaluated at 48h.
THP1 monocyte adhesion and spreading has been evaluated at 1h from the seeding. Additionally, the ability of SAPs to induce HUVECs' tubular structures formation both directly and mediated by the influence of polarized macrophages, has been assessed with matrigel assays. EAK showed a significant increase in HOB proliferation and YAP1 expression demonstrating that cells cultivated on this self-assembling peptide are directed towards new bone deposition. DAR was consistently the most successful peptide at inducing differentiation to a HUVEC's angiogenic phenotype, it increased YAP1 expression and formation of long and complex tubule structures. EAK showed good results in terms of cells morphology and formation of long tubule structures, too. All five SAPs were able to induce monocyte adhesion, which could potentially encourage cell survival and alter cellular function via non-integrin specific binding. DAR and EAK-polarised M1 were found to promote HUVEC network formation on matrigel.
All these results support the use of EAK as soft scaffold for bone tissue regeneration, promoting new bone formation by increasing HOB proliferation and YAP1 expression, and enhancing angiogenesis by direct and indirect HUVECs activation through a macrophages-mediated pathway.

2.2 Human Osteoblasts

2.2.1 Results and discussion

To understand how different self-assembling peptides can influence HOB behaviour, HOB were cultured on 5 individual peptides (EAK, EAbuK, DAR, EAOrn and EYK, see **Table I** of Gambaretto *et al.*[1]) or PBS, as control, in a proliferation assay over 72 hours from the seeding.

All SAPs with the exception of DAR, showed an increased proliferation when compared to the control, but this increase was statistically significant (p-value≤0.05), only with cells cultured on EAK (**Fig 2.1**).

It is interesting to note that DAR is the only SAP that seemed not to induce an increase in cell proliferation, but HOB cultured on it showed a more elongated shape (length average164.49±15.46µm), when compared to the control (medium length 101.28±19.32µm), EAK (medium length 109.06±24.23µm), EAbuK (medium length 80.64±14.84µm), EYK (medium length 133.41±22.10µm) and EAOrn (medium length 109.10±25.85µm), which all led to a lesser degree of elongation.

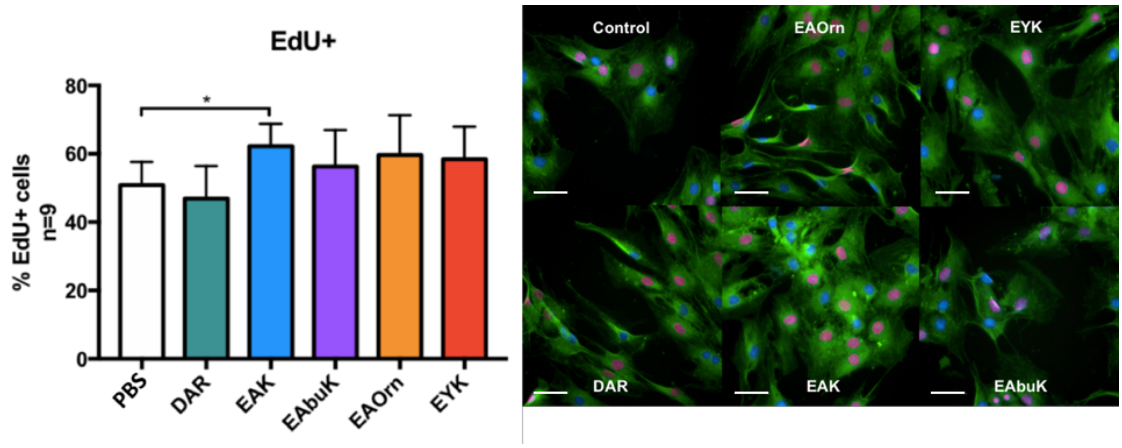


Figure 2.1. Effect of SAPs on HOB proliferation. Effect of SAPs coatings (DAR, EAK, EAbuk, EAOrn, EYK) on HOB proliferation for 48hrs using EdU as an index of proliferation (n=9). Error bars indicate standard deviation and *indicates p≤ 0.05. HOB morphology after 72h from the seeding (A488-Green CellBrite to label cell cytoplasmic membranes, A647-EdU+ cells represent the nuclei that divided at least once, Blue-Hoechst for nuclei; magnification = 20X OM, scale bar =50µm).

Due to the important role of mechanotransduction in HOB cells, we wanted to investigate it response to different SAPs.

When comparing the expression of activated YAP1 (immunohistochemistry analysis, see paragraph 2.2.3.4), all SAPs were able to upregulate YAP1 (YAP is retained in the nuclei rather than being distributed along the cytoplasm). There was a statistically significant

upregulation of YAP1 in cells cultured in DAR (p-value ≤ 0.01) and EAK (p-value ≤ 0.05) (**Fig 2.2**).

EAK produced the highest upregulated expression, and showed 2 times increase in YAP1 expression with respect to the control, suggesting that the properties of the EAK substrate were able to enhance mechanotransduction to modulate osteoblast activity and proliferation.

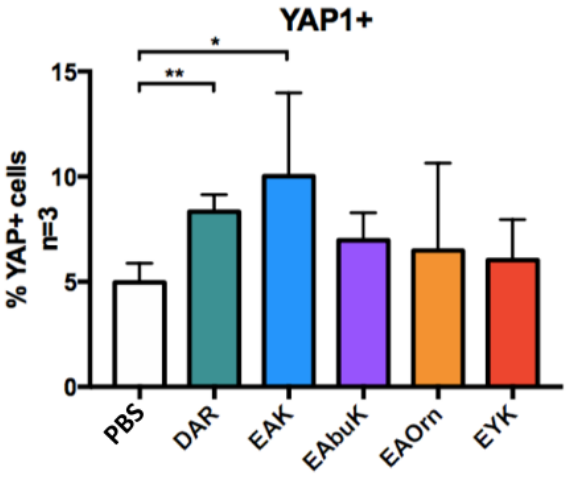


Figure 2.2. Analysis of nuclear and cytoplasmic YAP1 distribution for mechanotransduction. Graph represents comparison of the effect of SAP coatings (DAR, EAK, EAbuK, EAOrn and EYK) on HOB mechanotransduction, using YAP1+ as an indicator (n=3). Error bars indicate standard deviation and * indicates p-value ≤ 0.05; ** indicates p-value ≤ 0.01.

2.2.2 Conclusions

The aim of this part of the research study was to better understand the influence of different self-assembling peptides on human osteoblasts' behaviour. To achieve this, we screened five different SAPs to assess the direct impact on HOB proliferation, morphology and molecular effect of distribution of YAP1. As expected, SAPs showed a general tendency to increase HOB proliferation, but EAK was the only one between the five tested SAPs to give a statistically significant increase.

It is important to note that on the opposite side, DAR did not increase proliferation but induced a more elongated morphology.

All SAPs showed increased YAP1 expression, with statistically significant results for cells cultured on EAK and DAR. Indeed, YAP1 is a nuclear effector of the Hippo pathway and by interacting with TEA domain transcription factors, YAP1 has been involved in cell proliferation[2], thus linking YAP expression with proliferation in HOB cells cultured on EAK. Moreover, since mechanotransduction induces retention of YAP/TAZ into the nucleus[3] DAR could induced different intracellular pathways resulting in delayed cell proliferation.

Finally, YAP (together with its transcriptional coactivator with PDZ-binding motif, TAZ) expression promotes bone development through the regulation of osteoblast activity, matrix quality, and osteoclastic remodeling[4], and promote bone formation and inhibit bone resorption when expressed in mature osteoblasts and osteocytes[5].
All these results showed that SAPs, in particular EAK, could be a promising soft scaffold for bone tissue regeneration.

2.2.3 Materials and methods

All peptides used in this PhD project were synthetized, characterized and purified at the Biochemical Engineering Lab at the Department of Industrial Engineering, University of Padova (Prof. Monica Dettin). All bioassays and data analysis described in Chapter 2 were carried out during a collaboration with King's College London, at Tissue engineering & Biophotonics Department under the supervision of Prof. Lucy Di Silvio and PhD Lorenzo Veschini. I would like to acknowledge Shryam Patel and Jiawei Huang for their fundamental contribution in the developing of the *in vitro* bioassays with HUVEC and macrophages.

2.2.3.1 Peptide synthesis, purification and characterisation

Five different SAPs were used in this project: EAK, EAbuK, DAR, EYK and EAOrn (**Table I** of Gambaretto *et al.*[1] as follows).

Table I Peptide Sequences, Secondary Structure Attribution in Water, and an Estimation of Their Capacity to Form Film After Salt Addition and Drying Process

Name	Modification	Abbreviation	Sequence	Structure	Film
P1	–	EAK 16-II	A E A E A K A K A E A E A K A K	β	+ +
P2	Glu → Asp	DAK 16-II	A D A D A K A K A D A D A K A K	α	− −
P3	Lys → Orn	EAOrn 16-II	A E A E A Orn A Orn A E A E A Orn A Orn	α/β	+
P4	Lys → Orn, Glu → Asp	DAOrn 16-II	A D A D A Orn A Orn A D A D A Orn A Orn	α	− −
P5	Ala → Abu	EAbuK 16-II	Abu E Abu E Abu K Abu K Abu E Abu E Abu K Abu K	β	+ +
P6	Ala → Tyr	EYK 16-II	Y E Y E Y K Y K Y E Y E Y K Y K	β-hairpin	+ +
P7	Arg-Gly-Asp addition	RGD-(EAK 16-II)	R G D A E A E A K A K A E A E A K A K	β	+ +
P8	Arg-Gly-Asp + P1 scrambled	RGD-(EAK 16-II) Sc	R G D A K A K A E A E A A E K A K A E K	α	− −
P9	Glu → Asp, Lys → Arg	DAR 16-II	A D A D A R A R A D A D A R A R	α	−
P10	P9 inverted	RAD 16-II	R A R A D A D A R A R A D A D A	α	−

α stands for α-helix and β stands for β-sheet.
Orn = $-NH-CH(CH_2-CH_2-CH_2-NH_2)-CO-$.
Abu = $-NH-CH(CH_2-CH_3)-CO-$.

The SAPs were synthesised, characterized and purified following the protocol used in Gambaretto *et al*[1]. The SAPs were stored at -20°C.

2.2.3.2 Preparation of peptide solutions

Stock solutions of EAK, EAbuK, DAR, EYK and EAOrn were prepared in milliQ water, simply by vortexing and sonicating, at 0.5% w/v and sterilized by filtration, using 0.22µm pore size filter (Millex GP, Ø = 4mm).

2.2.3.3 Cell Tissue culture, seeding, fixation and permeabilisation

Primary human osteoblast (HOB) were commercially obtained (Cell Application, Inc) at passage 0, and cryopreserved for storage before beginning the experiments. The cells were stored at -80°C in freeze mix solution (90% FBS and 10% DMSO). The cells were maintained in osteoblast growth medium (PromoCell). Only cells from passage 1 to passage 5 were used. Cells were cultured in T-25 and T-75 flasks; once cells reached confluency, they were detached from the previous flask and splitted into 2 new flasks. Two ml of accutase (Gibco) was added for cell detachment, and then cells were centrifuged for 5 minutes at 1500 RPM. The supernatant was removed and the cell pellet was resuspended in adequate volume of medium. Before cell seeding, HOB were counted, and a cell suspension of the appropriate density was prepared, and subsequently pipetted into each well in either a 96 well tissue culture plate TCP (Nunc, Thermofisher). The culture plates were then incubated in a 37°C 5% CO_2 incubator (Heracell^{TM}, Thermo Scientific) and regularly observed for growth under a light microscope. Cells were fixed and permeabilised in order to preserve cell structures, maintain antigenicity for immunohistochemistry and allow cells to be immunostained with larger molecules such as antibodies. Culture medium was removed from the wells and cells were washed twice with PBS supplemented with Ca^{2+} and Mg^{2+}. Fixation was carried out using a cross linking agent, (paraformaldehyde, PFA). PFA (2%) in PBS enriched with Ca^{2+} and Mg^{2+} was then added and placed under agitation at room temperature for 15 minutes. The 2% PFA solution was then removed and cells were washed with PBS enriched with Ca^{2+} and Mg^{2+} twice. Permeabilisation was done using the detergent 0.1% TritonX-100. TritonX-100 (0.1%) in PBS was added to the cells and let at room temperature for 5 minutes. This was then removed and washed with PBS enriched with Ca^{2+} and Mg^{2+}. The PBS was removed and cells were placed in blocking solution, constituted of 1% FBS in PBS. Cells were left in blocking solution for at least 45 minutes before immunostaining.

2.2.3.4 Cell Staining

HOB were stained with CellBrite Green to label cell cytoplasmic membranes with fluorescent green dye. Before cell seeding, CellBrite Green was added directly to the culture medium in the tissue culture flask in the adequate concentration (1:100) and let act overnight. Immunostaining was used to localise specific structures and proteins of the cells. In general, cellular antigens are visualised using either direct detection, whereby the primary antibody is conjugated with a fluorophore, or indirect detection, which is a two steps method that involves an unconjugated primary antibody followed by a fluorophore conjugated secondary antibody.

The combination of various labelled antibodies allows detection of many target antigens within a single sample. In this project, the indirect immunostaining method was used to stain HOB on SAPs constructs.

The protocol was as follows. After cells had been incubated in blocking solution (1% FBS in PBS) for at least 45 minutes, the blocking solution was removed and the primary antibody solution was prepared at the required concentration.

The cells were then incubated in the primary YAP1 antibody solution (Abcam ab52771, dilution 1:200 in blocking solution) and placed under agitation at room temperature for one hour. The solution was removed and cells were washed thrice with blocking solution, agitating for 5 minutes each wash.

The secondary antibody Alexa-488 (Thermofisher, dilution 1:500 in blocking solution) was added and the cells were incubated in the secondary antibody solution for 45 minutes under agitation. Following addition of the secondary antibody, the well plate was covered with foil to limit light exposure of the conjugated fluorophore. The solution was removed and cells were washed twice with blocking solution, agitating for 5 minutes per wash.

The cells were then counterstained with Hoechst (Sigma, dilution 1:2000 in PBS plus Ca^{2+} and Mg^{2+} for 10 minutes) for nuclei staining. Finally, cells were washed twice with blocking solution and finally left in PBS. All stains used across experiments are reported in **Table 2.1**.

Table 2.1. Fluorescent dyes and target structures.

STAIN	TYPE	TARGET	SOURCE
CELLBRITE GREEN	Chemical	Cytoplasmic membrane	Biotium
HOECHST	Chemical	Nucleus	Sigma
ANTI-YAP1 antibody [EP1674Y] (ab52771)	Recombinant rabbit monoclonal antibody	Binds to YAP	Abcam
ALEXA FLUOR®-488) (AB150077)	Anti-Rabbit Goat polyclonal secondary	Binds to Anti-YAP1 antibody	Abcam

2.2.3.5 Preparation of SAPs coatings

Sterile PBS on TCP was used a control for all experiments, which respectively investigated HOB immunomorphology and proliferation on SAPs. PBS (100µl) was kept aside for use as the control, and 30µl was pipetted into the first set of triplicate wells of a 96 well plate. A solution of PBS and SAP, for each peptide, was then prepared at a dilution of 1:10 by mixing 10µl of each SAP's stock solution (paragraph 2.2.3.2) with 90µl of PBS. We pipetted 30µl of the solution into each triplicate well, corresponding to the peptide. Preparation of the solution and coating of the wells for each SAP was conducted separately one by one, to prevent peptide self-aggregation prior to coating.

The presence of the free ions within the solution would allow the peptides to immediately self-assemble. The coated plate was left for 24 hours in a 37°C 5% CO_2 incubator to allow the self-aggregation of the SAPs before cell seeding. 5×10^3 cells stained with CellBrite

Green were seeded per well in HOB growth medium, placed in a 37°C 5% CO_2 incubator and fixed after 72 hour to subsequently stain for Hoechst, and YAP1.

2.2.3.6 HOB proliferation assays

A proliferation assay was done to compare the extent of HOB proliferation for each SAP. 5×10^3 HOB suspended in osteoblast growth medium were seeded onto SAP/PBS coated wells on a 96 well plate (paragraph 2.2.3.5).
The plate was placed in a 37°C 5% CO_2 incubator for 24 hours and subsequently treated with the initial pulse of EDU (5- ethynyl-2'-deoxyuridine), according to the protocol outlined in Click-iT proliferation kit (ThermoFisher) After 48 hours in a 37°C 5% CO_2 incubator, cells were fixed and permeabilised (see protocol in paragraph 2.2.3.3).
The stain with EDU was added according to the protocol outlined in Click-iT proliferation kit. Cells were then stained for Hoechst and YAP1, and imaging was done using the Operetta High-Content imaging system. EDU is a thymidine nucleoside analogue, and represents an index of cell proliferation, as cells grown in the presence of EDU incorporate a thymidine base during the S phase, which is attached to a fluorophore label and allowing detection of proliferation cumulatively after addition of the initial EDU pulse. The experiment was repeated three times, and each time in triplicate.

2.2.3.7 Imaging and image analysis

The main imaging approach used was with the Operetta CLS™ High-Content Imaging System (Perkin Elmer), which is an automated high content confocal microscope with a vast range of filters for high quality fluorescence and bright field imaging, with reduced photobleaching. It is equipped with Harmony®, an image analysis software for data collection from cell samples.
Images were analysed to acquire quantitative data to provide morphological information on cell shape, identification and segmentation of nuclei, cytoplasm, sub-cellular characteristics, such as focal adhesions, and expression of certain cellular markers. This was done in accordance with the creation of a cell pipeline for image analysis.

2.2.3.8 Statistical Analysis

One-way Analysis of variance (ANOVA) was used to compare the effect of the different SAPs on HOB. Graphpad Prisim 7 software (Graphpad 7 for Mac OS-X, Version 7.0c) was used for statistical analysis. The Harmony® software provided graphing of results.
Mean differences between peptides was considered statistically significant when p-value < 0.05.

2.3 HUVECs

2.3.1 Results and discussion

To understand the impact of different self-assembling peptides on HUVEC proliferation, HUVECs were cultured on the 5 individual peptides or a gelatin, as positive control[6,7], to perform a proliferation assay at 72 hours from the seeding. There was a statistically significant (p-value ≤ 0.001) reduction in HUVEC proliferation after 48 hours amongst all SAPs when compared to the gelatin control (**Fig 2.3**). In particular, DAR and EAK had the least reduction in proliferation, with DAR (mean= 58.44, SD=4.50) exhibiting an approximate cumulative reduction of 16% vs the gelatin control (mean=74.81, SD=2.99) 48 hours after EdU treatment, and EAK (mean=51.84, SD=5.88) with an estimated cumulative reduction of 23% vs the gelatin control. The results showed that EAOrn (mean= 32.47, SD= 9.28) gave the greatest reduction in proliferation, in comparison to the gelatin control, with an approximate cumulative reduction of 40% at 48 hours.

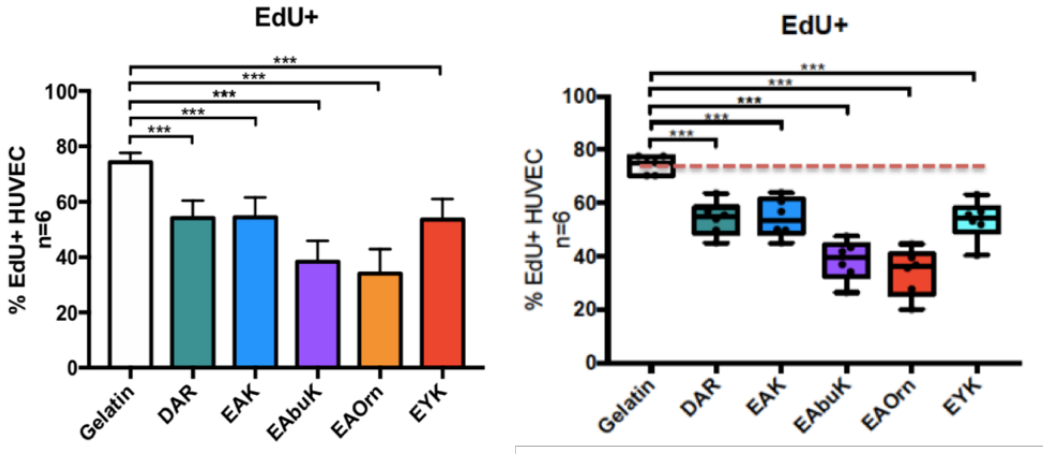


Figure 2.3. Effect of SAPs on HUVEC proliferation. Graph represents comparison of the effect of gelatin and SAPs coatings (DAR, EAK, EAbuk, EAOrn, EYK) on HUVEC proliferation at 48hrs using EdU as an index of proliferation (n=6). Error bars indicate standard deviation and *** indicates p≤ 0.001.

Qualitatively, cells cultured on SAPs expressed morphology analogous to specialised EC phenotypes such as elongated tip cells. The immunostained images highlighted a variation of morphology across the control and 5 peptides (**Fig 2.4**) consisting of elongated cells, migration and presence of cell clusters. It was clear that DAR induced a phenotype of elongation and migration, in comparison to the control, EAK, EAbuK, EYK and EAOrn, which all led to a lesser degree of elongation, with the development of cell clusters. Presence of clusters is a poor index of angiogenesis, and these were most prominent on cells on EAbuK, and minimal on DAR. Apoptotic ECs were more predominant on EAOrn, over the other peptides.

Overall, results from the proliferation assay support the notion that SAPs, in particular DAR, induced HUVECs to become less proliferative and adopt an angiogenic tip cell phenotype. Due to these findings, we investigated the mechanotransduction of HUVECs in response to different SAPs.

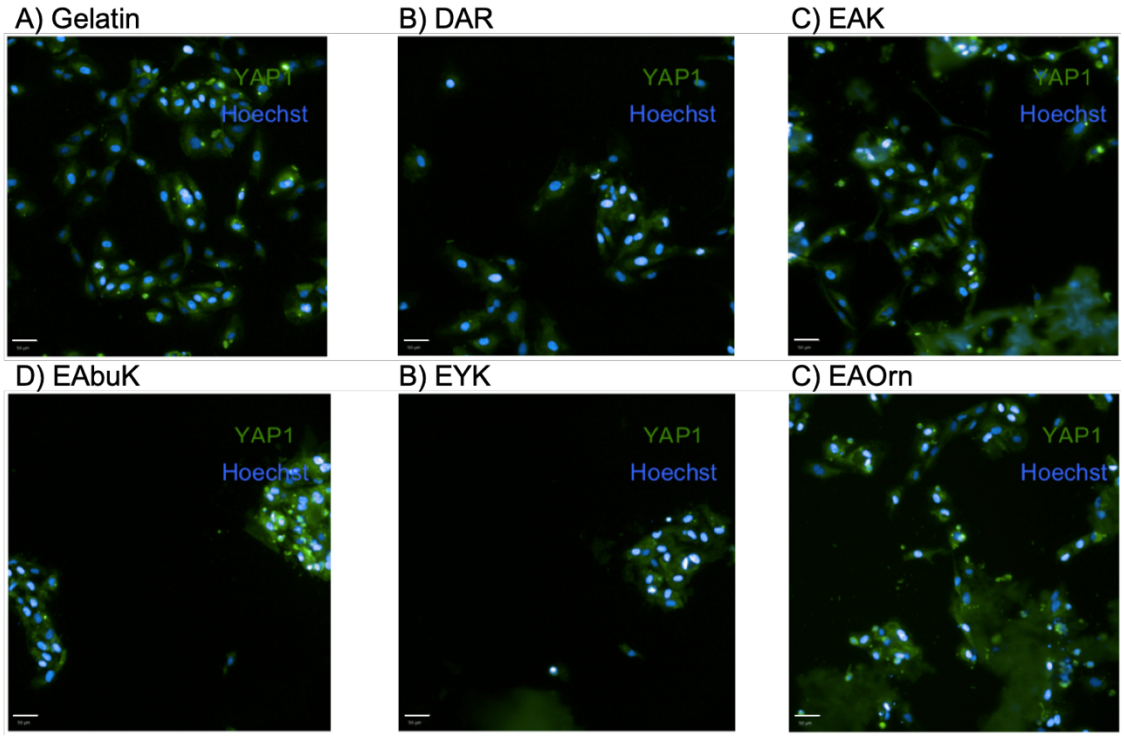


Figure 2.4. Immunomorphological analysis of HUVEC cultured on different self-assembling peptides for 72h. HUVECs were seeded onto the gelatin control and 5 SAPs and 72 hours after, cells were fixed and stained for YAP1 (green) and Hoechst for the nuclei (blue). Coatings used A) Gelatin, (B) DAR, (C), EAK, (D), EAbuK, (E), EYK, (F), EAOrn. (magnification = 10X OM, scale bar =50µm)

Mechanotransduction describes the induction of biochemical signals from mechanical forces and is an essential aspect of cellular function. We therefore sought to investigate how the ability to respond to mechanical stimuli is influenced by SAPs, using YAP1, a known mechanotransductor. HUVECs were cultured on five SAPs and gelatin as control. When comparing the expression of activated YAP1, there was a statistically significant (p-value ≤ 0.001) upregulation of YAP1+, (nuclear YAP1) in cells cultured in DAR, EAbuK and EAOrn (**Fig 2.5A**) DAR (mean=39.00, SD=4.82) had the highest upregulated expression, and showed 3 times increase in YAP1+ expression over the control (mean=12.45, SD=2.81), suggesting that properties of the DAR substrate were able to enhance mechanotransduction to modulate morphogenesis. However, there was no significant difference in YAP1+ expression in EAK (mean=19.77, SD=5.30) and EYK (mean=20.49, SD=5.90), when compared to the control. Immunostaining for YAP1 after 48 hours produced segmented images that demonstrated the distribution of varying

intensities of YAP1+ as cells experienced varied levels of stress during migration (**Fig 2.5C**). Varying YAP1 intensities across cells was used to construct a map of distribution (**Fig 2.5B**). The ratio of average intensity in the nucleus and average intensity in the cytoplasm was used to determine a threshold to identify cells positive or negative for YAP1, whereby ratio>1 was considered activated nuclear YAP1 and ratio<1 was inactivated cytoplasmic YAP1. This information was subsequently superimposed onto the segmented images, to produce a visible distribution map of YAP1+/- cells (**Fig 2.5D**).

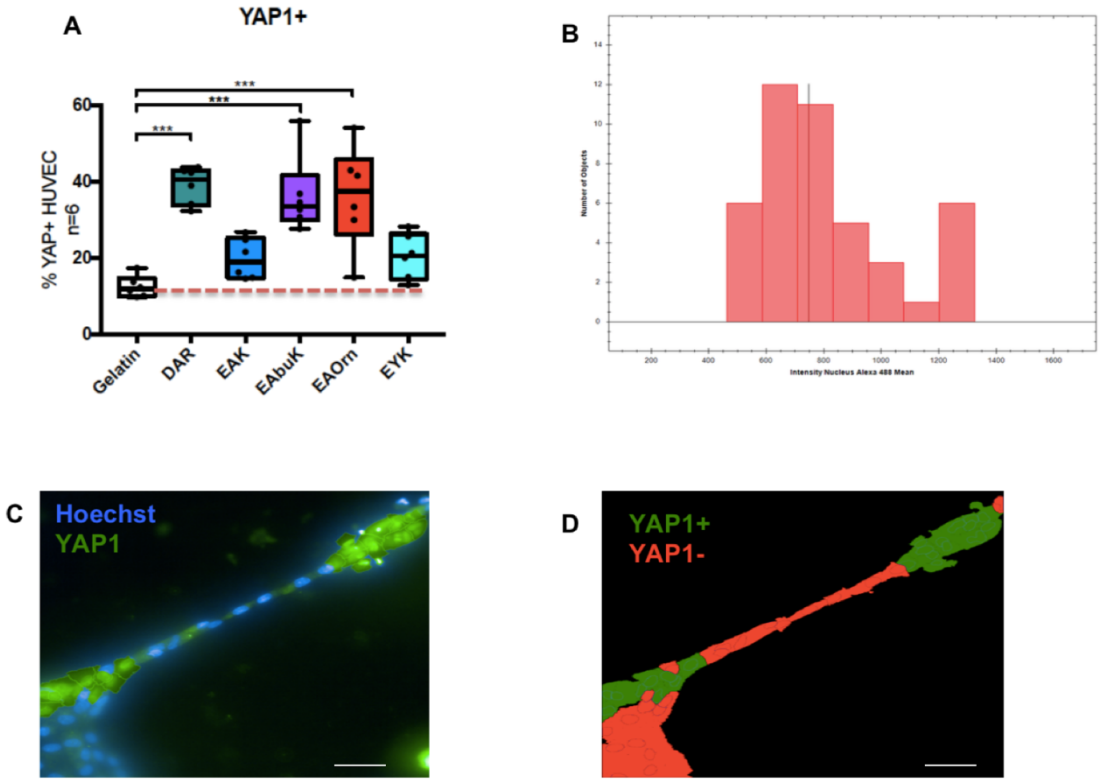


Figure 2.5. Analysis of nuclear and cytoplasmic YAP1 distribution for mechanotransduction **(A)** Graph represents comparison of the effect of gelatin and SAP coatings (DAR, EAK, EAbuK, EAOrn and EYK) on HUVEC mechanotransduction, using YAP1+ as an indicator (n=6). Error bars indicate standard deviation and *** indicates p-value ≤ 0.001. **(B)** Representation of the distribution of nuclear YAP1+ in cells with an established threshold to determine YAP1+/- cells. **(C)** Segmented image of HUVEC stained for Hoechst (nuclear stain, blue) and YAP1 (green) 48 hours after seeding (magnification = 20X OM, scale bar = 200µm). **(D)** Computer automated image of distribution of YAP1+/- across cell (magnification = 20X OM, scale bar =100µm).

HUVECs seeded onto matrigel form a network of tubular structures. Thus, we examined the ability of SAPs to influence tube-like structures' formation, by culturing HUVECs on matrigel alone or SAP-enriched matrigel. Since EYK gave the worst results both in terms of immunomorphological analysis and YAP1 expression on HUVECs, it has not been considered for the following experiments. Quantification of tubule length and nodes,

demonstrated a statistically significant increase in tubule length and number of nodes for all self-assembling peptides when compared to the matrigel control 24 hours after cell seeding (**Fig 2.6A**). EAbuK (mean= 1300.95μm, SD= 429.46μm) induced the highest tubule length formation, accounting for a 50.67% increase over the control. This was in comparison to EAK (mean= 1291.96μm, SD= 338.25μm), which had a 49.60% increase, and DAR (mean= 1240.43μm, SD= 402.04μm) with a 43.67% increase in tubule length.
The interquartile distance between 25th and 75th percentile was smallest for EAK and DAR, indicating these peptides had the most consistent and robust tubule length assay, which contrasted to the tube lengths formed on EAOrn (mean= 1299.08μm, SD= 494.22), with a significantly larger interquartile distance.
The number of nodes per assay was quantified as a measurement of network complexity. There was a statistically significant increase in the percentage number of nodes for all SAPs over the matrigel control, as demonstrated in **Figure 2.6B**. EAbuK (mean= 46.67μm, SD= 22.24μm) cultured cells formed the most complex networks with the highest number of nodes. Once again, DAR was the most consistent of the peptides, with the shortest interquartile distance between 25th and 75th percentile, suggesting it consistently induced complex network formation. This differed to EAOrn, which had the least consistency in number of nodes formed. Largely, we observed that cells cultured on SAPs, specifically DAR, induced the development of longer and more complex tubular structures.
Promotion of angiogenesis is essential to achieve the goal of tissue engineering. Along with fundamental parameters, such as biocompatibility, biodegradability, being sterilisable, optimal scaffold architecture and attaining minimise fibrosis, vascularisation of scaffolds is a crucial prerequisite for successful tissue engineering strategies, aiming to treat a variety of clinical problems. Many approaches for vascularisation have been explored, of which the use of a novel class of self-assembly peptides to enhance vessel formation is now being considered. Ionic self-assembly peptides are synthetic biomaterials that provide structural support to cells, similar to the ECM.
In this work, we screened five SAPs (DAR, EAK, EAbuK, EAOrn and EYK) in comparison to a gelatin or matrigel control, to assess the angiogenic potential and mechanotransduction response.
A recent work from our collaborating group at King's College investigated DAR for its role in promoting favourable angiogenesis (manuscript submitted). They demonstrated that DAR was able to induce HUVEC adhesion and activation towards an angiogenic tip cell, with development of morphogenetic changes, such as filopodia and lamellipodia, allusive to an activated migratory phenotype.
Furthermore, DAR coated scaffolds induced viable bone regeneration with vascularisation *in vivo*, highlighting the efficacy of functionalising biomaterials with DAR for implantation for bone tissue repair and regeneration.

Findings from the *in vitro* model were consistent with our observations that demonstrated HUVECs exposed to SAPs led to EC specification to an elongated migratory phenotype (**Fig 2.4**). This morphology was particularly prominent in cells cultured in DAR and EAK, and least expressed in EAbuK, which was characterised by the presence of apoptotic bodies and increased clusters of cells.

When compared to the control and other peptides, DAR exhibited the greatest amount of cell adhesion and phenotypical changes that allowed elongation and migration.

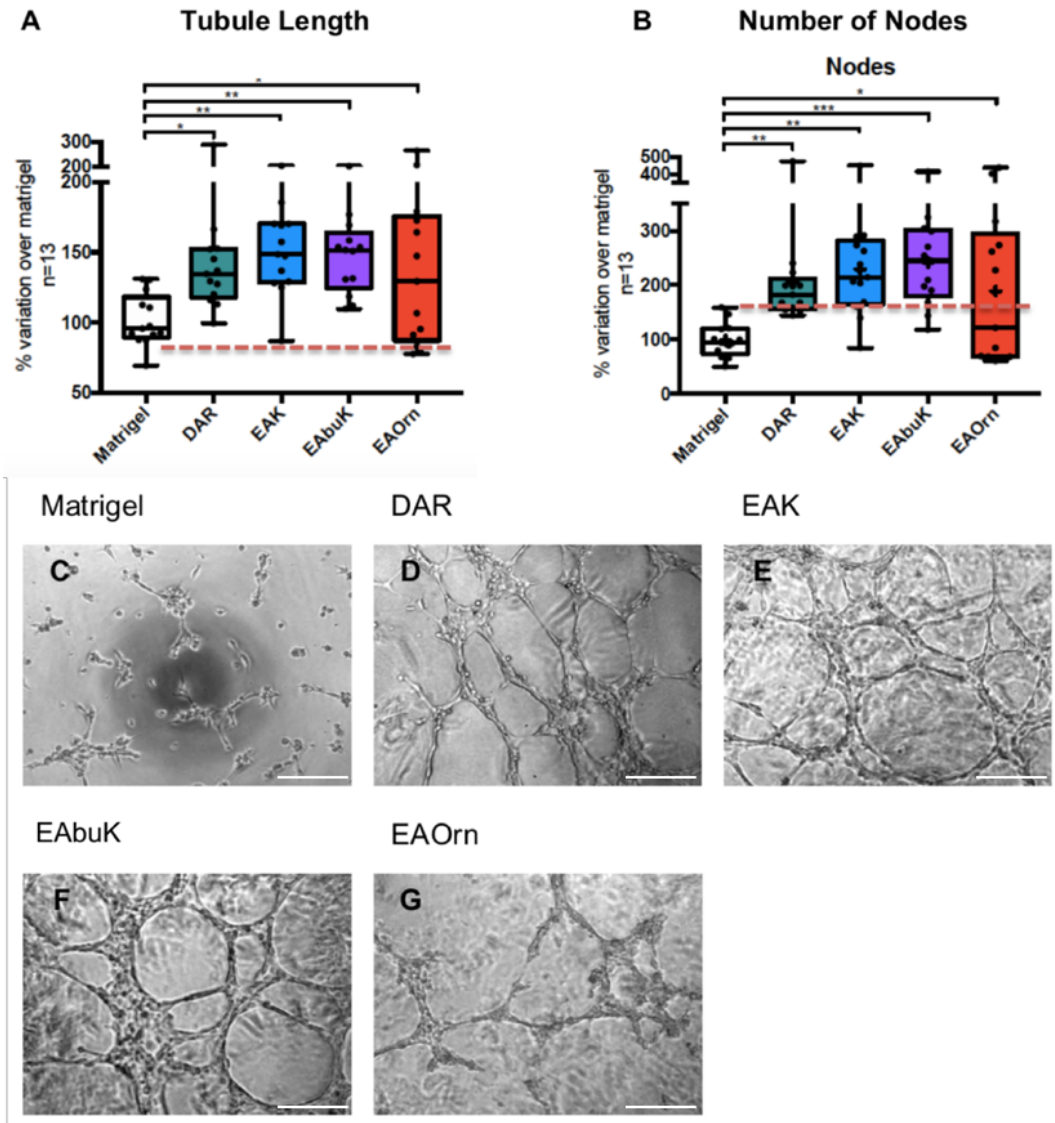


Figure 2.6. Tubule structure formation on SAPs and matrigel. **A**) Quantified tubule length formed by HUVECs cultured on matrigel and SAPs (DAR, EAK, EAbuK, EAOrn) after 24 hours. **B**) Number of nodes formed by HUVECs cultured on matrigel and SAPs after 24 hours (n=13). Error bars represent standard deviation, * indicates p-value≤ 0.05, ** indicates p-value≤ 0.01, and *** indicates p-value≤ 0.001. **C**), **D**), **E**), **F**), **G**) Characteristic images (10X, scale bars = 200µm) of tubular structure formation 24 hours after HUVEC cultured respectively on matrigel, DAR, EAK, EAbuK and EAOrn.

The variance in cell behaviour, concerning adhesion and migration, across the different peptides may be attributable to the differences in fibre architecture, as depicted by Siemenski *et al*, who compared capillary morphogenesis of peptides such as RAD16-II[8]. HUVECs cultured on RAD16-II formed complex elongated structures, in contrast to other peptides, KFE-8 and KLD-12, with different sequences. DAR16-II contains the same amino acids of RAD16-II but has different sequence, which may relate to the pro-angiogenic effects. This is in agreement with findings from Gambaretto and colleagues, who demonstrated the role of primary peptide sequences with varying polar/nonpolar amino acids still maintaining the periodicity of the EAK peptide family to form β-sheet structures, nanofibers and hydrogels[1].

We showed that the extent of angiogenic process such as adherence, elongation, migration and proliferation, correlated with the cellular perception of the mechanical environment. YAP1 is a mechanotransductor that regulates genes for proliferation and differentiation. In an activated state, YAP1 accumulates in the nucleus to facilitate transcription, and when inactivated, YAP1 is preserved in the cytoplasm. It has been illustrated that changes in matrix stiffness and bioavailability can upregulate YAP1 activity. As cells respond to the rigidity, organisation of stress fibres within the cytoskeleton occurs to impart cell spreading[9]. Furthermore, the EC lining of blood vessels are exposed to flow mediated stress and stimuli, which is one of the reasons why mechanotransduction occurs, to enable maintenance and remodelling. Along with tissue homeostasis, YAP1 has been associated with the development of malignant cancer, arising from growth of a metastatic niche due to changes in ECM mechanics and composition[10]. Although the molecular basis of how YAP1 controls downstream cellular responses is unknown, the knowledge would be of significant value to a plethora of fields, such as tissue engineering and oncology. In our work, we observed that nuclear YAP1+ expression was most prevalent in cells exposed to DAR, EAbuK and EAOrn, which links with our findings that cells exposed to DAR were more likely to adopt a migratory phenotype compared to the control and other peptides. This is in accordance with findings from Neto *et al*., demonstrating that nuclear YAP1+ is most present at the top of tip cells, responsible for migrating towards VEGF-A and sprout guidance[11]. This study also depicted the role of YAP/TAZ in encouraging the reorganisation of ECs by increasing junctional turnover, hence giving emphasis to the balance between stretch induced proliferation and remodelling to achieve adequate vascular patterning.

We perfumed a morphogenesis assay of HUVECs cultured on matrigel to investigate the formation of tubule like structures, similar to pre-vascular vessels. In our investigation of tubule length on matrigel alone and matrigel enriched with SAPs, DAR displayed the most consistent average tubule lengths, and along with EAK, formed the longest tubules. This could be associated with high YAP1+ activity at the tip cell, driving migration and thus

forming elongated structures. Quantification of nodes as a measure of structural complexity, showed the highest number of nodes for HUVECs seeded on EAbuK, however DAR had the most consistent findings. Greater numbers of nodes pertain to increased tip cell activity and would also contribute to total tubule length. The extent of tip cell branching could therefore be calculated in the future to support the notion that DAR and activated YAP1+ induce morphological differentiation of EC to exhibit less proliferation and more migration, leading to increased branching and interconnectivity. This functionally translates to an increase in tubule length and increase in number of nodes, which are an index of activated interconnected cells, able to form a network that is more angiogenic without being more proliferative. We found that the increase in differentiation was paralleled by a reduction in proliferative effects of the SAPs. There was a reduction in proliferation across all SAPs, particularly DAR, EAbuK and EAOrn. These peptides also expressed high levels of YAP1+ statistically, suggesting the negative effects of YAP1 on proliferation, regardless of changes in morphology towards a tip cell phenotype. However, this is in contrast to literature suggesting that YAP1+ activity leads to promotion of proliferation. Ragni *et al*. showed that nuclear translocation of YAP1 led to cardiomyoctye proliferation, and upregulation of genes involved in mesothelioma cell proliferation[12]. We hypothesise, that YAP1+ activity and regulation of cell proliferation and differentiation is still unclear, and may differ across cell types, warranting further research to understand this potential variance. Unfortunately, we have shown the peptide influence on angiogenesis in an *in vitro* setup, which is unable to mimic the complexity of the ECM, as doable *in vivo*. In terms of YAP1, it is still unclear why the peptides upregulated YAP1 expression, yet had varied proliferation and differential morphogenesis. We can speculate that DAR is more effective at supporting angiogenesis, and EAK for vascular maintenance for progression. However, to confirm this, further studies must be carried out, and further work is required to understand the wider context of the role of self-assembling peptides and YAP1 mediated activity. This would include repeating experiments, conducting 3D and *in vivo* assays, and integrating the use of induced pluripotent stem cell derived endothelial cells (IPSC-ECEF) and growth factors, such as VEGF and sonic hedgehog. These are established by cell to cell contact, and bound to the matrix at varying concentrations, and hence would provide further insight. Although we have developed a method to understand how YAP1+ is distributed in 3D, we are yet to analyse this to attain a detailed molecular understanding of this distribution.

In this study, we provide a viable strategy to investigate the use of SAPs to maximise EC cell differentiation to an angiogenic phenotype, for use in tissue engineering. Furthermore, this can be applied to aid design and screening of scaffolds to enhance vascularisation and tissue regeneration such as bone, incorporation of peptide motifs in SAPs to improve cell-material interactions, and for use in drug delivery. By studying the effect of mechanical

signals on vascular development, it can be used to as a tool to improve control over capillary organisation, through tuning stiffness of scaffolds to direct favourable cell behaviour.

2.3.2 Conclusions

The aim of this study with HUVECs was to understand the influence of self-assembly peptides on *in vitro* angiogenesis. To achieve this, we screened five different SAPs to assess the direct impact on HUVEC proliferation, molecular effect of distribution of YAP1 and functional influence on network formation. Using a combination of HUVEC cell culture assays, we found that SAPs were effective at inducing vascularisation vs gelatin and matrigel controls. We then used immunofluorescence to observe the morphological changes, as a result of SAP exposure.

DAR was consistently the most successful peptide at inducing differentiation to an angiogenic phenotype, increased YAP1+ expression and formation of long and complex tubule structures.

EAK showed good results in terms of cells morphology and formation of long tubule structures, too.

2.3.3 Materials and methods

2.3.3.1 Cell Tissue culture, seeding, fixation and permeabilisation

Human Umbilical Vein Endothelial Cells (HUVEC) were commercially obtained (PromoCell) at Passage 0, and cryopreserved for storage before initiating the experiments. The cells were stored at -80°C in freeze mix solution (90% FBS and 10% DMSO). The cells were maintained in endothelial growth medium 1 (EGM1) or endothelial growth medium 2 (EGM2) (PromoCell). EGM2 was used for fast proliferation of HUVEC cells because it contains a range of growth factors such as VEGF, insulin-like growth factor, epidermal growth factor and basic fibroblast growth factor (bFGF); whereas EGM1 contains very little or none of the growth factors in EGM2, hence it was used for normal HUVEC proliferation that resembles physiological environment. Only cells from passage 1 to passage 6 were used and cells from passages beyond 6 were discarded. Cells were seeded onto plates, coated with self-assembly peptides and either gelatin or matrigel (PromoCell) as the control. Once cells reached confluency, they were trypsinised. 2ml of trypsin-cell dissociation enzymatic solution was added to the cells and cells were allowed to detach, and the cells were centrifuged for 5 minutes at 1.2RPM. The supernatant was removed and the cell pellet was resuspended in 2ml of media. Cells were counted, and a cell suspension of the appropriate seeding density was prepared, and subsequently pipetted into each well in either a 96 well plate (Nunc, Thermofisher) or µ-slide Angiogenesis (Ibidi), depending on experiment. The culture plates were then incubated in a 37°C 5%

CO_2 incubator (Heracell™, Thermo Scientific) and regularly observed for growth under a light microscope till confluency. Cells were fixed and permeabilised in order to preserve cell structures, maintain antigenicity for immunohistochemistry and allow cells to be immunostained with larger molecules such as antibodies. Culture medium was removed from the wells and cells were washed twice with PBS with Ca^{2+} and Mg^{2+} and placed under agitation at room temperature for 5 minutes. Fixation was carried out using a cross linking agent, paraformaldehyde (PFA). 2% PFA with PBS enriched with Ca^{2+} and Mg^{2+} was then added and placed under agitation at room temperature for 15 minutes. The 2% PFA was then removed and cells were washed with PBS enriched with Ca^{2+} and Mg^{2+} twice. Permeabilisation was done using the detergent 0.1% TritonX-100. 0.1% TritonX-100 in PBS was added to the cells and let at room temperature for 5 minutes. This was then removed and washed with PBS enriched with Ca^{2+} and Mg^{2+}. The PBS was removed and cells were placed in blocking solution, constituted of 1% FBS in PBS. Cells were left in blocking solution for at least 45 minutes. When fixing matrigel assays, 4% PFA was added directly to the media with no preceded washes. Cells were agitated for a shorter time of 5 minutes, and then washed once with PBS enriched with Ca^{2+} and Mg^{2+}.

2.3.3.2 Cell Staining

In this project, the indirect immunostaining method was used to stain HUVECs on SAP constructs. The protocol followed for YAP1 immunostaining was the same of the one used for HOB (paragraph 2.2.3.4). The cells were counterstained with Hoechst (Sigma, diluition 1:2000 in PBS plus Ca^{2+} and Mg^{2+}.) for nuclei staining and Phalloidin (Sigma, diluition 1:5000 in PBS plus Ca^{2+} and Mg^{2+}) for actin cytoskeleton staining. To stain with Phalloidin, HUVECs were placed under agitation for one hour, and when Hoechst was used individually, they were agitated for only 10 minutes. The cells were then washed twice with blocking solution and finally left in PBS. All stains used across experiments are reported in **Table 2.2**.

Table 2.2. Fluorescent dyes and target structures.

STAIN	TYPE	TARGET	SOURCE
HOECHST	Chemical	Nucleus	Sigma
PHALLOIDIN	Chemical	Actin filaments of cytoplasm	Sigma
ANTI-YAP1 antibody [EP1674Y] (ab52771)	Recombinant rabbit monoclonal antibody	Binds to YAP	Abcam
ALEXA FLUOR®-488) (AB150077)	Anti-Rabbit Goat polyclonal secondary	Binds to Anti-YAP1 antibody	Abcam

2.3.3.3 Preparation of SAP/Gelatin coatings

Porcine gelatin was used a control for three experiments, which respectively investigated HUVEC adhesion, HUVEC immunomorphology and HUVEC proliferation with SAPs.

0.5% gelatin in PBS with Ca^{2+} and Mg^{2+} was prepared and sterilised by autoclave. 100µl of 0.5% gelatin in PBS was kept aside for use as the control, and 30µl was pipetted into the first set of triplicate wells of a 96 well plate. A solution of gelatin and SAP, for each peptide, was then prepared at a dilution of 1:10 by mixing 10µl of each SAP's stock solution (paragraph 2.2.3.2) with 90µl of gelatin. 30µl of the solution was pipetted into each triplicate well, corresponding to the peptide. Preparation of the solution and coating of the wells for each SAP was conducted separately one by one, to prevent peptide self-aggregation prior to coating. The presence of the free ions within the solution would allow the peptides to immediately self-assemble. The coated plate was left for 24 hours in a 37°C 5% CO_2 incubator to allow a better self-aggregation of the SAPs before cell seeding. For HUVEC adhesion experiment, 5×10^3 cells were seeded per well in EGM2, placed in a 37°C 5% CO_2 incubator and fixed after 1 hour to subsequently stain for Hoechst, Phalloidin, and YAP1. For HUVEC morphology, 1.5×10^4 cells were seeded per well in EGM1, kept in a 37°C 5% CO_2 incubator, and fixed after 48 hours, followed by immunostaining.

2.3.3.4 SAPs/matrigel assays

Matrigel was used as a control and in solution with the five SAPs to assess tube formation and HUVEC immunomorphology. A µ-slide Angiogenesis Slide (**Fig 2.6**) was used to provide enhanced image acquisition and visualisation without meniscus formation and allowing cells to be in one focal plane, due to the well within a well design.

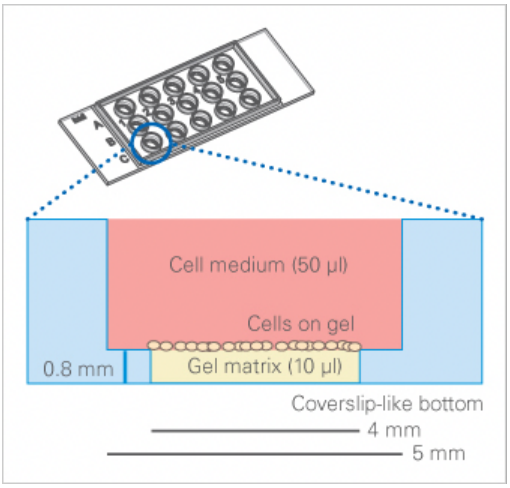


Figure 2.6 Schematic drawing of the well within a well design of the µ-slide Angiogenesis Slide (Ibidi)

For matrigel assays a 15 well µ-slide Angiogenesis plate was used. Whilst working on ice, 500µl of EGM2 was added 1:1 to dilute matrigel, and mixed thoroughly. 50µl of matrigel solution was kept aside, on ice, as the control, and 10µl was pipetted into the first set of triplicate wells. A solution of matrigel and SAP, for each respective peptide was prepared at a dilution of 1:10, with 40µl of peptide stock solution (paragraph 2.2.3.2) mixed with

400µl of matrigel. 10µl of the solution was then pipetted into each triplicate well, allocated to the peptide. The coated slide was then placed in a 37°C 5% CO_2 incubator for 30 minutes, to allow the matrigel to set. $1x10^4$ HUVECs were seeded per well in EGM1, placed in a 37°C 5% CO_2 incubator and fixed after 24 hours. The volume of SAP/matrigel solution, the HUVEC seeding density, the choice of growth medium and the method of fixation, were factors that were optimised.

Using a µ-slide Angiogenesis plate, wells were coated with 10µl and 11µl of SAP/matrigel solution, and incubated at a 37°C 5% CO_2 for 30 minutes, to assess which volume would have reduced meniscus formation and produce images with greater clarity. Once the matrigel had gelified, 3×10^3, 5×10^3 and 1×10^4 HUVECs were seeded onto the coated wells, half suspended in EGM1 and half in EGM2. The plate was placed in a 37°C 5% CO_2 incubator for 3 hours and observed under a light microscope.

Cord formation was well defined and markedly greater in wells coated with 10µl of SAP enriched matrigel with 1×10^4 cells in EGM1. Therefore, subsequent matrigel assays were carried out using these optimum conditions. Fixation of the matrigel assays originally consisted of washing with PBS twice, fixing 2% PFA with PBS, followed by washing twice before leaving cells in blocking solution. This protocol resulted in significant cell loss due to drying and excessive washing. To minimise cell loss, 4% PFA with PBS was directly added to the cell media without prior washing, followed by a single wash with PBS before leaving cells in blocking solution.

2.3.3.5 HUVEC proliferation assays

A proliferation assay was done to compare the extent of HUVEC proliferation for each SAP. 5×10^3 HUVECs suspended in EGM1 were seeded onto SAP/gelatin coated wells on a 96 well plate (paragraph 2.3.3.3). The plate was placed in a 37°C 5% CO_2 incubator for 24 hours and subsequently treated with the initial pulse of EDU (5- ethynyl-2'-deoxyuridine), according to the protocol outlined in Click-iT proliferation kit (ThermoFisher) After 48 hours in a 37°C 5% CO_2 incubator, cells were fixed and permeabilised. The stain with EDU was added according to the protocol outlined in Click-iT proliferation kit and agitated for 30 minutes. Cells were then stained for Hoechst and YAP1, and imaging was done using the Operetta High-Content imaging system. EDU is a thymidine nucleoside analogue, and is an index of cell proliferation, as cells grown in the presence of EDU incorporate a thymidine base during the S phase, which is attached to a fluorophore label and allowing detection of proliferation cumulatively after addition of the initial EDU pulse.

2.3.3.6. Imaging and image analysis

All images where taken with the Operetta CLS™ High-Content Imaging System (Perkin

Elmer), equipped with Harmony® software for image analysis. Images were analysed to acquire quantitative data to provide morphological information on cell shape, identification and segmentation of nuclei, cytoplasm, sub-cellular characteristics, such as focal adhesions, and expression of certain cellular markers. This was done in accordance with the creation of a cell pipeline for image analysis. Matrigel assays images were analysed using the Angiogenesis Analyser tool on ImageJ.

2.3.3.7 Measuring HUVEC networks' architecture

Each phase contrast image was processed before quantification. Backgrounds and artefacts found in the images were selected manually using the function "Freehand selections" and blurred using the "Blurring Mask Tool" of the Angiogenesis Analyser Macro in ImageJ.
In order to accurately select the background and artefact without including any HUVEC network, the "freehand selection" was done using an iPencil and iPad. An example of before and after blurring were shown in **Figure 2.7**.

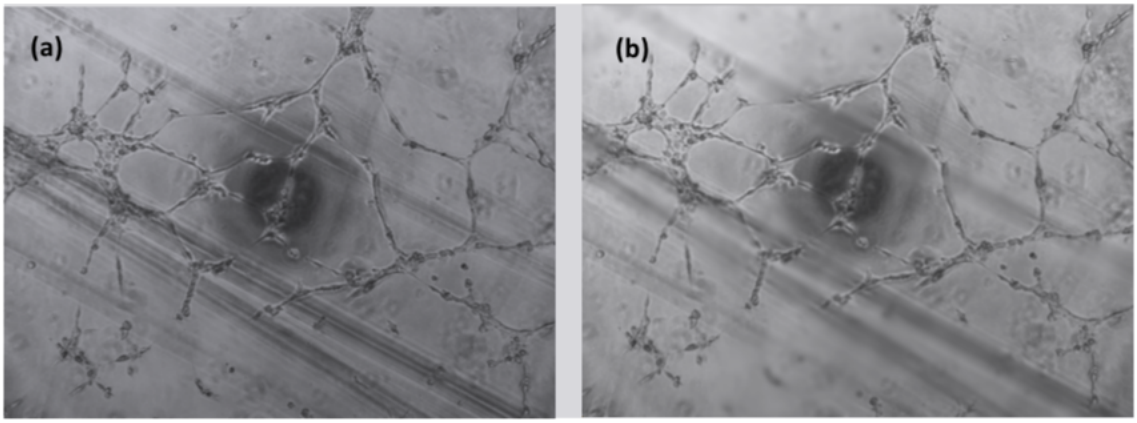


Figure 2.7. Phase contrast image before (**a**) and after (**b**) manual processing. Images were zoomed in for better illustration. Original phase contrast images were taken at 4X OM.

Total number of nodes and total length of network was determined using the "Analyse HUVEC Phase Contrast" function of the Angiogenesis Analyser Tool in ImageJ. Results were compiled into a Microsoft Excel document automatically by the software. The absolute values of total number of nodes and total length of network were converted to percentage change to control manually.

2.3.3.8 Statistical Analysis

One-way Analysis of variance (ANOVA) was used to compare the effect of the different SAPs on HUVECs. Graphpad Prisim 7 software (Graphpad 7 for Mac OS-X, Version 7.0c) was used for statistical analysis. The Harmony® software provided graphing of results. Mean differences between peptides was considered statistically significant when p-value < 0.05.

2.4 Macrophages

2.4.1 Results and discussion

Monocyte adhesion is a crucial step for its differentiation into macrophages[13]. Therefore, we designed an experiment to study how various SAP/gelatin coatings could induce monocyte adhesion. THP-1 cells were seeded on SAP/gelatin coated plates and the number of cells that adhered to the coating and their average cell area (i.e. cell spreading) were measured 1 hour after seeding.

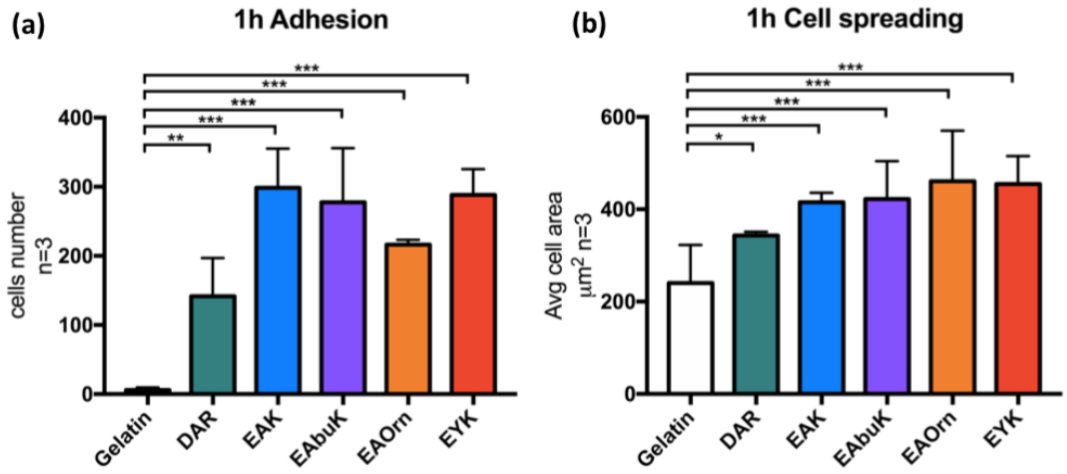


Figure 2.7. THP-1 adhesion assay on various SAP/gelatin coated wells (n=3). **a**) Number of cells adhered to the various SAP/gelatin coating 1 h after seeding. **b**) Average cell area of the adherent cells. Data are shown as mean ± SD. *p-value<0.05, **p-value<0.01, ***p-value<0.001

As shown in **Figure 2.7a**, the average number of cells adhered to the SAP/gelatin coated plates were all significantly higher than that of the gelatin coated plate (control). There was 25 to 53-fold increase in the number of cells adhered when various SAPs of the EAK family were added to the gelatin-based coating solution. The results were also highly significant, where the p-value of EAK, EAbuK, EAOrn and EYK when compared to gelatin were all less than 0.001 and the p-value for DAR was less than 0.01. The highest number of adhered cells to the lowest among the SAP/gelatin coated plates were detected for EAK, followed by EYK, EAbuK, EAOrn and DAR. It is interesting to note that the average number of cells adhered to the DAR/gelatin coated wells was the lowest among other SAP coated wells. To assess the THP-1 cells' affinity to the coating material, average cell area was measured as an indication of how flat the cells were spreading on top of the coating. As shown in **Figure 2.7b**, the THP-1 cells on SAP/gelatin-coated wells had significantly larger surface area as compared to gelatin-coated wells (control). We observed an average surface area of cells in SAP/gelatin-coated wells 1.4 to 1.9 times larger than those in gelatin/coated wells. Cells in EAOrn-gelatin coated wells exhibited the highest average cell spreading,

followed by EYK/gelatin, EAbuK/gelatin, EAK/gelatin and DAR/gelatin in descending order. It is once again interesting to note that cells in DAR/gelatin coated wells showed the least spreading when compared to cells on other SAP/gelatin coatings. Using the protocol outlined in section 2.4.3, we differentiated THP-1 cells into macrophages (M0) using PMA and further polarised them into M1 phenotypes using IFNγ and LPS and M2 phenotype using IL4. Qualitative observations were made based on the phase contrast images taken at various time points during this process (**Fig 2.8**).

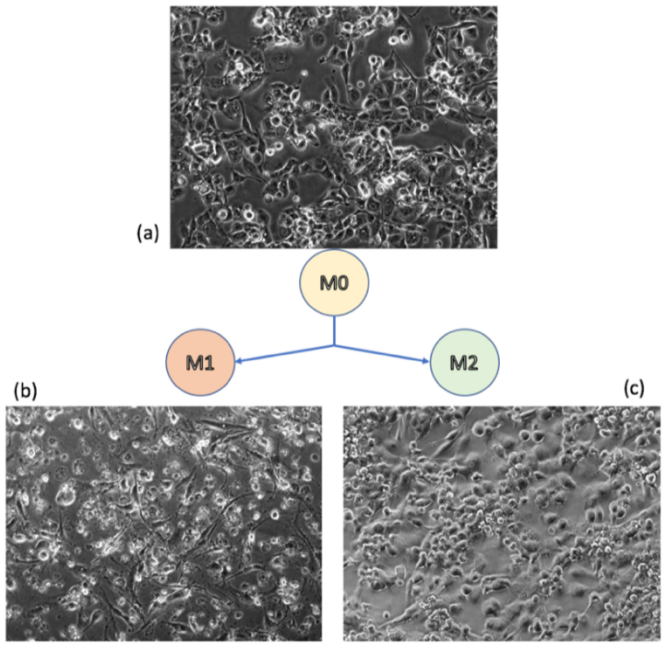


Figure 2.8. Phase contrast images of (**a**) macrophages derived from THP-1 cells (**b**) M1 macrophages and (**c**) M2 macrophages, showing distinct morphological differences. Images were taken from gelatin-coated wells at day 4 (**a**) and day 7"(**b**)(**c**). Images were zoomed in for better illustration. Original phase contrast images were taken at 20X OM.

We observed morphological changes to the THP-1 cells as they are differentiated into M0 and polarised to M1/M2 and these changes were consistent in every experimental condition that was treated according to the protocol. Three days after PMA was added to the THP-1s, the cells became adherent and developed lamellipodia and filopodia, stretching the cell into various irregular shapes. The M0 cells were also larger than THP-1 cells, with a lower nucleocytoplasmic ratio since we observed an increase in their cytoplasmic volume. Three days after adding the polarising agents (i.e. IFNγ, LPS and IL4), both M1 and M2 cells developed longer lamellipodia and filopodia, resulting the cells to adopt an elongated cell shape. In addition, M1 macrophages appeared to be more elongated than M2 macrophages. Immunofluorescence analysis was conducted to ascertain that THP-1 cells were polarised into M1/M2 and assess how various SAPs could influence M1 and M2 surface marker expression, which could in turn influence their angiogenic potentials. Unfortunately, we

were unable to obtain reproducible viable images suitable for data analysis, due to the large background noise, which made it impossible to distinguish cells from the background. A possible explanation was insufficient washing which resulted in the failure to remove unbound fluorescent antibodies witheld by the self-assembling peptides. As a result of time constraint, it was not possible to repeat this part of the study; hence future work would allow modification of the protocol to optimise the blocking step and washing solution.

To understand how SAP-polarised M1 or M2 can affect HUVEC cord network formation using their secreted factors without any cell-cell contact, we performed a functional matrigel-HUVECs assay, in which HUVECs were seeded on to matrigel that was conditioned with SAP-polarised M1/M2 secreted factors and we measured total length of the network and the number of nodes. As shown in **Figure 2.9a** and **2.9b**, HUVECs that were seeded on matrigel conditioned by DAR-polarised M1 formed networks with significantly greater total length (23% increase) and total number of nodes (26% increase) compared to HUVECs on matrigel conditioned by gelatin-polarised M1 (control).

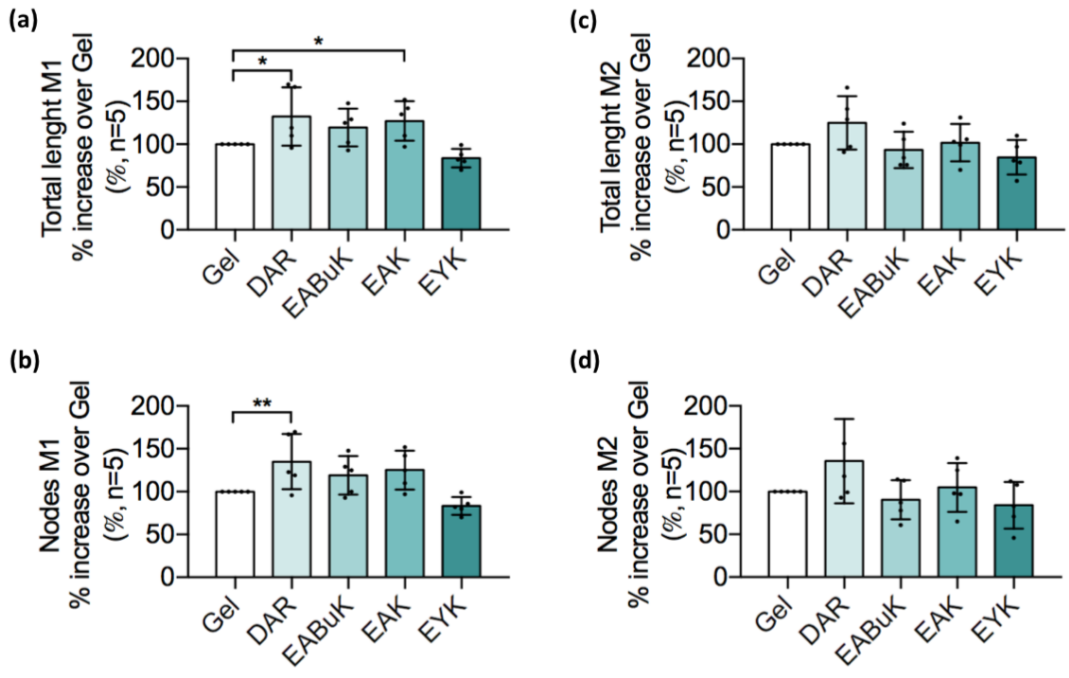


Figure 2.9. Matrigel-HUVECs angiogenesis assay on SAP-polarised M1/M2 (n=5) (**a**) Total length of HUVEC network on matrigel conditioned by SAP-polarised M1 macrophages. (**b**) Total number of nodes found in HUVEC network on matrigel conditioned by SAP-polarised M1 macrophages. (**c**) Total length of HUVEC network on matrigel conditioned by SAP-polarised M2 macrophages (**d**) Total number of nodes found in HUVEC network on matrigel conditioned by SAP-polarised M2 macrophages. Results were expressed as percentage over gelatin (control). Data are shown as mean ± SD. *p<0.05, **p<0.01.

In addition, EAK-polarised M1 also increased in total network length (20% increase) but did not significantly increase the total number of nodes. Although it was not statistically

significant, it was nonetheless interesting to note that EYK-polarised M1 was the only one that reduced the total length and total number of nodes in the HUVEC network. The trends in total length mirror the total number of nodes.

As shown in **Figure 2.9c** and **2.9d**, matrigel conditioned by SAP-polarised M2 macrophages did not significantly increase or decrease the total length or total number of nodes in the HUVEC network when compared to matrigel conditioned by gelatin-polarised M2 macrophages (control). Despite statistical insignificance, it is still interesting to note that DAR-polarised M2 was the one that resulted in the greatest network length and highest number of nodes. The trends in total length once again mirror the total number of nodes.

Numerous *in vitro* and *in vivo* studies have demonstrated that SAPs of the EAK family could induce angiogenesis and tissue regeneration at the site of injury[14]. However, their effects on macrophage polarisation, which play an important role in regulating angiogenesis and wound healing[15], is an area that has been ignored by the researchers and poorly understood. According to Spiller and Koh[16,17], M1 macrophages produce pro-inflammatory cytokines which initiates angiogenesis in the early stage of tissue repair while M2 macrophages stabilise angiogenesis by promoting fibroblast proliferation, recruiting pericytes and encouraging ECM production in the later stages. Therefore, it is essential understand if SAPs of the EAK family could modulate macrophage polarisation (i.e. upregulate or downregulate M1/M2 phenotype), so that appropriate SAP may be utilised to promote the timely shift from M1 to M2. Such strategy would be highly desired because it harnesses the body's own natural healing response to promote regeneration. In this study, we found all of the tested SAPs to promote monocyte adhesion while DAR and EAK-polarised M1 were able to promote HUVEC network formation via their secreted factors. The results suggest that SAPs could potentially be used to induce angiogenesis via their influence on macrophage polarisation.

We showed that all five SAPs could induce monocyte adhesion, which is the first step of a series cellular events that leads to macrophage polarisation. Adding SAPs of the EAK family to the gelatin-based coating solution led to a 25 to 53-fold increase the number of cells adhered. This finding is consistent with a similar study conducted using mouse neural cells and RAD16, another member of the EAK family, in which RAD16 promoted cell adhesion. Another study demonstrated that a variety of mammalian cell types were able to attach to RAD16 and EAK hydrogel, including fibroblasts and keratinocytes[18]. In addition, SAPs have been widely used in tissue engineering as nanofiber scaffolds and have demonstrate capacity to induce cell adhesion, and promote survival[14]. Since cell adhesion triggers a cascade of signal pathway that promote cell survival, proliferation and differentiation[19] in the same way, it is possible that when THP-1 cells adhere to the SAP/gelatin coating, their cellular function may be altered. Therefore, further mRNA and cell marker analysis are needed to test this hypothesis. Although the reason for their affinity

towards SAP coating was not formally explored in this study, past literature could offer potential explanations. It is established that SAPs can form hydrogel made of nanofibers when exposed to ionic solution and the structure of the hydrogel resembles the structure of extracellular matrix[19], which may lead to THP-1 adhesion. Moreover, cell attachment is often mediated by surface receptors such as integrin, selectin and cadherin. Hence, the molecular structure of the SAP hydrogel could bear resemblance to proteins these surface receptors can recognise. On the contrary, one study found that the cell attachment was not mediated by integrin. Instead, the author attributed the cell's affinity towards SAPs of the EAK family to the presence of uniformly distributed charged residue within the peptide[18]. Hence, further studies are needed to understand the underlying cellular mechanism of THP-1's affinity towards SAPs.

We observed clear morphological changes to the THP-1 cells as they are differentiated into M0. 3 days after PMA was added to the THP-1s, the cells became adherent and developed lamellipodia and filopodia, stretching the cell into various irregular shapes. Such change in morphology was also observed in other studies, despite the difference in the reagents used (e.g. Vitamin D3 and macrophage colony stimulating factor) and duration of treatment[15,20,21]. Macrophage differentiation is associated with a reduction in the nucleocytoplasmic ratio due to an increase in cytoplasm volume[22]. As anticipated, the M0 cells appeared to be larger than THP-1 cells, with a lower nucleocytoplasmic ratio. 3 days after adding the polarising agents (i.e. IFNγ, LPS and IL4), both M1 and M2 cells developed longer lamellipodia and filopodia, resulting the cells to adopt an elongated cell shape. In addition, M1 macrophages appeared to be more elongated than M2 macrophages. There are conflicting evidence regarding the morphological differences between M1 and M2: Zajac *et al*. found M1 appeared more elongated than M2, which is consistent with our finding while McWhorter *et al*. found the opposite where M1 appeared more rounded as compared to M2. This seemingly contradictory finding could be the result of using different polarizing agents. In the study conducted by McWhorter *et al*., IL13 was used in conjunction with IL4 as M2 polarising agent, while Zajac *et al*. used the same set of polarising agents as our study. Despite the difference in morphology, both studies were able to obtain functional M1 and M2 cells, with distinctive phenotype-specific gene expression pattern and surface markers. Such evidence supports our hypothesis that the 3-day PMA treatment followed by 3-day IFNγ or LPS/IL4 treatment was sufficient to differentiate THP-1 cells into M0 macrophages and further polarise them into M1/M2 phenotypes. However, flow cytometric analysis of macrophage phenotype markers such as CCR7, CD206, CD163 and HLADR could further strength such claim[15].

We were able to measure the total length and total number of nodes of the HUVEC networks using the "Analyse HUVEC Phase Contrast" function of the Angiogenesis Analyser Tool in ImageJ. However, every image must be manually processed using the

blurring function before the analysis because the software was unable to accurately detect HUVEC network based on unprocessed phase contrast images. Artefacts and background were often mistakenly detected as part of the network. Such issue could be avoided if fluorescent HUVECs were used to form network on matrigel, so that the images produced would contain significantly less artefacts and background noise.

Functional matrigel/HUVEC assay was performed to assess how SAP-polarised M1/M2 could influence HUVEC network formation with their secreted factor only without any cell-cell contact. This was achieved by incubating the matrigel on top of the macrophages for 24 hours, allowing the secreted factors such as VEGF to diffuse into the matrigel.

The fact that increase in HUVEC network formation (although not all statistically significant) was observed in matrigel conditioned by DAR, EAbuK and EAK polarised M1 cells suggests that macrophage secreted factors were able to diffuse across the matrigel and influence HUVEC network formation. Such diffusion-based experiment set-up is a novel approach to matrigel/HUVEC assay because it is more common to use macrophage conditioned media to influence HUVEC network formation instead of macrophage conditioned matrigel[15,23].

Matrigel/HUVEC is considered a 2.5D assay that only examines HUVEC network formation without cell-cell contact, therefore further studies should be conducted using 3D collagen or fibrin HUVEC assay, in which macrophages and HUVECs are suspended in the matrix and allowed to interact directly.

In this study, we found that the HUVEC network on matrigel conditioned by DAR-polarised M1showed 23% increase in total length and 26% increase total number of nodes compared to control. In addition, EAK-polarised M1 also increased in total network length (EAK) but did not increase the total number of nodes. However, no significant increase in network formation was observed for DAR or EAK-polarised M2. As previous studies have shown, MMP-9 expression level is the key factor that increase network formation in matrigel-HUVEC assays, since MMP-9 is a potent stimulator for vascular remodelling that allows endothelial cells to migrate[15,24]. Moreover, M1 phenotype express higher level of MMP-9 than M2, while M2 express high level of TIMP3, an inhibitor of MMP-9. In the context of *in vitro* HUVEC network formation, stiff and non-compliant gels tend to inhibit network formation while soft gels encourage HUVEC cell migration, thus promoting network formation[25]. Because the initial stiffness of the matrigel was the same across every experimental condition, the increase in network formation on matrigel conditioned by DAR and EAK-polarised M1 may be explained by the increased level of MMP-9, which cleave the ECM proteins in matrigel, making the gel softer and more compatible for HUVEC migration and network formation. Such evidence highly suggests DAR and EAK can increase M1's expression of MMP-9. The lack of increase in the SAP-polarised M2 could be due to their innate low expression of MMP-9 or high expression of TIMP3.

Gene expression analysis could further strengthen this hypothesis. It is worth noting that the M2 cells used in this study were in fact M2a, a subtype of M2 which can be obtained by IL4; while M2c, another M2 subtype obtained using IL-10, can produce highest level of MMP-9 and minimal level of its inhibitor, TIMP3 among all M1/M2 population[15]. Therefore, it would be worthwhile to explore the effect of DAR and EAK on M2c polarisation using Matrigel/HUVEC assay. M2a macrophages on the other hand produce high level of PDGF, a factor that recruits pericytes, which can in turn stabilise the newly form blood vessels. Hence, a 3D collagen assay that incorporates HUVECs, pericytes and SAP-polarised macrophages could further elucidate the effect of SAPs on M2 polarisation.
It is interesting to note that while DAR was the most effective SAP in promoting M1-induced HUVEC network formation, DAR was also the SAP to which THP-1 cells showed the least affinity (i.e. cell spreading); the opposite was true for EYK. Furthermore, we noticed the trend in M1-induced network formation (**Fig 2.9a** and **2.9b**) was the inverse of the trend in THP-1 cell spreading (**Fig 2.7b**). This finding suggests a possible link between THP-1 cell spreading and M1 protein expression.
The increase in THP-1 spreading may have triggered a signalling cascade that would later inhibit M1 polarisation and their cellular activity. We also observed that the trends in total length mirror the total number of nodes. This finding was consistent with previous studies[15,24], thus suggesting a possible correlation between the length and complexity of HUVEC network. Further studies are needed to test these hypotheses and reproducibility of the observed correlations.
EGM2 was used as the media for HUVECs during 18 hr incubation on matrigel because EGM2 contains a range of growth factors (e.g. VEGF and bFGF) that were implicated in inducing endothelial cell migration. Despite their pro-angiogenic roles, VEGF and bFGF may inhibit HUVEC network formation on matrigel. Previous studies found that VEGF and bFGF disrupts HUVEC network formation *in vitro* because they induce increased cell migration which leads to network instability[25]. Hence, it was possible that the use of EGM2 negatively affected the HUVEC network formation and EGM1, which has no VEGF and bFGF, should be used instead.
We plan to systematically characterise the SAP-polarised M1/M2 by conducting mRNA analysis and further repeating the immunofluorescence analysis, so that we can fully understand the effect of SAPs on macrophage polarisation.
We are currently developing a 3D collagen assay that incorporates HUVEC, pericytes and macrophages to assess how SAP-polarised M1/M2 could affect HUVEC vasculogenesis as well as stability of the newly formed network. The effect of various SAPs on M2c macrophages will also be explored using various *in vitro* models. Furthermore, THP-1 adhesion experiment and matrigel/ HUVEC assay will be performed to test for reproducibility.

2.4.2 Conclusions

This study aims to understand how SAPs of the EAK family could affect monocyte adhesion and macrophage polarisation in the context of angiogenesis. Our results showed all five SAPs were able to induce monocyte adhesion, which could potentially encourage cell survival and alter cellular function via non-integrin specific binding. DAR and EAK-polarised M1 were found to promote HUVEC network formation on matrigel, possibly by increasing M1's expression of MMP-9, a pro-angiogenic protease that promotes endothelial cell migration and network formation. However, no significant increase in network formation was observed for SAP-polarised M2. The lack of increase could be attributed to M2's innate low expression of MMP-9 or high expression of TIMP3, an inhibitor of MMP-9. We observed the trend in M1-induced network formation is the inverse of the trend in THP-1 cell spreading. For example, DAR polarised M1 induced highest network formation while THP-1s showed least spread on DAR/gelatin coating; the opposite was true for EYK. This finding suggests the increase in THP-1 spreading triggered some signalling cascades that would later inhibit M1 polarisation and their protein expression. In addition, we observed clear morphological changes to the THP-1 cells as they are differentiated into irregular-shaped M0 and further elongated when polarised into M1/M2. The morphological changes were consistent with the literature using the same differentiation and polarisation protocol. Further characterisation (mRNA and immunofluorescence) and *in vitro* studies (collagen/HUVEC assay) are needed to fully appreciate the intricate relationship between macrophages and SAPs. It may also be worthwhile to explore effect of various SAPs on M2c macrophages, considering DAR and EAK's potential influence on MMP-9 expression. THP-1 adhesion experiments and matrigel/HUVEC assay will be performed to test for reproducibility.

In summary, our findings support the hypothesis that SAPs of the EAK family are able to influence monocyte and macrophage's cellular functions favouring angiogenesis. Therefore, we believe SAPs of the EAK family holds great therapeutic potential in improving tissue engineered systems for clinical application in future.

2.4.3 Materials and methods

2.4.3.1 THP-1 Cell Culture

The monocytes used for this study was THP-1 cells (ATCC TIB-202™). They were purchased from ATCC and kept at -80°C. When resuscitated, the cells were maintained between 2×10^5 cells/ml and 4×10^5 cells/ml in THP-1 medium, which was made up of RPMI medium 1640 + L-glutamate (Gibco®) supplemented with penicillin and 10% foetal calf serum (FCS) or foetal bovine serum (FBS) (Sigma). Optimal cell density was determined using a TC20™ automated cell counter and was corrected by adding more THP-1 medium

or discarding THP-1 cells if they were in excess. The cells were cultured in sterile T75 cell culture flasks (Cellstar®), which was kept upright during the incubation period as THP-1 cells are non-adherent cells. As THP-1 cells proliferate, they formed clusters which could result in the death of cells in the centre due to lack of exposure to the media. To break the clusters, cells and medium were transferred from the T75 flasks to a 15ml or 50ml Falcon conical centrifuge tube (depending on the volume of the medium), and centrifuged at 1.5 RPM for 5 minutes. The remnant medium was discarded. The resultant pellet was re-suspended by adding 5 ml THP-1 medium to the falcon tube and repeated pipetting until the pellet is completely dispersed. Cells were then transferred back to the original flask and add suitable amount of medium so that the cell density was maintained between the optimal interval.

2.4.3.2 HUVEC Cell Culture

HUVECs were cultured as reported in paragraph 2.3.3.1.

2.4.3.3 SAP/gelatin coatings and incubation time optimization

The SAP/gelatin solutions for plates coating were prepared as reported in paragraph 2.3.3.3. Each sterile coating solution was pipetted into each well of a cell culture plate. Three types of cell culture plates were used, and different volume of coating solution was used as shown in **Table 2.3**:

Table 2.3. Volume of coating solution per well used in each type of plate.

TYPE OF PLATE	VOLUME OF COATING SOLUTION PER WELL
96/WELL PLATE (THERMOFISHER)	30 µL
24/WELL PLATE (CELLSTAR®)	150 µL
A µ/SLIDE ANGIOGENESIS (IBIDI®)	8 µL

The coated plates were left in the 37°C incubator for 24 hrs and the remaining coating solution (if there is any) was removed using a pipette. Following this, the coated plate was left in the sterile fume hood for 1 hr so that the SAP/gelatin (SAP/gelatin) coating would be completely dried. The ideal length of incubation was ascertained by coating three 96 well plates with the five different SAP/gelatin solutions and incubating at 37°C 5% CO_2. Each plate was incubated for 12 hours, 24 hours or 48 hours. After the respective times had elapsed for the SAPs to assemble, $5x10^3$ THP-1 (ATCC) cells, were seeded onto the wells, and incubated for a further hour. The plates were then fixed and stained with Hoechst, to stain the nuclei and Phalloidin, to stain the actin filaments.

The plates were imaged using high content microscope (Operetta Imaging System) and compared to determined which coating duration was the best. Based on this preliminary experiment, coating with SAPs for 24 hours prior to seeding was found to be the most optimal, when compared to coatings of 12 hours and 48 hours.

2.4.3.4 THP-1 Adhesion assay on SAP/gelatin coated plate

THP-1 cells were seeded on SAP/gelatin coated plates and the number of cells that adhered to the coating and their average cell area (i.e. cell spreading) was measured 1 hr after seeding. 3 wells of a 96 wells plate, were coated with the five different SAPs coating solutions according to the method outlined in section 2.4.3.4. 0.5% w/v gelatin/PBS solution without SAP was used as control of the experiment (n=3) Following this, $5x10^3$ THP-1 cells (in 100µl of THP-1 medium) were seeded into each coated well and the 96 well plate was left in the incubator for 1 hr to allow the THP-1 cells to adhere to the coating. After 1 hr, non-adherent cells were removed together with medium and the cells that adhered to the coating were fixed removing cell media, washing with PBS enriched with Ca^{2+} and Mg^{2+} for 5 min under agitation and adding 2% PFA in PBS enriched with Ca^{2+} and Mg^{2+} for 15 minutes under agitation. Finally, cells were washed with PBS enriched with Ca^{2+} and Mg^{2+} and kept in PBS in a 4 °C refrigerator.

2.4.3.5 Staining THP-1 cells with Hoechst and Phalloidin

The PBS was removed, 10mM Hoechst (ThermoFisher) and 0.1mM phalloidin (Sigma-Aldrich®) staining solutions were prepared in 0.01% w/v TritonX-100 in PBS enriched with Ca^{2+} and Mg^{2+}. 50 µl of Hoechst and Phalloidin staining solution was added to each well and the plate was covered with aluminium foil and left on the agitator for 1 hour. Finally, the wells were washed with PBS enriched with Ca^{2+} and Mg^{2+}.

2.4.3.6 Imaging and quantification of adherent cells

Fluorescent contrast images were taken using an automated confocal microscope (Operetta High-Content Imaging System). The number of cells adhered to the coating and the average area of the adherent cells were measured using the image analysis software Columbus by PerkinElmer.

The software was equipped with accurate image segmentation capacity, allowing it to find nuclei, cell boundaries and cytoplasm in a phase contrast / fluorescent image (**Fig 2.10**).

The software was able to quantify the relevant parameters such as total number nuclei detected (i.e. number of cells), average area of the nuclei, average area of cytoplasm and average area of the cells. Image analysis using Columbus instead of manual counting could greatly improve efficiency and avoid potential human error or biasness.

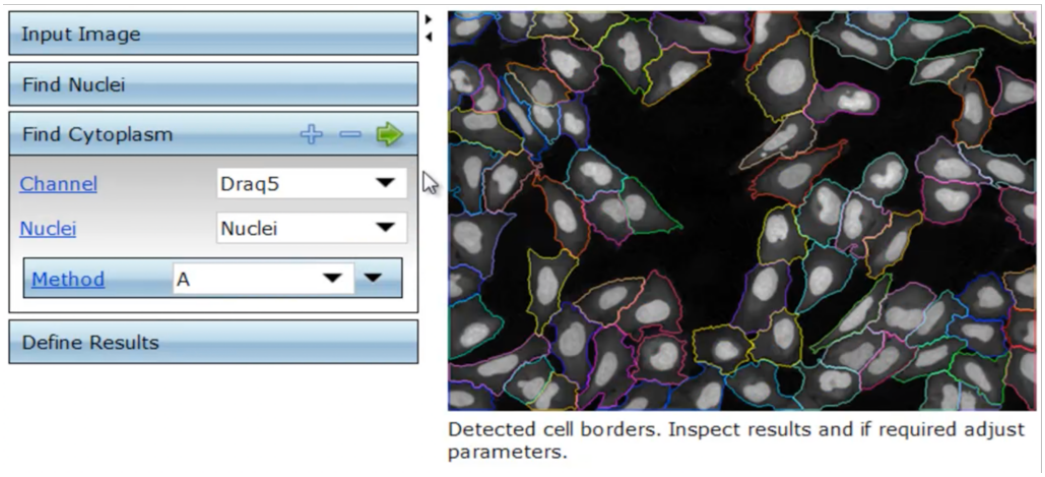


Figure 2.10. Screenshot of Columbus software interface demonstrating its capacity to detect nuclei, cytoplasm and cell boundaries. Adapted from http://insideinformatics.cambridgesoft.com/videosanddemos/273/columbus-image- segmentation.

2.4.3.7 Polarisation of THP-1 derived Macrophages

Cell culture plates were coated with various SAP/gelatin coating solution as outlined in paragraph 2.4.3.4. THP-1 cells can be differentiated into macrophages (M0) and polarised into M1 or M2 macrophages using the following protocol, which was developed based on literature[15]:

. 1. obtain suitable number of cells suspended in suitable amount of THP-1 medium based on the requirement of the experiment;
. 2. differentiating THP-1 cells to macrophages: add suitable amount of phorbol 12-myristate 13-acetate (PMA) to the THP-1 media containing THP-1 cells, so that the concentration of PMA is 5ng/ml;
. 3. seed THP-1 cells that are suspended in medium containing PMA to the SAP/gelatin coated wells;
. 4. incubate the cells at 37 °C and 5% CO_2 for 3 days;
. 5. remove media containing PMA;
. 6. polarise M0 to M1 or M2: obtain suitable amount of THP-1 medium to replenish the removed medium. Based on the target concentration shown in **Table 2.4**, add suitable amount of interferon gamma (IFNγ) and lipopolysaccharides (LPS) to the THP-1 medium for M1 polarisation and interleukin 4 (IL4) for M2 polarisation. Add the medium containing polarising agent(s) to each well that holds M0 macrophages;
. 7. incubate the cells at 37 °C and 5% CO_2 for 72 hrs (3 days) to allow polarisation to take place.

Table 2.4. Polarising reagents used to polarise M1/M2 and their target concentrations.

Polarisation	*Reagent*	*Target concentration*
M1	IFNγ (Peprotech)	1000 ng/ml
M1	LPS (Sigma)	20 ng/ml
M2	IL4 (Peprotech)	20 ng/ml

Brightfield images of the cells in different stages of polarisation were taken by an optical microscope (Olympus 1X51) at 20X original magnification (OM). All M1 or M2 cells that were used for the immunofluorescence analysis and matrigel/HUVEC angiogenesis assay were obtained using this this protocol.

Figure 2.11 shows the overall for timeline of obtaining SAP-polarised M1/M2.

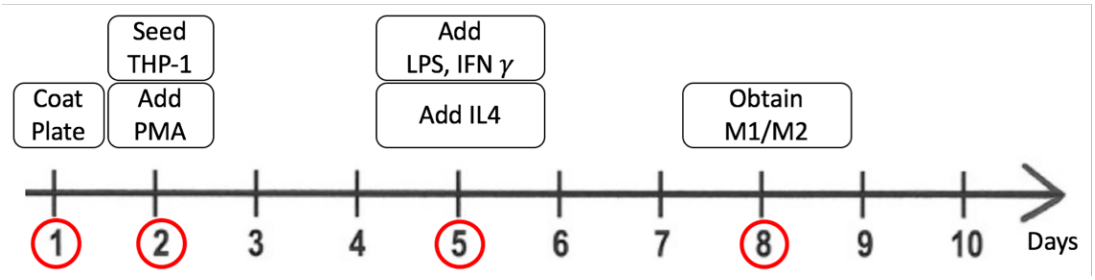


Figure 2.11. Overall for timeline of obtaining SAP-polarised M1/M2

2.4.3.8 M1 and M2 Immunofluorescence analysis

In a 96 well plate coated with various SAPs, THP-1 cells were differentiated and polarised into M1 and M2 cells using the protocol outlined in section 2.4.3.8, with gelatine-polarised M1/M2 as control, each well was seeded with 5×10^3 THP-1 cells in 100µl medium (n = 2). M1 and M2 cells were fixed using the method outlined in section 2.4.3.5, except for the last step, in which 150µl of blocking solution (10% FCS in sterile PBS) was used instead of 150µl of PBS.

Because immunostaining involves the use of antibodies, blocking solution was used to prevent non-specific bonding of the antibodies to the cells surface (ThermoFisher Scientific).

The list of antibodies used and their dilution factor in blocking solution are shown in **Table 2.5**.

These surface markers were chosen because their levels of expression differ greatly among M0, M1, M2 and THP-1[15].

Table2.5. Antibodies used for M1/M2 immunofluorescence analysis.

Antibody	Type	Diluition
Anti-CD64 (R&D system)	Monoclonal mouse IgG	1:500
Anti-mouse IgG (R&D system)	Conjugated Donkey IgG	1:200
Anti-CD14 (BD Pharmingen)	Conjugated mouse antibody	1:100
Anti-CD206 (BD Pharmingen)	Conjugated mouse antibody	1:100

For example, CD206, also known as Mannose receptor, is significantly upregulated in M2 phenotype[15]; CD14 is considered as a monocyte marker that is downregulated during differentiation[22] and CD64 is a M1 maker that is upregulated when macrophages encounter IFNγ[26].

Immunostaining was conducted diluting the antibody solutions according to **Table 2.4**, and adding 50µl of the prepared solution per well to the cells. The solutions are left in contact with the cells on the agitator for 45 minutes, covered in aluminium foil. Finally, the wells were washed twice with blocking solution and for 10 minutes under agitation, always covered in aluminium.

The cells were then stained with Hoechst as per section 2.4.3.6.

2.4.3.9 Matrigel/HUVEC angiogenesis assay on SAP-polarised M1/M2

The overall schematic is shown in **Figure 2.12a**. µ-angiogenesis slides (iBidi®) were used for this experiment because the well-within-a-well design prevents matrigel forming a meniscus and thus produce better and clearer image since all HUVECs would be aligned within a relatively flat surface (**Fig 2.12b**).

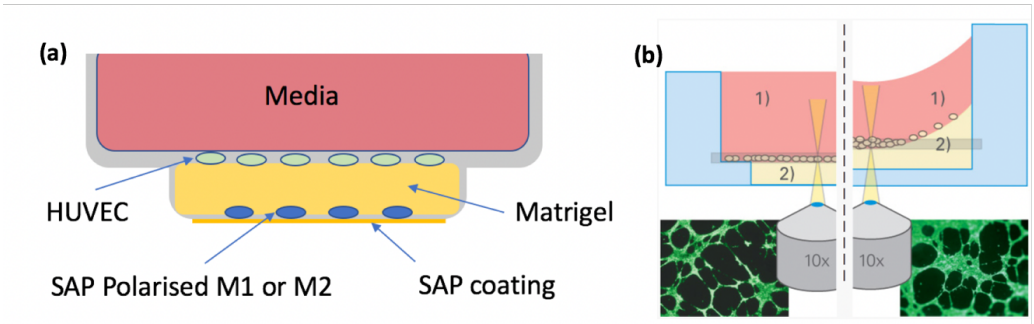


Figure 2.12. a) Schematic of a single well in matrigel/HUVEC assay. **b**) Illustration of difference in cell alignment between a normal well and a µ-angiogenesis well, adapted from https://ibidi.com/open-slides/41--slide-angiogenesis.html

In 2 µ-angiogenesis slides coated with various SAPs, THP-1 cells were differentiated and polarised into M1 and M2 cells using the protocol outlined in section 2.4.3.8, with gelatin-polarised M1/M2 as control. Each inner well contained 5×10^3 THP-1 cells and 100µl medium. Each experimental condition was conducted in triplicates and the entire experiment was repeated (n = 6).

Only 5 out of the 6 SAPs of the EAK family were used for this experiment due to limited columns in the iBidi µ-angiogenesis slides (i.e. 3 rows × 5 columns). Matrigel solution was prepared in ice by combining EGM2 and matrigel as supplied (PromoCells) at a 1:1 ratio. 10µl of matrigel was then added to the inner wells in a dropwise to avoid introducing any bubbles.

The slides were then incubated at 37 °C for 30 minutes to allow the matrigel to set. 50µl of EGM2 medium was added to each well. The 2 slides were left in the incubator for 24 hr to allow the angiogenic factors secreted by M1/M2 cells to diffuse into the matrigel.

After the 24 hours of incubation, HUVECs were seeded on top of the matrigel conditioned by SAP-polarised M1/M2 ($1x10^4$ cells in 40 µl EGM2 per well) and the cells were incubated overnight (18 hrs). On the next day, networks in each well were imaged in phase contrast using an optical microscope (Olympus 1X51) at 4X OM.

Figure 2.16 shows the overall timeline of the experiment over the course of 10 days.

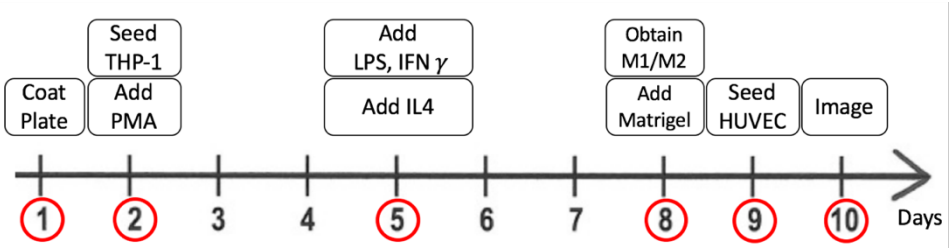


Figure 2.16. Overall for timeline of matrigel-HUVEC assay.

2.4.3.10 Measuring HUVEC networks' architecture

The absolute values of total number of nodes and total length of network were measured as reported in section 2.3.3.7.

2.4.3.11 Statistical analysis

Data are shown as Mean ± standard deviation (SD). Statistical analysis was performed using Graphpad Prism 7 for Mac OS X, Version 7.0c.

One way ANOVA tests were conducted for the THP-1 adhesion assay and matrigel/HUVEC angiogenesis assay with post/hoc Bonferroni analysis. P-value<0.05 was deemed as significant.

2.5 References

1. Gambaretto, R., Tonin, L., Di Bello, C. & Dettin, M. Self-assembling peptides: sequence, secondary structure in solution and film formation. *Biopolymers* **89,** 906–15 (2008).
2. Lee, K.-K. & Yonehara, S. Identification of Mechanism That Couples Multisite Phosphorylation of Yes-associated Protein (YAP) with Transcriptional Coactivation and Regulation of Apoptosis. *J. Biol. Chem.* **287,** 9568–9578 (2012).
3. Halder, G., Dupont, S. & Piccolo, S. Transduction of mechanical and cytoskeletal cues by YAP and TAZ. *Nat. Rev. Mol. Cell Biol.* **13,** 591–600 (2012).
4. Kegelman, C. D. *et al.* Skeletal cell YAP and TAZ combinatorially promote bone development. *FASEB J.* **32,** 2706–2721 (2018).
5. Xiong, J., Almeida, M. & O'Brien, C. A. The YAP/TAZ transcriptional co-activators have opposing effects at different stages of osteoblast differentiation. *Bone* **112,** 1–9 (2018).
6. Terramani, T. T. *et al.* Human macrovascular endothelial cells: optimization of culture conditions. *In Vitro Cell. Dev. Biol. Anim.* **36,** 125–32 (2000).
7. Schulz, C. *et al.* Monolayer formation and shear- resistance of human vein endothelial cells on gelatin-based hydrogels with tailorable elasticity and degradability. *Clin. Hemorheol. Microcirc.* **64,** 699–710 (2017).
8. Sieminski, A. L., Semino, C. E., Gong, H. & Kamm, R. D. Primary sequence of ionic self-assembling peptide gels affects endothelial cell adhesion and capillary morphogenesis. *J. Biomed. Mater. Res. A* **87,** 494–504 (2008).
9. Dupont, S. *et al.* Role of YAP/TAZ in mechanotransduction. *Nature* **474,** 179–183 (2011).
10. Pan, D. The Hippo Signaling Pathway in Development and Cancer. *Dev. Cell* **19,** 491–505 (2010).
11. Neto, F. *et al.* YAP and TAZ regulate adherens junction dynamics and endothelial cell distribution during vascular development. *Elife* **7,** (2018).
12. Ragni, C. V. *et al.* Amotl1 mediates sequestration of the Hippo effector Yap1 downstream of Fat4 to restrict heart growth. *Nat. Commun.* **8,** 14582 (2017).
13. Tattersall, I. W. *et al.* In vitro modeling of endothelial interaction with macrophages and pericytes demonstrates Notch signaling function in the vascular microenvironment. *Angiogenesis* **19,** 201–215 (2016).
14. Rad-Malekshahi, M., Lempsink, L., Amidi, M., Hennink, W. E. & Mastrobattista, E. Biomedical Applications of Self-Assembling Peptides. *Bioconjug. Chem.* **27,** 3–18 (2016).
15. Spiller, K. L. *et al.* The role of macrophage phenotype in vascularization of tissue

engineering scaffolds. *Biomaterials* **35,** 4477–4488 (2014).

16. Spiller, K. L. & Koh, T. J. Macrophage-based therapeutic strategies in regenerative medicine. *Adv. Drug Deliv. Rev.* **122,** 74–83 (2017).
17. Koh, W., Stratman, A. N., Sacharidou, A. & Davis, G. E. In vitro three dimensional collagen matrix models of endothelial lumen formation during vasculogenesis and angiogenesis. *Methods Enzymol.* **443,** 83–101 (2008).
18. Zhang, S. *et al.* Self-complementary oligopeptide matrices support mammalian cell attachment. *Biomaterials* **16,** 1385–1393 (1995).
19. Gelain, F., Bottai, D., Vescovi, A. & Zhang, S. Designer Self-Assembling Peptide Nanofiber Scaffolds for Adult Mouse Neural Stem Cell 3-Dimensional Cultures. *PLoS One* **1,** e119 (2006).
20. McWhorter, F. Y., Wang, T., Nguyen, P., Chung, T. & Liu, W. F. Modulation of macrophage phenotype by cell shape. *Proc. Natl. Acad. Sci.* **110,** 17253–17258 (2013).
21. Zajac, E. *et al.* Angiogenic capacity of M1- and M2-polarized macrophages is determined by the levels of TIMP-1 complexed with their secreted proMMP-9. *Blood* **122,** 4054–4067 (2013).
22. Daigneault, M., Preston, J. A., Marriott, H. M., Whyte, M. K. B. & Dockrell, D. H. The Identification of Markers of Macrophage Differentiation in PMA-Stimulated THP-1 Cells and Monocyte-Derived Macrophages. *PLoS One* **5,** e8668 (2010).
23. Forget, M. A. *et al.* Macrophage Colony-Stimulating Factor Augments Tie2-Expressing Monocyte Differentiation, Angiogenic Function, and Recruitment in a Mouse Model of Breast Cancer. *PLoS One* **9,** e98623 (2014).
24. Jadhav, U., Chigurupati, S., Lakka, S. S. & Mohanam, S. Inhibition of matrix metalloproteinase-9 reduces in vitro invasion and angiogenesis in human microvascular endothelial cells. *Int. J. Oncol.* **25,** 1407–14 (2004).
25. Saunders, R. L. & Hammer, D. A. Assembly of Human Umbilical Vein Endothelial Cells on Compliant Hydrogels. *Cell. Mol. Bioeng.* **3,** 60–67 (2010).
26. Akinrinmade, O. A. *et al.* CD64: An Attractive Immunotherapeutic Target for M1-type Macrophage Mediated Chronic Inflammatory Diseases. *Biomedicines* **5,** 56 (2017).

Chapter 3

Wollastonite-Diopside foams

3.1 Abstract

Bioceramic foams based on wollastonite ($CaSiO_3$) and diopside ($CaMgSi_2O_6$), can be obtained from the thermal treatment of preceramic polymers (silicone resins) containing micro- and nano-sized filler powders. This innovative process is advantageous because of its simplicity, the limited processing temperature and the microstructural homogeneity. These foams can simulate the natural porous internal structure of human bones and consequently can be considered as promising scaffolds for bone tissue engineering. Nowadays, the key role of many physiologically molecules in cell adhesion and growth has been elucidated: the acquired knowledge opens the perspective of a new approach to surface treatments, i.e. the so-called "biochemical functionalization" to improve surface-to-cells interactions.

Several adhesive peptides have been individuated: in particular, a nonapeptide (HVP) from the h-Vitronectin protein (sequence 352-360) is able to enhance osteoblast adhesion through an osteoblast-specific mechanism, involving interaction between membrane glycosaminoglycans (GAGs) and the heparin binding sites on extracellular matrix (ECM). The peptide HVP has been used to design biomimetic surfaces using both unselective or selective grafting. In this study, polymer-derived silicate foams were covalently and selectively functionalized with adhesive peptides.

In addition to HVP sequence, a dimeric analogue (2HVP) has been tested in order to increase ionic interactions with cellular GAGs. On the other side, we have synthesized two retro-inverted sequences of Vitronectin peptides (D-HVP and D-2HVP) in an effort to avoid the enzymatic degradation of HVP peptide, observed in serum-containing solution. Crushing strength test on functionalized scaffolds were carried out to study the influence of functionalization reactions on the mechanical properties of bioceramic foams. H-osteoblast adhesion and proliferation assays were carried out to compare the differently decorated bioactive foams.

Cell viability on rude foam-scaffolds will be promoted using the self-assembling peptide EAK as filler. In fact, EAK, in water solution, have the ability to penetrate the scaffold's pores and to aggregate in hydrogel-structure when immersed in buffer. In this way, the final

sample will be structured as "a soft scaffold inside a hard scaffold", where the latter is represented by the W/D foam that gave the adequate mechanical properties, and the first is the SAP hydrogel that creates a more suitable environment for cells. The bioactivity of SAPs has been widely investigated and their ability of stimulate the osteointegration was demonstrated in several literature articles.

A pro-angiogenic sequence will be covalently grafted to EAK (EAKG7TIM) to promote neoangiogenesis and vascularization, that represent fundamental key issues for implanted scaffolds' survival. This type of SAP functionalization of the bioglass scaffolds is characterized by the simplicity and biocompatibility of the treatments.

Finally, bioceramic foams covalently functionalized with the adhesive sequence that give the most promising *in vitro* results, embedded in EAK hydrogel and enriched with a pro-angiogenic sequence (EAKG7TIM), will be tested *in vivo* in ectopic site of a murine model, to evaluate osteoconductivity and osteoinductivity of D2HVP, furthermore new calcium deposition will be evaluated together with the angiogenic potential of EAK and EAKG7TIM treatments and how the latter can influence new calcium deposition on the scaffold.

3.2 Results and Discussion

3.2.1 *In vitro* assays

Since mechanical properties represent one of the most relevant key issue in bone reconstruction, it was important to verify that the selective and covalent functionalization protocol, consisting in a series of reactions with organic solution and including a final acid treatment did not cause a decrease in the mechanical properties of the wollastonite-diopside foams. Consequently, a compressive strength test was performed on functionalized samples, and the crushing strength of functionalized foams was measured at room temperature with a cross-head speed of 1 mm/min.

The results, reported in **Figure 3.1,** showed no significant decrease of mechanical strength at crushing due to functionalization treatment, with average values in accordance with the literature data[1].

The bulk density and the open porosity remained unchanged after the treatment.

Silanized W/D foams (Sil), and samples functionalized with a non–adhesive sequence $(GRADSP)_4K$ (ctrl) were used as control in all *in vitro* assays.

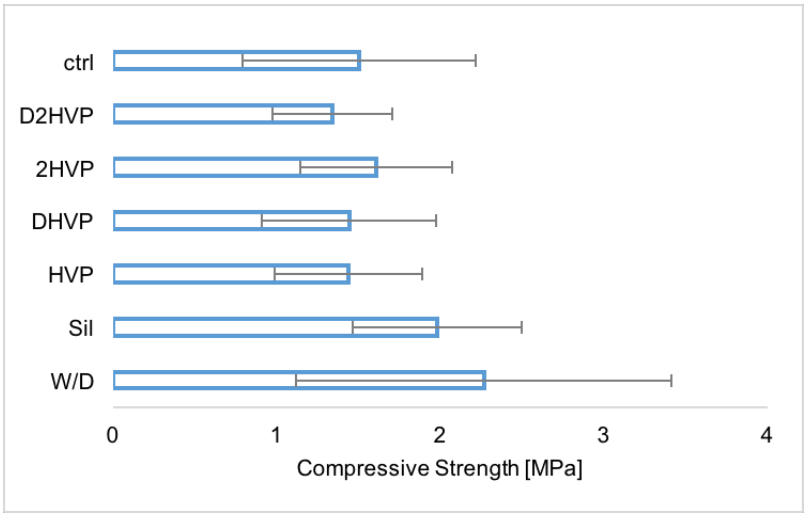


Figure 3.1. Crushing strength test. "Ctrl" refers to foams functionalized with $(GRADSP)_4K$, a non-adhesive peptide. "Sil" refers to silanized surface, while "W/D" are not-treated Wollastonite-Diopside foams

H-osteoblasts (3×10^5 cells/sample) were seeded onto bioceramic scaffolds (35mg/sample) and incubated at 37°C for 2 h. Cellular adhesion was assessed by MTT assay (**Fig 3.2**).

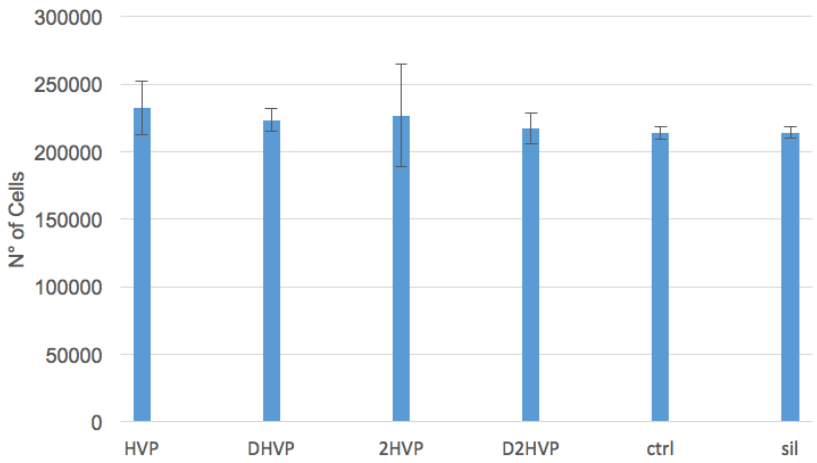


Figure 3.2. H-osteoblast adhesion on functionalized W/D foams, determined at 2h through MTT assay. "Sil" sample refers to the silanized scaffolds; "ctrl" refers to samples functionalized with a nonadhesive peptide.

The functionalization with the adhesive peptides didn't improve h-osteoblast adhesion at 2h in comparison with silanized (Sil) samples or foams functionalized with the not-adhesive peptide $(GRADSP)_4K$ (Ctrl).

This result was in disagreement with previous ones obtained on functionalized titanium oxide or functionalized glass surfaces[2,3], so other adhesion assays at different time points were carried out to confirm this experimental evidence, and HOB proliferation on functionalized bioceramic foams was then determined at 2, 4 and 6 days after the seeding, using CFSE probe assay (**Fig 3.3**).

All the samples functionalized with the adhesive peptides showed increased cell proliferation with respect to the control and silanized foams.
The proliferation increase was particularly dramatic for retro-inverted analogues (D-HVP and D-2HVP) and could be due to their capacity to maintain the bioactivity of natural sequences (HVP and 2HVP) jointed with their complete stability to enzymatic degradation[3].
The functionalization with the two retro-inverted sequences doubled the proliferation of HVP and 2HVP samples at 2 and 4 days, while the functionalization with D2HVP doubled the proliferation of HVP, DHVP and 2HVP samples at 6 days.
Furthermore, D2HVP covalently and selectively grafted to wollastonite-diopside foams gave a 15 times proliferation increase at 6 days with respect to the controls, suggesting that this is the most effective functionalization treatment among the proposed once also at longer time.

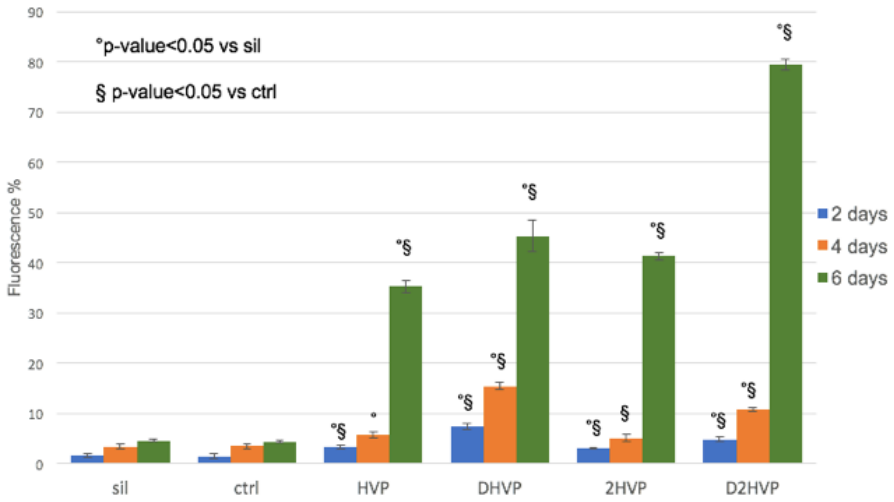


Figure 3.3. H-osteoblast proliferation on functionalized W/D foams, determined at 2, 4 and 6 days using CFSE probe assay. "Sil" sample refers to the silanized scaffolds; "ctrl" refers to samples functionalized with a non-adhesive peptide. *, ° P-value<0.05 Student's t-test compared to "Sil" and "ctrl" respectively.

LDH test demonstrated the absence of cytotoxicity induced by functionalization treatments at 4 and 6 days (**Fig 3.4**).
Human *SPP1* (Osteopontin, secreted phosphoprotein 1), Human *VTN* (Vitronectin), Human *IBSP* (Integrin-Binding Sialoprotein) and Human *RUNX2* (Runt-related transcription factor 2) mRNA specific transcript levels were evaluated by quantitative RT-PCR at 2 days after h-osteoblasts' seeding. The results are reported in **Figure 3.5**.

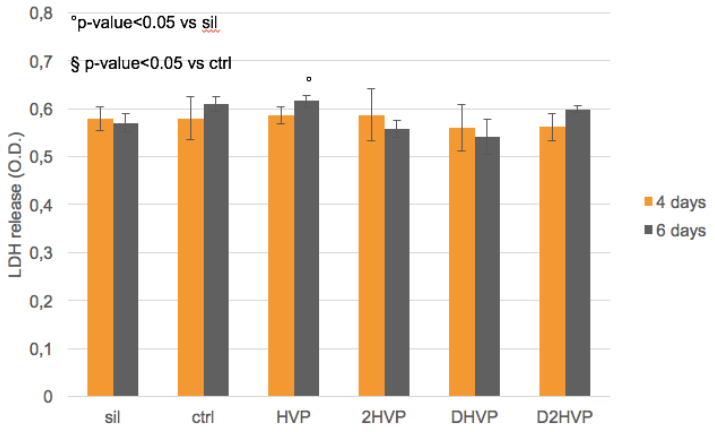


Figure 3.4. LDH test at 4 and 6 days demonstrated the absence of cytotoxicity induced by functionalization treatments. "Sil" sample refers to the silanized scaffolds; "ctrl" refers to samples functionalized with a non-adhesive peptide. *,° P-value<0.05 Student's t-test compared to "Sil" and "ctrl" respectively.

We demonstrated that all functionalised wollastonite-diopside foams were able to increase the expression of SPP1, VTN, RUNX2 and IBSP, proteins fundamental for bone formation, when compared to the controls.

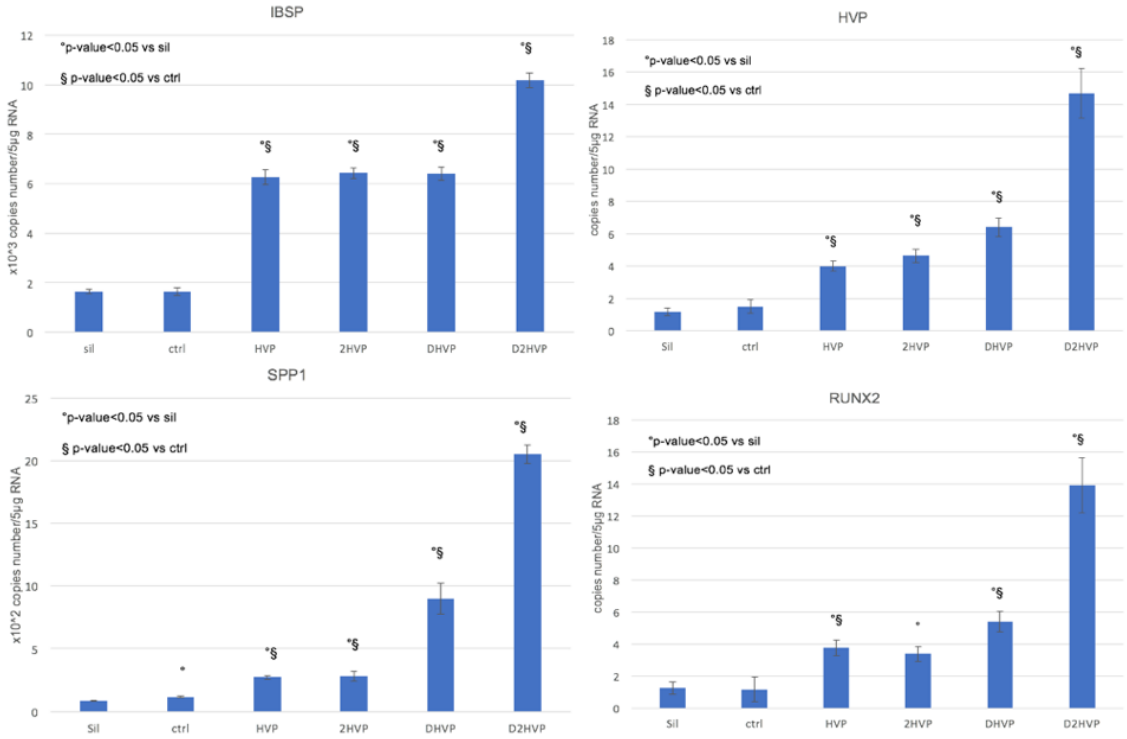


Figure 3.5. Human *SPP1* (secreted phosphoprotein 1), Human *VTN* (Vitronectin), Human *IBSP* (Integrin-Binding Sialoprotein) and Human *RUNX2* (Runt-related transcription factor 2) mRNA specific transcript levels evaluated by quantitative RT-PCR. "Sil" refers to silanized scaffolds; "ctrl" refers to surfaces functionalized with a non-adhesive peptide. °, § P-value<0.05 Student's t-test compared to "Sil" and "ctrl" respectively.

It is worth noting that the foams functionalised with the two retro-inverted analogues gave the best results. HVP, 2HVP and DHVP samples tripled IBSP expression while D2HVP foams gave a dramatic increase of more than 6 times when compared to the controls. Furthermore, D2HVP foams showed an increase of more than 9 times in VTN expression, more than 18 times in SPP1expression and more than 12 times in RUNX2 expression.
Since the retro-inverted sequence D2HVP gave the most promising results *in vitro*, it was then covalently and selectively grafted to W/D foams for subsequent *in vivo* assays.

3.2.2 *In vivo* assays

The final scaffold for *in vivo* assays was based on wollastonite-diopside foam covalently and selectively functionalised with D2HVP that was the adhesive sequence that gave the best *in vitro* results and subsequentially embedded in a solution of SAP. Bioceramic samples were embedded in a 0.15%w/v EAK solution, since EAK was the self-assembling peptide that gave the best results in the preliminary *in vitro* assay with HOB (**Fig. 2.1** and **2.2**) and induced a high tubule length formation in all matrigel assays (**Fig. 2.6** and **2.9**). *In vivo* assays were performed to evaluate scaffold colonization and mineralization inserting samples/controls under-skin in a murine model. The experimental plane was based on nine mice. Mice were randomly divided in three groups of three animals each. Each mouse of the first group received a scaffold functionalized with D2HVP (sample) and a silanized W/D (control). Each mouse of the second group received a scaffold functionalized with D2HVP and filled with EAK hydrogel (0.15% w/v) (sample) and a scaffold functionalized with D2HVP (control). Each mouse of the third group received a scaffold functionalized with D2HVP and filled with EAK hydrogel (0.15% w/v) containing 5×10^{-5} M of EAKG7TIM (sample) and a scaffold functionalized with D-2HVP and filled with EAK hydrogel (0.15% v/v) (control). Where EAKG7TIM is a pro-angiogenesis sequence TIM (see paragraph 1.3.1.3) covalently linked to the self-assembling peptide EAK, through *chemoselective ligation,* and G7 act as a spacer (made of Glycine and 7-aminoheptanoic acid). Following surgery, no abnormalities were detected in any animal and all vital functions returned to physiological levels in a short time. After 45 days, the mice were sacrificed and the implants were removed. At first glance, the macroscopic appearance of the wollastonite-diopside scaffolds was found to be normal, as well as the surrounding tissues. The normal macroscopic appearance of implants showed no inflammation, no vascularization and no encapsulation. Although in endosseous experiment it has been shown that adhesive peptides carry out their biological activity in a short time (~15 days)[4], for the evaluation of ectopic osteoinduction the timing has been prolonged because in this type of experimental model more time is needed to induce mineralization(~45-60 days)[5]. In particular, to obtain a good degree of mineralization in the subcutaneous area, periods

of time ranging from weeks to months are required[5]. This is due both to the absence of pro-osteogenic factors and cells capable of producing bone, and to the presence of a relatively small number of blood vessels, which provide the elements necessary to obtain an ectopic mineralization, such as nutrients, oxygen and mesenchymal stem cells. Moreover, these cells, once recalled by the circulation, must differentiate into mature pre-osteoblasts and osteoblasts before being able to produce mineralized matrix. All this represents the rational that led to consider an extension of the experimental timing to 45 days.

All the analyses carried out on functionalized W/D foams after the removal from the animals were conducted at the Department of Medicine and Surgery of the University of Parma (Prof. Antonio Cacchioli, Prof. Francesca Ravanetti).

3.2.2.1 Qualitative histological analysis

Wollastonite-diopside scaffolds were processed as non-decalcified samples and included in polymethyl-methacrylate, to be finally cut into sections with a circular diamond-coated rotary microtome, and then stained with Goldner's Trichrome and the Von Kossa method.

The qualitative analysis performed with light field optical microscopy showed, for all samples, scaffold colonization both in the internal and external portion, with the formation of new blood vessels (neoangiogenesis) (**Fig 3.6**).

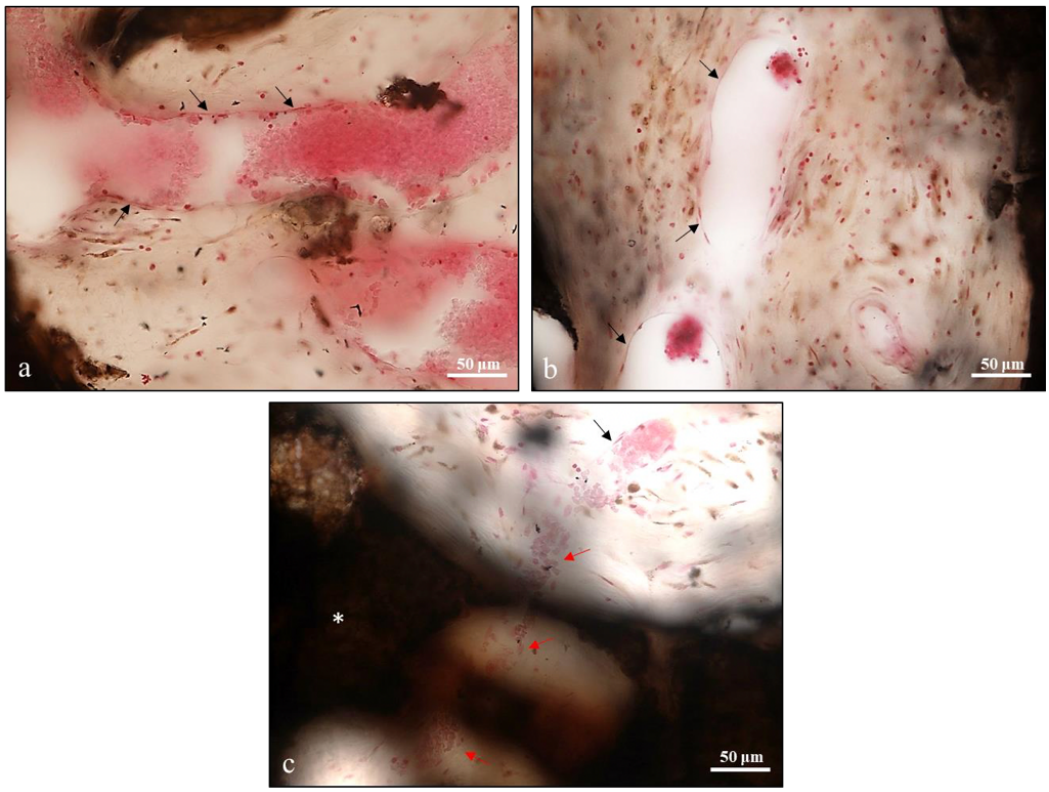


Figure 3.6. Blood vessels stained for Von Kossa. Figures (**a**) and (**b**) show the colonization of the scaffold by large vessels, the black arrows indicated vessels' endothelium. In figure (**c**) it is possible to notice a single blood vessel (red arrows) crossing several pores of the scaffold (*).

Colonizing cells showed an elongated appearance, with a predominantly fibroblast-like phenotype. All the scaffolds were surrounded by a layer of fibrous connective tissue and, in some cases, the internal matrix of the pores was mixed with adipose tissue, representative of a characteristic physiological reparative status (**Fig 3.7**, **a** and **b**). Goldner's Trichrome stain showed, in all samples, a matrix that has the same dye affinity as the bone matrix (green), but is weaker coloured (**Figure 3.7**, **c-f**). Its presence was variable among the different scaffolds and was limited only to some pores, generally on the periphery, as a deposition front. Among all, silanized samples (SIL) were found to be the less stained. Within the pores were also visible some areas with a dyeing affinity similar to that of connective tissue (purple). This coloration was not sufficient to demonstrate the presence of a bone or pre-bone matrix inside the scaffolds. Since the newly formed tissue didn't have the characteristics of endogenous mineralized bone tissue, the dyeing affinity of the staining was less specific; so, this histological staining was not used for quantitative analyses.

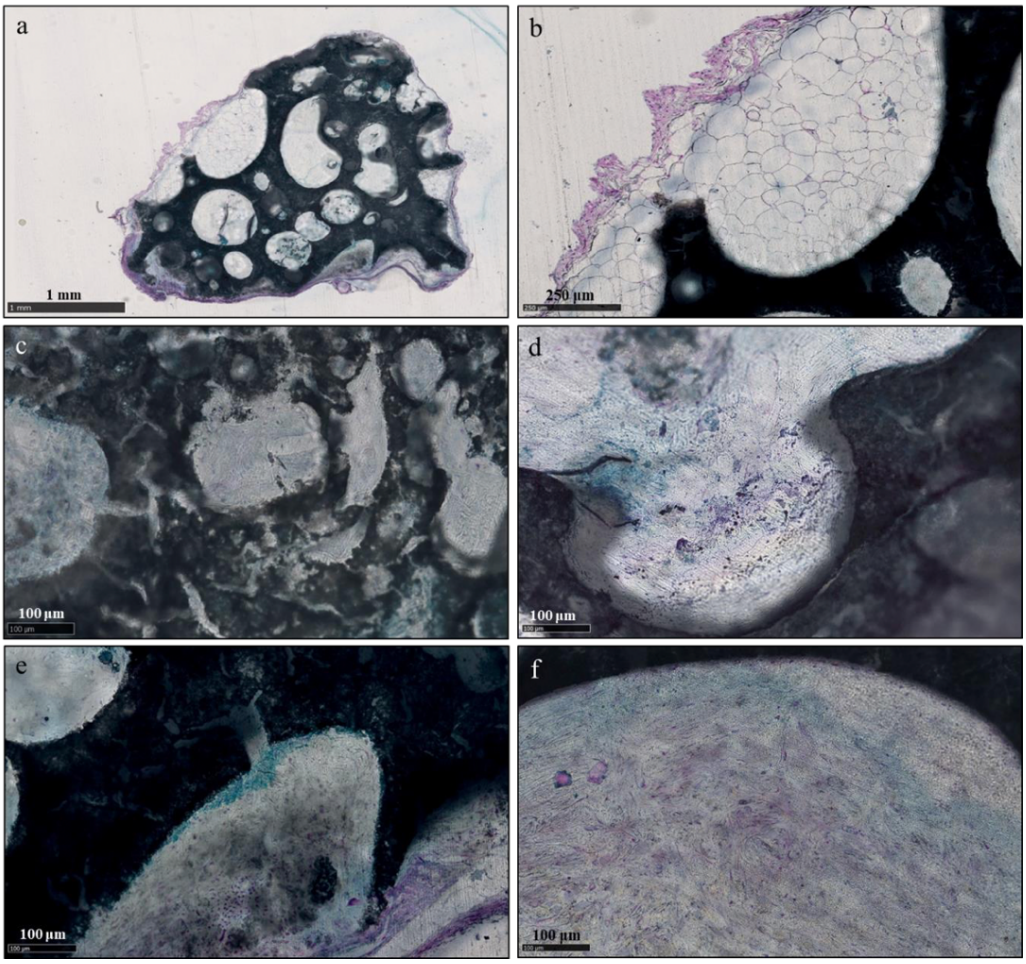


Figure 3.7. Goldner's Trichrome Staining. (**a-b**): Scaffold surrounded by fibrous connective tissue (violet) and a detail of adipose tissue mixed with the matrix (**b**). (**c-f**): The matrix inside the pores has a tintorial affinity similar to that of the bone matrix (green) but with lower intensity. SIL (**c**), D2HVP (**d**), D2HVP + EAK (**e**), D2HVP+EAK+EAKG7TIM (**f**). Magnification: 3X (**a**), 10X (**b**), 20X (**c, d, e, f**).

The sections were then stained using the Von Kossa method, specific for calcium and ideal to visualize bone matrix's mineralization. This staining allows to highlight the presence of calcium carbonate and phosphate salts through a substitution reaction of calcium ions with silver ions, which are subsequently reduced to metallic silver, that assumes the characteristic black colour.

A preliminary qualitative analysis, the negativity of the control group (SIL) was clear, while all the others showed positivity, visible as black precipitates (**Fig 3.8**). The D2HVP + EAK + EAKG7TIM group appeared to be the richest in calcium salts deposits. Since calcium is part of the chemical formula of the components of the scaffold ($CaSiO_3$ - $CaMgSi_2O_6$), this latter is also stained, but still quite distinguishable from the deposits.

The results obtained from qualitative histological analysis revealed the presence of calcium salts and fractions deposits of active mineral deposition in all types of functionalization (D2HVP, D2HVP+EAK and D2HVP+EAK+EAKG7TIM); the control group, on the other hand, did not show ectopic mineralization. This is in agreement with other studies carried out *in vivo*[6,7], in which it has been shown that wollastonite is not able to form ectopic bone in a subcutaneous place; for diopside, on the other hand, no studies are currently available to support the results obtained in this experiment.

From what has been observed, it is possible to state that the D2HVP peptide is able to induce an ectopic mineralization, and, consequently, has an osteoinductive activity[8], which, together with the osteoconductive properties demonstrated in endosseous study on titanium implants[4], represents a potentiality in regenerative approaches, besides being very important to promote an optimal osseointegration process.

The subcutaneous tissue was chosen as an ectopic implant site in order to have a microenvironment as free as possible from pro-osteogenic stimuli and confounding factors. It's known, in fact, that the subcutis is devoid of stem cells capable of forming bone[5]; therefore, the successful mineralization in this site can almost certainly be attributed to the presence of the peptide and its osteoinductive activity, which allowed to recall mesenchymal stem cells from the circulation, which were induced to differentiate into the osteoblastic lineage and to deposit calcium salts which grow by coalescence.

In various samples, we found calcium deposits classifiable with three distinct morphologies: fine dots, named *dot*; a thin filament staining appearance that tend to cluster in small aggregates, called *dash*, and deposition *fronts* located at the periphery of the pores.

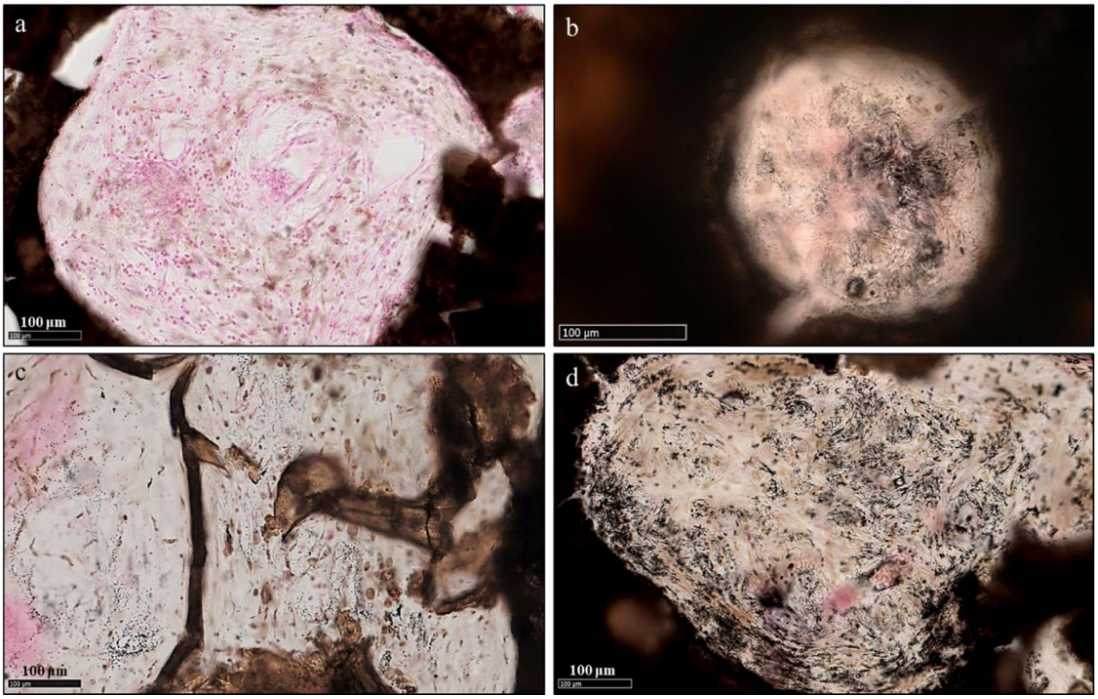
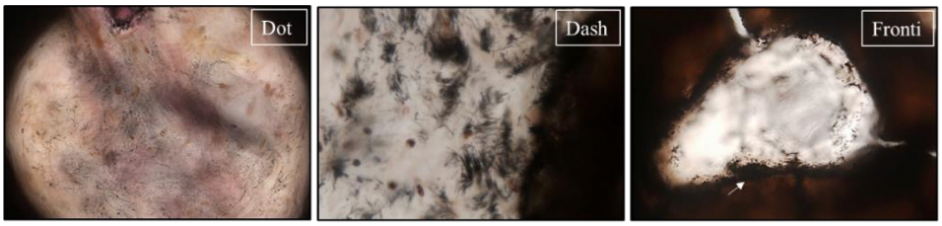


Figure 3.8. Von Kossa method for calcium deposits individuation. D2HVP (**b**), D2HVP+EAK (**c**) and D2HVP+EAK+EAKG7TIM (**d**) groups showed calcium deposits, visible as black precipitates. The silanized scaffolds (SIL) (**a**) are negative. Magnification: 20X.

The presence different morphologies in the differently functionalised scaffold was defined as a score and reported in **Figure 3.9**. The silanized foams, being negative to Von Kossa staining, didn't possess any of the indicated morphologies. Functionalization with D2HVP, on the other hand, showed all types of deposits whereas in the D2HVP+EAK group it is possible to display only the *dot* and *fronts* morphology. The D2HVP+EAK+EAKG7TIM group didn't present *dot*, but is characterized by a much greater amount of *dash* and *front*s than the others.



SIL	–	–	–
D2HVP	+	+	+
D2HVP + EAK	+	–	+
D2HVP + EAK + EAKG7TIM	–	++	++

Figure 3.9. Presence of different morphology of calcium deposits. Absent (-), present (+), present in visibly greater quantities (++)

The *fronts* morphology, located on the surface of scaffolds' pores, was found to be present in all types of functionalization, confirming the osteoconductive properties of the D2HVP peptide. Moreover, the *dot* and *dash* morphologies were observed in the internal pore matrix: *dot* morphology was found in the functionalizations with D2HVP and D2HVP+EAK, while *fronts* morphology was present in the D2HVP and D2HVP+EAK+EAKG7TIM groups. In this latter, calcium deposits with *dash* morphology are present in much higher quantities than D2HVP and *dot* morphology is completely absent. Considering that, both qualitatively and quantitatively, the D2HVP+EAK+EAKG7TIM group proved to be the one characterized by higher degree of mineralization, it is possible to suppose that *dot* and *dash* morphologies represent two consecutive stages of calcium deposition, which occurs by coalescence inside the pores: firstly, there is a matrix in an initial phase of mineralization, while in the second case, in a more advanced phase, the deposition of calcium is more consistent.

According to this assumption, it is possible to deduce that the D2HVP+EAK+EAKG7TIM group showed a more advanced mineralization phase than the other types of functionalization. The fact that the D2HVP+EAK group did not present *dash* morphology could therefore agree with the quantitative data obtained in paragraph 3.2.2.2, which indicate this functionalization as less suitable to induce mineralization, albeit not statistically significant with respect to the D2HVP group.

Although no signs of inflammation and encapsulation are macroscopically visible, at a microscopic level all scaffolds presented a layer of fibrous connective tissue on the outer surface. Some literature studies indicate that bioceramics implanted in the subcutaneous tissue can cause the formation of a fibrous capsule, depending both on the composition of the ceramic and on the implantation site[9,10].

However, the silicate-based bioceramics proved to be characterized by an excellent bioactivity in experiments performed at the endosseous site[11,12], probably due to their ability to form an apatite surface layer when in contact with biological fluids, thus allowing no foreign body reaction when implanted in the bone.

Further studies will be needed to verify the osseointegrative abilities of wollastonite-diopside scaffolds in the endosseous site.

The qualitative analysis in fluorescence microscopy allowed to highlight the presence of active mineralization fronts marked by Calcein Green in the days corresponding to its administration (i.e. at 40^{th}, 42^{nd} and 44^{th} day after surgery).

As shown in **Figure 3.10**, the group of non-functionalized samples (SIL) didn't show any signal, while for the other treatments there were visible fronts of active discontinuous mineralization on the inner surface of the pores, located mainly in the peripheral areas of

the scaffold. The D2HVP and D2HVP+EAK groups appear to be characterized by a greater number of fronts than D2HVP+EAK+EAKG7TIM.

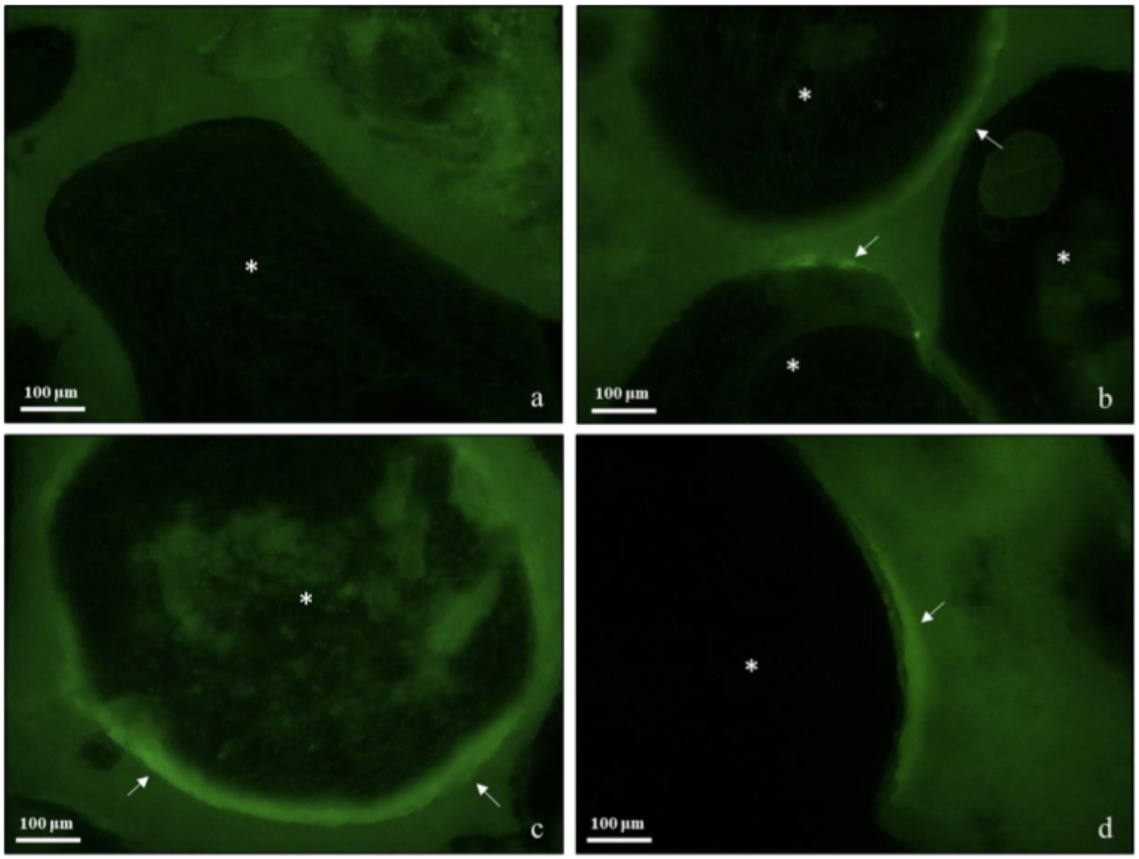


Figure 3.10. Images of the scaffolds in fluorescence microscopy. The groups D2HVP (b), D2HVP+EAK (c) and D2HVP+EAK+EAKG7TIM (d) present fronts of active mineralization (indicated by arrows) located on the inner surface of the pores (indicated by asterisks), which are absent in the SIL group (a). Magnification: 10X.

3.2.2.2 Histomorphometric analysis

Data obtained from the static and dynamic histomorphometry analysis were grouped and plotted as mean ± standard error.

The amount of calcium salts deposited inside the pores, measured with the static histomorphometry parameter Md.S/Po.S (Mineralized Surface versus Pores Surface), was calculated at the end of the experimental time (45th day after scaffold implant), in light field optical microscopy, as a percentage of the surface occupied by calcium deposits on the surface of the pores.

The results obtained from the comparison between the different functionalizations are shown in **Figure 3.11**.

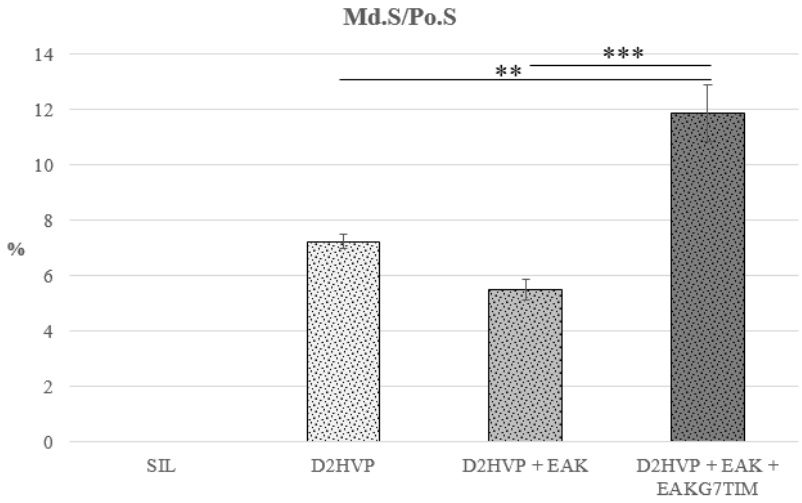


Figure 3.11 Histogram of Md.S/Po.S (Mineralized Surface versus Pores Surface). D2HVP+EAK+EAKG7TIM treatment statistically increased Md.S/Po.S compared to D2HVP (**p<0.005) and to D2HVP+EAK (***p<0.001).

The values obtained for the D2HVP+EAK+EAKG7TIM group were found to be significantly greater than those of the D2HVP group (p-value < 0.005) and of the D2HVP+EAK group (p-value < 0.001), indicating that this treatment is the one that determined a greater calcium deposition inside the pores. According to what was shown during the qualitative histological analysis, the silanized foams (SIL) did not show measurable signals for this parameter. This result indicates that the combination of all three treatments (D2HVP, EAK hydrogel and pro-angiogenic sequence) produced a synergistic action in promoting calcium salts deposition in the inner pore matrix. As previously specified, the role of the D2HVP adhesive peptide is probably to recall mesenchymal stem cells within the scaffold and induce their differentiation into osteoblastic lineage cells. Scaffold colonization by these cells could also be induced by the presence of the EAK hydrogel, which consisting of a nanofibrous structural matrix specifically mimic the architecture of the extracellular matrix[13]. Finally, the presence of the pro-angiogenic sequence could contribute to vessels development inside the scaffold, which bring the nourishment necessary for cell growth, so indirectly could contribute to cell colonization.
The values of Md.S/Po.S for the D2HVP group were greater than those of D2HVP+EAK but no statistically significant difference was detected by the statistical test used. Since the aim of the EAK hydrogel is to favour cell scaffold colonization, we could expect a greater mineralization compared to that obtained. The SAP hydrogel, in fact, consists of a woven nanofibrous structure that fills the pores, which gives the cells the possibility of colonizing the entire available area in a rapid, abundant and homogeneous way. The scaffold

functionalized only with the D2HVP peptide, on the other hand, presents empty pores, in which cell colonization will reasonably occur by stratification on the inner surface. However, the hypothesis of increased colonization stimulated by SAP hydrogel does not necessarily correlate with higher mineral deposition, since no analyses have been carried out to confirm neither the quantity nor the type of cells present in the scaffold, which could, for example, be predominantly fibroblasts rather than osteoblasts, thus representing a non-specific colonization.

The variability in the deposition of calcium salts, in addition to the type of functionalization, could be influenced by factors depending on the individual animal or by the different positioning of the implant in the subcutaneous region. Furthermore, the number of samples available for analysis is a fundamental factor to correctly interpret the data; in this preliminary study, the reduced number of analysed implants was certainly a limit. It will therefore be appropriate to extend the sample size of this preliminary study by carrying out further experiments.

The dynamic histomorphometry parameter of MS/Po.S (Mineralizing Surface versus Pores Surface) measures the active mineralization within the pores of the scaffold during the period of administration of the vital bone marker. It was calculated as the ratio between the surface occupied by Calcein Green marker signal, displayed in fluorescence microscopy, and the total surface of the pores. The results are shown in **Figure 3.12**.

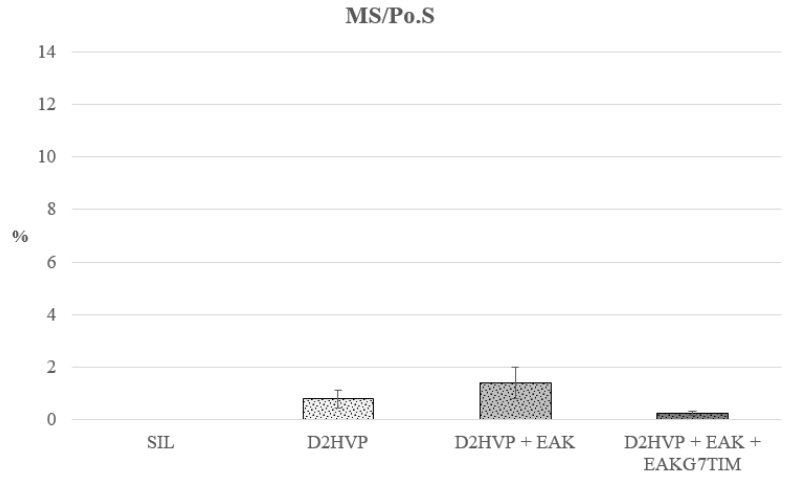


Figure 3.12. Histogram of MS/Po.S during the marking period with Calcein Green (40th, 42nd and 44th day). No statistically significant difference was found among the different functionalizations.

The highest MS/Po.S value was found for the D2HVP + EAK group, followed by the D2HVP group and by D2HVP+EAK+EAKG7TIM, which has the lower value. This means that the scaffolds functionalized with the D2HVP adhesive peptide and the EAK self-assembling peptide hydrogel are those with a higher mineralization activity in the period of administration of the vital bone marker (40^{th}, 42^{nd} and 44^{th} day). Despite this, the

statistical test used did not reveal any significant difference between the different functionalizations. For the control group (SIL), as anticipated by the qualitative analyses, no area of mineralization was measured.

The MAR-SL (Mineral Apposition Rate for Single Label) dynamic histomorphometry parameter indicates the rate of mineral deposition during the lifetime of the vital bone marker. It was calculated as the ratio between the average thickness (in μm) of the deposition fronts marked by Calcein Green, displayed in fluorescence microscopy, and the period of administration of the marker, expressed in days. As shown in **Figure 3.13**, the highest MAR-SL value was found to be that of the group characterized by the functionalization D2HVP+EAK+EAKG7TIM, followed by D2HVP and D2HVP+EAK, which showed the lowest value. Functionalization with the D2HVP adhesive peptide, the EAK self-assembling peptide hydrogel and the EAKG7TIM pro-angiogenic peptide (D2HVP+EAK+EAKG7TIM) thus determines a higher mineral deposition rate in the period corresponding to the administration of the Calcein Green vital bone marker (40^{th} ,42^{nd} and 44^{th} day). Despite this, the statistical test used did not reveal any significant difference between the values measured in the various treated groups. The control, having shown no marking with Calcein Green, presented no mineral deposition rate.

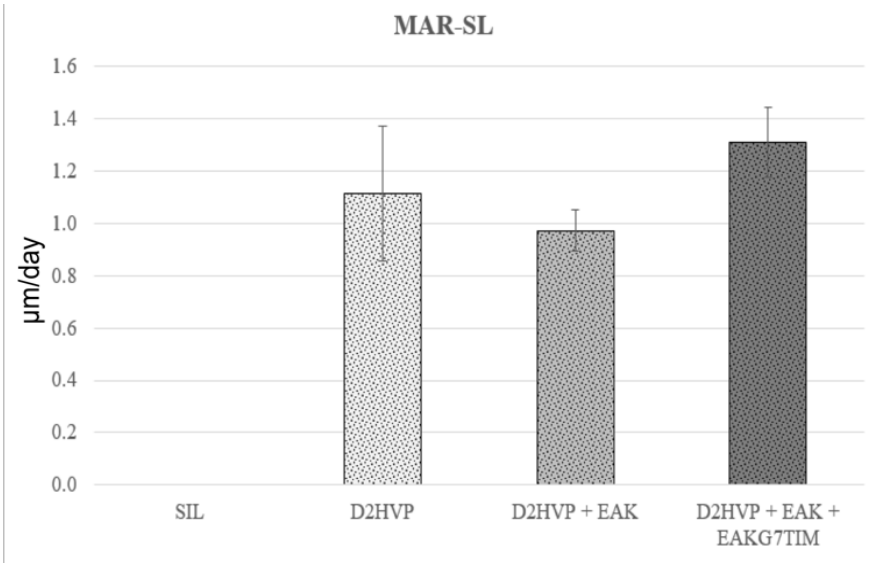


Figure 3.13. Histogram MAR-SL (Mineral Apposition Rate for Single Label) in the marking period with Calcein Green (40°, 42° and 44° day). There is no statistically significant difference between the treated groups.

The similarity of the MAR-SL values among the different types of functionalization could be interpreted as an index of the maximum activity of the D2HVP peptide in inducing mineralization, since, among the different peptides tested, it is the only one having a specific stimulatory activity for osteoblasts.

The fact that the mineralization at the end of the experiment (Md.S/Po.S) presented some statistically significant differences despite the MAR-SL values were almost uniform, can be attributed, to the combined action of the self-assembling peptide's hydrogel.
However, the trend of the MAR-SL parameter reflects the amount of calcium salts detected with the Von Kossa method (Md.S/Po.S), in which the highest value was found to be that of the D2HVP+EAK+EAKG7TIM group while the lower value was that of the D2HVP+EAK group. Considering that the MAR-SL parameter measures the mineral deposition rate only in the period of time corresponding to the Calcein Green marking, it is possible to suppose that its trend actually follows that of the parameter Md.S/Po.S and that the absence of statistical significance depends on the low power of the statistical test, caused by the reduced number of data.
Considering that D2HVP activity in stimulating the mineral deposition rate seemed to be uniform among all functionalized scaffolds, the difference, although not significant, between the mineralization areas could be attributed to the fact that the parameter MS/Po.S is measured within a limited time window, which cannot be considered as totally representative of the whole mineralization process.
The morphological observation of the fronts of mineralization within the various types of scaffolds can help to explain the variability between the measured values. In the D2HVP+EAK+EAKG7TIM group, compared to the other functionalizations, fewer fronts have been observed, but characterized by a greater thickness; this justifies the detection of a smaller surface of active mineralization despite the mineral deposition speed being greater: since the front is thicker, the velocity will be higher, but the scarcity of active fronts in the period of time considered will lead to a lower total area.
On the contrary, the D2HVP+EAK group presented a greater number of fronts, but characterized by a lower thickness; therefore, there is a greater surface of active mineralization at a lower mineral deposition rate. The D2HVP group, on the other hand, showed a surface in active mineralization consistent with the calculated mineral deposition rate.
The quantity of blood vessels present inside each pore of the scaffolds was calculated, at the end of the experimental time (45^{th} day), by manual counting, in light field optical microscopy. The average of the values obtained for each type of functionalization is shown in Table 3.1. The D2HVP+EAK+EAKG7TIM group was found to be the one with the highest average, while the D2HVP group the one with the lower average.
The statistical test used, however, found no statistically significant differences between any of the treatments considered.

Table 3.1. Average number of blood vessels displayed within the pores and standard deviation.

	Scaffold			
	SIL	**D2HVP**	**D2HVP + EAK**	**D2HVP + EAK + EAKG7TIM**
Average	1.00	0.82	1.08	1.50
St. Deviation	0.50	0.18	0.29	0.32

For each type of scaffold, the numerical distribution of blood vessels in the pores was evaluated, too. The data were categorized into three ranges of values, arbitrarily established as less than 2, between 2 and 4 and greater than 4, expressed as a percentage and represented as a histogram of percentage frequencies (**Fig 3.14**).

As shown in **Figure 3.14**, the D2HVP+EAK+EAKG7TIM group, whose treatment includes a pro-angiogenic peptide, is the only one characterized by the presence of pores containing a number of blood vessels higher than 4.

In addition, regarding the pores containing a number of pots between 2 and 4, it is the group that showed the largest percentage, but with a value more similar to the other types of functionalization tested.

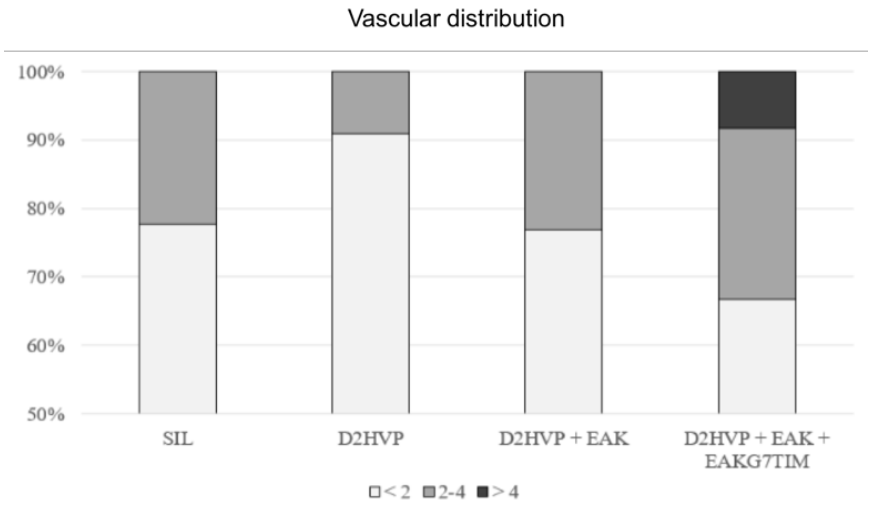


Figure 3.14. Histogram of percentage frequencies of the number of blood vessels within the individual pores of the scaffolds. D2HVP+EAK+EAKG7TIM functionalization is the only one characterized by pores containing a number of vessels higher than 4.

Since increased vascularization results in a greater supply of nutrients, oxygen and a greater possibility for mesenchymal stem cells to reach and colonize the scaffold, it can be hypothesized that, in the D2HVP+EAK+EAKG7TIM scaffolds, osteoblasts and osteoprogenitor cells, receiving more nutrients and oxygen, are more vital than cells in the scaffolds functionalized with D2HVP and D2HVP+EAK.

The colonization support provided by EAK hydrogel, together with a greater supply of nutrients and oxygen, could therefore provide a more suitable environment for bone cells,

which would result in higher vitality and, consequently, greater mineral deposition. Furthermore, the increased vascularization found in the scaffolds functionalized with EAKG7TIM, although not statistically significant with respect to the other types of scaffold, would indicate the ability of this peptide sequence to stimulate *in vivo* production of blood vessels within the scaffold.

For the pro-angiogenic peptide TIM derived from thymosin β4, which constitutes EAKG7TIM in combination with the self-assembling peptide EAK, the ability to stimulate endothelial cell growth and vessel formation *in vivo* has already been demonstrated[14].

The results of this work suggested that the EAKG7TIM peptide still maintained the pro-angiogenic properties of the native pro-angiogenic peptide. Further studies will be necessary to obtain an effective confirmation of the angiogenic properties of this new peptide sequence.

3.3 Conclusions

Wollastonite-diopside foams from preceramic polymer precursor and reactive oxide fillers were successfully synthetized, and subsequentially, covalently and selectively functionalized with HVP series' peptides. We demonstrated that the functionalization protocol didn't negatively affect the mechanical strength at crushing of W/D foams.

All functionalized samples showed increased cell proliferation *in vitro* with respect to the control and silanized foams; in particular, retro-inverted sequences doubled the proliferation with respect to HVP and 2HVP at 2 days. This result could be due to the capacity of DHVP and D2HVP to maintain the bioactivity of natural sequences (HVP and 2HVP) jointed with their complete stability to enzymatic degradation. These properties of the two retro-inverted sequences were confirmed in previous study[3],

In fact, in the synthesis of a retro-inverted peptide, D-amino acids assembled in the reverse order as compared to the parent L-sequence, leading to an analogue in which the side chains are usually arranged similarly to the native peptide[15–19], but, unfortunately, retro-inverted sequences not always maintain the bioactivity of the native peptide[20,21]. In this case, the bioactivity of the two retro-inverted sequences DHVP and D2HVP seemed to be further increased by their stability to enzymatic degradation when compared to the L-sequences in long time proliferation assays.

D2HVP anchored to W/D foams gave a dramatic proliferation increase of more than 15 times in respect to the controls at 6 days. All anchored peptides enhanced mRNA specific transcript levels coding *IBSP*, *VTN*, *RUNX2* and *SPP1*, proteins fundamental in bone development.

In most cases, it was shown that retro-inverted peptides do not induce cytotoxicity when compared to L-enantiomers, nevertheless, cytotoxicity has to be ascertained case by

case[22,23], and LDH test confirmed the absence of cytotoxicity induced by the functionalization treatment at 4 and 6 days.

D2HVP functionalized foams enhanced calcium deposition *in vivo* and histological analysis revealed the presence of new calcium deposits inside the pores only on functionalized bioceramics. *In vivo* assays demonstrated the osteoconductive and osteoinductive properties of D2HVP peptide.

The normal macroscopic appearance of the implants after 45 days from the surgery showed no inflammation and no encapsulation.

The qualitative analysis performed with light field optical microscopy showed external and internal colonization of all the scaffolds with formation of new blood vessels (neoangiogenesis).

All the functionalizations tested proved to be able to stimulate the process of ectopic mineralization, whilst the control didn't develop any degree of mineralization. Md.S/Po.S (Mineralized Surface versus Pores Surface), however, resulted to be significantly greater for the group characterized by the functionalization D2HVP+EAK+EAKG7TIM, which showed a greater vascularization, too. This demonstrated that the EAK self-assembling peptide, designed to aid scaffold colonization, and the pro-angiogenic EAKG7TIM sequence have a synergistic effect in promoting mineralization.

Future studies will confirm the results obtained in the present work, especially regarding the osteoinductive capacities of D2HVP+EAK and D2HVP+EAK+EAKG7TIM functionalizations, it will be necessary to carry out further *in vivo* experiments to assess reproducibility.

The next step will be to evaluate the efficacy, in regenerative endosseous approaches, of the W/D scaffold characterized by the most efficient functionalization in promoting osteogenesis. Finally, the same covalent and specific functionalization's strategy has to be tested on different types of bioceramic scaffolds, in order to assess if the proposed functionalization protocol can be easily transferred to all types of polymer-derived bioglass still improving in a comparable way the biological properties. This last topic will be investigated in Chapter 4.

3.4 Materials and methods

3.4.1 W/D foams synthesis and characterization

Wollastonite-Diopside(W/D) foams were prepared using the following method[1]: recipe for 10g of final W/D: 9.34g of H62C (preceramic precursor polymer, silica source, with a yield of 58%wt, Wacker-Chemie GmbH, Munich, Germany), 6.02g of $CaCO_3$ (<10µm, Industrie Bitossi, Vinci, Italy), 1.76g of $Mg(OH)_2$ (<10µm, Industrie Bitossi, Vinci, Italy). All dissolved in 9mL isopropanol (IPA). Then add 0.3g (3% of the total final amount) of Borax ($Na_2B_4O_7 \cdot 10H_2O$, foaming agent, Sigma-Aldrich). Let the mixture at 60°C overnight to dry IPA. Put 1.8g in each melting pot of aluminum to proceed with two following treatments: (i) foaming treatment: 350°C for 30min; (ii) ceramization step: 1100°C for 2h with a T ramp of 2°C/min (**Fig 3.15**).

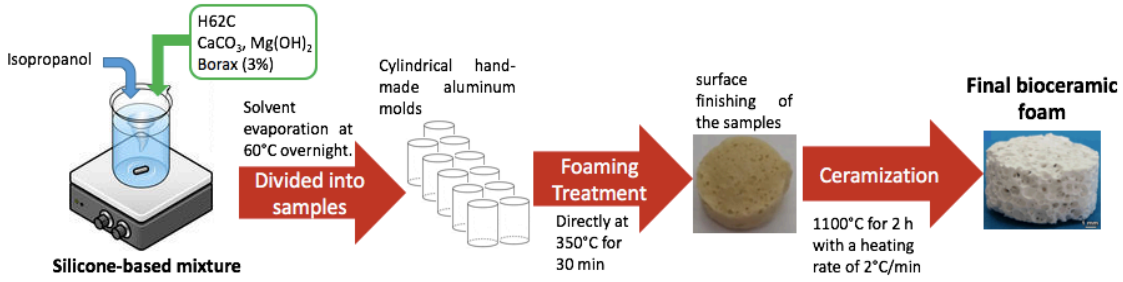


Fig 3.15. Schematic representation of W-D foams synthesis

The crystalline phase assemblage was investigated by X-ray diffraction (XRD, Bruker AXS-D8 advance, Karlsruhe, Germany-CuKα radiation, 0.15418 nm, 40 kV–40 mA, 2θ = 15°–70°, step size = 0.05°, 2 s counting time). A semi-automatic phase identification was provided by the Mach! Software package (crystal Impact GbR, Bonn, Germany), supported by data from the PDF-2 database (ICDD-International Centre for diffraction Data, Newton Square, PA, USA).

The bulk density of the foams was determined from the weight-to-volume ratio, using a caliper and a digital balance. The true density of the samples was measured by means of a gas pycnometer (Micromeritics AccuPyc 1330, Norcross, GA, USA), operating with He gas on finely-milled samples. The final properties of the obtained W/D are listed in **Table 3.2**. W/D foams were synthetized and characterized at the Department of Industrial Engineering, University of Padova (Prof. Enrico Bernardo).

Table 3.2. Final properties of Wollastonite-Diopside foams

	Bulk Density [g/cm^3]	Open Porosity [%]	Wollastonite [wt%]	Diopside [wt%]	Other phases [wt%]	Glass [wt%]
W/D foams	0.73 ± 0.02	77.0	29.3	45.3	8.2	10.2

3.4.2 Adhesive peptides synthesis and characterization

All adhesive peptides were synthesized by standard Fmoc chemistry using Sieber Amide resin (0.72 mmol/g; scale 0.125 mmoles, Novabiochem, Merck KGaA, Darmstadt, Germany) and a fully automated peptide synthesizer (Syro I, Multisynthec, Witten, Germany). The synthetized sequences are reported in **Table 3.3** (the underlined sequences refer to D-amino acids).

All Fmoc-protected amino acids were from Novabiochem.

Table 3.3 HVP series of synthetic peptides

Name	*Sequence*
HVP	FRHRNRKGY
2HVP	FRHRNRKGYFRHRNRKGY
DHVP	YGKRNRHRF
D2HVP	YGKRNRHRFYGKRNRHRF

The side chain protection employed were: Arg, Pbf; His and Asn, Trt; Lys, Boc; Tyr, tBu. The coupling reaction was carried out using 5 eq of Fmoc protected amino acid, 5 eq of HOBt/HBTU and 10 eq of DIPEA. The coupling reagents 2-(1H-Benzotriazole-1-yl)-1,1,3,3-tetramethyluronium hexafluorophosphate (HBTU) and 1-Hydroxybenzotriazole (HOBt) were from Advanced Biotech (Seveso, MI, Italy). N,N-diisopropylethylamine (DIEA) and piperidine were from Biosolve (Leenderweg, Valkenswaard, The Netherlands). All the couplings were double. The peptides were cleaved from the solid support without contemporary side-chain deprotection using the following mixture: 1% 2,2,2-trifluoroacetic acid (TFA) in dichloromethane (DCM).

Solvents, such as N,N-dimethylformamide (DMF), trifluoroacetic acid (TFA), N-methyl-2-pyrrolidone (NMP), dichloromethane (DCM), and acetonitrile were from Biosolve. A sample of each crude peptide was completely deprotected using the following mixture: 2.5% H_2O MilliQ, 2.5% TES, and 95% TFA (90 min, under magnetic stirring). After cleavage, the resin was filtered, the reaction mixture concentrated and the crude peptide precipitated with cold ethyl ether. Peptides identity and homogeneity were ascertained by mass (ESI-TOF Mariner System 5220, Applied Biosystems, Perkin-Elmer, Norfolk, CT) and RP-HPLC analyses (Waters Corporation, Milford, MA), respectively.

The peptides used for W/D functionalization were crude peptides.

3.4.2.1 HVP characterization

The native nona-peptide HVP was characterized as reported in Dettin et al[24].

3.4.2.2 2HVP characterization

The chromatogram of crude peptide was carried out in the following conditions: column, Jupiter C18 (5µm, 300Å, 4.6×250 mm, Phenomenex); injection volume, 10µL of 1 mg/mL peptide solution; flow rate, 1 mL/min; eluent A, 0.05% TFA in water; eluent B, 0.05% TFA in CH_3CN; gradient, from 10%B to 30%B in 20 min, detection at 214 nm. The retention time results 11.6 min. Experimental mass: 2447.43 Da, Theoretical mass: 2447.79 Da (ESI-TOF, Mariner System 5220, Applied Biosystem, Perkin-Elmer, California, USA).

3.4.2.3 DHVP characterization

The chromatogram of crude peptide was carried out in the following conditions: column, Jupiter C18 (5µm, 300Å, 4.6×250 mm, Phenomenex); injection volume, 10µL of 1 mg/mL peptide solution; flow rate, 1 mL/min; eluent A, 0.05% TFA in water; eluent B, 0.05% TFA in CH_3CN; gradient, from 10%B to 20%B in 20 min, detection at 214 nm. The retention time results 10.8 min. Experimental mass: 1232.75 Da, Theoretical mass: 1232.39 Da (ESI-TOF, Mariner System 5220, Applied Biosystem, Perkin-Elmer, California, USA).

3.4.2.4 D2HVP characterization

The chromatogram of crude peptide was carried out in the following conditions: column, Vydac C18 monomeric (5µm, 300Å, 4.6×250 mm, Grace); injection volume, 20µL of 1 mg/mL peptide solution; flow rate, 1 mL/min; eluent A, 0.05% TFA in water; eluent B, 0.05% TFA in CH_3CN; gradient, from 8% B to 18%B in 20 min, detection at 214 nm. The retention time results 12.4 min. Experimental mass: 2448.32 Da, Theoretical mass: 2447.82 Da (ESI-TOF, Mariner System 5220, Applied Biosystem, Perkin-Elmer, California, USA).

3.4.3 Non-adhesive peptide synthesis and characterization

A non-adhesive sequence $(GRADSP)_4K$ (Sequence: H-Gly-Arg-Ala-Asp-Ser-Pro-Gly-Arg-Ala-Asp-Ser-Pro-Gly-Arg-Ala-Asp-Ser-Pro-Gly-Arg-Ala-Asp-Ser-Pro-Lys-NH_2) was synthetized as a control for all *in vitro* biological assays. The non-adhesive peptide was synthesized by standard Fmoc chemistry using Sieber Amide resin (0.72 mmol/g; scale 0.125 mmoles, Novabiochem, Merck KGaA, Darmstadt, Germany) and a fully automated peptide synthesizer (Syro I, Multisynthec, Witten, Germany). All Fmoc-protected amino acids were from Novabiochem. The side chain protection employed were: Arg, Pmc; Ser, tBu; Asp, OtBu; Lys, Boc. The coupling reaction was carried out using 5 eq of Fmoc protected amino acid, 5 eq of HOBt/HBTU and 10 eq of DIPEA. The coupling reagents 2-(1H-Benzotriazole-1-yl)-1,1,3,3-tetramethyluronium hexafluorophosphate (HBTU) and 1-Hydroxybenzotriazole (HOBt) were from Advanced Biotech (Seveso, MI, Italy). N,N-diisopropylethylamine (DIEA) and piperidine were from Biosolve (Leenderweg, Valkenswaard, The Netherlands). The loading of the resin with the first amino acid was

carried out with a double coupling, the following 18 couplings were single and all the remaining were double. The peptide was cleaved from the solid support without contemporary side-chain deprotection using the same procedure used for all adhesive peptides. A sample of crude peptide was completely deprotected using the following mixture: 2.5% H_2O MilliQ, 2.5% TES, and 95% TFA (90 min, under magnetic stirring). After cleavage, the resin was filtered, the reaction mixture concentrated and the crude peptide precipitated with cold ethyl ether. Peptide identity and homogeneity were ascertained by mass (ESI-TOF Mariner System 5220, Applied Biosystems, Perkin-Elmer, Norfolk, CT) and RP-HPLC analyses (Waters Corporation, Milford, MA), respectively. The chromatogram of crude peptide was obtained in the following conditions: column, Vydac C18 (5µm, 300Å, 4.6×250 mm, Grace); injection volume, 30µL of 1 mg/mL peptide solution; flow rate, 1 mL/min; eluent A, 0.05% TFA in water; eluent B, 0.05% TFA in CH_3CN; gradient, from 0%B to 30%B in 30 min, detection at 214 nm. The retention time results 20.8 min. Experimental mass: 2479.20 Da, Theoretical mass: 2479.59 Da (ESI-TOF, Mariner System 5220, Applied Biosystem, Perkin-Elmer, California, USA). The peptide used for W/D functionalization was crude peptide.

3.4.4 Self-assembling peptide synthesis and characterization

3.4.4.1 EAK

The synthesis of EAK (H-Ala-Glu-Ala-Glu-Ala-Lys-Ala-Lys-Ala-Glu-Ala-Glu-Ala-Lys-Ala-Lys-NH_2) was carried out on 0.72 mmol/g Rink Amide MBHA resin (Novabiochem, Merck KGaA, Darmstadt, Germany) using Fmoc chemistry by a Syro I synthesizer (Multisynthec, Witten, Germany). All Fmoc- protected amino acids were from Novabiochem. The side chain protecting groups were: OtBu, Glu and Boc, Lys. The loading of the first amino acid was carried out with a double coupling (5 eq. of Fmoc-amino acid, 5 eq. HBTU, 5 eq. HOBt and 10 eq. DIEA, for 45 min). The following four insertions were carried out with single couplings and the remaining ones with double couplings. The coupling reagents 2-(1H-Benzotriazole-1-yl)-1,1,3,3-tetramethyluronium hexafluorophosphate (HBTU) and 1-Hydroxybenzotriazole (HOBt) were from Advanced Biotech (Seveso, MI, Italy). N,N-diisopropylethylamine (DIEA) and piperidine were from Biosolve (Leenderweg, Valkenswaard, The Netherlands). Solvents, such as N,N-dimethylformamide (DMF), trifluoroacetic acid (TFA), N-methyl-2-pyrrolidone (NMP), dichloromethane (DCM), and acetonitrile (CH_3CN) were from Biosolve. At the end of the synthesis the last inserted amino acid was Fmoc-deprotected. Crude peptide was cleaved from the resin and protecting groups were removed using a 95% TFA, 2.5% TES, 2.5% H_2O MilliQ (v:v:v). Purification of the crude product was performed through reverse phase high performance liquid chromatography (RP-HPLC). The homogeneity (>99%) of the

purified product was calculated by the integration of the analytical chromatogram peaks, whereas the identity of each product was ascertained by ESI-TOF (ESI-TOF, Mariner System 5220, Applied Biosystem, Perkin-Elmer, Foster City, CA, USA) and mass spectrometry (experimental mass = 1614.84 Da; theoretical mass = 1614.83 Da). The chromatogram of purified peptide was carried out in the following conditions: column, Jupiter C18 (5µm, 300Å, 4.6x250 mm, Phenomenex); injection volume, 100µL of 1 mg/mL peptide solution; flow rate, 1 mL/min; eluent A, 0.05% TFA in water; eluent B, 0.05% TFA in CH_3CN; gradient, from 7%B to 27%B in 20 min, detection at 214 nm. The retention time results 10.9 min.

3.4.4.2 AoaEAK

The peptide AoaEAK (sequence: NH_2-O-CH_2-CO-Ala-Glu-Ala-Glu-Ala-Lys-Ala-Lys-Ala-Glu-Ala-Glu-Ala-Lys-Ala-Lys-NH_2, Aoa represents the aminooxyacetic acid at N-terminus) was synthesized by standard Fmoc chemistry using Rink Amide MBHA resin (0.7 mmol/g; scale 0.125 mmoles, Novabiochem, Merck KGaA, Darmstadt, Germany) and a fully automated peptide synthesizer (Syro I, Multisynthec, Witten, Germany). All Fmoc-protected amino acids were from Novabiochem. The side chain protection employed were: Glu, OtBu; Lys, Boc; Aoa, BisBoc. The Fmoc removal was accomplished by two treatments with 40% and 20% piperidine/DMF for 3 min and 12 min respectively. The coupling reaction was carried out using 5-fold excess of Fmoc protected amino acid and HOBt/HBTU/DIPEA (5-fold excess in HOBt/HBTU and 10-fold excess in DPEA; 45 min) in DMF. The coupling reagents 2-(1H-Benzotriazole-1-yl)-1,1,3,3-tetramethyluronium hexafluorophosphate (HBTU) and 1-Hydroxybenzotriazole (HOBt) were from Advanced Biotech (Seveso, MI, Italy). N,N-diisopropylethylamine (DIEA) and piperidine were from Biosolve (Leenderweg, Valkenswaard, The Netherlands). The loading step was a double coupling with Fmoc-Lys(Boc)-OH, the following four couplings were single and the remaining 12 cycles were double. Solvents, such as N,N-dimethylformamide (DMF), trifluoroacetic acid (TFA), N-methyl-2- pyrrolidone (NMP), dichloromethane (DCM), and acetonitrile (CH_3CN) were from Biosolve. After the Fmoc deprotection the resin was washed with DCM and dried for 1 hr under vacuum. The peptide was cleaved from the solid support with contemporary side-chain deprotection using the following mixture: 0.125 mL H_2O MilliQ, 0.125 mL TES, 4.750 mL TFA (90 min, under magnetic stirring). Triethoxysilane (TES) was from Sigma-Aldrich (Steinheim, Germany). After cleavage the resin was filtered, the reaction mixture concentrated and the crude peptide precipitated with ethyl ether. The chromatogram of crude peptide was obtained in the following conditions: column, Vydac C18 monomeric (5µm, 300Å, 4.6x250mm, Grace), Injection volume, 200µL of 1 mg/mL peptide solution; flow rate, 1 mL/min; eluent A, 0.05% TFA in water; eluent B, 0.05% TFA in CH_3CN; gradient, from 0%B to 30%B in 30 min, detection at 214

nm. The retention time results 12.97 min. Experimental mass: 1687.9 Da, Theoretical mass: 1687.8 Da (ESI-TOF, Mariner System 5220, Applied Biosystem, Perkin-Elmer, California, USA).

3.4.5 Pro-angiogenic peptide synthesis and characterization

The peptide G7TIM (Sequence: H-Gly-7-aminoheptanoic acid-Ser-Lys-Leu-Lys-Lys-Thr-Glu-Thr-Gln-Glu-NH_2, 7 represents 7-aminoheptanoic acid and the flexible spacer G7 at the N-terminus of the TIM peptide was inserted as it was demonstrated to increase the yield of site-specific bioconjugation through N-terminal transamination[25]) was synthesized by standard Fmoc chemistry using Rink Amide MBHA resin (0.7 mmol/g; scale 0.125 mmoles, Novabiochem, Merck KGaA, Darmstadt, Germany) and a fully automated peptide synthesizer (Syro I, Multisynthec, Witten, Germany). All Fmoc-protected amino acids were from Novabiochem. The side chain protection employed were: Ser and Thr, But; Glu, OtBu; Gln, Trt; Lys, Boc. The Fmoc removal was accomplished by two treatments with 40% and 20% piperidine/DMF for 3 min and 12 min respectively. The coupling reaction was carried out using 5-fold excess of Fmoc protected amino acid and HOBt/HBTU/DIPEA (5-fold excess in HOBt/HBTU and 10-fold excess in DPEA; 45 min) in DMF. The coupling reagents 2-(1H-Benzotriazole-1-yl)-1,1,3,3-tetramethyluronium hexafluorophosphate (HBTU) and 1-Hydroxybenzotriazole (HOBt) were from Advanced Biotech (Seveso, MI, Italy). N,N-diisopropylethylamine (DIEA) and piperidine were from Biosolve (Leenderweg, Valkenswaard, The Netherlands). All the couplings were double. After the Fmoc deprotection the resin was washed with DCM and dried for 1hr under vacuum. Solvents, such as N,N-dimethylformamide (DMF), trifluoroacetic acid (TFA), N-methyl-2- pyrrolidone (NMP), dichloromethane (DCM), and acetonitrile (CH_3CN) were from Biosolve. The peptide was cleaved from the solid support with contemporary side-chain deprotection using the following mixture: 0.125 mL H_2O MilliQ, 0.125 mL TES, 4.750 mL TFA (90 min, under magnetic stirring). Triethoxysilane (TES) was from Sigma-Aldrich (Steinheim, Germany). After cleavage the resin was filtered, the reaction mixture concentrated and the crude peptide precipitated with cold ethyl ether. Thirty mg of crude peptide dissolved in 20 mL of MilliQ water were loaded on Jupiter C18 (5µm, 300Å, 10×250 mm, Phenomenex) and separated in the following conditions. Eluent A, 0.05% TFA in MilliQ water; Eluent B, 0.05% TFA in CH_3CN; gradient, from 0%B to 5%B in 2 min, then from 5%B to 25%B in 40 min; flow rate, 4 mL/min; detection at 214 nm. The identity of the peptide was ascertained by ESI-TOF (ESI-TOF, Mariner System 5220, Applied Biosystem, Perkin-Elmer, Foster City, CA, USA) and mass spectrometry (experimental mass = 1373.61 Da; theoretical mass = 1372.86 Da). The chromatogram of purified peptide was carried out in the following conditions: Jupiter C18 (5µm, 300Å, 4.6×250 mm, Phenomenex); injection volume, 10µL of 1 mg/mL peptide solution; flow

rate, 1 mL/min; eluent A, 0.05% TFA in water; eluent B, 0.05% TFA in CH_3CN; gradient, from 10%B to 30%B in 20 min, detection at 214 nm. The retention time results 7.4 min and the purity grade, 97%.

3.4.6 Chemoselective ligation of EAK and G7TIM

In this research project the pro-angiogenic sequence G7TIM was covalently linked to the self-assembling peptide EAK through chemoselective ligation. The N-terminal amino acid of pure G7TIM was converted into a α-ketoaldehyde, using the method proposed by J.M. Gilmore *et al.*[26] (Paragraph 1.3.1.4, **Fig 1.10,** reaction **1+2→3**), in which the peptide was treated with 20 eq. PLP in buffer solution (25 mM NaH_2PO_4, pH 6.5) at 37°C for 18 h. Once the transamination reaction was carried out successfully, the α-ketoaldehyde product was purified and characterized by HPLC and mass spectrometry. The chromatogram of purified α-ketoaldehyde G7TIM was obtained in the following conditions: column, Symmetry Shield RP8 (5µm, 100Å, 4.6×250 mm, Waters); injection volume, 20 µL of 1 mg/mL peptide solution; flow rate, 1 mL/min; eluent A, 0.05% TFA in water; eluent B, 0.05% TFA in CH_3CN; gradient, from 10%B to 25%B in 25 min, detection at 214 nm. The retention time results 18.8 min and the purity grade, 82%. Experimental mass: 1373.78 Da, Theoretical mass: 1372.8 Da (ESI-TOF, Mariner System 5220, Applied Biosystem, Perkin-Elmer, California, USA).

The final reaction (Paragraph 1.3.1.4, **Fig 1.10**, **3+4→5**), leading to the formation of the oxime bond between the purified α-ketoaldehyde G7TIM and crude AoaEAK, functionalized at N-terminus with aminooxyacetic acid (Aoa), was carried out for 24 hours at room temperature, with a ratio between α- ketoaldehyde peptide and SAP of 1:10 eq, in 1mM SAP aqueous solution.

The final product EAKG7TIM was purified and characterized by HPLC and mass analyses. The chromatogram was obtained in the following conditions: column, Jupiter C18 (5µm, 300Å, 4.6×250 mm, Phenomenex); injection volume, 20 µL of 1 mg/mL peptide solution; flow rate, 1 mL/min; eluent A, 0.05% TFA in water; eluent B, 0.05% TFA in CH_3CN; gradient, from 0%B to 35%B in 35 min, detection at 214 nm. The retention time results 22.9 min and the purity grade, 85%. Experimental mass: 3042.65 Da, Theoretical mass: 3042.73 Da (ESI-TOF, Mariner System 5220, Applied Biosystem, Perkin-Elmer, California, USA)

3.4.7 W/D foams functionalization

3.4.7.1 Selective and covalent functionalization

A specific functionalization of Wollastonite-Diopside foams (mass: 35mg) was carried out following the procedure reported in **Figure 3.16**. The side- chain deprotection was obtained

treating each sample with a solution of 95% TFA, 2,5% MilliQ water and 2,5% TES, for 1h at room temperature. The samples underwent the following washings: once in TFA, twice in acetone, three times in MilliQ water and finally twice in acetone. The W/D were dried under vacuum for 30 min. The coupling reagents 2-(1H-Benzotriazole-1-yl)-1,1,3,3-tetramethyluronium hexafluorophosphate (HBTU) and1-Hydroxybenzotriazole (HOBt) were from Advanced Biotech (Seveso, Italy). N, N-diisopropyle- thylamine (DIPEA) and piperidine were from Biosolve (Leenderweg, Valkenswaard, The Netherlands). Triethoxysilane (TES) and acetone were from Sigma-Aldrich (Steinheim, Germany). Solvents for synthesis such as trifluoroacetic acid (TFA), N-methyl-2-pyrrolidone (NMP) and dichloromethane (DCM) were from Biosolve. (3-Aminopropyl)triethoxysilane (APTES 2%) was from Sigma-Aldrich.

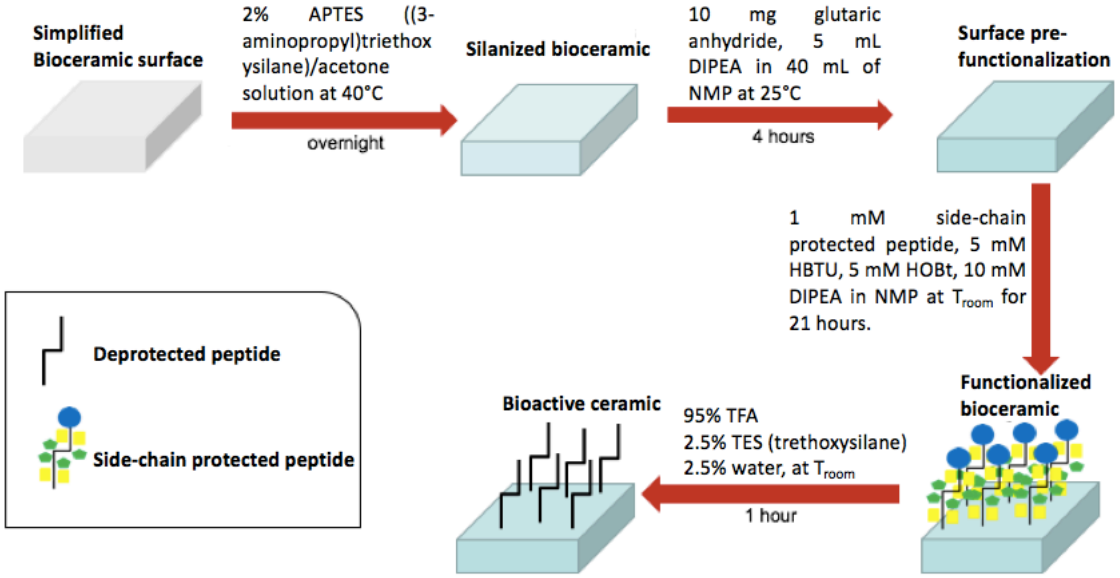


Figure 3.16. Scheme of the covalent and specific functionalization of wollastonite-Diopside foams.

Previous studies[27] carried out with titanium surfaces demonstrated that this functionalization strategy leads to a superficial peptide density between 0.016 and 0.063 nmol/cm^2.

3.4.7.2 SAP embedding

Wollastonite-Diopside foams, after selective and covalent functionalization, were completely covered in a 0.3% w/v EAK solution in milliQ H_2O and let at 37°C for 30 min to allow the solution to completely fill the open porosity of the material. Then an equal volume of PBS was added to each sample and let at 37°C for other 30 min, EAK self-aggregated at the final concentration of 0.15% w/v. A 0.15% w/v SAP concentration was used for *in vivo* assays as it showed promising *in vitro* results in previous studies[28].

3.4.8 Crushing strength test

The crushing strength of functionalized foams was measured at room temperature using an Instron 1121 UTM (Instron Danvers, MA), equipped with 10kN load cell with a cross-head speed of 1 mm/min. The mean value of five to ten samples was used for each data point.

3.4.9 *In vitro* bioassays

All *in vitro* bioassays were carried out at the Department of Molecular Medicine, University of Padova (Prof. Paola Brun). Primary human (h) osteoblast cells were obtained from explants of cortical mandible bone collected during a surgical procedure from healthy subjects. The study was approved by the Ethical committee of the University Hospital of Padova. Patients were informed of the study aims and protocol and gave their written informed consent.

Bone fragments were cultured in Dulbecco's Modified Eagle Medium (DMEM, provided from Gibco, Thermo Scientific) supplemented with 20% heat inactivated FBS, 10,000 units/mL of penicillin, 10,000 µg/mL of streptomycin (Gibco) and incubated at 37°C until cells migrated from the bone fragments. At cell confluence, bone fragments were removed, cells were detached using trypsine-EDTA (Gibco) and cultured in DMEM supplemented with 50 mg/mL ascorbic acid, 10 nM dexametasone, and 10 mM β-glycerophosphate (all purchased from Sigma-Aldrich).

Osteoblast phenotype was confirmed by the von Kossa staining[29]. Cells were used at passage 3th and 8th in culture.

For biological assays, bioceramic foams were placed into non-treated sterile plates (Corning) and incubated with h-osteoblasts ($3x10^5$ cells/cm^2) in complete culture medium.

3.4.9.1 Adhesion assay

Cell viability was assessed using the MTT (3-(4,5-dimethylthia- zole-2-yl)-2,5-diphenyl tetrazoliumbromide; Sigma) assay on h-osteoblasts cultured on bioceramic foams at 37°C for 2 hrs, incubation time previously reported ensuring the optimal adhesion of h-osteoblasts to functionalized surfaces[2].

At the end of incubation, samples were rinsed three times with PBS in order to remove non-adherent cells and then incubated with MTT solution (5 mg/mL) at 37°C for 4 h under continuous gentle shaking.

Reaction was stopped by adding 0.01N HCl in 10% v/v SDS and absorbance was recorded 16h later at 620nm using a plate reader (Sunrise, Tecan; Switzerland). To quantify cells adhering to bioceramic foams, a standard curve was obtained for each experiment by seeding a known number of h-osteoblasts on tissue-treated sterile culture plates.

3.4.9.2 Proliferation assay

To assess cell proliferation, h-osteoblasts were at first loaded with 25µM carboxyfluorescein diacetate succinimidyl ester (CFSE, Molecular Probe, Invitrogen), cell-permeable fluorescent probe that is equally partitioned among daughter cells. Cells were incubated with CFSE at 37°C for 10 min in pre-warmed PBS containing 0.1% v/v BSA (Sigma) and reaction was stopped by adding 5 volumes of ice-cold culture media. Cells were then washed, counted using Trypan blue, and seeded on bioceramic foams. After 2, 4, and 6 days on culture, cells were detached using trypsine-EDTA. Cell proliferation was assessed using BD FACS-Calibur flow cytometer by evaluating the percentage of CFSE-positive cells.

3.4.9.3 Cytotoxity assay

To investigate whether bioceramic foams have a toxic effect, cell death was assessed on h-osteoblasts by measuring the lactate dehydrogenase (LDH), a soluble cytoplasmic enzyme released into extracellular space when membranes are damaged[30].

Culture medium of h-osteoblasts seeded on bioceramic foams for 4 or 6 days was harvested and added of lysis buffer following the instructions of the kit (Lactate Dehydrogenase Activity Assay Kit; Sigma-Aldrich). Samples were incubated at 37°C for 45 min and centrifuge to eliminate cell debris. Supernatants were incubated with LDH assay buffer and the reaction was stopped 30 min later by acidification.

Absorbance was measured at 520nm using a plate reader (Sunrise, Tecan; Switzerland). Positive control was set by incubating cells for 30 min with 1% Triton, a membrane detergent agent.

3.4.9.4 Quantitative real time polymerase chain reaction

Specific mRNA transcript levels coding human Integrin Binding Sialoprotein (IBSP), human Vitronectin (VTN), Secreted Phosphoprotein 1 (SPP1), and Runt Related Transcription Factor 2 (Runx2) were quantified in osteoblast cells cultured for 48 h on bioceramic foams.

At the end of incubation, total RNA was extracted using the SV Total RNA Isolation System kit (Promega, Milan, Italy).

Contaminating DNA was removed by DNase I digestion. cDNA synthesis and subsequent polymerization was performed in a one-step using the iTaq Universal SYBR Green One-Step Kit (Bio-Rad). The reaction mixture contained 200 nM forward primer, 200 nM reverse primer, iTaq universal SyBR Green reaction mix, iScript reverse transcriptase, and 200 ng total RNA. Real time PCR was performed using ABI PRISM 7700 Sequence Detection System (Applied Biosystems). Human GAPDH was used as reference gene.

Target and reference genes were amplified with efficiencies near 100%. Oligonucleotides used for PCR are listed in **Table 3.4**.

Table 3.4. Oligonucleotides used in qPCR experiments. [a]Fw: forward; [b]Rv: reverse.

GENE[ACCESSION#]	SEQUENCE
GAPDH	[a]Fw: 5'-cgggaagcccatcacca-3'
[NM_002046]	[b]Rv: 5'-ccggcctcaccccatt-3'
IBSP	Fw: 5'-ttactaccaccaccagtgaagc-3'
[NM_004967]	Rv: 5'-gatgcaaagccagaatggat-3'
VTN	Fw: 5'- ggaggacatcttcgagcttct-3'
[NM_000638]	Rv: 5'- gctaatgaactggggctgtc-3'
SPP1	Fw: 5'- aagtttcgcagacctgacatc-3'
[NM_000582]	Rv: 5'- ggctgtcccaatcagaagg-3'
RUNX2	Fw: 5'- cagtgacaccatgtcagcaa-3'
[NM_001024630]	Rv: 5'- gctcacgtcgctcattttg-3'

3.4.10 *In vivo* bioassays

All *in vivo* bioassays were carried out at the Department of Molecular Medicine, University of Padova (Prof. Paola Brun). Surgical procedures and animal care were performed with the approval of Animal Care and Use Committee of the Padova University under supervision of the Health Italian Ministry and following the European directive for animal experiments. C57BL/6J male mice 6-week-old were anesthetized by inhalation of isoflurane 5%. The dorsal skin of animals was shaved and washed with 70% ethanol and an incision of 1 cm was made in skin to create a pocket under the cutaneous tissue. Immediately, a ceramic foam was inserted in each side and the incision was sutured. In compliance with the 3R (Replace, Reduce, Refine) guiding principles for the use of animals in scientific research, two ceramic samples per animal were implanted (**Fig. 3.17**, **a-d**). After surgical procedures, animals were returned to their cages and daily observed for any sign of pain. Mice were euthanized 45 days after implantation. Ceramic samples were collected and fixed in 10% formalin.

Four different types of functionalised scaffolds were used: SIL = silanized W/D scaffold (control); D2HVP = W/D scaffold functionalized with the D2HVP peptide; D2HVP+EAK = W/D scaffold functionalized with the D2HVP peptide and enriched with EAK (0.15% w/v); D2HVP+EAK+EAKG7TIM = W/D scaffold functionalized with the D2HVP peptide and enriched with EAK (0.15% w/v) and $5x10^{-5}$M EAKG7TIM (a pro-angiogenic sequence grafted to EAK via chemoselective ligation through the protocol reported in paragraph 3.4.6). The previously sterilized scaffold was placed above the subcutaneous musculature.

For each mouse two scaffolds were inserted, bilaterally and randomly, taking care not to insert the same type of sample into the same animal. Finally, the skin has been closed and sutured. At 40, 42 and 44 day after samples' implantation, the vital bone marker Calcein Green (50 mg/kg) was administered intraperitoneally, in order to highlight the osteogenic activity inside the scaffold during the period of administration. On the 45th day, the animals were sacrificed and the implants were removed. For the histological analyses 8 scaffolds were provided, two for each type of functionalization (**Fig. 3.17**, **e**). The experimental plan is reported in **Figure 3.12f**.

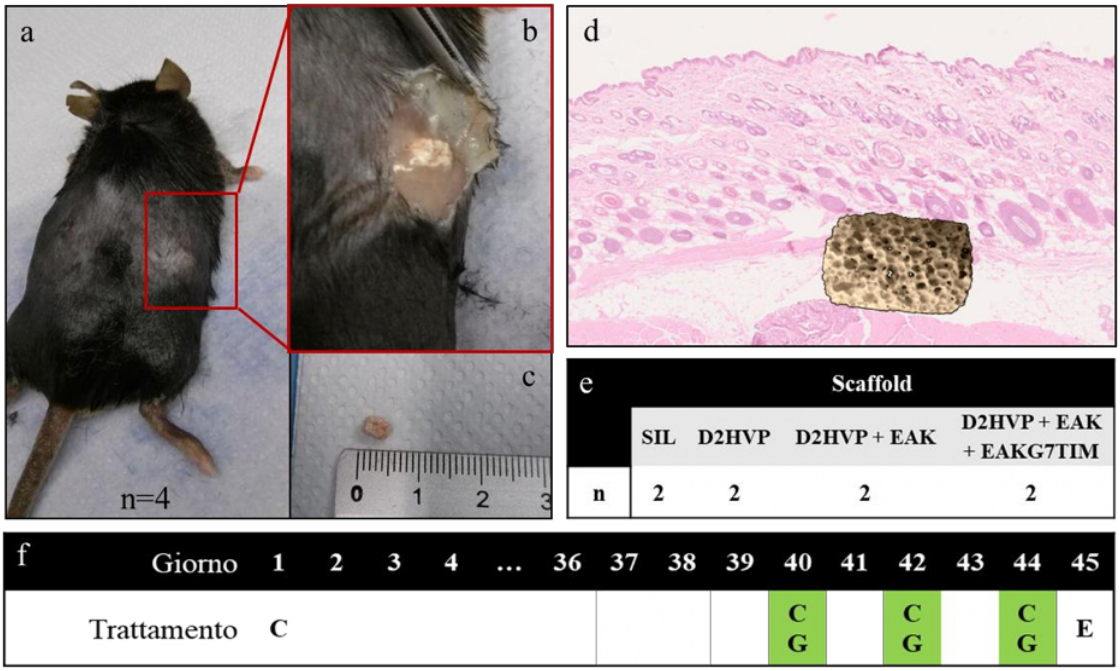


Fig. 3.17. Mouse in ventral position (**a**) and enlargement of the para-median lumbar region (**b**), and the W/D scaffold subcutaneously positioned. (**c**): Dimensions of implanted scaffolds. (**d**): Histological image of murine skin, coloured in haematoxylin-eosin, in which the location of the scaffold in the subcutis is schematized. (**e**): Numerosity of samples for histological analyses. SIL: silanized scaffold; D2HVP: scaffold functionalized with the D2HVP peptide; D2HVP+EAK: scaffold functionalized with the D2HVP peptide and enriched with EAK self-assembling peptide hydrogel (0.15% w/v); D2HVP+EAK+EAKG7TIM: scaffold functionalized with D2HVP and enriched with EAK self-assembling peptide hydrogel (0.15% w/v) and with the EAKG7TIM pro-angiogenic sequence ($5x10^{-5}$ M). (**f**): Scheme of the experimental plan. The experiment started with surgery (C) and ended the 45th day with euthanasia (E) of the animals. The Calcein Green (CG) vital marker was administered at the 40th, 42nd and 44th day.

Wollastonite-diopside scaffolds were kept in a 4% formalin solution. The formalin fixation passage lasted 3 days. Subsequently, they were washed in water and dehydrated in an ascending series of alcohols. First, they were immersed overnight in 70% alcohol, then for 4 hours in 95% alcohol and finally for 3 hours in 100% alcohol. For the last two steps, a

change was made with a renewed alcohol solution during the indicated period of time. The samples were included in polymethyl-methacrylate using the Osteo-Bed Plus kit (Polysciences, Warrington, PA). Three steps were required: infiltration, pre-polymerization and polymerization. The infiltration step was performed at room temperature, embedding the samples overnight in an un-catalyzed methyl methacrylate solution. The samples were then incubated for 2 hours, at room temperature, in a solution composed of methyl methacrylate and benzoyl peroxide (catalyst) at a concentration of 1.40g/100mL renewing the solution each 40 min. The last step was performed by soaking the samples in a solution of methyl methacrylate with added benzoyl peroxide (3.5g/100mL) and placing them in the incubator at 34.5°C in an aqueous bath, to activate the radical polymerization for 3 days. The samples were cut into 50µm thick sections with a diamond-coated circular blade with water cooling (Leica 1600, Leica Biosystems, Nussloch, Germany), obtaining abrasion cuts. Histological and histomorphometric analyses on W/D samples from *in vivo* bioassays were assessed at the Department of Veterinary Science, University of Parma, (Prof. Francesca Ravanetti and Prof. Antonio Cacchioli)

3.4.10.1 Histological analysis

One section for each sample was coloured with Goldner's Trichrome, using the following protocol:

- Immerse the blue section of toluidine 1% (Carlo Erba Reagents, Milan, Italy) for 3 minutes;
- Rinse in 100% alcohol;
- Immerse in basic fuchsin 1% (Carlo Erba) for 3.5 min;
- Rinse in 100% alcohol;
- Immerse in fast green FCF 1% (Sigma) for 4 min;
- Rinse in 95% alcohol;
- Rinse in 100% alcohol;
- Allow to dry and cover with a coverslip.

The same number of sections was also colored using the Von Kossa method (Bio-Optica kit, Milan, Italy), using the following protocol:

- De-resinate the xylene sections (Histo-Line Laboratories) at 37°C for 3h;
- Bring to distilled water: 100% alcohol for 5 minutes; 95% alcohol for 5 minutes; 70% alcohol for 5 minutes; two steps in distilled water for 5 min each;
- Put 10 drops of saturated carbonate solution on the section and leave to act for 10 min;
- Washe twice in distilled water;
- Put 10 drops of silver nitrate solution on the section and leave to act in the dark for 1h;

- Make two washes in distilled water;
- Put 5 drops of distilled water on the section, add 10 drops of reducing solution and leave to act 5 min (until blackening of silver salts);
- Wash in distilled water;
- Put 10 drops of sodium hyposulphite solution on the section and leave to act for 5 minutes;
- Wash in distilled water;
- Put 10 drops of Mayer's carmallume on the section and leave to act for 5 minutes;
- Wash in distilled water;
- Dehydrate in the ascending series of alcohols: rinsing in 70% alcohol; 95% alcohol for 45sec; 100% alcohol for 5 min;
- Clarify the sections in xylene for 5 min and fit the coverslip.

The sections were analysed in light field optical microscopy and fluorescence microscopy, using a motorized microscope (Eclipse 90i, Nikon) equipped with a digital camera (Nikon model DS-5M) and a software for image analysis (NIS-Elements AR 3.10; Nikon). Furthermore, the images of the entire sections (Whole Slide Image, WSI) were acquired using the NanoZoomer S60 slide scanner (Hamamatsu Photonics, Shizuoka, Japan).
The qualitative analysis was carried out in bright-field: to verify the presence of fibrous tissue, scaffold colonization and calcium deposition, and in fluorescence: to confirm the presence of fronts of active mineral deposition.

3.4.10.2 Histomorphometric analysis

The degree of mineralization and the number of blood vessels within the scaffold pores were measured through the following static and dynamic histomorphometry parameters[31]:

- Mineralized Surface versus Pores Surface (%) [Md.S/Po.S]: measured in bright-field optical microscopy as the ratio between the surface of calcium deposits present in the pores and the surface of the pores. For each section, three representative images were acquired in three different fields, at a magnification of 20X. The surface of the pores was selected by creating ROIs, specific for each image, using the Binary function of the image analysis software; subsequently, a threshold was applied within the above ROIs, which allowed to identify, in a semi-automatic way, the surface occupied by calcium deposits.
- Mineralizing Surface versus Pores Surface (%) [MS/Po.S]: calculated manually on the WSI as the ratio between the surface marked by Calcein Green, displayed in fluorescence microscopy, and the total surface of the pores. The WSIs were imported into the image analysis software to make the measurements.
- Mineral Apposition Rate for Single Label (μm/day) [MAR-SL]: calculated manually on the WSI as the ratio between the average thickness of the deposition

fronts marked by Calcein Green, displayed in fluorescence microscopy, and the period of administration of the marker vital bone. Measurements were made using the NDP.view2 image display software (Hamamatsu Photonics).

- Number of vessels: calculated in bright-field optical microscopy, manually counting the number of blood vessels contained in each pore of the scaffold, and presented as frequency distribution of the categories (<2, 2-4, >4).

3.4.11 Statistical analysis

For *in vitro* assays data are expressed as mean ± standard deviation of three experiments. Statistical analysis was performed using the program Microsoft Excel®. Statistical significance of the values was assessed by Student's t-test. Data were considered statistically significant for p-values≤0.05.

For *in vivo* results, data are reported as mean ± standard error. Data obtained from static and dynamic histomorphometry analyses were statistically analysed through one-way analysis of variance (ANOVA) with Tukey multiple comparison test and by Kruskal-Wallis test with Dunn multiple comparison test, using the statistical software GraphPad Prism 7.0 (GraphPad Software, Inc. La Jolla, CA). The values expressed as a percentage were previously converted by angular transformation. The value of p-value≤0.05 was considered statistically significant.

3.5 References

1. Fiocco, L. *et al.* Bioactive Wollastonite-Diopside Foams from Preceramic Polymers and Reactive Oxide Fillers. *Materials (Basel).* **8,** 2480–2494 (2015).
2. Brun, P. *et al.* Mechanisms underlying the attachment and spreading of human osteoblasts: from transient interactions to focal adhesions on vitronectin-grafted bioactive surfaces. *Acta Biomater.* **9,** 6105–15 (2013).
3. Zamuner, A. *et al.* Smart biomaterials : Surfaces functionalized with proteolytically stable osteoblast-adhesive peptides. *Bioact. Mater.* **2,** 121–130 (2017).
4. Ravanetti, F. *et al.* Enhancement of peri-implant bone osteogenic activity induced by a peptidomimetic functionalization of titanium. *Ann. Anat.* **218,** (2018).
5. Scott, M. A. *et al.* Brief Review of Models of Ectopic Bone Formation. *Stem Cells Dev.* **21,** 655–667 (2012).
6. Minarelli Gaspar, A. M. *et al.* Comparison of the Biological Behavior of Wollastonite Bioceramics Prepared from Synthetic and Natural Precursors. *Key Eng. Mater.* **361–363,** 1083–1086 (2007).
7. Minarelli Gaspar, A. M. *et al.* Biological Response to Wollastonite Doped α-Tricalcium Phosphate Implants in Hard and Soft Tissues in Rats. *Key Eng. Mater.*

396–398, 7–10 (2008).

8. Albrektsson, T. & Johansson, C. Osteoinduction, osteoconduction and osseointegration. *Eur. Spine J.* **10 Suppl 2,** S96-101 (2001).
9. Butler, K., Benghuzzi, H., Tucci, M. & Cason, Z. A comparison of fibrous tissue formation surrounding intraperitoneal and subcutaneous implantation of ALCAP, HA, and TCP ceramic devices. *Biomed. Sci. Instrum.* **34,** 18–23 (1997).
10. Butler, K. R., Benghuzzi, H., Tucci, M. & Puckett, A. D. The Tissue Implant Response Surrounding Subcutaneous TCP, HA, And ALCAP Bioceramics. *Biomed. Sci. Instrum.* **51,** 407–14 (2015).
11. Wu, C. & Chang, J. A review of bioactive silicate ceramics. *Biomed. Mater.* **8,** 32001 (2013).
12. Xu, S. *et al.* Reconstruction of calvarial defect of rabbits using porous calcium silicate bioactive ceramics. *Biomaterials* **29,** 2588–2596 (2008).
13. Zamuner, A. *et al.* Design of decorated self-assembling peptide hydrogels as architecture for mesenchymal stem cells. *Materials (Basel).* **9,** (2016).
14. Conconi, M. T. *et al.* Effects on in vitro and in vivo angiogenesis induced by small peptides carrying adhesion sequences. *J. Pept. Sci.* **16,** 349–57 (2010).
15. Li, Y. *et al.* Potent Retro-Inverso <scp>d</scp> -Peptide for Simultaneous Targeting of Angiogenic Blood Vasculature and Tumor Cells. *Bioconjug. Chem.* **24,** 133–143 (2013).
16. Parthsarathy, V. *et al.* A Novel Retro-Inverso Peptide Inhibitor Reduces Amyloid Deposition, Oxidation and Inflammation and Stimulates Neurogenesis in the APPswe/PS1ΔE9 Mouse Model of Alzheimer's Disease. *PLoS One* **8,** e54769 (2013).
17. Ngoei, K. R. W., Catimel, B., Milech, N., Watt, P. M. & Bogoyevitch, M. A. A novel retro-inverso peptide is a preferential JNK substrate-competitive inhibitor. *Int. J. Biochem. Cell Biol.* **45,** 1939–1950 (2013).
18. Carmona, A. K. & Juliano, L. Inhibition of angiotensin converting enzyme and potentiation of bradykinin by retro-inverso analogues of short peptides and sequences related to angiotensin I and bradykinin. *Biochem. Pharmacol.* **51,** 1051–1060 (1996).
19. de la Fuente-Núñez, C. *et al.* D-Enantiomeric Peptides that Eradicate Wild-Type and Multidrug-Resistant Biofilms and Protect against Lethal Pseudomonas aeruginosa Infections. *Chem. Biol.* **22,** 196–205 (2015).
20. Li, C. *et al.* Limitations of Peptide Retro-inverso Isomerization in Molecular Mimicry. *J. Biol. Chem.* **285,** 19572–19581 (2010).
21. Nair, D. T. *et al.* Mimicry of Native Peptide Antigens by the Corresponding Retro-Inverso Analogs Is Dependent on Their Intrinsic Structure and Interaction

Propensities. *J. Immunol.* **170,** 1362–1373 (2003).

22. Wang, J. *et al.* Retro-Inverso CendR Peptide-Mediated Polyethyleneimine for Intracranial Glioblastoma-Targeting Gene Therapy. *Bioconjug. Chem.* **25,** 414–423 (2014).
23. Gu, J., Chen, X., Fang, X. & Sha, X. Retro-inverso d -peptide-modified hyaluronic acid/bioreducible hyperbranched poly(amido amine)/pDNA core-shell ternary nanoparticles for the dual-targeted delivery of short hairpin RNA-encoding plasmids. *Acta Biomater.* **57,** 156–169 (2017).
24. Dettin, M. *et al.* Effect of synthetic peptides on osteoblast adhesion. *Biomaterials* **26,** 4507–4515 (2005).
25. Zamuner, A., Sica, G. & Dettin, M. Insertion of a Flexible Spacer Increases the Yield of Site-Specific Bioconjugation through N-Terminal Transamination. *Lett. Org. Chem.* **14,** (2017).
26. Gilmore, J. M., Scheck, R. A., Esser-Kahn, A. P., Joshi, N. S. & Francis, M. B. N-terminal protein modification through a biomimetic transamination reaction. *Angew. Chem. Int. Ed. Engl.* **45,** 5307–11 (2006).
27. Dettin, M. *et al.* Assessment of novel chemical strategies for covalent attachment of adhesive peptides to rough titanium surfaces: XPS analysis and biological evaluation. *J. Biomed. Mater. Res. Part A* **91A,** 463–479 (2009).
28. Dettin, M. *et al.* Driving h-osteoblast adhesion and proliferation on titania: Peptide hydrogels decorated with growth factors and adhesive conjugates. *J. Pept. Sci.* **20,** 585–594 (2014).
29. Luna, L. G. *Manual of histologic staining methods of the Armed Forces Institute of Pathology*. (Blakiston Division, McGraw-Hill, 1968).
30. Chan, F. K.-M., Moriwaki, K. & De Rosa, M. J. in 65–70 (2013). doi:10.1007/978-1-62703-290-2_7
31. Dempster, D. W. *et al.* Standardized nomenclature, symbols, and units for bone histomorphometry: a 2012 update of the report of the ASBMR Histomorphometry Nomenclature Committee. *J. Bone Miner. Res.* **28,** 2–17 (2013).

Chapter 4

Mg/Sr doped Hardystonite foams

4.1 Abstract

Novel hardystonite-based bioceramics were obtained by thermal treatment, in air, of silicone resins and reactive fillers. Using commercial silicones embedding SrO and MgO precursors (in addition to CaO and ZnO precursors), a quite complex solid solution ($Ca_{1.4}Sr_{0.6}Zn_{0.85}Mg_{0.15}Si_2O_7$) could be achieved, at 1100°C, instead of pure hardystonite ($Ca_2ZnSi_2O_7$), with improvements in biocompatibility and bioactivity.

The aim of this part of the PhD project consisted in understanding whether the proposed covalent and specific functionalization strategy (Chapter 3) could also be transferred to other types of polymer-derived bioceramics, such as Mg/Sr doped hardystonite (HT). For this reason, HT foams were covalently and selectively functionalized with D2HVP adhesive sequence and preliminary *in vitro* assays were carried out.

Controversial results showing no human osteoblasts (HOB) proliferation at 2, 4 and 6 days underlined the need to develop a different functionalization method that, requiring only mild reaction conditions and aqueous solutions, could be suitable for most of the bioceramic materials.

Consequently, a novel functionalization strategy was designed, in which the NH_2^- group of APTES reacts with D2HVPF (that differs from D2HVP for an additional phenylalanine, F, with an aldehyde group at the C-terminus).

Functionalized HT showed a dramatic increase in HOB proliferation at 6 days when compared to silanized foams or non-functionalized samples.

A LDH assay confirmed the total absence of cytotoxicity induced by functionalization treatment. D2HVPF enhanced mRNA specific transcript levels coding *IBSP*, *VTN*, *RUNX2* and *SPP1* at 2 days after seeding. These final results were in total agreement to the previously obtained ones concerning wollastonite-diopside foams functionalized with D2HVP (Chapter 3).

4.2 Results and discussion

Synthesized Mg/Sr doped hardystonite foams showed a homogeneous structure (**Fig 4.1**). The homogeneity of the cellular structure was preserved after firing, as shown in **Fig. 4.1** b; the cell size (approximately 500µm) and, above all, the cell windows size (approximately 200µm) match well the morphological requirements for bone tissue engineering scaffolds, in order to optimize cell ingrowth and vascularization[1,2].

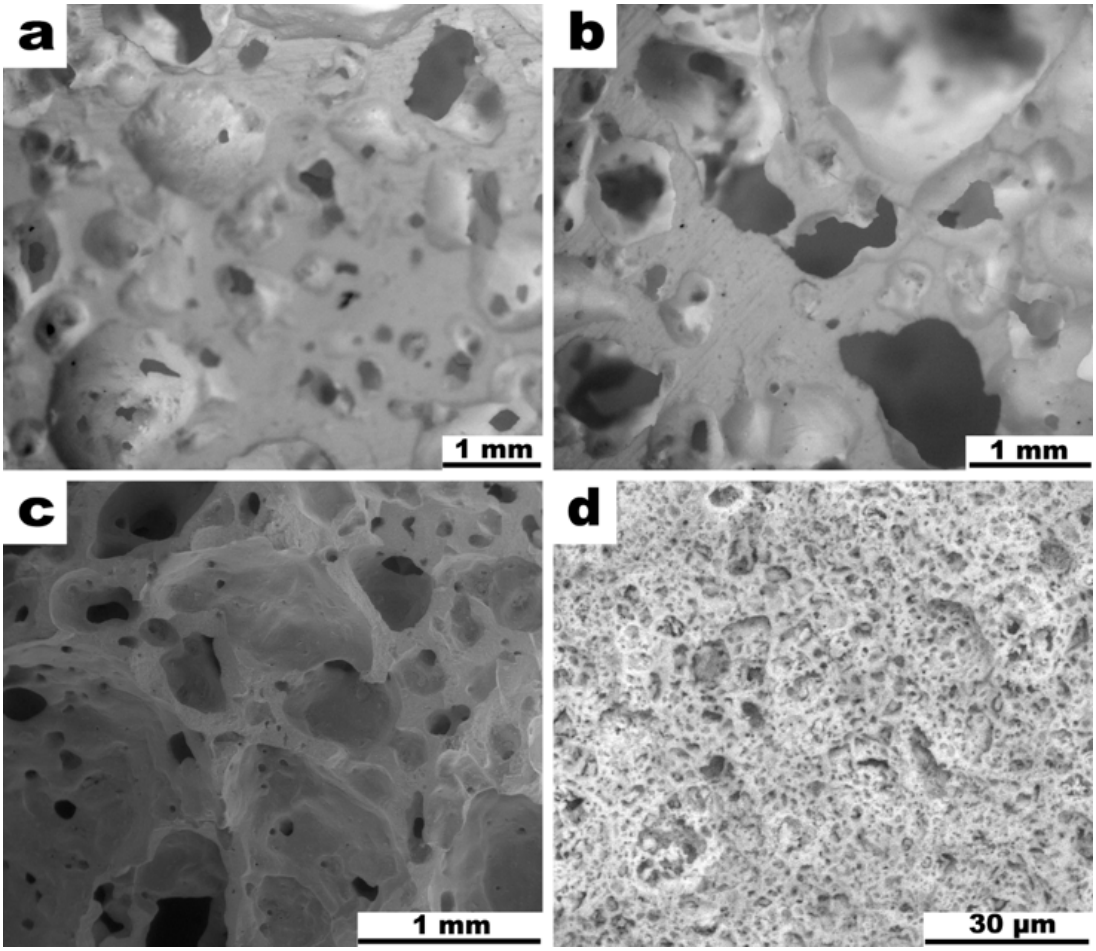


Figure 4.1. Microstructural details of cellular Sr/Mg-doped hardystonite ceramics; **a**) before firing; **b**, **c**) after firing; **d**) high magnification detail of a foam.

Possessing a higher open porosity (83%), compared to foams based on pure hardystonite (77% with 1.8 MPa of compressive strength), the new Sr/Mg-doped hardystonite exhibited a compressive strength of about 1 MPa, that can be considered to be a sort of threshold limit for scaffolds operating *in vivo*[3–5].

Elsayed *et al.* demonstrated that the densification and the integrity of cellular Sr/Mg-doped hardystonite ceramic scaffolds can be enhanced over 2 MPa by using fine glass powders as

additional fillers, with positive impacts on the mechanical properties without modifying the overall phase assemblage of the fired material (paper under submission).

This study by Elsayed *et al.* also demonstrated that Polymer-derived Sr/Mg-doped hardystonite ceramics, according to preliminary biological assays, were definitely more promising than pure hardystonite, in terms of biocompatibility and bioactivity.

Figure 4.2 clearly shows the excellent phase purity that can be obtained when producing stoichiometric hardystonite from the reaction of preceramic polymers with $CaCO_3$ and ZnO fillers[6,7].

The experimental pattern matches very well with all the peaks of the reference pattern for pure $Ca_2ZnSi_2O_7$ (PDF#35-0745), in terms of both 2θ position and relative intensities.

The same figure also highlights the effective incorporation of Sr^{2+} and Mg^{2+} ions, in newly developed samples, considering the 2θ shifts and some changes in the relative intensities. In particular, all peaks moved to lower 2θ values, in analogy with what happens for pure $Sr_2ZnSi_2O_7$ (strontium hardystonite, PDF#35-0235), due to the enhanced spacing between $ZnSi_2O_7^{4-}$ layers. Since the replacement of Ca^{2+} with Sr^{2+} was not complete, it is not surprising to find the patterns for the solid solution in intermediate positions.

The replacement of Zn^{2+} with Mg^{2+} is hardly detectable, owing to the strong similarity of the reference patterns of pure $Ca_2ZnSi_2O_7$ and pure $Ca_2MgSi_2O_7$ (akermanite, PDF#35-0592), but we suppose that a synergy occurs between Sr^{2+} and Mg^{2+} ions in leading to a much less pronounced peak at 2θ≈17.7°. In fact, this specific peak is well distinguishable in pure hardystonite, while it is practically absent in the Sr- and Mg-rich melilites.

No peak ascribable to additional phases could be detected.

Strontium (Sr) as a trace element (nearly 0.00044% of 70-kg standard man body mass corresponding to ~0.32g[8]) in human body has been found to produce beneficial effects on bone formation, inducing osteoblast activity by stimulating bone formation[9–12] and reducing bone resorption[13,14].

The amount of Sr in the skeleton is only 0.035 of its Ca content[8].

Toxic symptoms due to overdosing of Sr have not been reported in man, however, intravenous administration of high doses of Sr induces hypocalcaemia due to increased renal excretion of Ca[8,15].

A direct effect of high doses of Sr in bone *in vitro* was demonstrated by Verberckmoes *et al.*[14] who found evidence of deficient hydroxyapatite formation at high medium doses of Sr, who create special problems of osteomalacia.

It was also reported that Sr ions have been used as a sintering additive to improve $PbTiO_3$ ceramic density[16] and the improvement of the density would decrease the dissolution rate of ceramics[17].

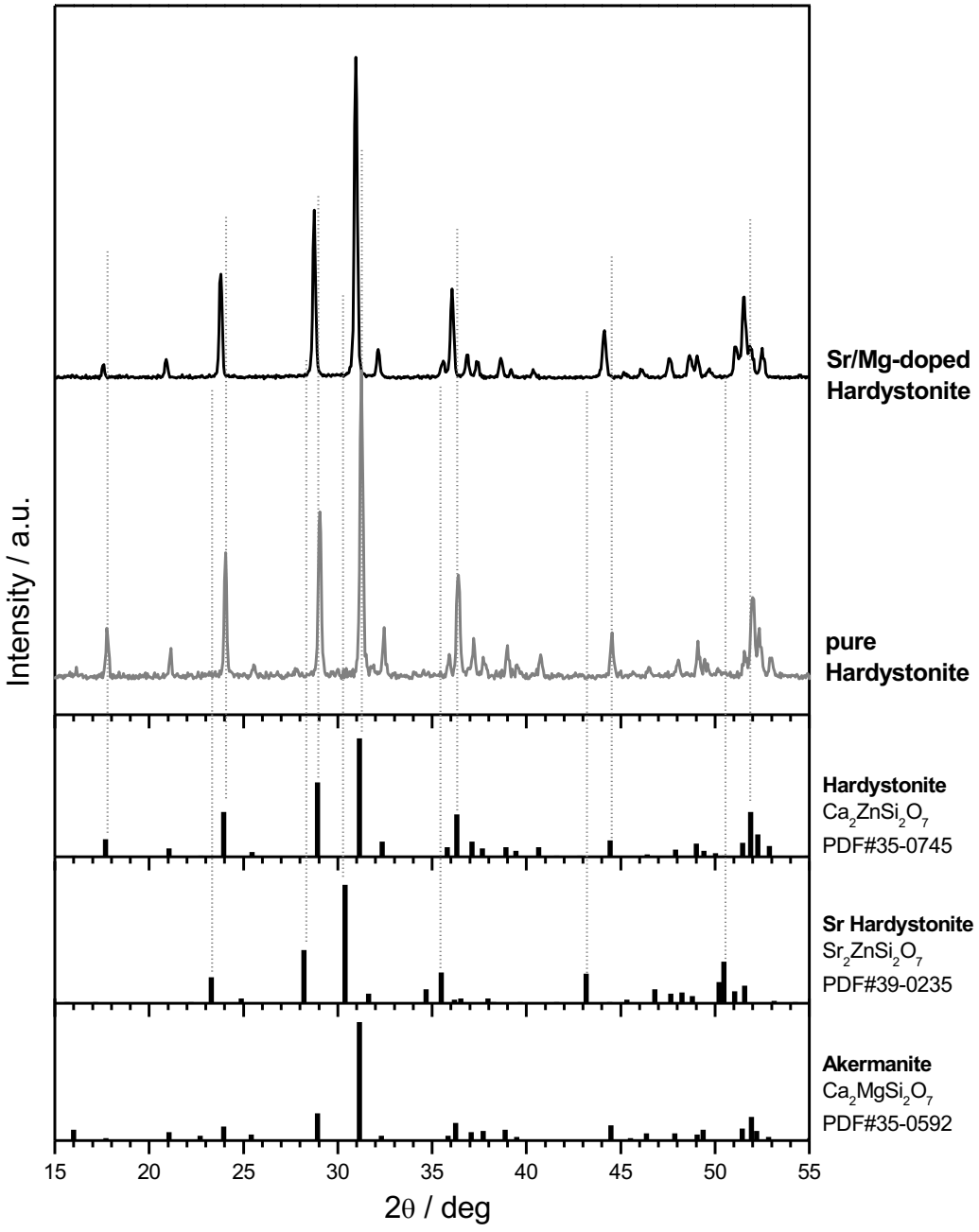


Fig. 4.2. Experimental diffraction patterns of pure hardystonite and Sr/Mg-doped hardystonite pellets, compared to reference patterns.

It was demonstrated that Sr doped $CaSiO_3$ ceramics possess improved physical and biological properties as compared with pure $CaSiO_3$ ceramics[18].

Magnesium ions have been demonstrated to stimulate new bone formation[19] and increase bone cell adhesion and stability (probably due to interactions with integrins)[19–21].

Bioactive glasses doped with Mg have been shown to improve dissolution behavior due to the Mg effect disrupting the silica network and exhibit decreased crystallization of the HAp layer on the bioglass surface[22].

Preliminary *in vitro* bioassays on Mg/Sr doped hardystonite foams functionalized with the same protocol applied to wollastonite-diopside foams (paragraph 3.4.7.1) gave very controversial results in terms of cell viability.
No proliferation was detected at 2, 4 and 6 days after HOB seeding on all covalently and selectively functionalized HT foams (data not shown). Furthermore, comparing the images taken after 6 days from the seeding at Operetta CLS high-content microscope, it was quite evident that non-functionalized HT samples were colonized by many more cells than the functionalized samples (**Fig 4.3**).

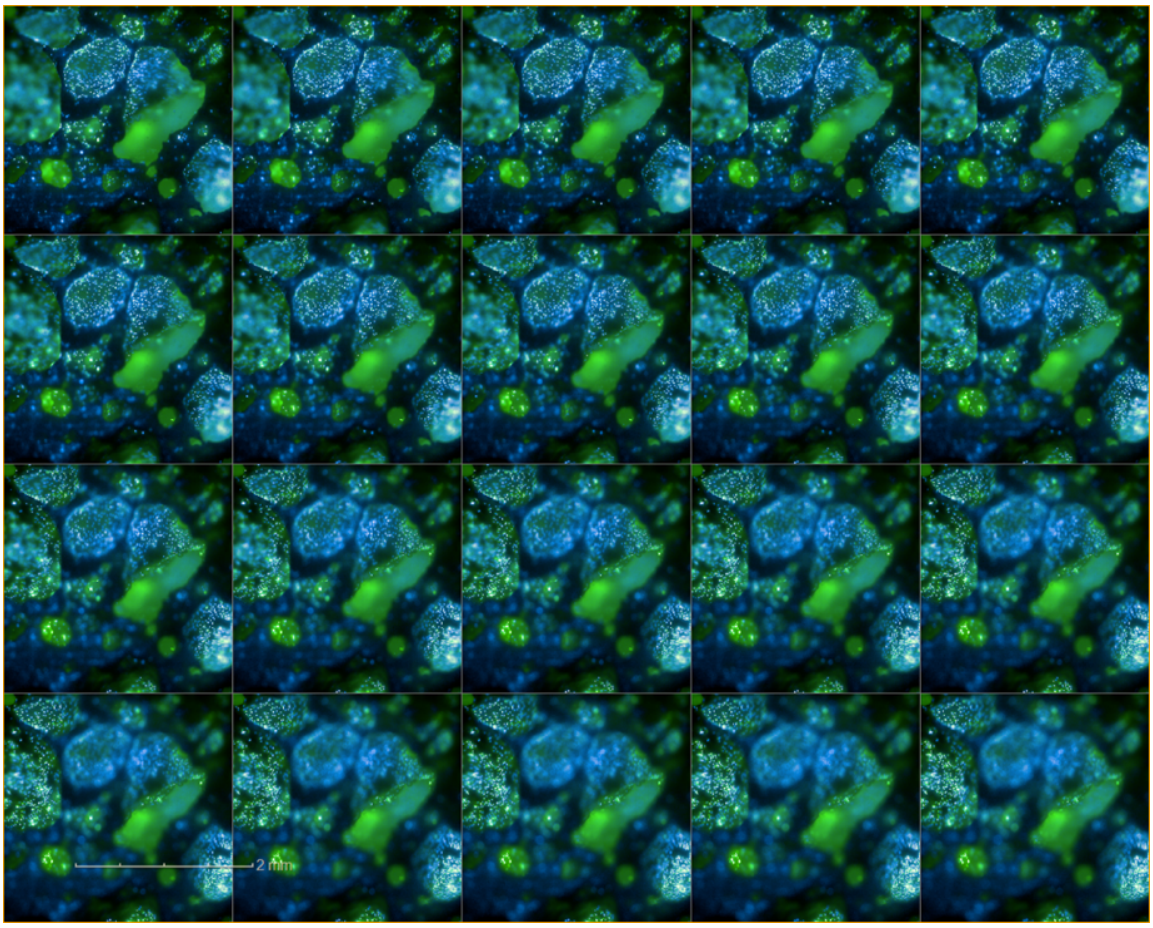


Figure 4.3. Human Osteoblasts seeded on Sr/Mg-doped hardystonite foams completely colonized the scaffold. Images taken with Operetta CLS (PerkinElmer) 5X magnification, z-stacks of 30µm, scale bar = 2mm. Each image corresponds to a z-stack. Blue corresponds to the nuclei (Hoechst) and Green to the entire cell (CellBrite Green).

Moreover, HOB seeded on simple HT foams appeared more spreaded, whilst cells on functionalized foams showed a more roundish shape that could denote suffering (**Fig 4.4** and **Fig 4.6**). These results were in contrast with the promising results obtained previously with functionalized wollastonite-diopside foams.

Cells seeded on silanized HT foams (SIL) show the same elongated morphology as HOB seeded on non-functionalized foams (**Fig 4.5** and **Fig. 4.6**), suggesting that the bad impact on cell behavior is probably due to the following functionalization steps (Paragraph 3.4.7.1).

One possible explanation that can be hypothesized to explain these results is that Mg/Sr doped hardystonite could be more sensitive to the acid treatment used to covalently graft D2HVP.

Future studies will be carried out to understand whether this functionalization treatment modifies the composition of the bioceramic, inducing the release of Mg^{2+} and Sr^{2+} ions into cells medium, moving the bioceramic's ions-balance toward a higher percentage of Zn that can produce cytotoxicity if de-adsorbed up to 50 μg/ml concentration[23,24].

The partial replacement of sodium with zinc in bioactive glasses has been proposed to stimulate bone cells proliferation and differentiation and improve bone-bonding ability of bioglass[25].

In fact, Zinc is fundamental for cell growth, development and differentiation[26], as it is a cofactor for many enzymes, stimulates protein synthesis and is essential for DNA replication[27].

Zinc is also thought to activate bone formation[28] and inhibit bone resorption[29].

Another important role played by Zinc, that promotes its incorporation in bioglass, is the ability to prolong chemical durability of glass, by retarding glass dissolution, and improving glass mechanical properties[30].

However, a study from Aina V. *et al.* demonstrated that the effect of Zn on glass durability is not sufficient to prevent a complete dissolution of the material[24].

The dissolution causes an increased concentration of Zn^{2+} ions in solution, which, when occurring *in vivo*, might be relevant in eliciting changes of cell functions and metabolism. Aina *et al.* demonstrated that the presence of Zn increases, in a dose-dependent way, the release of LDH in the extracellular medium (an index of cytotoxicity), the accumulation of intracellular MDA (an index of lipoperoxidation), and increased PPP activity and HO-1 expression (two sensitive signals of cell response to oxidative stress).

In parallel, the level of intracellular thiols and the GSH/GSSG ratio were decreased, in inverse relationship with the zinc content of glass powders[24].

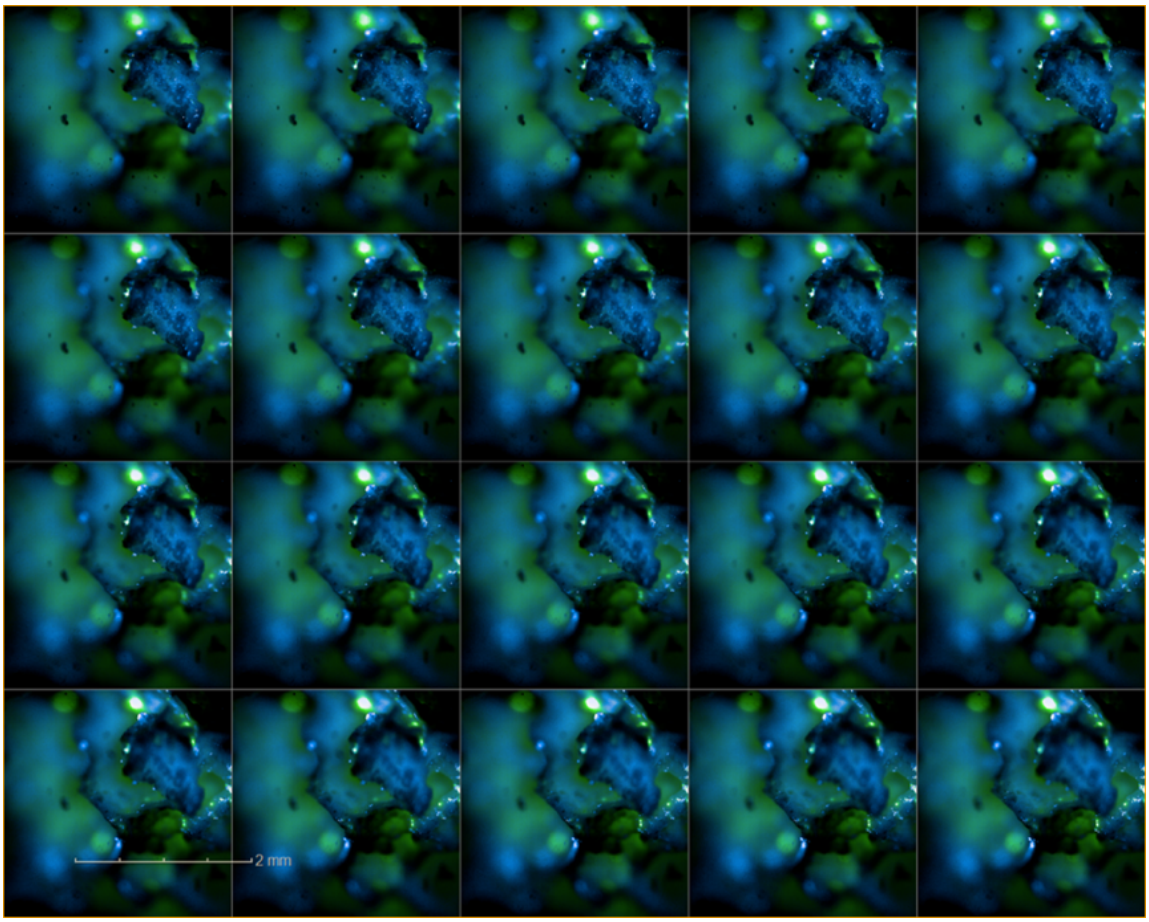


Figure 4.4. Human Osteoblast seeded on D2HVP functionalized Sr/Mg-doped hardystonite foams. Images taken with Operetta CLS (PerkinElmer) 5X magnification, z-stacks of 30µm, scale bar = 2mm. Each image corresponds to a z-stack. Blue corresponds to the nuclei (Hoechst) and Green to the entire cell (CellBrite Green).

Further studies involving the quantification of Zinc release (e.g. using an inductively coupled plasma, ICP, spectrometer equipped with ultrasonic nebuliser for trace elements) from Mg/Sr doped HT will be carried out to explain these previous results.

To overcome the non-encouraging results and to correlate indirectly the results to the use of acid solutions during D2HVP grafting, in this part of the research project we designed a different covalent and selective functionalization strategy that, after samples silanization, requires only mild reaction conditions and aqueous solutions.

This strategy involves a simple modification of D2HVP peptide's sequence (D2HVPF), with the introduction of an aldehyde group at C-terminus, that can selectively react with the amine groups of silanized surfaces.

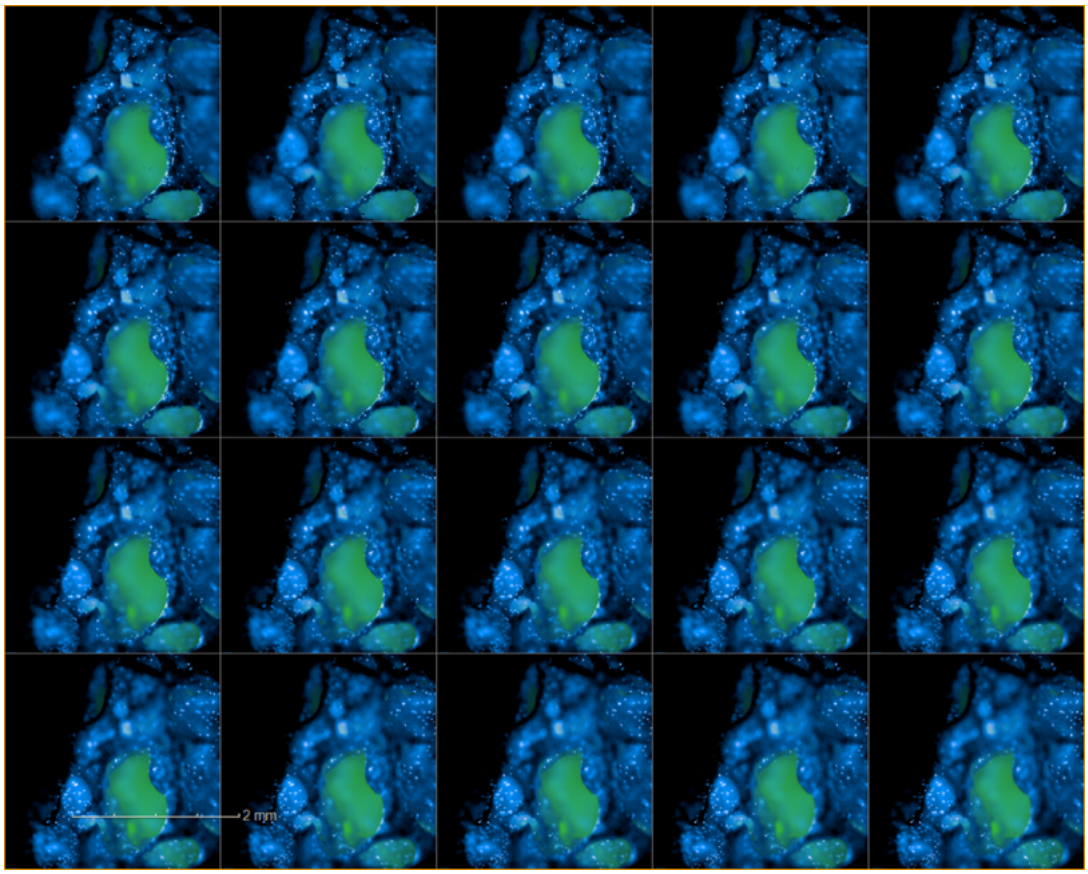


Figure 4.5. Human Osteoblast seeded on silanized Sr/Mg-doped hardystonite foams. Images taken with Operetta CLS (PerkinElmer) 5X magnification, z-stacks of 30µm, scale bar = 2mm. Each image corresponds to a z-stack. Blue corresponds to the nuclei (Hoechst) and Green to the entire cell (CellBrite Green).

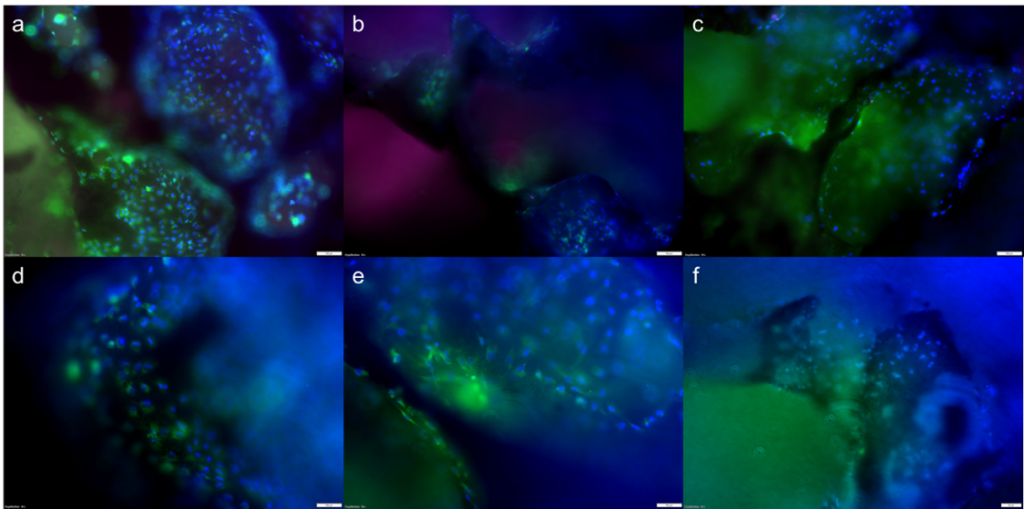


Figure 4.6. Human Osteoblast seeded on **a-d**)Sr/Mg-doped hardystonite foams, **b-e**) silanized Sr/Mg-doped hardystonite foams and **c-f**) D2HVP functionalized Sr/Mg-doped hardystonite foams. Images taken in fluorescent microscopy with Olympus 1X51microscope **a-b-c**) 10X magnification, scale bar = 100µm, and **d-e-f**) 20X magnification, scale bar = 20µm. Each image corresponds to a z-stack. Blue corresponds to the nuclei (Hoechst) and Green to the entire cell (CellBrite Green).

HT was functionalized with D2HVPF following the protocol reported in paragraph 4.4.1. H-osteoblasts (3×10^5 cells/sample) were seeded onto bioceramic scaffolds (35mg/sample) and incubated at 37°C for 6 days.

Cellular proliferation was assessed by CFSE probe assay (**Fig 4.7**). Both the HT foams functionalized with D2HVPF and D2HVPF+EAK showed 14-folds increased cell proliferation with respect to the non-functionalized (HT) and silanized (SIL) foams.

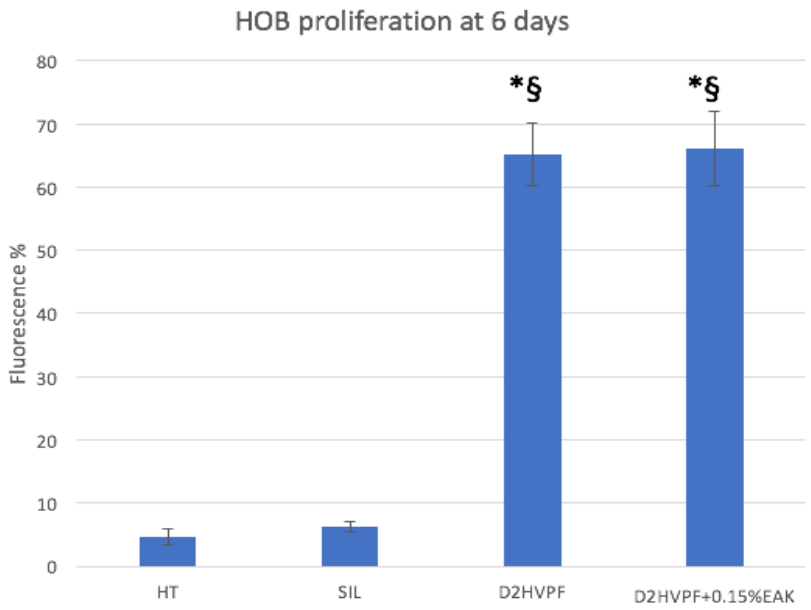


Figure 4.7. H-osteoblast proliferation on functionalized HT foams, determined at 6 days using CFSE probe assay. "HT" refers to non-functionalized Mg/Sr doped hardystonite foams; "SIL" refers to silanized scaffolds; *, § P-value<0.05 Student's t-test compared to "HT" and "SIL" respectively.

These results are in accordance with the previously obtained with W/D foams, suggesting again that the results obtain with HT foams functionalized with the first chemical strategy were to impute to the use of organic/acid solutions and not to the failure of the adhesive peptide.

As shown in **Figure 4.7**, the enrichment with a 0.15% EAK hydrogel did not further increase HOB proliferation when compared to the foams functionalized only with D2HVPF.

LDH assay at 6 days from the seeding demonstrated the complete absence of cytotoxicity induced by the new functionalization treatment (**Fig 4.8**).

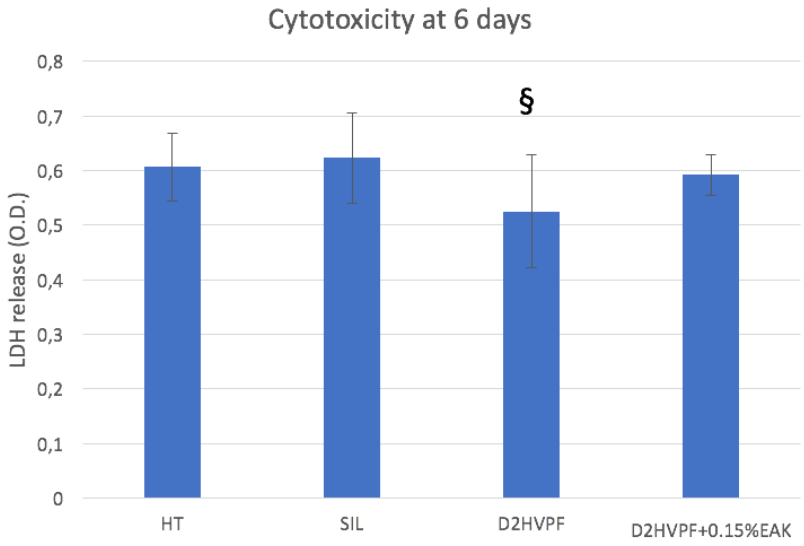


Figure 4.8. LDH test at 6 days demonstrated the absence of cytotoxicity induced by functionalization treatments. "HT" refers to non-functionalized Mg/Sr doped hardystonite foams; "SIL" refers to silanized scaffolds; *, § P-value<0.05 Student's t-test compared to "HT" and "SIL" respectively.

Human *SPP1* (secreted phosphoprotein 1, Osteopontin), Human *VTN* (Vitronectin), Human *IBSP* (Integrin-Binding Sialoprotein) and Human *RUNX2* (Runt-related transcription factor 2) mRNA specific transcript levels were evaluated by quantitative RT-PCR at 2 days after h-osteoblast seeding.

The results are reported in **Figure 4.9**. HT foams functionalised with D2HVPF were able to increase the expression of SPP1, VTN, RUNX2 and IBSP, proteins fundamental for bone formation, when compared to the controls.

The enrichment of D2HVPF functionalized HT foams with the self-assembling peptide EAK (0.15%w/v) did not further increase gene expression with respect to the functionalized foams.

The gene expression results are comparable with the results obtained with wollastonite-diopside foams functionalized with D2HVP, in fact, both functionalization increase gene expression of all the four considered proteins more than 10-times in comparison with the controls.

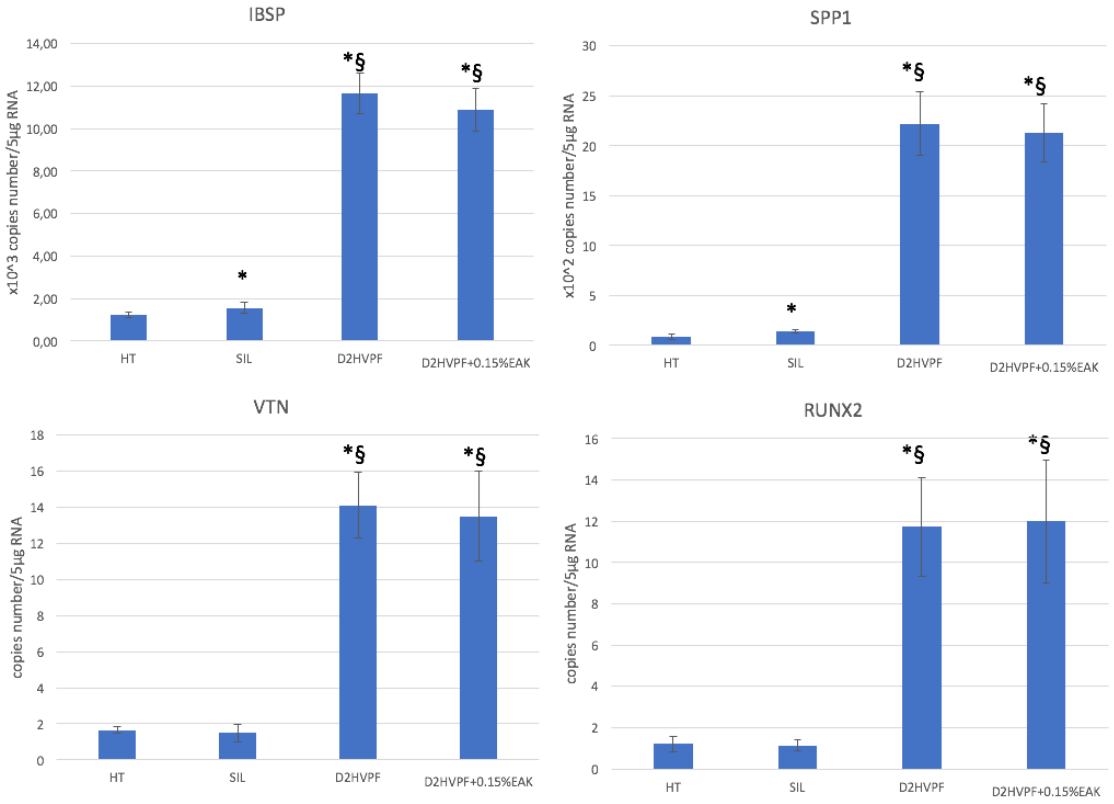


Figure 4.9. Human *SPP1* (secreted phosphoprotein 1, Osteopontin), Human *VTN* (Vitronectin), Human *IBSP* (Integrin-Binding Sialoprotein) and Human *RUNX2* (Runt-related transcription factor 2) mRNA specific transcript levels evaluated by quantitative RT-PCR at 2 days from the seeding. "HT" refers to non-functionalized Mg/Sr doped hardystonite foams; "SIL" refers to silanized scaffolds; *, § P-value<0.05 Student's t-test compared to "HT" and "SIL" respectively.

4.3 Conclusions

Single-phase Sr/Mg-doped hardystonite ceramics were easily achieved by the heat treatment, in air, of commercial silicones mixed with reactive oxide fillers, with higher open porosity than pure hardystonite still maintaining a mechanical strength at crushing that can be considered between the limits for bone tissue engineering scaffolds.

In this section of the PhD project we tried to understand if the promising results obtained with wollastonite-diopside functionalized foams were transferable to bioceramics with other compositions. For this reason, the same covalent and specific functionalization's strategy used with success for W/D foams was tested on Mg/Sr doped hardystonite but the results were negative.

Hypothesizing that the controversial results in terms of cell viability were due to the aggressive treatments involved in the functionalization protocol, we proposed a different functionalization method that, requiring mild reaction conditions and aqueous solutions

could overcome this problem. The new functionalization strategy proposed in this chapter required a simple modification of the adhesive peptide sequence that consists in the introduction of an aldehyde group at peptide's C-terminus. This single modification allows (i) to avoid organic solutions and the final acid treatment necessary to remove side-chain protecting groups of the peptide, and (ii) introduce a selective group (aldehyde group) directly in the peptide sequence, reducing the functionalization procedure to one reaction. Furthermore, HOB proliferation increase obtained with the second method (via aldehyde peptide) is comparable to the HOB enhancement observed with the first protocol (via side-chain protected peptide). In addition, gene expression results are similar in both functionalized bioceramics.

4.4 Materials and methods

4.4.1 Mg/Sr doped Hardystonite foams synthesis and characterization

Mg/Sr doped Hardystonite (HT) foams were prepared using the following method: recipe for 10g of final HT: 6.39g of H62C (preceramic precursor polymer, silica source, with a yield of 58%wt, Wacker-Chemie GmbH, Munich, Germany), 4.17g of $CaCO_3$ (<10µm, Industrie Bitossi, Vinci, Italy), 2.06g of ZnO (<1.48µm, Sigma Aldrich, Germany), 2.64g of $SrCO_3$ (<10µm, Industrie Bitossi, Vinci, Italy) and 1.76g of $Mg(OH)_2$ (<10µm, Industrie Bitossi, Vinci, Italy). All dissolved in 15mL isopropanol (IPA). Then add 0.1g (1% of the total final amount) of HZ (N'-Dicarbamoylhydrazine, or biurea; $C_2H_6N_4O_2$, 98%, Alfa Aesar, England, foaming agent, Sigma-Aldrich). Let the mixture at 60°C overnight to dry IPA. Put 1.8g in each melting pot of aluminum to proceed with two following treatments: (i) foaming treatment: 350°C for 30min; (ii) ceramization step: foams are fired at 1100°C for 1h, with a heating rate of 0.3°C/min and dwelling steps at 590°C for 3h and 880°C for 2h. The cooling rate is set at 2°C/min. (**Fig 4.10**).

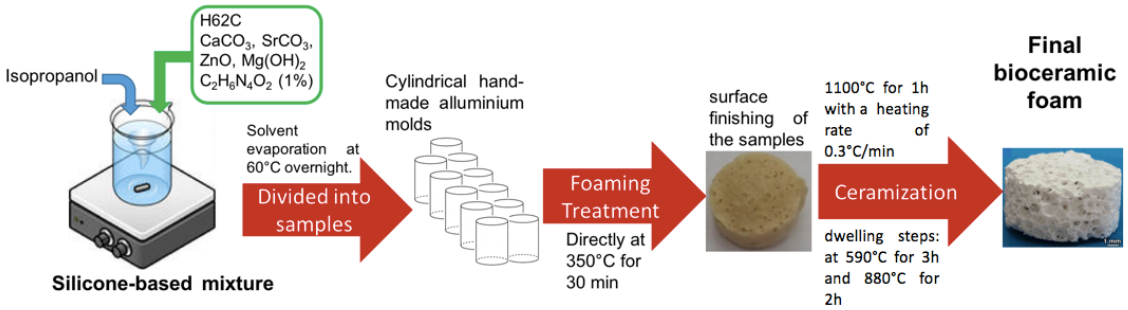


Fig 4.10. Schematic representation of Mg/Sr doped Hardystonite foams synthesis

In **Figure 4.11** is reported in a schematic way the thermal treatments used with Mg/Sr doped Hardystonite foams.

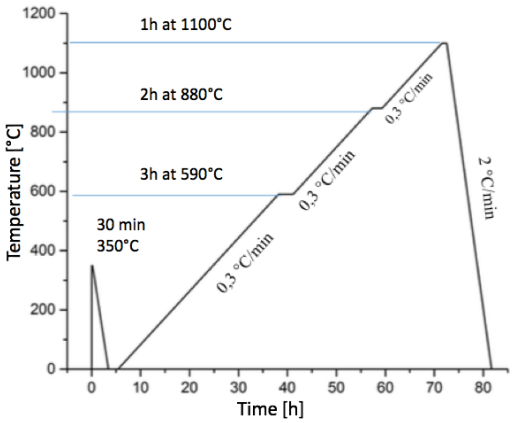


Fig 4.11. Schematic representation of foaming and firing treatments of Mg/Sr doped Hardystonite.

The crystalline phase identification was performed by means of X-ray diffraction on powder samples (XRD; Bruker AXS D8 Advance, Bruker, Germany), supported by data from the PDF-2 database (ICDD-International Centre for Diffraction Data, Newtown Square, PA) and the Match! program package (Crystal Impact GbR, Bonn, Germany).
The density of the ceramic parts was determined geometrically and by weighing with an analytical balance. The apparent and true densities of the various samples were measured by means of a gas pycnometer (Micromeritics AccuPyc 1330, Norcross, GA), operating with He gas on samples in bulk (foam scaffold) and powder forms. Morphological and microstructural characterizations were performed by optical stereomicroscopy (AxioCam ERc 5s Microscope Camera, Carl Zeiss Microscopy, Thornwood, New York, USA) and SEM (FEI Quanta 200 ESEM, Eindhoven, The Netherlands and JSM JEOL 6490 SEM microscope, JEOL, Tokyo, Japan) equipped with EDS. The compressive strength of porous ceramic components was measured at room temperature, by means of an Instron 1121 UTM (Instron Danvers, MA) operating with a cross-head speed of 0.5 mm/min. Each data point represents the average value of at least 10 individual tests. The final properties of the obtained HT foams are listed in **Table 4.1**. Mg/Sr doped hardystonite foams were synthetized and characterized at the Department of Industrial Engineering, University of Padova (Dr. Hamada Elsayed and Prof. Enrico Bernardo).

Table 4.1. Physical and mechanical properties of Sr/Mg-doped hardystonite ceramics, compared to porous ceramics based on pure hardystonite

Formulation	Bulk density [g/cm^3]	True density [g/cm^3]	Total porosity [%]	Compressive strength [MPa]
Pure $Ca_2ZnSi_2O_7$*	0.75 ± 0.02	3.30 ± 0.02	77 ± 1	1.8 ± 0.1
Sr/Mg-doped hardystonite	0.59 ± 0.05	3.45 ± 0.03	83 ± 2	1.0 ± 0.3
*Data from literature[7]				

4.4.2 Adhesive peptides synthesis and characterization

The retro-inverted dimeric analogue D2HVP used for the HT selective and covalent functionalization following the protocol of paragraph 3.4.7.1 was synthetized and characterize as reported in paragraph 3.4.2. The D2HVPF peptide with an aldehyde group at C-terminus (Sequence: H-Tyr-Gly-Lys-Arg-Asn-Arg-His-Arg-Phe-Tyr-Gly-Lys-Arg-Asn-Arg-His-Arg-Phe-Phe-CHO, this peptide differently from the D2HVP peptide of paragraph 3.4.7.1 presents the aldehyde group at C-terminus, and a phenylalanine in C-terminus, as this amino acid was pre-loaded on the resin) was synthetized, characterized and purified as followed. The peptide was synthesized by standard Fmoc chemistry using H-Phe-H NovaSyn®TG resin (0.18 mmol/g; scale 0.09 mmoles, Novabiochem, Merck KGaA, Darmstadt, Germany) and a fully automated peptide synthesizer (Syro I, Multisynthec, Witten, Germany). The side chain protection employed were: Arg, Pbf; His and Asn, Trt; Lys, Boc; Tyr, tBu. The coupling reaction was carried out using 5 eq of Fmoc protected amino acid, 5 eq of HOBt/HBTU and 10 eq of DIPEA. The coupling reagents 2-(1H-Benzotriazole-1-yl)-1,1,3,3-tetramethyluronium hexafluorophosphate (HBTU) and 1-Hydroxybenzotriazole (HOBt) were from Advanced Biotech (Seveso, MI, Italy). N,N-diisopropylethylamine (DIEA) and piperidine were from Biosolve (Leenderweg, Valkenswaard, The Netherlands). All the couplings were single. The side-chain protections were removed using 5mL of pure 2,2,2-trifluoroacetic acid (TFA) for 1h at room temperature under magnetic stirring. The peptide was subsequentially cleaved from the resin using 4mL of the following mixture: AcOH/H_2O MilliQ/DCM/MeOH (10:5:63:21) for 1h at room temperature under magnetic agitation, then, the solution was filtered and collected to be lyophilized overnight. Solvents, such as N,N-dimethylformamide (DMF), trifluoroacetic acid (TFA), N-methyl-2- pyrrolidone (NMP), dichloromethane (DCM), and acetonitrile were from Biosolve. The obtained lyophilized peptide was then treated as follows: 2.5% H_2O MilliQ, 2.5% TES, and 95% TFA (90 min, under magnetic stirring). The reaction mixture was concentrated and the crude peptide precipitated with cold ethyl ether. Peptides identity and homogeneity were ascertained by mass (ESI-TOF Mariner System 5220, Applied Biosystems, Perkin-Elmer, Norfolk, CT) and RP-HPLC analyses (Waters Corporation, Milford, MA), respectively. The chromatogram of crude peptide was carried out in the following conditions: column, Vydac 238EV54 Everest (5µm, 300Å, 4.6x250 mm, Grace); injection volume, 100µL of 1 mg/mL peptide solution; flow rate, 1 mL/min; eluent A, 0.05% TFA in water; eluent B, 0.05% TFA in CH_3CN; gradient, from 10% B to 25%B in 30 min, detection at 214 nm. The retention time results 17.6 min. Experimental mass: 2580.59 Da, Theoretical mass: 2579.97 Da (4800 MALDI-TOF/TOF™ Analyzer, AB Sciex Pte Ltd., Singapore, with 4000 Series Explorer™ software, Applied Biosystems, Foster City, CA, USA). Purification of the crude product was performed through reverse phase high performance liquid chromatography (RP-

HPLC) as follows: thirty mg of crude peptide dissolved in 15 mL of MilliQ water were loaded on Jupiter C18 (5µm, 300Å, 10×250 mm, Phenomenex) and separated in the following conditions. Eluent A, 0.05% TFA in MilliQ water; Eluent B, 0.05% TFA in CH_3CN; gradient, from 0%B to 10%B in 2 min, then from 10%B to 25%B in 45 min; flow rate, 4 mL/min; detection at 214 nm. The final homogeneity was >98%.

4.4.3 Self-assembling peptide synthesis and characterization

The self-assembling peptide EAK was synthetized, purified and characterized as reported in paragraph 3.4.4.1.

4.4.4 HT foams functionalization

4.4.4.1 Selective and covalent functionalization

Firstly, a specific functionalization of Mg/Sr doped hardystonite foams (mass: 35mg) with D2HVP peptide was carried out using the procedure reported in paragraph 3.4.7.1. In a second time, HT foams were covalently and selectively functionalized with D2HVPF through the protocol reported in **Figure 4.12**:

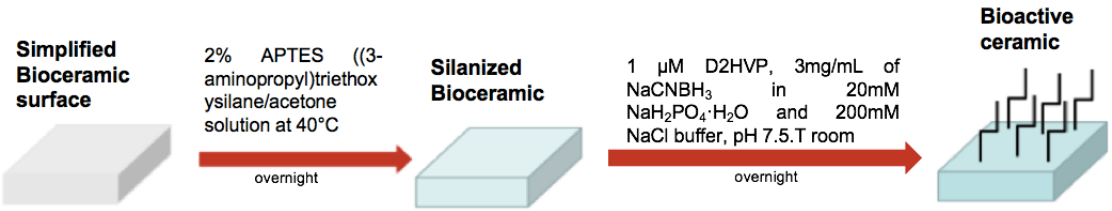


Figure 4.12. Scheme of the covalent and specific functionalization of Mg/Sr doped hardystonite foams.

After the silanization with APTES, Mg/Sr doped hardystonite foams were treated with D2HVPF specifically synthetized carrying in C-terminal an aldehyde group, dissolved in an aqueous buffer. This aldehyde group allows a selective anchoring. The reaction takes place between the aldehyde group and the exposed amine group on the silanized surface, and does not require side chain protections. In **Figure 4.13** is represented the formation of the covalent bond between the surface and the peptide. Since the formation of a Schiff base, with the liberation of a water molecule is reversible, to create a more stable bond, the imines can be reduced to amines by using sodium cyanoborohydride ($NaCNBH_3$, Sigma-Aldrich).

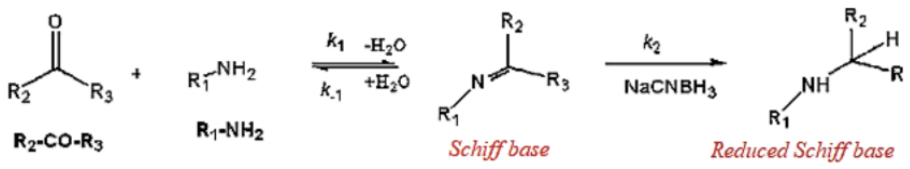


Figure 4.13. Reduction of the Schiff base by sodium cyanoborohydride.

Finally, the functionalized foams were rinsed with milliQ water three times to remove all the unreacted reagents, and dried under vacuum. Differently from the first functionalization chemistry, requiring side-chain protected peptides (paragraph 3.4.7.1), it is evident that this last procedure summarized in **Figure 4.11**, does not therefore need the use of any organic solvent or acid treatment.

4.4.4.2 SAP embedding

HT foams, after selective and covalent functionalization, were embedded in a 0.15% w/v EAK solution following the procedure reported in paragraph 3.4.7.2

4.4.5 *In vitro* bioassays

Biological assays *in vitro* were carried out as previously done with W/D foams at the Department of Molecular Medicine, University of Padova (Prof. Paola Brun). All the protocols are reported in paragraph 3.4.9. HOB proliferation and cytotoxicity was measured at 6 days after the seeding. Quantitative real time polymerase chain reaction was carried out after 2 days from the seeding. Human osteoblasts were stained with Hoechst (nuclei) and CellBrite Green (cell-mask) following the protocols of paragraph 2.2.3.4.

4.4.6 Statistical analysis

Data are expressed as mean ± standard deviation of three experiments. Statistical analysis was performed using the program Microsoft Excel®. Statistical significance of the values was assessed by Student's t-test. Data were considered statistically significant for p-values≤0.05.

4.5 References

1. Baino, F. & Vitale-Brovarone, C. Three-dimensional glass-derived scaffolds for bone tissue engineering: Current trends and forecasts for the future. *J. Biomed. Mater. Res. Part A* **97A,** 514–535 (2011).
2. Rahaman, M. N. *et al.* Bioactive glass in tissue engineering. *Acta Biomater.* **7,** 2355–2373 (2011).
3. Pereira, M. M., Jones, J. R. & Hench, L. L. Bioactive glass and hybrid scaffolds prepared by sol–gel method for bone tissue engineering. *Adv. Appl. Ceram.* **104,** 35–42 (2005).
4. Jones, J. R. & Hench, L. L. Regeneration of trabecular bone using porous ceramics. *Curr. Opin. Solid State Mater. Sci.* **7,** 301–307 (2003).

5. Xynos, I. D. *et al.* Bioglass 45S5 stimulates osteoblast turnover and enhances bone formation In vitro: implications and applications for bone tissue engineering. *Calcif. Tissue Int.* **67,** 321–9 (2000).
6. Elsayed, H. *et al.* Development of bioactive silicate-based glass-ceramics from preceramic polymer and fillers. *J. Eur. Ceram. Soc.* **35,** 731–739 (2015).
7. Elsayed, H., Zocca, A., Franchin, G., Bernardo, E. & Colombo, P. Hardystonite bioceramics from preceramic polymers. *J. Eur. Ceram. Soc.* **36,** 829–835 (2016).
8. Pors Nielsen, S. The biological role of strontium. *Bone* **35,** 583–588 (2004).
9. Guo, D., Xu, K., Zhao, X. & Han, Y. Development of a strontium-containing hydroxyapatite bone cement. *Biomaterials* **26,** 4073–4083 (2005).
10. Wong, C. T. *et al.* In vivo cancellous bone remodeling on a strontium-containing hydroxyapatite (sr-HA) bioactive cement. *J. Biomed. Mater. Res.* **68A,** 513–521 (2004).
11. Wong, C. T. *et al.* Ultrastructural study of mineralization of a strontium-containing hydroxyapatite (Sr-HA) cementin vivo. *J. Biomed. Mater. Res.* **70A,** 428–435 (2004).
12. Qiu, K., Zhao, X. J., Wan, C. X., Zhao, C. S. & Chen, Y. W. Effect of strontium ions on the growth of ROS17/2.8 cells on porous calcium polyphosphate scaffolds. *Biomaterials* **27,** 1277–1286 (2006).
13. Marie, P. J., Ammann, P., Boivin, G. & Rey, C. Mechanisms of action and therapeutic potential of strontium in bone. *Calcif. Tissue Int.* **69,** 121–9 (2001).
14. Verberckmoes, S. C., De Broe, M. E. & D'Haese, P. C. Dose-dependent effects of strontium on osteoblast function and mineralization. *Kidney Int.* **64,** 534–543 (2003).
15. Morohashi, T., Sano, T. & Yamada, S. Effects of strontium on calcium metabolism in rats. I. A distinction between the pharmacological and toxic doses. *Jpn. J. Pharmacol.* **64,** 155–62 (1994).
16. Chen, T.-Y., Chu, S.-Y. & Juang, Y.-D. Effects of sintering temperature on the dielectric and piezoelectric properties of Sr additive Sm-modified PbTiO3 ceramics. *Sensors Actuators A Phys.* **102,** 6–10 (2002).
17. Li, J., Liao, H. & Hermansson, L. Sintering of partially-stabilized zirconia and partially-stabilized zirconia-hydroxyapatite composites by hot isostatic pressing and pressureless sintering. *Biomaterials* **17,** 1787–90 (1996).
18. Wu, C., Ramaswamy, Y., Kwik, D. & Zreiqat, H. The effect of strontium incorporation into CaSiO3 ceramics on their physical and biological properties. *Biomaterials* **28,** 3171–81 (2007).
19. Zreiqat, H. *et al.* Mechanisms of magnesium-stimulated adhesion of osteoblastic cells to commonly used orthopaedic implants. *J. Biomed. Mater. Res.* **62,** 175–184 (2002).

20. Yamasaki, Y. *et al.* Synthesis of functionally graded MgCO3 apatite accelerating osteoblast adhesion. *J. Biomed. Mater. Res.* **62,** 99–105 (2002).
21. Hoppe, A., Güldal, N. S. & Boccaccini, A. R. A review of the biological response to ionic dissolution products from bioactive glasses and glass-ceramics. *Biomaterials* **32,** 2757–2774 (2011).
22. Dietrich, E., Oudadesse, H., Lucas-Girot, A. & Mami, M. In vitro bioactivity of melt-derived glass 46S6 doped with magnesium. *J. Biomed. Mater. Res. Part A* **88A,** 1087–1096 (2009).
23. Aina, V., Malavasi, G., Fiorio Pla, A., Munaron, L. & Morterra, C. Zinc-containing bioactive glasses: Surface reactivity and behaviour towards endothelial cells. *Acta Biomater.* **5,** 1211–1222 (2009).
24. Aina, V. *et al.* Cytotoxicity of zinc-containing bioactive glasses in contact with human osteoblasts. *Chem. Biol. Interact.* **167,** 207–218 (2007).
25. Oki, A., Parveen, B., Hossain, S., Adeniji, S. & Donahue, H. Preparation andin vitro bioactivity of zinc containing sol-gel-derived bioglass materials. *J. Biomed. Mater. Res.* **69A,** 216–221 (2004).
26. J. Brandao-Neto, V. Stefan, B.B. Mendonca, W. Bloise, A. V. B. C. The essential role of zinc in growth. *Nutr. Res* **15,** 335–358 (1995).
27. Tang, Z.-L., Wasserloos, K., St. Croix, C. M. & Pitt, B. R. Role of zinc in pulmonary endothelial cell response to oxidative stress. *Am. J. Physiol. Cell. Mol. Physiol.* **281,** L243–L249 (2001).
28. Yamaguchi, M. & Yamaguchi, R. Action of zinc on bone metabolism in rats. Increases in alkaline phosphatase activity and DNA content. *Biochem. Pharmacol.* **35,** 773–7 (1986).
29. Holloway, W. R., Collier, F. M., Herbst, R. E., Hodge, J. M. & Nicholson, G. C. Osteoblast-mediated effects of zinc on isolated rat osteoclasts: Inhibition of bone resorption and enhancement of osteoclast number. *Bone* **19,** 137–142 (1996).
30. Lusvardi, G., Malavasi, G., Menabue, L. & Menziani, M. C. Synthesis, Characterization, and Molecular Dynamics Simulation Of Na 2 O−CaO−SiO 2 −ZnO Glasses. *J. Phys. Chem. B* **106,** 9753–9760 (2002).

Chapter 5

Final conclusions

In the last few decades the scientific scenario has seen a quick evolution in the field of tissue engineering, proposing increasingly sophisticated and complex scaffolds that try to mimic the human extracellular matrix.

As an example of this evolution, first-generation scaffolds were represented by bi-dimensional surfaces, with obvious application limitations that led the scientific research to move onto 3D scaffolds mimetic of the cellular environment in human body. In a similar way, the previous *in vitro* biological assays to understand cell response to different scaffolds' stimuli, were carried out taking in consideration only one cell lineage at a time, while, nowadays innovative bioassays combining different cell types are becoming more and more interested not only in investigating the direct influence of external/internal agents to a certain cell lineage, but also in studying the indirect influence of different stimuli through another cell type mediated pathway.

In this perspective, this PhD project has considered not only the direct influence of different self-assembling peptides (SAPs) to human umbilical vein endothelial cells (HUVEC) behaviour, but how the activation of this type of cells toward an angiogenic phenotype was mediated by SAP-polarized macrophages. This kind of approach is relevant in the study of neo-angiogenesis process since the first human body reaction after surgery is always represented by inflammation response, and the presence of macrophages and their secreted factors has to be taken into consideration as it can influence deeply other cell types' behaviour.

Recently, the study of angiogenesis process and how it can be directed toward the obtainment of a stable and interconnected vascularization of implanted scaffolds is gaining interest due to its fundamental importance for implant's survival, jointed to the improvement of nourishment and gas diffusion necessary for cell growth and proliferation.

In this research study, we demonstrated that the synergy between different strategies could represent a valid alternative to obtain a next-generation scaffold for bone-tissue engineering, able to osteointegrate and to promote angiogenesis. With this in mind, we combined in the same proposal:

- polymer-derived bioceramic foams with high and interconnected porosity and adequate compressive strength, able to mimic the trabecular bone structure and mineral composition;
- covalent and selective functionalization to add protease-resistant biochemical motifs able to enhance h-osteoblast (HOB) proliferation and gene expression through an HOB-specific pathway.
- EAK self-assembling peptide properties with the aim of improving HOB viability and, especially, triggering HUVEC activation toward a pro-angiogenic phenotype to improve *in vivo* angiogenesis.
- the ability of EAK to be used as a carrier of pro-angiogenic factor such as TIM from Tß4, to further increase *in vivo* scaffold vascularization.

During the experimental development of the project, preliminary *in vitro* bioassays were performed to study the influence of self-assembly peptides on angiogenesis. To achieve this, five different SAPs were screened to assess the direct impact on HUVEC proliferation, molecular effect of distribution of YAP1 and functional influence on network formation. Using a combination of HUVEC cell culture assays, we found that SAPs were effective at inducing vascularisation vs gelatin and matrigel controls. Immunofluorescence evidenced the morphological changes, as a result of cell-SAP interaction. DAR was consistently the most successful peptide at inducing differentiation toward an angiogenic phenotype, increased YAP1 expression and formation of long and complex tubule structures. EAK showed good results in terms of cells morphology and formation of long tubule structures, too, and determined the highest increase in HOB proliferation and YAP1 expression.

All five SAPs were able to induce monocyte adhesion, which could potentially encourage cell survival and alter cellular function via non-integrin specific binding. DAR and EAK-polarised M1 were found to promote HUVEC network formation on matrigel, possibly by increasing M1's expression of MMP-9, a pro-angiogenic protease that promotes endothelial cell migration and network formation. However, no significant increase in network formation was observed for SAP-polarised M2. The lack of increase could be attributed to M2's innate low expression of MMP-9 or high expression of TIMP3, an inhibitor of MMP-9. We observed the trend in M1-induced network formation is the inverse of the trend in THP-1 cell spreading. For example, DAR polarised M1 induced highest network formation while THP-1s showed least spread on DAR/gelatin coating; the opposite was true for EYK. This finding suggests the increase in THP-1 spreading triggered some signalling cascades that would later inhibit M1 polarisation and their protein expression.

Further characterisation (mRNA and immunofluorescence) and *in vitro* studies (collagen/HUVEC assay) are needed to fully appreciate the intricate relationship between macrophages and SAPs.

Wollastonite-diopside foams were successfully functionalized with HVP series' peptides (HVP, 2HVP, DHVP and D2HVP) without negatively affecting the mechanical strength at crushing that still remained between the appropriate interval suitable for scaffolds for bone tissue engineering.

All functionalized samples showed increased h-osteoblast proliferation with respect to the control and silanized foams: retro-inverted sequences doubled the proliferation with respect to HVP and 2HVP at 2 days; D2HVP gave a dramatic proliferation increase (more than 15 times) at 6 days. All anchored peptides enhanced mRNA specific transcript levels coding *IBSP*, *VTN*, *RUNX2* and *SPP1*, four proteins fundamental during the process of new bone deposition.

LDH test confirmed the absence of cytotoxicity at 4 and 6 days from HOB seeding.

D2HVP functionalized W/D foams enhanced calcium deposition *in vivo* when inserted in an ectopic site in a murine model. Furthermore, histological analysis revealed the presence of new calcium deposits inside the pores only on functionalized bioceramics. *In vivo* assays demonstrated the osteoconductive and osteoinductive properties of D2HVP peptide.

The normal macroscopic appearance of implants after the removal from the animals, showed no inflammation and no encapsulation. The qualitative analysis performed with light field optical microscopy showed external and internal colonization of all the scaffolds with formation of new blood vessels (neoangiogenesis).

All the functionalizations tested proved to be able to stimulate the process of ectopic mineralization, whilst the control didn't develop any degree of mineralization. Md.S/Po.S, however, results to be significantly greater for the group characterized by the functionalization D2HVP+EAK+EAKG7TIM, which has a greater vascularization, too. This demonstrates that the EAK self-assembling peptide, designed to aid scaffold colonization, and the pro-angiogenic EAKG7TIM sequence grafted to the SAP itself, have a synergistic effect in promoting mineralization.

Future studies will confirm the results obtained in the present work, especially regarding the osteoinductive capacities of D2HVP+EAK and D2HVP+EAK+EAKG7TIM functionalizations, it will be necessary to carry out further *in vivo* experiments to assess reproducibility. The next step will be to evaluate the efficacy, in regenerative endosseous approaches, of the W/D scaffold characterized by the most efficient functionalization in promoting osteogenesis.

Another relevant aspect considered in the development of the final BTE scaffold was the transferability and the simplification of the functionalization protocol. In fact, the main strength point of this functionalization strategy is to be applicable to all ceramic scaffold, thus leaving space for further improvement of the ceramic composition, such as through the introduction of trace ions that may lead to therapeutic effects such as promotion of angiogenesis and antibacterial effect.

Nevertheless, although the selective and covalent anchoring of bioactive peptides to wollastonite-diopside foams gave promising *in vitro* and *in vivo* results, the same functionalization strategy showed not-encouraging results when transferred to Mg/Sr doped hardystonite foams. Since the selective and covalent functionalization protocol involves organic/acid treatments, this could lead to a fast release of Mg^{2+} and Sr^{2+} ions, changing the ions balance in the functionalized bioceramic to a higher content level of Zinc, that is known to induce cytotoxicity on h-osteoblast when de-adsorbed up to 50 μg/ml concentration (Aina, V. *et al*. Cytotoxicity of zinc-containing bioactive glasses in contact with human osteoblasts, Chemico-Biological Interactions 167 (2007) 207–218 doi:10.1016/j.cbi.2007.03.002). Further studies will be planned to prove this hypothesis.

The setup of a new and simplified functionalization method still able to anchor bioactive motifs in a covalent and selective way (via aldehyde peptide), but requiring mild reaction conditions and aqueous solutions, well-endured by scaffold for medical applications, allowed to obtain good results.

An important advantage of the final proposed covalent and selective functionalization strategy consists not only in being easily transferred to all types of ceramics, but even to biological matrices thanks to its less aggressive protocol.

Abbreviations

A / Ala - Alanine
AA - Amino acid
Abs - Absorbance
Abu - Aminobutyric acid
AcOH - Acetic acid
ALP - Alkaline phosphatase
bFGF - Basic fibroblast growth factor
BMP - Bone morphogenetic protein
BSP - Bone sialoprotein
BTE - Bone tissue engineering
C / Cys - Cysteine
c-HAP - carbonated Hydroxyapatite
Cbfa1 - Core binding factor alpha1
D / Asp - Aspartic acid
DCM - Dichloromethane
DIEA / DIPEA - N,N-Diisopropylethylamine
DLL4 - Delta-like ligand
Dlx5 - Distal-less homeobox 5
DMF - N,N-Dimethylformamide
E / Glu - Glutamic acid
EC - Endothelial cells
ECM - Extracellular matrix
EHS - Engelbreth Holm Swarm
ESI - Electrospray ionization
EtOH - Ethanol
F / Phe - Phenylalanine
FGF - Fibroblast growth factors
Fmoc - 9-Fluorenylmethoxycarbonyl
G / Gly - Glycine
G7 - Glycine-7-aminoheptanoic acid

GAGs - Glycosaminoglycan's
H / His - Histidine
HA - Hydroxyapatite
HATU - 1-[Bis(dimethylamino)methylene]-1H-1,2,3-triazolo[4,5-b]pyridinium 3-oxid hexafluorophosphate, N-[(Dimethylamino)-1H-1,2,3-triazolo-[4,5-b]pyridin-1-ylmethylene]-N-methylmethanaminium hexafluorophosphate N-oxide
HBTU - N,N,N′,N′-Tetramethyl-O-(1H-benzotriazol-1-yl)uronium hexafluorophosphate, O-(Benzotriazol-1-yl)-N,N,N′,N′-tetramethyluronium hexafluorophosphate
HOB - Human osteoblasts
HOBt - 1-Hydroxybenzotriazole
HT - Hardystonite
HUVEC - Human umbilical vein endothelial cells
I / Ile - Isoleucine
IBSP - Integrin-Binding Sialoprotein
IGF - Insulin-like growth factor
KGF - Keratinocyte growth factor
L / Leu - Leucine
M / Met - Methionine
M1 - Pro-inflammatory / activated macrophages
M2 - Anti-inflammatory / alternatively activated macrophages / pro-angiogenic macrophages
MALDI - Matrix assisted laser desorption/ionization
MeOH - Methanol
MMP-9 - Matrix metalloproteinase-9
MMPs - Matrix metalloproteinases
MSCs - Mesenchymal stem cells
N / Asn - Asparagine
NCPs: Non-collagenous proteins
NMP - N-Methyl-2-pyrrolidone
OCN - Osteocalcin
Orn - Ornithine
Osx - Osterix
OtBu - tert-Butyloxy
P / Pro - Proline
PCL - Polycaprolactone
PDGF - Platelet derived growth factor
PGA - Polyglycolic acid
PLA - Polylactic acid

PLGA - Copolymer of polylactic acid and polyglycolic acid
PLP - Pyridoxal-5-phosphate
Pmc - 2,2,5,7,8-Pentamethylchromane-6-sulfonyl
Q / Gln - Glutamine
R /Arg - Arginine
RGD - Arginine-Glycine-Aspartic Acid
RP-HPLC - Reverse Phase - High Performance Liquid Chromatography
RUNX2 - Runt-related transcription factor 2
Runx2 - Runt-related transcription factors 2
S / Ser - Serine
SAPs - Self-assembling peptides
SMCs - Smooth muscle cells
SPP1 - Secreted phosphoprotein 1 / Osteopontin
SPPS - Solid Phase Peptide Synthesis
ß-TCP - beta Tricalcium phosphate
T / Thr - Threonine
t-Boc / Boc - tert-Butoxycarbonyl
t-Bu / But - di-tert-Butyl
TAZ - paralog WW domain containing transcription regulator 1 of YAP
TCP1 - Human leukemic monocytes
TE - Tissue engineering
TES - Triethylsilane
TFA - Trifluoroacetic acid
TGFβ - Transforming growth factor beta
TIMP-1 - Tissue inhibitor of metalloproteinases-1
TOF - Time of flight
Trt - Trityl
Tß4 - Thymosin-ß4
V / Val - Valine
VEGF - Vascular Endothelial Growth Factor
VEGFR2 - VEGF receptors
VTN - Vitronectin
W/D - Wollastonite-Diopside
Wnt - Members of the Wingless pathways
Y / Tyr - Tyrosine
YAP - Yes-associated protein